

# **Bio-relevant Characterisation of Lipidic Formulations and Prediction of *In Vivo* Exposure**

**Paloma Benito-Gallo**

Thesis submitted to The University of Nottingham for the degree of  
Doctor in Philosophy

Nottingham, United Kingdom – September 2016

## **Thesis supervisor**

Pavel Gershkovich, PhD

Assistant Professor, School of Pharmacy, The University of Nottingham

## **Thesis co-supervisors**

Maria Marlow, PhD

Associate Professor, School of Pharmacy, The University of Nottingham

Vanessa Zann, PhD

Senior Research Fellow, Quotient Clinical Ltd.

Peter Scholes, PhD

Chief Scientific Officer, Quotient Clinical Ltd.

# Thesis Declaration

---

I, Paloma Benito Gallo, hereby certify that I am the sole author of this thesis and neither any part of this thesis nor the whole of the thesis has been submitted for a degree to any other University or Institution.

I state that this thesis is the result of my own independent work/investigation, except for otherwise stated.

I certify that, to the best of my knowledge, my thesis does not contain any material previously published or produced by another party in fulfilment, partial or otherwise, except for when due acknowledgment is made in the text. I understand the nature of plagiarism and that it is a serious academic offence. I confirm that no material in this thesis has been plagiarised and I consent to my work being run through a plagiarism checker.

I authorise the University of Nottingham to reproduce this thesis for the purpose of research either the whole or any portion of the contents in any manner whatsoever.

Signature:.....Date:.....

## I. Abstract

---

Lipidic formulations (LFs) are increasingly utilised for the delivery of poorly–water soluble drugs to improve oral bioavailability. *In vitro* lipolysis is capable of mimicking the lipid digestion process and therefore it is a suitable method for assessing the fate of drugs administered in LFs. Intestinal micellar solubilisation and first–pass metabolism are the main contributors to the oral bioavailability of drugs that belong to class II of the Biopharmaceutics Classification System (BCS). The intraluminal solubility of BCS II drugs in LFs can be estimated with the *in vitro* lipolysis model, whereas the first–pass extraction ratio can be assessed by performing microsomal stability assays. This thesis work proposes, for the first time, the combination of *in vitro* lipolysis and microsomal metabolism studies for the quantitative prediction of human oral bioavailability of BCS II drugs administered in LFs. Marinol® ( $\Delta^9$ –tetrahydrocannabinol dissolved in sesame oil) and Neoral® (a lipidic self–emulsifying drug delivery system of cyclosporin A), were selected as model LFs. The observed oral bioavailability ( $F_{\text{observed}}$ ) values were obtained from published clinical studies that described the oral administration of the selected LFs to human subjects. Two different lipolysis buffers, differing in the level of surfactant concentrations, were used for digestion of the LFs. The predicted fraction of absorbed dose ( $F_{\text{abs}}$ ) was calculated by measuring the drug concentration in the micellar phase, obtained after ultra–centrifugation of the lipolysis medium. To determine the fraction of drug dose that escapes metabolism in the gut wall and in the liver ( $F_g \cdot F_h$ ), microsomal metabolism stability studies with human intestinal and hepatic microsomes were performed. Clearance values were determined by applying the “*in vitro* half–life approach”, which is based on the measurement of the first–order rate depletion constant of a drug substrate. The estimated  $F_{\text{abs}}$  and  $F_g \cdot F_h$  values were combined for the calculation of the predicted oral bioavailability ( $F_{\text{predicted}}$ ). For the model LFs tested, results showed there was a correlation between  $F_{\text{observed}}$  and  $F_{\text{predicted}}$  values only when  $F_{\text{abs}}$  was calculated with the buffer characterised by more bio–relevant (lower) surfactant levels. The general accuracy of the predicted values, and the strong correlation shown with the clinical ones, suggests the novel *in vitro* lipolysis/metabolism approach could satisfactorily quantitatively estimate the oral bioavailability of BCS II drugs administered in LFs.

## II. Acknowledgements

---

Firstly, I would like to express my most sincere gratitude to my main supervisor, Dr. Pavel Gershkovich, for always being there whenever I needed, for his constant advice, for the provided freedom in the research, for the fruitful discussions, and for making me see this PhD topic was much more interesting than I originally thought.

I would also like to thank my other supervisors Dr. Maria Marlow, Dr. Vanessa Zann and Dr. Peter Scholes for their trust in me, and for their constructive feedback and continuous support.

I would like to make a special mention to my lab mates who gave up their time to help and support my work. Thanks to Atheer Zgair and Jonathan Wong for their help with the *in vitro* lipolysis experiments; thanks to Jong Bong “JB” Lee and Dhiaa Taha for their help with the microsomal metabolism and HPLC–MS/MS assays, respectively; and thanks to Sally Gittings for making the office hours being much more bearable and entertaining.

I would like to thank Zoe Kane and Alison Wilby for their help with GastroPlus® software.

I would like to acknowledge the funding sources of these studies: the UK Engineering and Physical Sciences Research Council (EPSRC), the University of Nottingham, and Quotient Clinical Ltd. (grant number EP/I01375X/I).

I would like to thank my internal and external assessors, Dr. Martin Garnett and Prof. Abdul Basit, for generously giving their time and expertise to evaluate my work. I appreciate their feedback to improve my work.

I would like to express my gratitude as well to the staff and technicians at Boots Science Building and at the Centre for Biomolecular Sciences (School of Pharmacy), where the experimentation of this thesis was carried out.

Last but not least, I would like to thank my family in Spain. *Gracias mamá y papá por siempre apoyarme, por vuestro cariño y por vuestra confianza ciega en mí. Gracias Marina por tus ánimos en momentos cuando ni siquiera los tenías para ti. Gracias Alberto por tu compañía durante tu estancia en Nottingham. Y gracias Lía y Kyra, mis perrinas, por sacarme siempre una sonrisa. Os quiero.*

## III. Table of Contents

<b>Thesis Declaration .....</b>	<b>iii</b>
<b>I. Abstract .....</b>	<b>iv</b>
<b>II. Acknowledgements .....</b>	<b>v</b>
<b>III. Table of Contents .....</b>	<b>vi</b>
<b>IV. List of Publications .....</b>	<b>xi</b>
<b>V. List of Abbreviations .....</b>	<b>xiii</b>
<b>VI. List of Symbols.....</b>	<b>xvii</b>
<b>VII. List of Figures .....</b>	<b>xviii</b>
<b>VIII. List of Tables .....</b>	<b>xxiii</b>
<b>IX. List of Equations.....</b>	<b>xxvi</b>
<b>X. Thesis Format and Author's Statement.....</b>	<b>xxviii</b>
<b>Chapter I: Introduction.....</b>	<b>I</b>
I.1. Introduction .....	I
I.2. Bioavailability of orally administered drugs .....	I
I.3. Oral drug delivery strategies for poorly water-soluble drugs .....	4
I.3.1. Salt formation .....	4
I.3.2. Polymorphic and amorphous forms .....	5
I.3.3. Solid dispersions .....	5
I.3.4. Cyclodextrin complexation .....	6
I.3.5. Particle size reduction.....	6
I.4. Lipidic formulations .....	7
I.4.1. Rationale behind the use of lipidic formulations .....	7
I.4.2. Digestion and absorption of lipids in the gastrointestinal tract .....	8
I.4.3. Mechanisms of bioavailability enhancement by lipidic formulations .....	11
I.4.3.1. Mechanisms that enhance solubilisation.....	11
I.4.3.2. Mechanisms that facilitate permeability.....	12
I.4.3.3. Mechanisms that reduce pre-systemic metabolism: Stimulation of the lymphatic transport.....	13
I.4.4. Lipidic excipients: The Lipid Formulation Classification System .....	15
I.5. Assessment of oral drug delivery systems .....	18
I.5.1. Bio-relevant media .....	18
I.5.2. <i>In vitro</i> testing of oral dosage forms.....	19

1.6. <i>In vitro</i> lipolysis model .....	20
1.6.1. Bio-relevant medium of the <i>in vitro</i> lipolysis model .....	21
1.6.2. Predictability power of the <i>in vitro</i> lipolysis model: IVIVCs .....	23
1.7. First-pass metabolism .....	24
1.7.1. The small intestine, the enterocytes and enzyme gut activity .....	25
1.7.2. The liver, the hepatocytes, and enzyme hepatic activity .....	26
1.7.3. Estimation of first-pass metabolism .....	27
1.7.3.1. Direct and indirect methods in humans .....	27
1.7.3.2. <i>In vivo</i> methods: Allometric scaling .....	28
1.7.3.3. <i>In vitro</i> methods .....	28
1.7.3.3.1. Recombinant enzymes .....	28
1.7.3.3.2. Cell systems .....	29
1.7.3.3.3. Tissue slices .....	29
1.7.3.3.4. Subcellular fractions .....	29
1.7.3.3.5. Determination of human clearance .....	30
1.8. Research proposal and Objectives .....	32
<b>Chapter 2: Optimisation of the <i>In Vitro</i> Lipolysis Model Working Conditions.....</b>	<b>34</b>
2.1. Introduction .....	34
2.2. Materials and Methods .....	36
2.2.1. Materials .....	36
2.2.2. Lipidic formulations .....	37
2.2.3. Preparation of digestion buffers .....	37
2.2.4. Preparation of lipase/co-lipase extract .....	38
2.2.5. Determination of lipase/co-lipase extract activity .....	38
2.2.6. Optimisation of the <i>in vitro</i> lipolysis model working conditions .....	38
2.2.7. Statistical data analysis .....	40
2.3. Results .....	40
2.3.1. Lipase extract activity .....	40
2.3.2. Optimisation of the <i>in vitro</i> lipolysis model working conditions .....	41
2.3.2.1. 0.5 M NaOH, 1 mL/min maximum rate, 10 µL/min minimum rate .....	41
2.3.2.2. 1 M NaOH, 1 mL/min maximum rate, 10 µL/min minimum rate .....	42
2.3.2.3. 1 M NaOH, 1 mL/min maximum rate, 3 µL/min minimum rate .....	42
2.3.2.4. 1 M NaOH, 3.5 mL/min maximum rate, 3 µL/min minimum rate .....	42
2.4. Discussion .....	47
2.4.1. Lipase extract activity .....	47
2.4.2. Optimisation of the <i>in vitro</i> lipolysis model working conditions .....	47

2.5. Conclusions.....	48
<b>Chapter 3: Assessment of Pancreatic Lipase Activity: <i>In Vitro</i> Digestion of Equimolar Amounts of Lipids.....</b>	<b>50</b>
3.1. Introduction .....	50
3.2. Materials and Methods .....	51
3.2.1. Materials.....	51
3.2.2. Preparation of simulated digestion buffers .....	52
3.2.3. Preparation of lipase/co-lipase extract .....	52
3.2.4. Experimental procedure: Lipolysis of equimolar amounts of different triglycerides .....	52
3.2.5. Experimental procedure: Back-titrations .....	53
3.2.6. Solubility effect of glyceryl triacetate on the extent of lipolysis.....	53
3.2.7. Measurement of the droplet size and total surface area of equimolar triglyceride emulsions following dispersion in the lipolysis buffer .....	53
3.2.8. Statistical data analysis.....	54
3.3. Results .....	54
3.3.1. <i>In vitro</i> lipolysis of equimolar amounts of different triglycerides .....	54
3.3.2. Back-titration studies .....	57
3.3.3. Solubility effect of glyceryl triacetate on the extent of lipolysis.....	58
3.3.4. Droplet size and total surface of the equimolar triglyceride emulsions following dispersion in the lipolysis buffer .....	58
3.4. Discussion.....	59
3.5. Conclusions .....	63
<b>Chapter 4: Estimation of the Fraction Absorbed of BCS II Drugs in Lipidic Formulations by <i>In Vitro</i> Lipolysis .....</b>	<b>65</b>
4.1. Introduction .....	65
4.2. Materials and Methods .....	68
4.2.1. Materials.....	68
4.2.2. Lipidic formulations, clinical data, and PK analysis .....	68
4.2.2.1. Selection of lipidic formulations and associated clinical data.....	68
4.2.2.2. PK analysis .....	71
4.2.3. Composition and preparation of blank lipidic formulations.....	71
4.2.4. <i>In vitro</i> lipolysis studies .....	72
4.2.4.1. Scaling down from in vivo to in vitro conditions.....	72
4.2.4.2. Simulated intestinal buffers .....	73
4.2.4.3. Experimental procedure .....	73
4.2.5. HPLC–UV analysis.....	74



4.2.5.1. Sample preparation.....	74
4.2.5.2. Chromatographic conditions .....	75
4.2.5.3. Method validation .....	75
4.2.6. Calculation of the predicted fraction absorbed ( $F_{abs}$ ) .....	76
4.2.7. Statistical data analysis.....	76
4.3. Results .....	77
4.3.1. PK analysis of selected clinical data .....	77
4.3.2. HPLC–UV method development and validation .....	78
4.3.3. <i>In vitro</i> lipolysis.....	79
4.3.3.1. Drug distribution across lipolysis phases. The effect of the assumed <i>in vivo</i> dissolution volume: 250 versus 100 mL .....	79
4.3.3.2. Effect of the surfactant concentrations: “classic” versus “new” buffer .....	81
4.4. Discussion.....	83
4.4.1. PK analysis of selected clinical data .....	83
4.4.2. HPLC–UV method development and validation .....	84
4.4.2.1. HPLC–UV method development.....	84
4.4.2.2. HPLC–UV method validation .....	85
4.4.3. <i>In vitro</i> lipolysis.....	85
4.4.3.1. Drug distribution across the lipolysis phases. The effect of the assumed <i>in vivo</i> dissolution volume: 250 versus 100 mL .....	86
4.4.3.2. Effect of the surfactant concentrations: “classic” versus “new” buffer.....	88
4.5. Conclusions.....	90
<b>Chapter 5: <i>In Vitro</i> Lipolysis/Microsomal Metabolism Model for the Estimation of the Oral Bioavailability of BCS II Drugs in Lipidic Formulations .....</b>	<b>92</b>
5.1. Introduction .....	92
5.2. Materials and Methods .....	94
5.2.1. Materials.....	94
5.2.2. <i>In vitro</i> microsomal incubations.....	94
5.2.3. Analytical procedures.....	95
5.2.3.1. HPLC–UV analysis .....	95
5.2.3.1.1. Sample preparation .....	95
5.2.3.1.2. Chromatographic conditions .....	96
5.2.3.2. HPLC–MS/MS analysis .....	96
5.2.3.2.1. Sample preparation .....	96
5.2.3.2.2. Chromatographic conditions .....	97
5.2.4. Data analysis .....	97
5.2.4.1. Determination of <i>in vitro</i> intrinsic clearance values .....	97
5.2.4.2. Calculation of the predicted fraction escaping hepatic metabolism ( $F_h$ ) .....	99

5.2.4.3. Calculation of the predicted fraction escaping gut metabolism ( $F_g$ ) .....	99
5.2.4.4. Calculation of the predicted oral bioavailability ( $F_{\text{predicted}}$ ).....	100
5.2.5. Statistical data analysis.....	100
5.3. Results .....	101
5.3.1. HPLC–MS/MS detection method .....	101
5.3.2. Hepatic microsomal metabolism: Prediction of the fraction non–metabolised in the liver ( $F_h$ ).....	101
5.3.3. Intestinal microsomal metabolism: Prediction of the fraction non–metabolised in the gut ( $F_g$ ).....	103
5.3.4. Linking <i>in vitro</i> lipolysis and metabolism studies: Prediction of the oral bioavailability ( $F_{\text{predicted}}$ )... ..	104
5.4. Discussion.....	106
5.4.1. Prediction of the fraction non–metabolised in the liver .....	108
5.4.2. Prediction of the fraction non–metabolised in the gut.....	109
5.4.3. Prediction of oral bioavailability.....	110
5.5. Conclusions .....	112
<b>Chapter 6: Ongoing Experimentation and Recommendations for Future Work</b>	<b>113</b>
6.1. Introduction .....	113
6.2. <i>In vitro</i> lipolysis/microsomal metabolism model for the prediction in pre–clinical species of oral bioavailability of BCS II drugs in lipidic formulation.....	114
6.2.1. Introduction.....	114
6.2.2. Materials and Methods.....	115
6.2.2.1. Materials .....	115
6.2.2.2. Model formulation and associated pharmacokinetic data .....	115
6.2.2.3. <i>In vitro</i> lipolysis experiments.....	116
6.2.2.4. <i>In vitro</i> microsomal incubations .....	117
6.2.2.5. Calculation of the predicted oral bioavailability and statistical analysis .....	118
6.2.3. Results and Discussion.....	118
6.2.3.1. <i>In vitro</i> lipolysis .....	118
6.2.3.2. Microsomal metabolism .....	120
6.2.3.3. Prediction of the oral bioavailability in rats.....	122
6.2.4. Conclusions.....	123
6.3. <i>In vitro-in silico/in vivo</i> Correlation: Prediction of the performance of BCS II drugs in lipidic formulations.....	123
6.3.1. Introduction.....	123
6.3.2. Materials and Methods.....	124
6.3.2.1. Software .....	124
6.3.2.2. <i>In silico</i> and <i>in vitro</i> input parameters .....	125

6.3.2.3. <i>In vivo</i> data.....	126
6.3.3. Results and Discussion.....	126
6.3.4. Conclusions.....	128
<b>Chapter 7: General Discussion and Concluding Remarks.....</b>	<b>130</b>
7.1. General Discussion: Summary, Future Perspectives, Impact on the Research Field, and Advantages and Limitations of the <i>In Vitro</i> Lipolysis/Microsomal Metabolism Model	130
7.2. Concluding remarks .....	133
<b>Appendix.....</b>	<b>136</b>
Appendix A. Pharmacokinetic data following administration of model drugs and lipidic formulations.....	136
Appendix B. HPLC–UV Method development for the determination of $\Delta^9$ –tetrahydrocannabinol and cyclosporin A in lipolysis samples.....	140
Appendix C. HPLC–MS/MS Method development for the determination of $\Delta^9$ –tetrahydrocannabinol and cyclosporin A in microsomal incubation samples....	145
Appendix D. Additional data derived from the microsomal metabolism of $\Delta^9$ –tetrahydrocannabinol, cyclosporin A, and control compounds.....	148
Appendix E. Pharmacokinetic data derived from the intravenous and oral administration of $\Delta^9$ –tetrahydrocannabinol to rats.....	151
Appendix F. Additional data resulting from the <i>in vitro</i> lipolysis of the lipidic and lipid-free formulations of $\Delta^9$ –tetrahydrocannabinol.....	152
Appendix G. Additional data derived from the <i>in silico</i> simulations of the oral profiles of Marinol® and Neoral®.....	154
<b>References.....</b>	<b>156</b>

## IV. List of Publications

---

### Original Research Papers

- Benito-Gallo, P., Marlow, M., Zann, V., Scholes, P., & Gershkovich, P. (2016). Linking *In Vitro* Lipolysis and Microsomal Metabolism for the Quantitative Prediction of Oral Bioavailability of BCS II Drugs Administered in Lipidic Formulations, *Molecular Pharmaceutics*, 13 (10): p. 3526–3540.
- Benito-Gallo, P., Franceschetto, A., Wong, J.C.M., Marlow, M., Zann, V., Scholes, P., and Gershkovich, P. (2015). Chain length affects pancreatic lipase activity and the extent and pH–time profile of triglyceride lipolysis. *European Journal of Pharmaceutics and Biopharmaceutics*, 93(0): p. 353–362.

### Book Chapter

- Benito-Gallo, P., Gershkovich, P., Marlow, M., Zann, V., & Wasan, K.M. (2016). Smart Lipid-Based Drug Delivery Systems. In V.P. Torchilin (Ed.), *Smart Pharmaceutical Nanocarriers* (pp. 309–371). Imperial College Press. ISBN: 978-1-78326-722-4 (hardcover), 978-1-78326-724-8 (ebook).

### Abstracts and Conference Proceedings

- Benito-Gallo, P., Marlow, M., Zann, V., Scholes, P., & Gershkovich, P. (2016). Improvement of *In Vitro* Lipolysis Predictability Power: Studies with Physiologically Relevant Surfactant Concentrations. *10<sup>th</sup> World Meeting on Pharmaceutics, Biopharmaceutics and Pharmaceutical Technology*. Glasgow, UK.
- Benito-Gallo, P., Marlow, M., Zann, V., Scholes, P., & Gershkovich, P. (2015). *In Vitro* lipolysis/metabolism approach for the quantitative prediction of oral bioavailability of lipophilic drugs administered in lipid-based formulations. *AAPS Meeting and Exposition*. Florida, Orlando, USA.
- Benito-Gallo, P., Franceschetto, A., Wong, J.C.M., Marlow, M., Zann, V., Scholes, P., & Gershkovich, P. (2014). The effect of triglyceride chain length on pH–time profiles,

pancreatic lipase activity, and the extent of reaction during *in vitro* lipolysis studies. *APS UK PharmSci*. University of Hertfordshire, Hatfield, UK.

- Benito-Gallo, P., Franceschetto, A., Wong, J.C.M., Marlow, M., Zann, V., Scholes, P., & Gershkovich, P. (2014). Optimisation of an *in vitro* lipolysis model: Effect of triglyceride chain length on pH-time profiles and lipase activity. *PhysChem Forum (14<sup>th</sup> Symposium)*. East Grinstead, Surrey, UK.
- Franceschetto, A., Wong, J.C.M., How, X.Y., Amin, J., Benito-Gallo, P., & Gershkovich, P. (2013). Establishment and optimization of *in vitro* lipolysis model to guide development of lipid-based formulations with different fatty acid chain lengths of triglyceride component. *NC3Rs*. London, UK.

## V. List of Abbreviations

---

ACAT	Advanced compartmental absorption and transit
ADME	Absorption, distribution, metabolism and excretion
ANOVA	Analysis of variance
API	Active pharmaceutical ingredient
AUC	Area under the plasma/blood concentration–time curve
AUC <sub>t</sub>	AUC from time zero to the last measurable concentration point
AUC <sub>∞</sub>	AUC extrapolated to infinity
BCS	Biopharmaceutics classification system
BDDCS	Biopharmaceutics Drug Disposition Classification System (BDDCS)
B/P	Blood to plasma drug concentration ratio
BS	Bile salt
C <sub>0</sub>	Compound concentration at the beginning of the incubation process
CBD	Cannabidiol
C <sub>GI,pH</sub>	<i>In vivo</i> solubility in a compartment of the gastrointestinal tract with specific pH and bile salt concentration (GastroPlus®)
CL	Clearance
CL <sub>g</sub>	Gut clearance
CL <sub>h</sub>	Hepatic clearance
CL <sub>int</sub>	Intrinsic clearance
CL <sub>u, int</sub>	Intrinsic clearance corrected for the fraction of drug unbound
C <sub>MP</sub>	Drug concentration in the micellar phase
C <sub>max</sub>	Maximum peak plasma/blood concentration
CL <sub>perm</sub>	Permeability clearance
CP	Liquid–crystalline phase
C <sub>t</sub>	Compound concentration remaining at each time point
CsA	Cyclosporin A
CV	Coefficient of variation
CYP	Cytochrome P450 monooxygenase
DG	Diglyceride
d <sub>H</sub>	Hydrodynamic droplet size
DLS	Dynamic light scattering

$E_g$	Intestinal drug extraction
$E_h$	Hepatic drug extraction
$F$	Systemic bioavailability
FA	Fatty acid
$F_{abs}$	Fraction of drug dose absorbed
FaSSIF	Fasted state simulated intestinal fluid
FeSSIF	Fed state simulated intestinal fluid
$F_g$	Fraction of drug dose that escapes extraction in the gut wall.
$F_h$	Fraction of drug dose that escapes extraction in the liver
$F_{observed}$	Observed oral bioavailability in human subjects
$F_{predicted}$	Predicted oral bioavailability using the <i>in vitro</i> lipolysis/metabolism approach
$fu_b$	Fraction of drug unbound in blood
$fu_{inc}$	Fraction of drug unbound in the microsomal incubation
$fu_g$	Fraction of drug unbound in the enterocyte
$fu_p$	Fraction of drug unbound in plasma
GRAS	Generally recognised as safe
GST	Glutathione S-transferase
HLB	Hydrophobic-lipophilic balance
HQC	High quality control
IV	Intravenous
IVIVC	<i>In vitro–in vivo</i> correlation
$k_{dep}$	First-order substrate depletion rate constant
$k_{dep,[S] \rightarrow 0}$	Theoretical depletion constant at infinitesimally low substrate concentration
$k_L$	Rate of lipolysis
$K_M$	Michaelis–Menten constant
LCT	Long-chain triglyceride
LF	Lipidic formulation
LFCS	Lipid formulations classification system
LLOQ	Lowest validated limit of quantification

---

logD	Decimal logarithm of the distribution coefficient (D)
logP	Decimal logarithm of the partition coefficient (P)
LQC	Low quality control
MCT	Medium-chain triglyceride
MG	Monoglyceride
MP	Micellar phase
MQC	Medium quality control
MS/MS	Tandem mass spectrometry
MW	Molecular weight
NADPH	Nicotinamide adenine dinucleotide phosphate
NaTC	Sodium taurocholate
NaTDC	Sodium taurodeoxycholate
NCA	Non-compartmental analysis
OSD	Overall standard deviation
OSSE	Overall sum of squared errors
$p$	probability
PBPK	Physiology-based pharmacokinetic
PC	Phosphatidylcholine
$P_{\text{eff}}$	Effective permeability
PEG	Polyethylene glycol
PG	Propylene glycol
PK	Pharmacokinetic
PL	Phospholipid
$Q_{\text{gut}}$	Gut blood flow
$Q_{\text{h}}$	Hepatic blood flow
$Q_{\text{villi}}$	Villous blood flow
RE	Relative error
Ref.	References
RSD	Relative standard deviation



S	Drug substrate; [S] drug substrate concentration
SCT	Short-chain triglyceride
SD	Standard deviation (also represented as <i>s</i> )
SEDDS	Self-emulsifying drug delivery system
SIF	Simulated intestinal fluids
<i>sn</i>	Stereospecific number
SR	Solubilisation ratio
$S_s$	Specific surface area
$t_{1/2}$	Half-life
$t_{1/2,z}$	Half-life at the terminal phase
TBU	Tributylin unit
THC	$\Delta^9$ -Tetrahydrocannabinol
TG	Triglyceride
$t_{max}$	Time at which the maximum peak plasma/blood concentration occurs
Tri-C2	Glycerol triacetate
Tri-C4	Glycerol tributyrate
Tri-C8	Glycerol trioctanoate
Tri-C10	Glycerol tridecanoate
Tri-C18	Peanut oil
UGT	Uridine 5'-diphospho-glucuronosyltransferase
USP	United States pharmacopeia
UV	Ultraviolet
$V_d$	Volume of distribution
VitD <sub>3</sub>	Vitamin D <sub>3</sub>
$V_{max}$	Maximum rate of metabolism
$V_{ss}$	Steady-state volume of distribution
$V_z$	Volume of distribution at the terminal phase
<i>v/v</i>	Volume per volume
<i>w/w</i>	Weight per weight
WX	Weighted mean

## VI. List of Symbols

---

$g$	Relative centrifugal force
$\lambda$	Wavelength
$n$	Sample size
pH	Decimal logarithm of the reciprocal of the hydrogen ion activity, $a_{H^+}$ , in a solution: $pH = -\log_{10}(a_{H^+})$
$pK_a$	Decimal logarithm of the reciprocal of the acid dissociation constant, $K_a$ : $pK_a = -\log_{10}(K_a)$
$\pi$	Mathematical constant equal to 3.14159
$\rho$	Density
$r$	Pearson's coefficient
$r^2$	Correlation coefficient
$s$	Standard deviation
$s^2$	Variance
$x_{calc}$	Regressed concentration computed from the calibration curve
$x_{nom}$	Nominal standard concentration
$\Sigma$	Sum
$\bar{x}$	Average
$\infty$	Infinity

## VII. List of Figures

- Figure 1-1.** Biopharmaceutical Classification System. (Reprinted with permission from Ref. [11], Copyright© 2008, Nature Publishing Group) ..... 2
- Figure 1-2.** Schematic representation of the barriers a drug must overcome to reach systemic circulation and the site of action.  $F_{abs}$ : Fraction absorbed;  $F$ : absolute bioavailability;  $F_g$ : intestinal bioavailability;  $F_h$ : hepatic bioavailability;  $E_g$ : intestinal extraction;  $E_h$ : hepatic extraction. (Adapted with permission from Ref.[18], Copyright© 2003, Nature Publishing Group)..... 4
- Figure 1-3.** Lipolysis of a triglyceride (TG) by pancreatic lipase. Pancreatic lipase shows the same selectivity towards the hydrolysis at positions *sn*-1 and *sn*-3 of the triglyceride when the fatty acid (FA) side chains are identical. DG: diglyceride; MG: monoglyceride. (Modified from Ref. [53], under the terms of the Creative Commons Attribution License, CC BY, 2016) ..... 9
- Figure 1-4.** The unstirred water layer and mechanism of lipid absorption. FA: fatty acid. (Reprinted with permission from Ref. [58], Copyright© 2007, Nature Publishing Group)..... 10
- Figure 1-5.** Access to the lymphatic system by lipids and lipophilic drugs within the enterocyte. TG: Triglyceride; MG: monoglyceride; FA: fatty acid; LP: lipoprotein. (Adapted with permission from Ref. [76], Copyright© 2015, Nature Publishing Group) ..... 14
- Figure 1-6.** Schematic representation of the phases commonly present after the ultra-centrifugation of the lipolysis medium. .... 21
- Figure 1-7.** Preparation method of subcellular fractions. S9 is the supernatant fraction obtained from a tissue homogenate by low speed centrifugation (~9000 g). Whilst, the pellet contains unbroken cells, nuclei, and mitochondria. After high speed centrifugation (~100,000 g) of the S9 fraction, pieces of the endoplasmic reticulum sediment out as a pellet (microsomes), and soluble components remain as a supernatant (cytosol)..... 30
- Figure 1-8.** Three-stage strategy for extrapolation of in vitro clearance to in vivo hepatic metabolic clearance.  $CL$ : human clearance (hepatic or intestinal);  $CL_{int}$ : intrinsic clearance;  $k_e$ : drug elimination constant;  $K_m$ : Michaelis–Menten constant;  $SI$ : small intestine;  $v_{max}$ : maximum rate of metabolism. .... 31
- Figure 2-7.** pH dependence of Michaelis–Menten constant ( $K_m$ , green circles) and maximum reaction rate ( $V_m$ , blue squares). (Adapted with permission from Ref. [197], Copyright© 1971, American Chemical Society) ..... 36
- Figure 2-1.** Set-up of the *in vitro* lipolysis model in the laboratory. The main components and their functions are indicated with arrows. .... 39
- Figure 2-2.** pH–time (green) and volume of NaOH–time (blue) profiles of the lipolysis of 6 mL of glyceryl tributyrate by 20  $\mu$ L of lipase/co-lipase extract. Conditions: 1 M NaOH, 3.5 mL/min maximum and 3  $\mu$ L/min minimum dosing rate..... 41
- Figure 2-3.** pH–time lipolysis profiles (mean  $\pm$  SD,  $n = 5$ ) for 200, 500 and 1000  $\mu$ L of glyceryl triacetate (tri-C2), tributyrate (tri-C4), trioctanoate (tri-C8), tridecanoate (tri-C10), and peanut oil (tri-C18). Conditions: 0.5 M NaOH, 1 mL/min maximum and 10  $\mu$ L/min minimum dosing rate. Only the first 800 s of the process are represented for ease of comparison. (Modified from Ref. [53], under the terms of CC BY, 2015)..... 43
- Figure 2-4.** pH–time lipolysis profiles (mean  $\pm$  SD,  $n = 5$ ) for 200, 500 and 1000  $\mu$ L of glyceryl triacetate (tri-C2), tributyrate (tri-C4), trioctanoate (tri-C8), tridecanoate (tri-C10), and peanut oil (tri-C18). Conditions: 1 M NaOH, 1 mL/min maximum and 10  $\mu$ L/min minimum

dosing rate. Only the first 800 s of the process are represented for ease of comparison. (Modified from Ref. [53], under the terms of CC BY, 2015)..... 44

**Figure 2-5.** pH–time lipolysis profiles (mean  $\pm$  SD,  $n = 5$ ) for 200, 500 and 1000  $\mu$ L of glyceryl triacetate (tri–C2), tributyrates (tri–C4), trioctanoate (tri–C8), tridecanoate (tri–C10) and peanut oil (tri–C18). Conditions: 1 M NaOH, 1 mL/min maximum and 3  $\mu$ L/min minimum dosing rate. Only the first 800 s of the process are represented for ease of comparison. (Modified from Ref. [53], under the terms of CC BY, 2015)..... 45

**Figure 2-6.** pH–time lipolysis profiles (mean  $\pm$  SD,  $n = 5$ ) for 200, 500 and 1000  $\mu$ L of glyceryl triacetate (tri–C2), glyceryl (tri–C4), glyceryl (tri–C8), glyceryl (tri–C10), and peanut oil (tri–C18). Conditions: 1 M NaOH, 3.5 mL/min maximum and 3  $\mu$ L/min minimum dosing rate. Only the first 800 s of the process are represented for ease of comparison. (Modified from Ref. [53], under the terms of CC BY, 2015). ..... 46

**Figure 3-1.** pH–time profiles obtained during the *in vitro* lipolysis of equimolar amounts of: (A) glyceryl triacetate, (B) tributyrates, (C) trioctanoate (D) tridecanoate, and (E) peanut oil. Conditions: pH  $6.80 \pm 0.05$ , 0.5 M NaOH titrant concentration, 1 mL/min and 10  $\mu$ L/min maximum and minimum titrant dosing rate, respectively. Values are expressed as mean  $\pm$  SD ( $n = 5$ ). (Modified from Ref. [53], under the terms of CC BY, 2015) ..... 55

**Figure 3-2.** Apparent extent of lipolysis (green) and volume of titrant (0.5 M NaOH) consumed over time (blue) during the direct *in vitro* lipolysis at pH  $6.80 \pm 0.05$  of equimolar amounts of: (A) glyceryl triacetate, (B) tributyrates, (C) trioctanoate, (D) tridecanoate, and (E) peanut oil. Values are expressed as means ( $n = 5$ )  $\pm$  SD. Note the difference in the time scales (X- axes) among the graphs. (Modified from Ref. [53], under the terms of CC BY, 2015) ..... 56

**Figure 3-3.** Comparison of the total extent of lipolysis for the *in vitro* lipolysis of equimolar amounts of different triglycerides: glyceryl triacetate (tri–C2), tributyrates (tri–C4), trioctanoate (tri–C8), tridecanoate (tri–C10) and peanut oil (tri–C18). Blue colours represent the apparent extent of lipolysis calculated during direct titration experiments (pH  $6.80 \pm 0.05$ ). Green-shade areas represent the underestimated extent of lipolysis calculated after back-titration experiments (pH  $11.50 \pm 0.05$ ). Values are expressed as means ( $n = 5$ )  $\pm$  SD. One-way ANOVA followed by post hoc Tukey–Kramer test was used for statistical analysis. .... 57

**Figure 3-4.** Proposed molecular mechanism of triglyceride lipolysis by pancreatic lipase focused on the catalytic triad. (Reprinted from Ref. [53], under the terms of the CC BY, 2016) ..... 62

**Figure 4-1.** Fraction of absorbed dose of  $\Delta^9$ -tetrahydrocannabinol (THC) in Marinol® estimated from lipolysis studies. Coral and blue colours correspond to the lipolysis of the formulations using the “classical” buffer, assuming an *in vivo* dissolution volume of 250 mL and 100 mL, respectively. Whilst, green colours represent the lipolysis in the “new” buffer, assuming 100 mL of dissolution volume. Values are expressed as means ( $n = 6$ )  $\pm$  SD. A one-way ANOVA followed by Tukey–Kramer multiple comparison test were used for statistical analysis. Statistically significantly different: \*\*\*\*,  $p < 0.0001$ ; \*\*,  $p < 0.01$  ..... 81

**Figure 4-2.** Fraction of absorbed dose of cyclosporin A (CsA) in Neoral® estimated from lipolysis studies assuming an *in vivo* dissolution volume of 100 mL. Blue colours correspond to the lipolysis of the formulations using the “classical” buffer; whereas green colours represent the “new” buffer. Values are expressed as means ( $n = 6$ )  $\pm$  SD. An unpaired *t*-test followed by Welch’s correction were used for statistical analysis. Statistically significantly different: \*\*\*\*,  $p < 0.0001$ ; \*\*,  $p < 0.01$ . ..... 83

**Figure 5-1.** Proposed *In vitro* lipolysis/microsomal metabolism model for the prediction of the human oral bioavailability of lipophilic drugs administered in lipidic formulations.  $F_{abs}$ : Fraction absorbed;  $F$ : absolute bioavailability;  $F_g$ : intestinal bioavailability;  $F_h$ : hepatic bioavailability;  $E_g$ : intestinal extraction;  $E_h$ : hepatic extraction ..... 93

**Figure 5-2.** Depletion curves at different concentration levels derived from hepatic microsomal incubations of  $\Delta^9$ -tetrahydrocannabinol (**A**) and cyclosporin A (**B**). The ratio between the drug concentration remaining at each time point (C) and the concentration of drug at the beginning of the incubation process ( $C_0$ ), is represented versus time. Values are expressed as means ( $n = 6$ )  $\pm$  SD. Note the difference in the time scales (X-axes) between the two figures..... 102

**Figure 5-3.** Depletion curves derived from intestinal microsomal incubations of 1  $\mu$ M  $\Delta^9$ -tetrahydrocannabinol (THC) and 1  $\mu$ M cyclosporin A (CsA). The ratio between the drug concentration remaining at each time point (C) and the concentration of drug at the beginning of the incubation process ( $C_0$ ), is represented versus time. Values are expressed as means ( $n = 6$ )  $\pm$  SD. .... 104

**Figure 5-4.** Most common metabolic pathways and metabolites of  $\Delta^9$ -tetrahydrocannabinol (THC) in humans, catalysed by CYP2C9 and CYP3A4 enzymes. Biotransformations are highlighted in colour red..... 106

**Figure 5-5.** Most common metabolic pathways and metabolites of cyclosporin A (CsA) in humans, catalysed by CYP3A4 enzyme. Biotransformations are highlighted in colour red. AA stands for amino acid..... 107

**Figure 6-1.** Fraction of absorbed dose of  $\Delta^9$ -tetrahydrocannabinol (THC) following the lipolysis of 3.2 mL of a lipidic (sesame oil) and lipid-free (propylene glycol/ethanol/water (80:10:10, v/v)) formulations (12 mg/mL) with different amounts of pancreatic lipase and albumin. Coral, blue, and green colours correspond to 1 g of pancreatic lipase ( $n = 6$ ), 0.2 g of pancreatic lipase ( $n = 3$ ), and 0.2 g of pancreatic lipase plus 0.8 g of bovine serum albumin ( $n = 3$ ), respectively. Values are expressed as means  $\pm$  SD. A one-way ANOVA followed by Tukey–Kramer multiple comparison test were used for statistical analysis. Statistically significantly different: \*\*,  $p < 0.01$ ; \*,  $p < 0.05$ ; ns, not significantly different. .... 120

**Figure 6-2.** Depletion curves derived from rat (**A**) hepatic ( $n = 8$ ) and (**B**) intestinal ( $n = 3$ ) microsomal incubations of 1  $\mu$ M  $\Delta^9$ -tetrahydrocannabinol (THC). The ratio between the drug concentration remaining at each time point (C) and the concentration of drug at the beginning of the incubation process ( $C_0$ ), is represented versus time. Values are expressed as mean  $\pm$  SD. Note the difference in the time scales (X-axes) between the two figures..... 121

**Figure 6-3.** Advanced compartmental absorption and transit (ACAT) model, by GastroPlus®..... 125

**Figure 6-4.** Simulated (blue line) and observed (red circles) plasma concentration–time profiles following single oral administration of (**A**) 20 mg and (**B**) 10 mg Marinol® to humans..... 127

**Figure 6-5.** Simulated (blue line) and observed (red circles) plasma concentration–time profiles following single oral administration of (**A**) 200 mg and (**B**) 300 mg Neoral® to humans. .... 127

**Figure A-1.** Observed mean  $\pm$  SD plasma concentration–time profiles following intravenous administration of THC, extracted from literature. (Figures **A** and **B**, and **D** adapted with permission from Ref. [277] and [289], Copyright© 1983 and 1980, respectively, American Society for Clinical Pharmacology and Therapeutics; Figure **C** from [288], Copyright© 1981, Plenum Publishing Corporation; Figures **E** and **F** from [290], Copyright© 1992, Oxford University Press; and Figure **G** from [291], Copyright© 2004, Wiley–Liss, Inc.)..... 135

**Figure A-2.** Observed mean  $\pm$  SD plasma concentration–time profiles following oral administration of Marinol®, extracted from literature. (Figure **A** adapted with permission from Ref. [237], Copyright© 2003, Lippincott Williams; and Figure **B** from [238], under the terms of the US Patent and Trademark Office, 2012)..... 136

**Figure A-3.** Observed mean  $\pm$  SD blood concentration–time profiles following intravenous administration of CsA, extracted from literature. (Figures **A** and **B** adapted with permission

from Ref. [292] and [138], Copyright© 1995 and 1992, respectively, American Society for Clinical Pharmacology and Therapeutics)..... 136

**Figure A-4.** Observed mean  $\pm$  SD plasma concentration–time profiles following oral administration of Neoral®, extracted from literature. (Figure **A** adapted with permissions from Ref. [241], Copyright© 2003, Elsevier B.V.; and Figure **B** from Ref. [240], under the terms of the US Patent and Trademark Office, 1999)..... 136

**Figure A-5.** Representative HPLC–UV chromatograms ( $\lambda = 220$  nm), spiked with the internal standard vitamin D<sub>3</sub> (VitD<sub>3</sub>), of micellar (**A**), sediment (**B**) and lipid (**C**) phases obtained after lipolysis and ultra-centrifugation of Marinol® ( $\Delta^9$ -tetrahydrocannabinol, THC, in sesame oil). ..... 139

**Figure A-6.** Representative HPLC–UV chromatograms ( $\lambda = 211$  nm), spiked with the internal standard cannabidiol (CBD), of micellar (**A**) and sediment (**B**) phases obtained after lipolysis and ultra-centrifugation of Neoral® (cyclosporin A, CsA, in a mixture of corn oil, ethanol, propylene glycol, and Kolliphor® RH 40). ..... 140

**Figure A-7.** Plot of peak area ratios of  $\Delta^9$ -tetrahydrocannabinol (THC) and internal standard (IS) versus sample concentration in (**A**) micellar (MP), (**B**) sediment (SP), and (**C**) lipid (LP) phases, obtained for the intra-day validation of the HPLC–UV detection method..... 140

**Figure A-8.** Plot of peak area ratios of cyclosporin A (CsA) and internal standard (IS) versus sample concentration in (**A**) micellar (MP) and (**B**) sediment (SP) phases, obtained for the intra-day validation of the HPLC–UV detection method. .... 141

**Figure A-9.** Residuals plotted against low, medium and high quality control concentration samples in (**A**) micellar (MP), (**B**) sediment (SP), and (**C**) lipid (LP) phases, obtained for the intra-day validation of the HPLC–UV detection method of  $\Delta^9$ -tetrahydrocannabinol (THC).  $x_{\text{calc}}$  is the regressed concentration computed from the non-weighted calibration curve, and  $x_{\text{nom}}$  is the nominal standard concentration. .... 141

**Figure A-10.** Residuals plotted against low, medium and high quality control concentration samples in (**A**) micellar (MP) and (**B**) sediment (SP) phases, obtained for the intra-day validation of the HPLC–UV detection method of cyclosporin A (CsA).  $x_{\text{calc}}$  is the regressed concentration computed from the non-weighted calibration curve, and  $x_{\text{nom}}$  is the nominal standard concentration. .... 142

**Figure A-11.** HPLC–MS/MS chromatograms of 2.5 ng/mL of  $\Delta^9$ -tetrahydrocannabinol (**A**) and 9.5 ng/mL cyclosporin A (**C**) in 0.1% (v/v) formic acid in acetonitrile. Representative chromatograms of the internal standards vitamin D<sub>3</sub> (**B**) and cannabidiol (**D**) are also included. .... 144

**Figure A-12.** MS/MS spectra of  $\Delta^9$ -tetrahydrocannabinol (**A**) and cyclosporin A (**B**) in 0.1% (v/v) formic acid in acetonitrile. .... 145

**Figure A-13.** Proposed mechanism for the fragmentation for  $\Delta^9$ -tetrahydrocannabinol (**A**), vitamin D<sub>3</sub> (**B**), cyclosporin A (**C**) and cannabidiol (**D**), in positive ionisation mode. Numbers indicate the  $m/z$  values for each fragment. .... 146

**Figure A-14.** Observed mean  $\pm$  SD plasma concentration–time profiles of  $\Delta^9$ -tetrahydrocannabinol (THC) following (**A**) intravenous (4 mg/kg,  $n = 5$ ) and (**B**) oral (12 mg/kg) administration to rats. Red colours represent the lipidic formulation (sesame oil,  $n = 6$ ), whereas green colours represent the lipid-free formulation (propylene glycol/ethanol/water (80:10:10, v/v),  $n = 5$ ). (Adapted with permission from Ref. [367], under the terms of CC BY, 2016) ..... 150

**Figure A-15.** Representative HPLC–UV chromatograms ( $\lambda = 220$  nm) of the liquid-crystalline phase obtained after lipolysis and ultra-centrifugation of 3.2 mL 12 mg/mL  $\Delta^9$ -

tetrahydrocannabinol (THC) in sesame oil, spiked with the internal standard vitamin D<sub>3</sub> (VitD<sub>3</sub>).  
..... 151

**Figure A-16.** Plot of peak area ratios of  $\Delta^9$ -tetrahydrocannabinol (THC) and internal standard (IS) versus sample concentration in the liquid-crystalline phase (CP), obtained for the intra-day validation of the HPLC-UV detection method. .... 152

**Figure A-17.** Residuals plotted against low, medium and high quality control concentration samples in the liquid-crystalline (CP) phase, obtained for the intra-day validation of the HPLC-UV detection method of  $\Delta^9$ -tetrahydrocannabinol (THC).  $x_{\text{calc}}$  is the regressed concentration computed from the non-weighted calibration curve, and  $x_{\text{nom}}$  is the nominal standard concentration. .... 152

## VIII. List of Tables

<b>Table 1-1.</b> The Lipid Formulation Classification System by Colin W. Pouton. ....	17
<b>Table 2-1.</b> Comparison of the composition of digestion media between the human jejunal fluids and several bio-relevant media. Values are expressed as means $\pm$ SD, or ranges (–). ..	35
<b>Table 2-2.</b> Sets of conditions assessed during the optimisation of the lipolysis model (n = 5). ....	40
<b>Table 3-1.</b> Volumes of titrant used, and calculated apparent and total extent of lipolysis (see <b>Equation 3-1</b> ), during the hydrolysis of different amounts of glyceryl triacetate representing values below and above its solubility limit. Conditions: 0.5 M NaOH, 1 mL/min maximum and 10 $\mu$ L/min minimum dosing rate. Values are expressed as mean $\pm$ SD. ....	58
<b>Table 3-2.</b> Hydrodynamic droplet size ( $d_H$ ) and specific surface area ( $S_S$ ) of the diluted ( $5 \cdot 10^{-2}\%$ v/v) triglyceride (TG) emulsions formed upon dispersion of equimolar amounts of oil in the digestion buffer after the equilibration period, prior to enzyme addition (mean $\pm$ SD, n $\geq$ 8). One way ANOVA followed by post hoc Tukey–Kramer test was used for statistical analysis. ....	59
<b>Table 4-1.</b> Physicochemical properties of $\Delta^9$ -tetrahydrocannabinol (THC) and cyclosporin A (CsA), and formulation details of Marinol® and Neoral®,.....	67
<b>Table 4-2.</b> Scaled amounts of lipidic formulation (Marinol® and Neoral®) dispersed in the <i>in vitro</i> lipolysis model (~40 mL) calculated from the quantities administered <i>in vivo</i> , according to <b>Equation 4-1</b> , assuming different <i>in vivo</i> dissolution volumes. ....	72
<b>Table 4-3.</b> Comparison of the two different lipolysis media used for the intraluminal processing of Marinol® and Neoral®. ....	73
<b>Table 4-4.</b> Bioavailability of selected formulations estimated from published clinical data. Absolute oral bioavailability values ( $F_{\text{observed}}$ ) were obtained following the administration of Marinol® [237, 238] and Neoral® [239–241]; hepatic bioavailability values ( $F_h$ ) were calculated from the intravenous administration of $\Delta^9$ -tetrahydrocannabinol (THC) [277, 288–291] and cyclosporin A (CsA) [138, 292], assuming strictly liver clearance. The fraction absorbed and non-metabolised in the gut ( $F_{\text{abs}} \cdot F_g$ ) were derived from $F_{\text{observed}}$ and $F_h$ . Values are expressed as weighted mean $\pm$ overall SD.....	78
<b>Table 4-5.</b> Distribution of recovered drug across micellar (MP), sediment (SP) and lipid (LP) phases after the lipolysis (in the “classical” buffer) of diverse doses of Marinol® and Neoral®, assuming two different <i>in vivo</i> dissolution volumes. Values are expressed as mean (n = 6) $\pm$ SD. ....	80
<b>Table 5-1.</b> Concentrations of microsomal incubations components at t = 0 minutes.....	95
<b>Table 5-2.</b> Absolute oral bioavailability values calculated from the data reported in published clinical studies ( $F_{\text{observed}}$ ), and calculated with the <i>in vitro</i> lipolysis/metabolism approach ( $F_{\text{predicted}}$ ), using two different digestion buffers. Values are expressed as weighted means $\pm$ overall SD ( $F_{\text{observed}}$ ) or as means $\pm$ SD ( $F_{\text{predicted}}$ ). ....	105
<b>Table 6-1.</b> Distribution of recovered drug across micellar (MP), sediment (SP), lipid (LP), and liquid-crystalline (CP) phases after the lipolysis of 3.2 mL of formulations containing $\Delta^9$ -tetrahydrocannabinol (12 mg/mL) with different amounts of pancreatic lipase and albumin. Data are presented as means $\pm$ SD.....	119



<b>Table 6-2.</b> Absolute oral bioavailability values calculated from the data reported in Ref. [367] ( $F_{\text{observed}}$ ), and calculated with the <i>in vitro</i> lipolysis/metabolism approach ( $F_{\text{predicted}}$ ). Values are expressed as means $\pm$ SD.....	123
<b>Table A-1.</b> Pharmacokinetic parameters reported in literature [237, 238, 277, 289–291] or calculated from the extracted plasma concentration–time profiles (in blue colours), after intravenous and oral (as Marinol®) administration of $\Delta^9$ -tetrahydrocannabinol. Values are expressed as means $\pm$ SD, unless otherwise stated. ....	137
<b>Table A-2.</b> Pharmacokinetic parameters reported in literature [138, 239–241, 292] or calculated from the extracted blood concentration–time profiles (in blue colours), after intravenous and oral (as Neoral®) administration of cyclosporin A. Values are expressed as means $\pm$ SD, unless otherwise stated.....	138
<b>Table A-3.</b> Sum of relative errors (RE) for various curve–weighting values and <i>F</i> values corresponding to data obtained during intra–day validation of the HPLC–UV detection method of $\Delta^9$ -tetrahydrocannabinol (THC) and cyclosporin A (CsA) in lipolysis phases. ....	142
<b>Table A-4.</b> Intra–day and inter–day accuracy and precision for the detection of $\Delta^9$ -tetrahydrocannabinol (Marinol®) and cyclosporin A (Neoral®) in lipolysis phases.....	143
<b>Table A-5.</b> Rate depletion constants ( $k_{\text{dep}}$ , $\text{min}^{-1}$ ) obtained following the incubation of $\Delta^9$ -tetrahydrocannabinol (THC), cyclosporin A (CsA), and control compounds at different initial substrate concentrations with hepatic microsomes. Values are expressed as means ( $n = 6$ ) $\pm$ SD. ....	147
<b>Table A-6.</b> Hepatic microsomal data for $\Delta^9$ -tetrahydrocannabinol, calculated assuming different fractions of drug unbound in the incubations ( $f_{\text{u,inc}}$ ). Values are expressed as means ( $n = 6$ ) $\pm$ SD.....	147
<b>Table A-7.</b> Hepatic microsomal data for cyclosporin A, calculated assuming different fractions of drug unbound in the incubations ( $f_{\text{u,inc}}$ ). Values are expressed as means ( $n = 6$ ) $\pm$ SD. ....	148
<b>Table A-8.</b> Intestinal microsomal data for $\Delta^9$ -tetrahydrocannabinol, calculated assuming different fractions of drug unbound in the incubations ( $f_{\text{u,inc}}$ ). Values are expressed as means ( $n = 6$ ) $\pm$ SD.....	148
<b>Table A-9.</b> Intestinal microsomal data for cyclosporin A, calculated assuming different fractions of drug unbound in the incubations ( $f_{\text{u,inc}}$ ). Values are expressed as means ( $n = 6$ ) $\pm$ SD. ....	148
<b>Table A-10.</b> Predicted oral bioavailability values of $\Delta^9$ -tetrahydrocannabinol in Marinol® using the <i>in vitro</i> lipolysis/metabolism approach. Values are expressed as means $\pm$ SD.....	149
<b>Table A-11.</b> Predicted oral bioavailability values of cyclosporin A in Neoral® using the <i>in vitro</i> lipolysis/metabolism approach. Values are expressed as means $\pm$ SD.....	149
<b>Table A-12.</b> Pharmacokinetic parameters (means $\pm$ SD) derived from the intravenous and oral administration of $\Delta^9$ -tetrahydrocannabinol to rats.....	150
<b>Table A-13.</b> Intra–day and inter–day accuracy and precision for the detection of $\Delta^9$ -tetrahydrocannabinol in the liquid–crystalline phase obtained after lipolysis and ultra–centrifugation of 3.2 mL of 12 mg/mL sesame oil. ....	151
<b>Table A-14.</b> <i>In silico</i> estimates and <i>in vitro</i> experimental values for $\Delta^9$ -tetrahydrocannabinol and cyclosporin A physicochemical and biopharmaceutical properties. ....	153
<b>Table A-15.</b> Pharmacokinetic output parameters obtained following the simulations of the oral profiles of Marinol® and Neoral® at different dose levels with GastroPlus®.....	154

## IX. List of Equations

$$F = \frac{AUC_{\text{oral}}/Dose_{\text{oral}}}{AUC_{\text{IV}}/Dose_{\text{IV}}} \quad \text{Equation 1-1}$$

$$\text{Activity (TBU)} = k_L \cdot \left( \frac{\text{mL 1 M NaOH}}{s} \right) \cdot \frac{60 s}{\text{min}} \cdot \frac{1000 \mu\text{mol NaOH}}{1 \text{ mL 1 M NaOH}} \cdot \frac{1 \mu\text{mol butyric acid}}{1 \mu\text{mol NaOH}} \quad \text{Equation 2-1}$$

$$\text{Extent of lipolysis (\%)} = \frac{V \cdot 0.5 \cdot MW}{3 \cdot \rho \cdot v} \cdot 100 \quad \text{Equation 3-1}$$

$$S_s = \frac{S_T}{V_T} = \frac{n \cdot S_i}{V_T} = \frac{V_T/V_i \cdot S_i}{V_T} = \frac{S_i}{V_T} = \frac{\pi \cdot d_H^2}{1/6 \cdot \pi \cdot d_H^3} = 6 \cdot \frac{1}{d_H} \quad \text{Equation 3-2}$$

$$\text{Formulation volume } in \text{ vitro} = \frac{40 \text{ mL} \cdot \text{Formulation volume } in \text{ vivo}}{250 \text{ or } 100 \text{ mL}} \quad \text{Equation 4-1}$$

$$RE(\%) = \frac{|\Delta x|}{x} = \frac{|x_{\text{calc}} - x_{\text{nom}}|}{x_{\text{nom}}} \cdot 100 \quad \text{Equation 4-2}$$

$$RSD(\%) = \frac{s_x}{\bar{x}} \cdot 100 \quad \text{Equation 4-3}$$

$$F_{\text{abs}} = C_{\text{MP}} \left( \frac{\text{mg}}{\text{mL}} \right) \cdot \frac{250 \text{ or } 100 \text{ mL}}{\text{Clinical dose (mg)}} \quad \text{Equation 4-4}$$

$$OSSE = \sum_{i=1}^n [(SD_i^2 + x_i^2) \cdot n_i] - N \cdot WX^2 \quad \text{Equation 4-5}$$

$$OSD = \sqrt{OSSE/N} \quad \text{Equation 4-6}$$

$$CV(\%) = 100 \cdot \sqrt{OSD/WX} \quad \text{Equation 4-7}$$

$$\frac{C_t}{C_0} = e^{-k_{\text{dep}} \cdot t} \quad \text{Equation 5-1}$$

$$k_{\text{dep}} = k_{\text{dep}([S] \rightarrow 0)} \cdot \left( 1 - \frac{[S]}{[S] + K_M} \right) \quad \text{Equation 5-2}$$

$$\frac{1}{k_{\text{dep}}} = \frac{1}{k_{\text{dep},[S] \rightarrow 0}} + \frac{1}{k_{\text{dep},[S] \rightarrow 0} \cdot K_M} \cdot [S] \quad \text{Equation 5-3}$$

$$fu_{100\%} = \frac{fu_{X\%}}{100 - (100 - X) \cdot fu_{X\%}} \quad \text{Equation 5-4}$$

$$CL_h = \frac{Q_h \cdot fu_b \cdot CL_{u_{h,int}}}{Q_h + fu_b \cdot CL_{u_{h,int}}} \quad \text{Equation 5-5}$$

$$F_h = \left(1 - \frac{CL_h}{Q_h}\right) \quad \text{Equation 5-6}$$

$$F_g = \frac{Q_{gut}}{Q_{gut} + fu_g \cdot CL_{ug,int}} \quad \text{Equation 5-7}$$

$$Q_{gut} = \frac{Q_{villi} \cdot CL_{perm}}{Q_{villi} + CL_{perm}} \quad \text{Equation 5-8}$$

$$F_{predicted}(\%) = F_{abs} \cdot F_g \cdot F_h \cdot 100 \quad \text{Equation 5-9}$$

$$C_{GI,pH} = C_{aq,pH} \cdot \left(1 + \frac{MW_{H_2O}}{\rho_{H_2O}} \cdot SR \cdot C_{bile}\right) \quad \text{Equation 6-1}$$

## **X. Thesis Format and Author's Statement**

---

This dissertation presents roughly the format of a thesis by publications. The author of this dissertation appears as the first author in such publications, since the vast majority of the information contained in them are a result of her own work.

Material from Chapter 1 has been published in the form of a book chapter printed by the Imperial College Press, in March 2016:

Benito-Gallo, P., Gershkovich, P., Marlow, M., Zann, V., & Wasan, K. M. (2016). Smart Lipid-Based Drug Delivery Systems. In V. P. Torchilin (Ed.), *Smart Pharmaceutical Nanocarriers* (pp. 309–371). Imperial College Press.

Information from Chapters 2 and 3 formed the basis of a publication in the European Journal of Pharmaceutics and Biopharmaceutics, in June 2015:

Benito-Gallo, P., Franceschetto, A., Wong, J. C. M., Marlow, M., Zann, V., Scholes, P., & Gershkovich, P. (2015). Chain length affects pancreatic lipase activity and the extent and pH–time profile of triglyceride lipolysis. *European Journal of Pharmaceutics and Biopharmaceutics*, 93(0), 353–362.

And finally, text included in Chapters 4 and 5 has been summarised in the form of a research paper submitted to the journal Molecular Pharmaceutics:

Benito-Gallo, P., Marlow, M., Zann, V., Scholes, P., & Gershkovich, P. (2016). Linking *In Vitro* Lipolysis and Microsomal Metabolism for the Quantitative Prediction of Oral Bioavailability of BCS II Drugs Administered in Lipidic Formulations. *Molecular Pharmaceutics*, 13 (10). 3526–3540.

# **Chapter I: Introduction**

## **I.1. Introduction**

The application of high-throughput screening techniques in non-aqueous media, and the development of combinatorial chemistry to generate large pharmacologically-active compound libraries, are considered to be responsible for the marked lipophilicity and low water solubility of the new chemical entities in development [1, 2]. The investigation of previously unexplored drug targets associated with lipidic architectures, intracellular signalling pathways, and highly lipophilic endogenous ligands, further boost the prerequisite of lipophilic drug candidates to gain access and interact with the target [3]. Moreover, the need for increased potency, together with the realisation that receptor binding is partially mediated by hydrophobic interactions, further amplifies the probability that drug candidates will have limited aqueous solubility. All these factors bias the recognition of poorly water-soluble drugs as hits during the early drug screening [4].

Despite efforts to develop drugs with favourable biopharmaceutical properties during lead optimisation phases, it was estimated that in 2005 around 40% of the top 200 marketed oral drugs were poorly water-soluble [5]. Subsequently in 2007, it was reported that up to 70% of the new active molecules in the development pipeline exhibited poor aqueous solubility [6]. Since low aqueous solubility can be associated with poor oral bioavailability, it is clear that one of the main challenges for pharmaceutical scientists is finding novel formulations capable of improving the intraluminal solubility of poorly water-soluble drugs.

## **I.2. Bioavailability of orally administered drugs**

Oral drug delivery is the most acceptable route of administration due to patient compliance and ease of administration. Besides, the manufacture of oral formulations is low cost, since they do not need to be produced under sterile conditions [7]. Analysis of the top 200

prescribed pharmaceutical agents in 2011 showed that in, the US, 87% were administered orally [8].

Solubility and permeability are thought to be the most important barriers to oral absorption. The Biopharmaceutics Classification System (BCS) was proposed by Amidon *et al.* with the aim of predicting the *in vivo* performance of drug products from *in vitro* measurements of permeability and solubility [9] (**Figure I-1**). A compound is considered highly soluble if the highest dose strength is soluble in less than 250 mL of over a pH range of 1 to 7.5 at 37 °C. Whilst, a drug substance is regarded as highly permeable when the extent of absorption in humans is greater than 90% of the administered dose, in comparison to an intravenous reference dose [10].

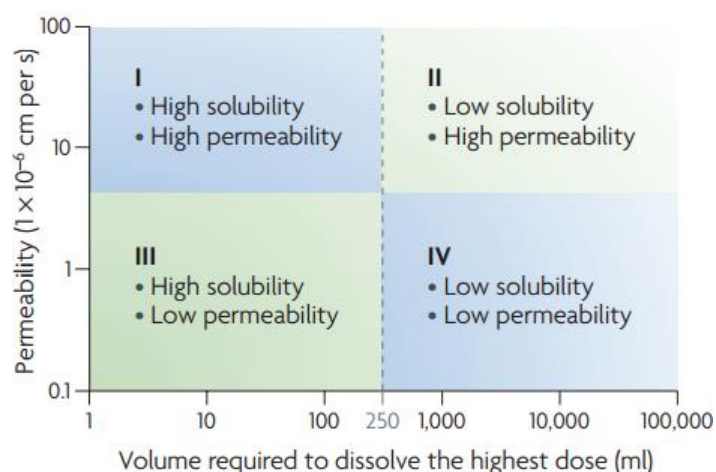


**Figure I-1.** Biopharmaceutical Classification System. (Reprinted with permission from Ref. [11], Copyright© 2008, Nature Publishing Group)

Formulation strategies cannot do much to increase the poor membrane permeability of class III and IV drugs, with the best solution to improve the oral bioavailability of these drugs being at the chemical level, i.e. to go back to the lead optimisation phase of drug discovery and select a candidate with more suitable physicochemical properties [12]. On the other hand, the aqueous solubility of class II drugs can be increased through formulation approaches, so as to achieve a biopharmaceutical behaviour similar to class I drugs. These formulation strategies (further described in sections 1.3 and 1.4) are either solid dosage forms designed to increase dissolution rate, or liquid dosage forms incorporating the compound already in solution [13].

It is generally acknowledged that although there are some difficulties in differentiating solubility classes, the major uncertainty relates to the permeability assignment. Thus, Wu and Benet [14, 15] proposed a revision of the BCS, the Biopharmaceutics Drug Disposition Classification System (BDDCS), where the extent of permeability criterion is replaced with extent of metabolism ( $\geq 70\%$  of the oral dose). BDDCS class I compounds would then be designated as highly soluble and extensively metabolised; BDDCS class II drugs as poorly soluble and extensively metabolised; BDDCS class III drugs as highly soluble and poorly metabolised; and BDDCS class IV compounds as poorly soluble and poorly metabolised. Benet and colleagues believed it will be easier and less ambiguous to determine the assignment of BDDCS classes based on the extent of metabolism than using permeability (i.e., extent of absorption) in BCS assignments. The usefulness of these new system and its implementation by regulatory agencies is yet to be seen. On the contrary, the BCS has been widely applied for a long time, and has been adopted by several regulatory agencies, such as the World Health Organisation, the US Food and Drug Administration, and the European Medicines Agency [16].

However, the BCS only focus on the drug absorption processes, e.g. drug movement from the lumen into the enterocytes, as it is a formulation tool. At this point, it is important to distinguish fraction absorbed from systemic bioavailability, which is often limited by first-pass biotransformations. In general, before reaching the systemic circulation and exerting its pharmacological action, drugs that are orally absorbed must first escape metabolism in the gut lumen and in the liver (**Figure I-2**). Once in the enterocyte, a drug molecule can either be effluxed back into the lumen by transporter proteins, undergo intestinal metabolism, or be transported to the portal vein (or mesenteric lymph). The fraction of drug in the portal vein is then transferred to the liver, where it can undergo hepatic extraction, which includes metabolism and/or excretion into the bile. The combination of the extraction that a drug suffers in the intestine and in the liver is known as first-pass or pre-systemic metabolism. Consequently, apart from limited solubility in the intestinal lumen restricting absorption, the other main barriers to a BCS class II drug having sufficient bioavailability are gastrointestinal metabolism and hepatic extraction/metabolism processes [9]. Alterations in any of the factors that determine the oral bioavailability will affect systemic drug concentrations, and therefore will determine the drug's efficacy and adverse effects [17].

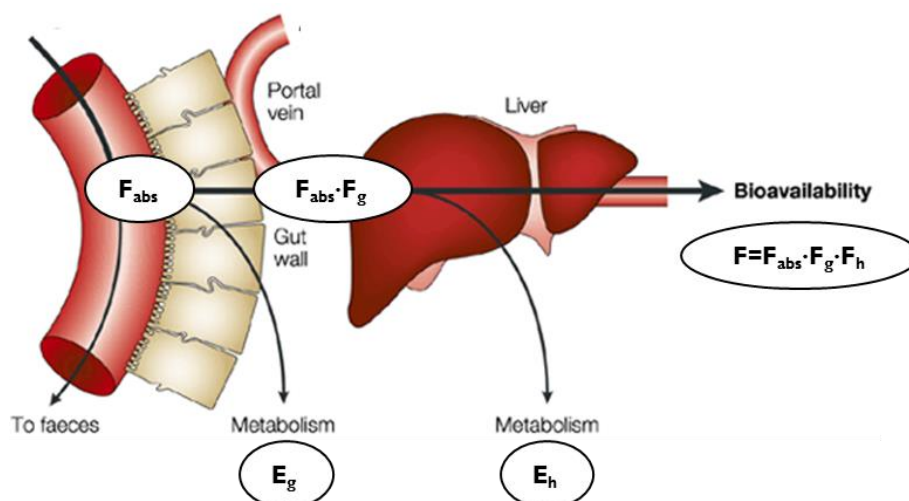


**Figure I-2.** Schematic representation of the barriers a drug must overcome to reach systemic circulation and the site of action.  $F_{abs}$ : Fraction absorbed;  $F$ : absolute bioavailability;  $F_g$ : intestinal bioavailability;  $F_h$ : hepatic bioavailability;  $E_g$ : intestinal extraction;  $E_h$ : hepatic extraction. (Adapted with permission from Ref.[18], Copyright© 2003, Nature Publishing Group)

### I.3. Oral drug delivery strategies for poorly water-soluble drugs

As indicated above, the rate-limiting factor in the absorption of poorly water-soluble drugs is intraluminal solubilisation. Therefore, increasing the dissolution rate could potentially enhance absorption. The following section summarises briefly the most common principles (excluding lipidic formulations, which are discussed in section I.4) that have been applied to improve oral absorption of hydrophobic drugs in recent years.

#### I.3.1. Salt formation

Salt formation is the most common and successful method of increasing dissolution rate and solubility of drugs with ionisable functional groups. Salts of weakly acidic and weakly basic drugs have, in general, higher solubilities than their corresponding acidic or basic forms [19]. The risk of precipitation out into the free acidic or basic forms upon pH changes in gastrointestinal fluids, represents the main challenge to formulation scientists when using this approach [20].



### **1.3.2. Polymorphic and amorphous forms**

Generally, the lowest energy crystalline polymorph is chosen for development. However, when the most thermodynamically stable polymorph of a drug has limited solubility and thus cannot achieve the systemic exposure required for efficacious therapy, an amorphous form or a metastable polymorph can be developed to provide medical benefit [21]. The reason for the improvement with these forms, is that the rate of dissolution of a high energy polymorph or amorphous form can be many times faster than that of the equivalent low energy material [4]. However, isolation of thermodynamically unstable polymorphs or amorphous forms is challenging since, over time, they can recrystallize reverting back to the thermodynamically stable form. This transformation can occur in solid state during storage or very quickly in solution [22, 23].

### **1.3.3. Solid dispersions**

The term solid dispersions refers to formulations containing drug dispersed in an inert carrier matrix. They are categorised in different classes, based on the molecular arrangement within the carrier: (a) crystalline solid dispersions, where the drug is partially dissolved and the excess is suspended in the crystalline form; (b) amorphous solid dispersions, where the drug is partially dissolved and the excess is suspended in the amorphous state; and (c) solid solutions, where the drug is completely dissolved, this is molecularly dispersed [24]. The dissolution rate of a poorly water-soluble drug in a solid dispersion is increased *via* several mechanisms, including but not limited to increasing the surface area as a result of a reduction in drug particle size up to the molecular level and the impediment of aggregation and enhancing solubility by formation of a supersaturated solution and stabilisation of the drug in more soluble metastable polymorphic or amorphous form [25]. There are few marketed solid dispersion products. This is a reflection of the difficulties in their use, in particular the thermodynamic instability of the drug in the non-crystalline state [4].

### **1.3.4. Cyclodextrin complexation**

Cyclodextrins are macrocyclic oligosaccharides produced by enzymatic conversion of starch. Their molecular structure consists of a hydrophilic outer surface and a non-polar inner cavity.

Hydrophobic drug molecules are capable of interacting with cyclodextrins through non-covalent bonds and form inclusion complexes [26]. The higher solubility of these complexes, compared to the solubility of the drug alone, can increase apparent solubility by several orders of magnitude [27]. Besides, compounds labile to chemical or enzymatic degradation can be effectively protected if incorporated into cyclodextrins. However, the nature of the drug-cyclodextrin interactions dictates that solubilisation within cyclodextrins is molecularly specific, thus only molecules that “fit” in the inner cavity can be incorporated in these macrocyclic structures [28].

#### **I.3.5. Particle size reduction**

The dissolution rate of a drug is a function of its intrinsic solubility and its particle size. When the particle size is reduced, the larger surface area available for solvation allows an increase in the rate of dissolution [29, 30]. Micronisation using dry-impact processes has been used for many years to obtain particles commonly between 2 and 5  $\mu\text{m}$  [31]. Despite micronisation leading to an enhancement of the drug dissolution rate, it does not change the saturation solubility. The development of wet-milling technologies together with the more extended utilisation of surfactant and polymeric stabilisers, led to the production of particles in the nanometre range (200–500 nm) [32]. Nanoparticles present a dramatic enlargement of the surface area to mass ratio. In addition, drug nanoparticles are capable of increasing the saturation solubility, since the size-dependency of this property only plays a role when particles are smaller than 1  $\mu\text{m}$  [33]. However, the formulation of drug nanoparticles is not trivial. Nanoparticles are very cohesive and tend to aggregate, therefore stabilisation of drug powders is needed. Furthermore, the high shear forces required to reduce particles to nano-size ranges, might induce changes in the crystal lattice, and introduce undesired amorphous behaviour [4].

### **I.4. Lipidic formulations**

Lipidic and surfactant excipients are commonly used to formulate drugs already in solution [13, 34]. These formulation platforms are known as lipid-based drug delivery systems, lipid-based

formulations, or simply lipidic formulations (LFs). The following sub-sections will review the development, characterisation and utilisation of oral LFs.

#### **I.4.1. Rationale behind the use of lipidic formulations**

Lipids are a group of naturally occurring hydrophobic and amphipathic small molecules, that include fatty acids, mono-, di- and triglycerides, phospholipids, waxes, eicosanoids, sphingolipids, sterols, terpenes, prenols and fat-soluble vitamins. Their main biological functions are to store energy, form structural components of cell membranes, and act as signalling molecules. In addition, lipids play an important role in enhancing the desirability and palatability of many food products [35, 36].

Both lipids and hydrophobic drugs are characterised by low water solubility and relatively high lipophilicity. However, whereas the oral absorption of poorly water-soluble drugs is low and erratic, dietary lipids are typically well absorbed (around 95%), even at “doses” as high as those characteristic of the Western diet (100 g or more, which constitutes 40% of the total energy intake). The efficiency of lipid absorption reflects the existence of a specialised lipid-digesting pathway that avoids the problems of low intraluminal solubility and lead to efficient solubilisation of dietary lipids within the gastrointestinal tract [37–39].

For many years now, it has been realised that the intake of food, notably lipids, can have positive effects on the absorption and bioavailability of drugs [40]. However, the variability of food ingestion patterns and food components as a function of health condition, time of the day, age, or cultural environment, makes clinical prescription of drugs co-administered with food very difficult [4]. The co-administration of poorly water-soluble drugs with formulated lipids reduces the variability associated with the food effect, and provides the advantages of the endogenous lipid processing pathway to support drug solubilisation and absorption.

#### **I.4.2. Digestion and absorption of lipids in the gastrointestinal tract**

The digestion process of triglycerides – the major components of dietary lipids – starts almost immediately after food ingestion. In the mouth, food is broken down and mixed with saliva by chewing, whereby the surface area is increased and a food bolus is formed. This bolus is swallowed and transferred from the oesophagus to the stomach, where enzymatic hydrolysis

of triglycerides begins. Around 10% to 30% of the total triglycerides may be digested in the stomach by the action of gastric and lingual lipases, secreted by the chief cells in the gastric mucosa and the serous glands on the tongue, respectively [38, 39]. Both enzymes hydrolyse triglycerides preferentially at the *sn*-3 position resulting in the formation of diglycerides and fatty acids [37, 41, 42]. The action of lingual and gastric lipases together with the mechanical mixing by peristaltic and segmental contractions, promotes the formation of coarse lipid emulsions that increase the surface area, and facilitates subsequent intestinal lipolysis. Digestion and absorption of lipids occurs mostly at the upper part of the gastrointestinal tract [43]. When chyme enters the duodenum, cholecystokinin secretion from epithelial cells is triggered by the presence of fatty acids, which in turn stimulates the release of pancreatic juice and bile into the duodenum, from the pancreas and gall bladder, respectively. Furthermore, it has been demonstrated that the presence of lipid emulsion in the distal part of the small intestine activates the so called “ileal brake”, which leads to a delay in gastric time and small intestine motility, and therefore increases the time available for digestion and absorption [44].

Pancreatic juice contains digestive enzymes, including pancreatic lipase, pancreatic co-lipase, and phospholipase A<sub>2</sub> [45]. Water (~84%), bile salts (~11.5%, mainly sodium glycolate and sodium taurocholate), phospholipids (~3%, essentially phosphatidylcholine), and cholesterol (~0.5%) are the major solutes of bile [40]. Additionally, bile contains bicarbonate that, together with the alkaline mucus secreted by the Brunner’s glands in the duodenum, neutralises the acidic chyme providing an optimum pH for the action of pancreatic lipase. Bile components are natural surfactants that decrease the lipid–water interfacial tension facilitating the formation of smaller oil droplets and stabilising the oil–in–water emulsion. This emulsification is important as pancreatic lipase can only act at the oil–water interface of lipid droplets [40]. Nonetheless, high concentrations of bile salts may have an inhibitory effect and restrict the access of pancreatic lipase to emulsion interfaces [46]. The action of the co-factor pancreatic co-lipase is crucial, since it binds to the interface of lipid droplets acting as an anchor site for pancreatic lipase, which otherwise would be desorbed by bile salts. In addition, recent studies of the X-ray crystal structure of the lipase/co-lipase complex suggest that another function for co-lipase is maintaining the active conformation of pancreatic lipase by stabilising the lid domain in the open conformation, thereby facilitating lipolysis [47, 48].

Pancreatic lipase hydrolyses triglycerides at the *sn*-1 and *sn*-3 positions generating one 2-monoglyceride and two fatty acids per triglyceride. It has been reported that 2-monoglycerides can slowly isomerise to 1/3-monoglycerides and be subsequently lipolysed releasing a third fatty acid and glycerol, as depicted in **Figure I-3** [49–52].

In addition to triacylglycerol lipases, there are other important lipolytic enzymes that act within the gastrointestinal tract. Phospholipase A<sub>2</sub> hydrolyses phospholipids at the *sn*-2 position releasing lysophospholipids and fatty acids, whereas carboxylester hydrolase breaks down cholesteryl ester to yield cholesterol. Lysophospholipids, cholesterol and bile salts arrange themselves into mixed micelles [71]. Mixed micelles incorporate the products of lipid digestion and serve as vehicles to the apical brush border membrane of the enterocytes.

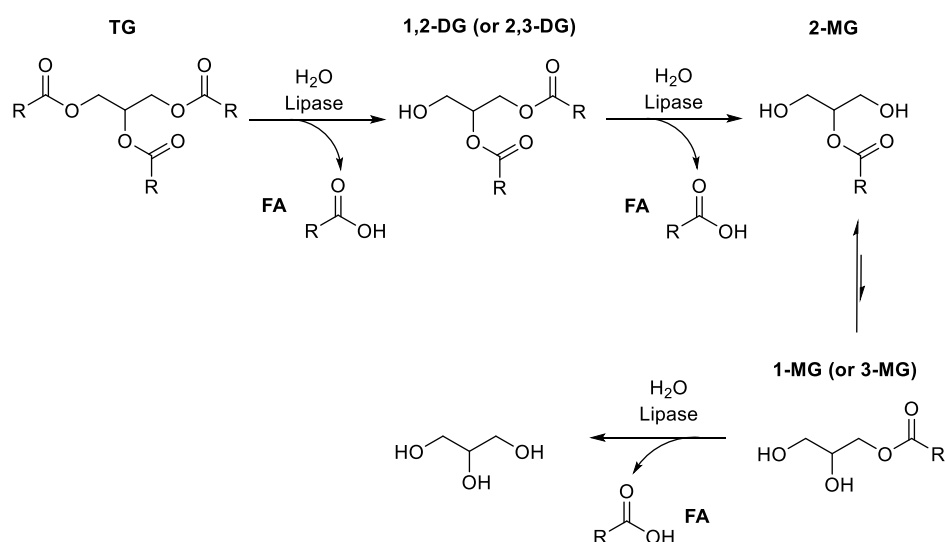


**Figure I-3.** Lipolysis of a triglyceride (TG) by pancreatic lipase. Pancreatic lipase shows the same selectivity towards the hydrolysis at positions *sn*-1 and *sn*-3 of the triglyceride when the fatty acid (FA) side chains are identical. DG: diglyceride; MG: monoglyceride. (Modified from Ref. [53], under the terms of the Creative Commons Attribution License, CC BY, 2016)

The unstirred water layer represents the next barrier for lipid absorption, as it is situated on the apical side of the enterocytes. It consists of a complex aqueous glycoprotein network, characterised by a lower pH compared with the bulk adjacent intestinal fluid, with which it is poorly mixed. Inclusion of lipolytic products into mixed micelles, which are characterised by high surface area–mass ratios, is necessary to maintain solubilisation and to generate structures that are small enough to quickly diffuse across the unstirred water layer [39, 54]. The exact

mechanism by which lipolysis products are absorbed into the enterocytes remains unknown (**Figure I-4**). Mixed micelles are not thought to be absorbed intact. It is assumed that due to the lower pH area within the unstirred water layer, micelles are destabilised so fatty acids, and 2-monoglycerides can cross the apical membrane alone [55]. It has been proposed lipolytic products can be absorbed by passive diffusion [56] or by carrier-mediated transport [57]. It is believed that the former dominates at high lipid concentrations, whereas the latter is more common at low fatty acid and 2-monoglyceride levels. Alternatively, lipolytic products can be directly transferred through collision of mixed micelles against the brush border; or colloidal vehicles may undergo vesicular-mediated uptake and this may be initiated by binding to a transport protein on the apical membrane. In addition to influx transporters, several transport proteins have been identified (e.g. P-glycoprotein) that efflux lipidic compounds back into the intestinal lumen [58].

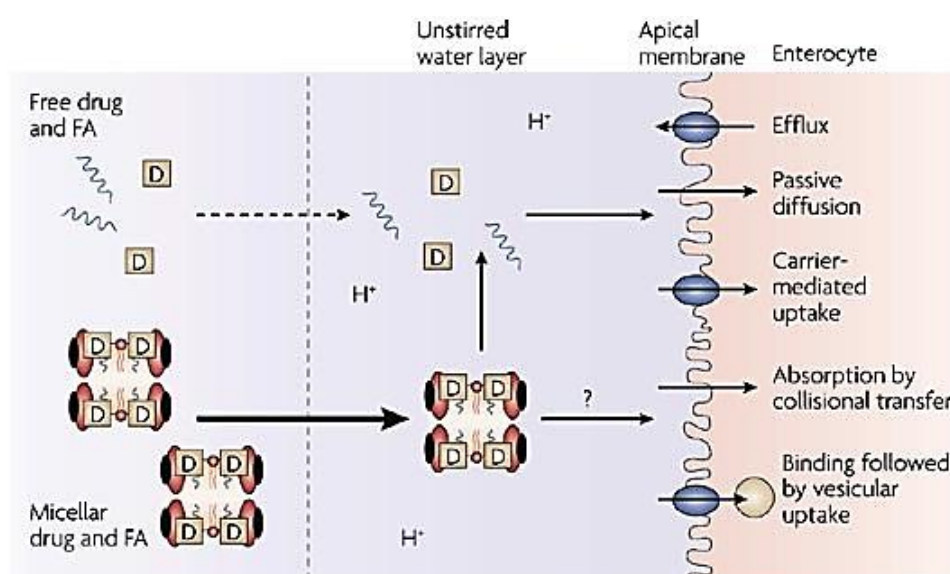


**Figure I-4.** The unstirred water layer and mechanism of lipid absorption. FA: fatty acid. (Reprinted with permission from Ref. [58], Copyright© 2007, Nature Publishing Group)

Once in the enterocyte, digestion products derived from short- and medium-chain triglyceride diffuse across the cytosol, enter the underlying lamina propria, and get access to the portal vein. By contrast, the lipolysis products resulting from the lipolysis of long-chain triglycerides (which are more lipophilic than their shorter counterparts) travel to the endoplasmic reticulum, and are re-esterified and incorporated into lipoproteins. Analogously, absorbed lysophospholipids can be re-esterified to phospholipids, and cholesterol can be esterified to form cholesterol

esters by the enzyme acyl-CoA cholesterol acyltransferase. Re-synthesised triglycerides, phospholipids, free cholesterol and cholesterol esters are then assembled into lipoproteins. Chylomicrons are the largest major type of lipoproteins (ranging from 75 to 1200 nm), and consist of a hydrophobic core of triglycerides and a polar outer surface of apolipoproteins and phospholipids [59–61]. After formation, chylomicrons are transported to the Golgi apparatus, exocytosed from the enterocyte into the intercellular space, where they are unable to enter the systemic circulation due to their large size and are taken up into the lymphatic system instead [58, 62].

#### **1.4.3. Mechanisms of bioavailability enhancement by lipidic formulations**

Dietary and formulation lipids, together with lipidic excipients, can affect the bioavailability of co-administered poorly water-soluble drugs *via* several mechanisms, which can be broadly grouped into those that promote solubilisation in the intestinal lumen, those that facilitate permeability into the enterocytes, and those that reduce pre-systemic metabolism [4].

##### **1.4.3.1. Mechanisms that enhance solubilisation**

LFs deliver the drug to the gastrointestinal tract in solution, avoiding the need for wetting and dissolution associated to solid dosage forms. Upon contact with the gastrointestinal fluids, LFs form emulsions in which the drug remains solubilised. Simple solutions of drug in oils are unlikely to suffer drug precipitation since they are dispersed in the gastrointestinal fluids. LFs that include large quantities of water-soluble co-solvents and surfactants, facilitate the formation of emulsions of particles with sizes in the nano-size range, and therefore increase the surface area available for lipolysis. However, these sophisticated LFs could increase the risk of drug precipitation since the solubilising capacity of hydrophilic co-solvents and surfactants might be lost upon dilution in the intestinal milieu. In general, highly lipophilic drugs would accumulate in any remaining undigested oil, whereas less lipophilic drugs would more easily travel from the processed LFs into solubilising colloidal species, such as mixed micelles.

LFs further influence solubilisation by stimulating the secretion of endogenous solubilising agents (cholesterol, phospholipids, and bile salts), and by supplying additional exogenous solubilising components (formulation-derived lipids, surfactants and co-solvents), in the intestinal lumen.

The arrangement of lipolytic products with biliary-derived components leads to swollen mixed micelles, characterised by high solubilisation capacities for poorly water-soluble drugs, and capable of promoting mass transfer across the unstirred water layer [63–65].

Furthermore, LFs are capable of triggering the “ileal brake”, leading to an increase in the time available for digestion and absorption [44]

#### I.4.3.2. Mechanisms that facilitate permeability

LFs may promote absorption across the apical membrane of the enterocytes by enhancing passive membrane diffusion, and by inhibiting drug efflux transporters.

Digestion products derived from short- and medium-chain triglycerides are known to induce paracellular transport through tight junction permeability changes [66, 67]. Whilst, surfactants in LFs have been reported to enhance transcellular diffusion by increasing the membrane fluidity of enterocytes [68, 69].

Recently, numerous publications have focused on studying the ability of LFs to facilitate drug permeation through direct and indirect inhibition effects on efflux transporters. Proposed mechanisms for transporter inhibition include direct interaction with the transporter [70], changes to transporter expression [71], and indirect destabilisation of the protein by changing the fluidity of the membrane lipidic domain [72].

#### I.4.3.3. Mechanisms that reduce pre-systemic metabolism: Stimulation of the lymphatic transport

Lipidic excipients may have an impact on first-pass metabolism either indirectly by interaction with efflux transporters, or directly by stimulation of the lymphatic system.

The “drug efflux–metabolism alliance” is a model that links the activity of metabolic enzymes and efflux transporters in the gut wall, and proposes that efflux increases the time available for enterocyte-based metabolism [73, 74]. Accordingly, the inhibition of efflux proteins by lipidic components might be expected to decrease pre-systemic extraction in the gastrointestinal tract, by reducing the time available for metabolism.

As previously mentioned in section I.4.2, after enterocyte uptake, some digestion products (specifically, fatty acids and 2-monoglycerides derived from long-chain triglycerides) are re–



esterified and incorporated into chylomicrons (**Figure I-5**). After formation, chylomicrons are expelled from the intracellular space, and enter the lymphatic capillaries near the small intestine (lacteals). Taking into account the differences in flow between blood and lymph (500:1, v/v), and that only 1% of lymph is made of chylomicrons, a drug requires a partition coefficient of at least 50,000 ( $\log D_{7.4} > 5$ ) in favour of lymph rather than blood to be transported *via* the lymphatic pathway [58]. Another requirement specified by Charman and Stella [59] is that drug solubility in triglycerides needs to be higher than 50 mg/mL for solubilisation within the chylomicron core. However, it has been shown that these two physicochemical properties are not sufficient alone to quantitatively predict association with chylomicrons [75], which seems to be a critical step in estimating the degree of intestinal lymphatic transport of lipophilic molecules [61]. Gershkovich *et al.* [61] suggested that the combination of  $\log D_{7.4}$ , degree of ionization, polar surface area, number of hydrogen acceptors and donors, density, molar volume and freely rotatable bonds describes the process of uptake of drugs by chylomicrons more accurately than any single physicochemical property.

Intestinal lymphatic transport provides two clear advantages over portal blood transport. First, the mesenteric lymph drains directly into the systemic circulation<sup>i</sup> bypassing the liver. Therefore, drugs that are transported through the lymph experience an increase in systemic exposure as a result of a reduction in first-pass metabolism [76]. For poorly water-soluble drugs suffering from very high first-pass metabolism, lymphatic transport accounts for the delivery of most of the bioavailable drug to the systemic circulation, even when the overall extent of lymphatic transport is very low (e.g. testosterone) [4]. The second advantage is the possibility of effectively targeting the lymphatic system with drugs transported in chylomicrons. Lymphatic targeting can be potentially beneficial in the treatment of autoimmune diseases [58], HIV [77], and metastatic processes [78].

LFs are capable of stimulating lipoprotein formation and therefore intestinal lymphatic lipid flux [58]. Examples of compounds formulated in long-chain lipids, in which lymphatic transport has been shown to improve oral bioavailability in animal models, include lipophilic cannabinoids in

---

<sup>i</sup> The thoracic lymph duct drains into the systemic circulation at the left subclavian vein.

peanut oil [79], halofantrine in soybean oil and glycerol monolinoleate [80], and dichlorodiphenyltrichloroethane in oleic acid [81].

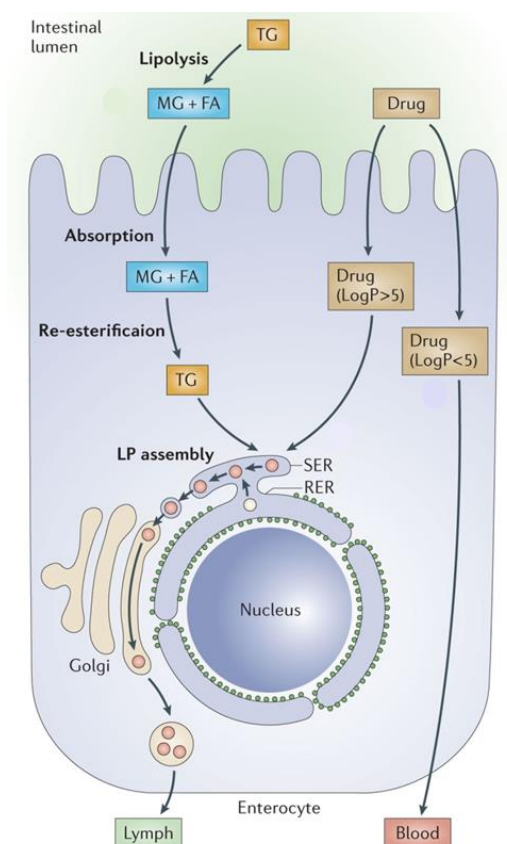


**Figure I-5.** Access to the lymphatic system by lipids and lipophilic drugs within the enterocyte. TG: Triglyceride; MG: monoglyceride; FA: fatty acid; LP: lipoprotein. (Adapted with permission from Ref. [82], Copyright© 2015, Nature Publishing Group)

#### I.4.4. Lipidic excipients: The Lipid Formulation Classification System

Oral LFs may be liquid, semi-solid, or solid at room temperature, and comprise a wide range of formulations, spanning from solutions, to emulsions, liposomes, and lipid nanoparticles. Liquid LFs are convenient for patient populations with swallowing difficulties (children and the elderly), and useful in pre-clinical studies, since they are relatively fast to formulate, and may be administered by oral gavage at a range of doses to animals [83]. Nonetheless, soft or hard gelatine capsules containing LFs in the liquid state, are commonly preferred for clinical applications. Lately, solid and semi-solid LFs, although more time- and money-consuming to develop, are gaining popularity, as they diminish the possibility of leakage and incompatibilities on storage [84].

Because LFs include such a diverse group of formulations with different properties, some classification systems have been proposed over time. Pouton [12, 85] proposed the Lipid Formulations Classification System (LFCS) to aid comparison of published data from other laboratories (**Table I-I**). In time, the LFCS has become the most common system for categorising LFs into four classes, depending on their composition, and the effect of digestion and dilution on their ability to prevent drug precipitation [13].

Type I LFs consist of drug solubilised in triglycerides, and/or mixed di- and monoglycerides. Commonly used excipients are vegetable oils, Labrafac™, and Capmul®. Type I LFs show the advantage of being simple, biocompatible (excipients are classified as GRAS<sup>ii</sup> by regulatory agencies), easy to fill in capsules, and resistant to precipitation on capsule rupture in the stomach. However, Type I LFs require digestion (except for monoglycerides) in order to generate more amphiphilic lipolytic products, and subsequently promote drug partitioning into the aqueous micellar phase. Moreover, due to their high lipophilicity, the solvent capacity is limited to drugs with high logPs (above 4).

The addition to Type I LFs of a lipid-soluble surfactant with a hydrophilic-lipophilic balance (HLB) lower than 12, transforms them into Type II LFs. Examples of lipophilic surfactants include fatty acid esters of propylene glycol (lauroglycol, capryol), and fatty acid esters of sorbitan (Spans®). The inclusion of a surfactant (20–60% w/w) creates an isotropic mixture that promotes emulsification, and may improve solvent capacity. Upon contact with water and with energy input, Type II LFs emulsify to give lipidic particle sizes that range from 200 nm to 1 µm. These formulations minimise the risk of drug precipitation upon dilution in the gastrointestinal fluids, as they are comprised of hydrophobic compounds, and the importance of digestion is not as critical as in Type I LFs. However, the limited number of approved lipophilic surfactants have limited the number of Type II systems, and there does not seem to currently be any marketed product using this type of formulation.

Type III LFs are comprised of a drug dissolved in a mixture of lipids and water-soluble surfactants (HLB > 12). These LFs may or may not contain co-solvents (0–40% w/w) such as ethanol, propylene glycol, or polyethylene glycol. Typical examples of hydrophilic surfactants

---

<sup>ii</sup> GRAS: Generally Recognised as Safe

are polyethylene glycol esters of fatty acids (Labrasol®, Gelucire®), castor oil ethoxylates (Kolliphor®), sorbitan ester ethoxylates (Tween®), and tocopheryl polyethylene glycol succinate. In contrast to Type II systems, Type III LFs are self-emulsifying drug delivery systems, since they are able to spontaneously form very fine and thermodynamically stable dispersions (particle size < 250 nm), upon contact with gastrointestinal fluids. Type III systems are further divided in two categories, based on the proportions of hydrophilic components and the particle size of the generated emulsions. Accordingly, Type IIIA LFs are characterised by a lower amount of surfactants and co-solvents (20–60% w/w) and bigger lipid droplets (100–250 nm), compared to Type IIIB systems (> 80% w/w non lipidic excipients, 50–100 nm particle size). Type III LFs offer enhanced solubilisation capacity, and reduce the importance of lipolysis, since drug absorption is possible even without excipient digestion. Nonetheless, the chance of precipitation upon dilution is increased, as they contain higher amounts of hydrophilic components.

Type IV LFs are lipid-free mixtures of surfactants (water- and/or lipid-soluble) and co-solvents. Because lipids are not incorporated, Type IV systems are characterised by the highest solvent capacity. They allow the solubilisation of drugs that are hydrophobic but not lipophilic, permit higher drug loading, and are barely influenced by digestion. However, Type IV systems are the most susceptible category to drug precipitation upon dispersion, as the majority of their components are water-miscible. In addition, when drugs are administered chronically, high content of surfactants may cause local irritation in the gastrointestinal mucosa [86].

The LFCS is a useful and practical attempt to classify the large variety of lipidic systems, but it shows some limitations. As such, numerous LFs in the market or reported in research articles do not strictly fit in any of the categories defined by Pouton and co-workers.

**Table I-I.** The Lipid Formulation Classification System by Colin W. Pouton.

		Type I	Type II	Type III		Type IV
				Type IIIA	Type IIIB	
Content of formulation (% w/w)	TG or mixed MG and DG	100	40-80	40-80	< 20	-
	Water-insoluble surfactants (HLB < 12)	-	20-60	-	-	0-20
	Water-soluble surfactants (HLB > 12)	-	-	20-40	20-50	30-80
	Co-solvents	-	-	0-40	20-50	0-50
Characteristics		Non-dispersing; requires digestion	SEDDS without water-soluble components	SEDDS/ SMEDDS with water-soluble components	SMEDDS with water-soluble components and low oil content	Oil-free formulation based on surfactants and co-solvents
Advantages		GRAS status; simple; excellent capsule compatibility	Unlikely to lose solvent capacity on dispersion	Clear or almost clear dispersion; drug absorption without digestion	Clear dispersion; drug absorption without digestion	Good solvent capacity for many drugs; disperses to micellar solution
Disadvantages		Poor solvent capacity unless drug is highly lipophilic	Turbid o/w dispersion (particle size 0.25–2 µm)	Possible loss of solvent capacity on dispersion; less easily digested	Likely loss of solvent capacity on dispersion	Loss of solvent capacity on dispersion; may not be digestible

MG, DG, TG: mono-, di-, tri-glyceride; HLB: hydrophilic-lipophilic balance; S(M)EDDS: self (micro) emulsifying drug delivery system; GRAS: generally recognised as safe; o/w: oil in water. (Adapted with permission from Ref. [12], Copyright© 2006, Elsevier B.V.)

## I.5. Assessment of oral drug delivery systems

*In vitro* tests for reliable prediction of the solubilisation behaviour of a drug under bio-relevant conditions are essential at early stages of formulation development. Unfortunately, *in vitro* tests often fail the *in vitro*–*in vivo* correlations (IVIVCs) for BCS class II drugs mainly due to poorly reproduced physiological conditions such as composition, volume, and static environment of classical dissolution tests, that also do not account for intestinal permeability and/or metabolism [87].

### I.5.1. Bio-relevant media

Prediction of the fate of a drug in the gastrointestinal tract generally requires adequate simulation of the conditions in the stomach and the proximal part of the small intestine [88]. The United States Pharmacopeia (USP) proposed the Simulated Intestinal Fluid (SIF) [89] consisting of phosphate buffer pH 7.5 and large amounts of pancreatin. SIF was later modified to pH 6.8 to better represent the pH environment of the proximal small intestine [90]. Dressman and co-workers [91, 92] introduced the Fasted State Simulated Intestinal Fluid (FaSSIF), which contained bile salts and lecithin. Recently, it was upgraded to FaSSIF–V2 [88], where the buffer was modified to maleic acid (to comply with physiological osmolality and pH), and the concentration of phospholipid was decreased, to better reflect the *in vivo* situation, and increase the stability over time. Alternatively, buffers based on bicarbonate species which incorporate a sophisticated double purging system of carbon dioxide and helium to establish and maintain the required pH, have been proposed as better surrogates for small intestinal fluid [93, 94]. Numerous media reflecting the contents of the small intestine in the post-prandial state have been developed. In general, all these Fed State Simulated Intestinal Fluids (FeSSIFs) contain higher amounts of bile salts and phospholipids, and include monoolein and oleic acid to simulate lipid loading [95]. Despite the hard work dedicated towards the development of bio-relevant media to better mimic *in vivo* drug dissolution/solubilisation, there are still a limited number of studies showing successful IVIVCs in humans [96].

### **1.5.2. *In vitro* testing of oral dosage forms**

Disintegration testing is conducted to determine whether tablets or capsules disintegrate within the prescribed time when placed in a liquid medium at 37 °C [97]. The majority of LFs are oral solutions, or liquids loaded into soft or hard gelatine capsules that take up to 3 and 6 minutes, respectively, to disintegrate in the stomach [98]. Accordingly, disintegration tests do not seem to be useful for LFs assessment.

After ingestion, LFs are presented to the gastrointestinal fluids in solution, and subsequently disperse. Dispersion tests are performed to discriminate formulations that disperse slowly compared to those that disperse rapidly, and thus lead to drug precipitation [4]. This test is particularly important for Types III and IV LFs which may lose solvent capacity upon contact with water, as a result of their water-miscible components migrating to the bulk water phase. Since the properties of LFs change dramatically by dilution and digestion, the assessment of drug solubilisation in bio-relevant media is critical. The most commonly used and wide-spread dissolution tests are the USP apparatus. The basket (type I) and the paddle (type II) apparatus allow dissolution testing in a single medium, at a defined pH. The reciprocating cylinder (type III) apparatus allows better hydrodynamics and enables flexibility in the composition of the medium. In the USP IV apparatus, the formulation is placed in a cell, where a medium passes through at a pre-defined rate.

Most dissolution tests are performed using USP apparatus because they are quite simplistic [99]. However, these tests can often reflect poorly the *in vivo* situation, and thus additional models that reproduce drug transfer were introduced to improve predictability. In these more sophisticated biopharmaceutical transfer tests, the formulation is initially dispersed in a gastric compartment and then is transferred to an intestinal compartment [100], and it could even be subjected to an absorption step [101]. Despite these tests being more bio-relevant than the USP apparatuses, they are still missing a key factor for LFs performance: the digestion step. For this reason, the *in vitro* lipolysis model was developed.

## I.6. *In vitro* lipolysis model

*In vitro* lipolysis model is capable of mimicking the lipid digestion process, and is consequently a suitable method to trace the solubilisation state of drugs delivered by means of LFs. Although biochemists have been performing lipolysis experiments for many years, the implementation of this technique by pharmaceutical scientists has been slow. Reymond and colleagues [102] published in 1988 the first *in vitro* lipolysis study in which the solubilisation of cyclosporin in olive oil was assessed. Numerous studies have been reported since then [49, 103–109], and although experimental conditions and parameters vary among them, the concept and fundamental principles remain the same.

The general protocol for *in vitro* lipolysis is based on the dispersion of the tested LF in the experimental medium consisting of FaSSIF. The addition of the digestive enzyme (pancreatic lipase/co-lipase) to the medium initiates the lipolysis process which is allowed to proceed until the triglycerides breakdown is completed (or deliberately stopped by the addition of an enzyme inhibitor). As a consequence of the triglycerides being hydrolysed, fatty acids are released, inducing a drop in pH. In order to keep pH at a constant value throughout the experiment (to mimic *in vivo* conditions), a pH-stat titrator is used. The instrument continuously measures and controls this transient drop in pH by equimolar titration with a basic solution.

After completion of the lipolysis process, the digestion medium is commonly subjected to density-gradient separation. Ultra-centrifugation of the lipolysis mixture usually affords three distinct layers (**Figure I-6**): (i) an upper lipid phase, containing undigested tri- and diglycerides; (ii) a middle aqueous-micellar phase, containing colloidal structures (mixed micelles formed by bile salts, lysophospholipids, fatty acids and monoglycerides) within which poorly water-soluble drugs are solubilised, and (iii) a lower sediment phase, comprising fatty acids' calcium soaps. Drug concentration in the micellar phase is of particular interest, as the working hypothesis of the researcher groups working with the model, is that only drug solubilised in the micellar layer is available for absorption. On the other hand, drug contained in the lipid and pellet phases is expected to have delayed or no absorption.



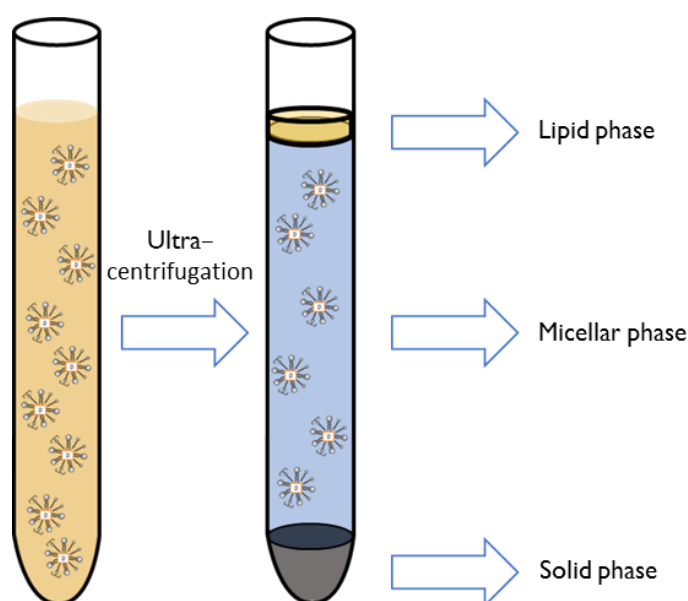


**Figure I-6.** Schematic representation of the phases commonly present after the ultra-centrifugation of the lipolysis medium.

### I.6.1. Bio-relevant medium of the *in vitro* lipolysis model

The main difference between *in vitro* lipolysis simulated medium and real intestinal contents is the buffer system. The principal physiological buffer ion present in the gastrointestinal tract is bicarbonate ( $\text{HCO}_3^-$ ), which is secreted by cells from the stomach, duodenum and pancreas [110]. Instead, simulated fluids use maleate buffer which is not produced naturally in the human gastrointestinal tract. There are two main reasons for using a different buffer system for *in vitro* lipolysis experiments. Firstly, bicarbonate buffer is unstable over time and experimentally difficult to handle, since it constantly seeks equilibrium with atmospheric  $\text{CO}_2$  resulting in pH changes, unless continuously sparged with  $\text{CO}_2$  and titrated with NaOH [111]. And secondly, the high buffer capacity of bicarbonate in the fasted state (reported average values range from 2.4 to 5.6 mM/ $\Delta\text{pH}$  [112–114]) would not allow the monitoring of lipolysis by direct titration as the ionisation of fatty acids would not provoke a drop in pH, as with the maleate buffer systems. Nevertheless, *in vitro* lipolysis models try to mimic the bicarbonate physiological buffer capacity by setting a tight pH control band (usually target  $\text{pH} \pm 0.05$ ).

The choice of pH depends partially on which region of the intestine is represented in the model. Therefore, while some groups focus on the duodenum (pH 6.5), others decide to mimic the jejunum (pH 6.8), where the absorption of the majority of nutrients takes place [115]. However, the election of pH value has been often a compromise between physiological

conditions, the optimum activity profile of pancreatic lipase (pH 6.5–8) [116], and the apparent pKa of the released fatty acids that are being monitored (e.g. pH for oleic acid ionisation is 9.85 [117]).

Bile salts in the human body are a complex mixture of steroid acids conjugated to taurine or glycine. By contrast, simulated media are rather simplistic and are usually formed by a single bile salt, with sodium taurocholate and sodium taurodeoxycholate being the most common ones. Although the use of these purified bile acids might be less representative of the *in vivo* situation, it facilitates the design and interpretation of lipolysis experimentation.

Lecithin consists of a mixture of phospholipids (phosphatidylcholine, phosphatidylethanolamine, etc.) and other traces of lipids such as triglycerides, and fatty acids. Lecithin derived from egg yolk is the most common source of phospholipids, although the current general trend is shifting towards higher purity sources such as soy-purified phosphatidylcholine.

Almost all research groups utilise porcine pancreatin powder as lipase source because of its availability and the common enzymatic features porcine and human pancreatic lipase share [118]. Besides, porcine pancreatin is also a good source of co-lipase and other relevant intestinal enzymes such as phospholipase A<sub>2</sub> and cholesterol esterase.

The inclusion of liberated fatty acids within mixed micelles is thought to be, *in vivo*, the most important mechanism of solubilisation and removal of fatty acids from the oil–water interface. However, *in vitro*, the precipitation of fatty acids in the form of calcium soaps is believed to be the main way of removing them from oil droplets surface. Therefore, the presence of calcium cations (Ca<sup>2+</sup>) is essential to avoid the inhibition of the enzyme and allow the lipolysis to proceed. The difference in Ca<sup>2+</sup> addition might be the most critical discrepancy between the research group at the University of Copenhagen (where Ca<sup>2+</sup> is added continuously during the experiment) and the rest of research institutions (where Ca<sup>2+</sup> is added as a bolus at the beginning of the experiment). Zangenberg *et al.* [103] developed the *in vitro* “dynamic” lipolysis model, where Ca<sup>2+</sup> is pumped into the digestion medium at a certain rate, and thus the rate of lipolysis can be artificially controlled. Both approaches can lead to a change in micellar composition and consequently to an altered dissolution capacity. Whether one technique is better than the other it is still a topic for discussion.

As previously mentioned, gastric lipase is partially responsible for the lipolysis process, and approximately 17.5% of ingested triglycerides are broken down in the stomach [119]. The majority of *in vitro* lipolysis studies have focused on the intestinal digestion, thus events occurring in the stomach that might be relevant for predictability purposes are potentially overlooked. The main barrier to the establishment of a gastric step has been the fact that gastric lipase is not commercially available, which limits the use to a few laboratories. Recombinant dog gastric lipase and the microbial lipase *Candida Antarctica* lipase A, which have comparable activity to human gastric lipase, have been used as a surrogate for the human enzyme in some published studies [120–122].

There have been very few attempts to establish *in vitro* lipolysis in the fed state [121]. The reasons for this may include the difficulty in developing an appropriate digestion media, and the impossibility of ranking LFs based on their performance, as their solubilisation enhancement capacity gets masked by the food effect (i.e. all formulations perform equally well).

#### **1.6.2. Predictability power of the *in vitro* lipolysis model: IVIVCs**

The development of IVIVCs is key in all drug development programs, as this is the basis for understanding how product performance *in vitro* is likely to relate to performance *in vivo*. Traditionally, an IVIVC is defined as a mathematical relationship between *in vitro* dissolution and some aspect of *in vivo* exposure, such as the area under the plasma concentration–time curve (AUC) or the maximum concentration ( $C_{\max}$ ). However, in literature and in practice, the term IVIVC is used to link some aspect of the *in vitro* formulation behaviour to the measured clinical performance of dosage forms [87].

Even though experimental conditions are still under evaluation, lipolysis testing has already demonstrated suitability with respect to predictability of the *in vivo* situation. Several publications have shown rank–order correlations between *in vitro* lipolysis solubilisation data and exposure data in animals [104, 123–127]. This was achieved by correlating the percentage of drug solubilised in the micellar phase with the AUC or the  $C_{\max}$  obtained after oral administration of the tested LF to animals (rats, mini–pigs or dogs). As an example, Dahan and Hoffman [105, 108] reported a linear relationship between *in vitro* data and bioavailability data for progesterone and griseofulvin when administered to rats in short–, medium–, and long–

chain triglycerides. However, when these experiments were applied to the study of Vitamin D<sub>3</sub> and dexamethasone, no linear IVIVC was obtained.

## I.7. First-pass metabolism

The liver is usually assumed to be the major site of metabolism because of its size and high content of metabolic enzymes. However, there are other potential metabolism sites, such as the lungs, the kidneys, the blood, and specifically, the intestinal mucosal cells in the small intestine [128–132]. Systemic bioavailability (F), defined as the ratio of AUCs, after oral and intravenous (IV) drug administration (normalised by the dose), is often used as a measure of the extent of first-pass metabolism (**Equation I-1**).

$$F = \frac{AUC_{\text{oral}} / \text{Dose}_{\text{oral}}}{AUC_{\text{IV}} / \text{Dose}_{\text{IV}}} \quad \text{Equation I-1}$$

Overall, metabolic processes will increase the polarity of a drug and transform it into a more-water soluble substance to enable excretion in body fluids (urine or bile). Phase I metabolism may involve reduction, hydrolysis, cyclisation, or de-cyclisation; but the most common reaction that occurs is oxidation. The vast majority of these oxidative reactions are catalysed by cytochrome 450 monooxygenases (CYPs), which are located at the endoplasmic reticulum and mitochondria within the cell. When the products of these reactions (metabolites) are polar enough, they may be readily excreted. When that is not the case, metabolites undergo subsequent phase II reactions. Phase II metabolism consists of the attachment (conjugation) of an ionised group to the electrophilic or nucleophilic group of the metabolite to form a highly water-soluble compound with increased molecular weight, to facilitate excretion. Phase II biotransformation include methylation, acetylation, glucurodination, sulphation, glutathione conjugation and glycine conjugation. These reactions are catalysed by transferases, mainly located in the cytosol of cells [133].

### **1.7.1. The small intestine, the enterocytes and enzyme gut activity**

Although the small intestine is commonly regarded as an absorptive organ, it is also considered the most important extra-hepatic site of drug biotransformation, due to its large surface area, significant metabolic content and low blood out-flow [132, 134, 135]. Interestingly, several clinical studies have shown the substantial contribution of the gut to overall first-pass metabolism of verapamil [136], midazolam [137] and cyclosporine A [138, 139], among other drugs. Furthermore, it has been suggested that for some substances the extent of intestinal metabolism is quantitatively greater than that of hepatic metabolism [140, 141].

The dominant cell type in the small intestinal epithelium (90% of total epithelial cells) is the enterocyte [142]. Enterocytes are responsible for the majority of the absorption of nutrients and drugs, and contain both influx and efflux transporters together with metabolic enzymes. The main absorption mechanism for lipophilic xenobiotics is the transcellular route (across the cell), while small hydrophilic molecules are able to diffuse across the tight junctions in between the cells (paracellular route) [143]. The route by which a drug is absorbed is of particular importance, since compounds using the paracellular pathway will not be metabolised by the intestinal enzymes [135]. Usually, drugs cross the enterocyte membrane by passive diffusion, driven by a concentration gradient. However, active mechanisms such as carrier-mediated transport may co-exist as well, and can either facilitate (influx transporters) or slow (efflux transporters) the drug uptake process [144]. The main efflux transporters expressed at the apical membrane are P-glycoprotein (P-gp), breast cancer resistance protein, and multidrug resistance protein (MRP) [15]. P-gp shares with CYP3A the same extremely broad substrate specificity, and together they form the “drug efflux-metabolism alliance”, acting as a coordinated absorption barrier against xenobiotics [134]. Drugs that are dual substrates of CYP3A and P-glycoprotein (e.g. cyclosporin A) show very limited bioavailability, as efflux transporters re-circulate the drug, giving the enzymes numerous opportunities to metabolise it [73, 74].

Enterocytes contain both phase I (CYPs) [135] and phase II (glucosyltransferase, UGT; glutathione S-transferase, GST; etc.) [145, 146] enzymes. Intestinal enzyme expression demonstrates a large intra- and inter-individual variability, with specific content and activity declining sharply from the proximal region to the distal ileum. The most abundant P450

subfamily expressed in the small intestine is CYP3A4, which accounts for around 82% of the total CYP content, followed by CYP2C9 (~14%), CYP2C19 (~2%), CYP2J2 (~1.4%), and CYP2D6 (~0.7%) [135, 147]. It has been estimated that the total amount of CYP3A in the human small intestine represents around 1% of the hepatic levels. Nonetheless, when intestinal and hepatic activities are corrected for the enzyme mean population relative abundance, the metabolic activities of gut and liver are comparable [148, 149].

### **1.7.2. The liver, the hepatocytes, and enzyme hepatic activity**

The liver is the largest solid organ and the most important site for drug biotransformation in humans. Besides, it is responsible for other important functions, such as bile production, plasma protein synthesis, hormone production, or regulation of glycogen storage, among others.

Hepatocytes are the main cell type in the liver (make up around 70-85% of liver's mass), and are responsible for the vast majority of metabolism occurring in the liver. They are characterised by abundant cellular organelles associated with metabolic (e.g. endoplasmic reticulum) and secretory (e.g. Golgi apparatus) functions. Furthermore, the membrane of hepatocytes is constituted with microvilli, enabling increased exchange of substances with the perfusing blood [150]. Hepatocytes are well equipped at both the apical (canalicular) and basolateral (sinusoidal) membranes, with active transporters for efficient uptake of drugs and excretion into bile [151]. Unbound compounds in sinusoidal blood are taken up into hepatocytes by transporter-mediated mechanisms or by diffusion across the basolateral membrane [152]. Drugs that are excreted into the bile reach the duodenum and can be either eliminated with faeces, or be re-absorbed (enterohepatic circulation) [153].

Hepatocytes contain a great number of metabolic enzymes, which can be found either freely moving in the cytosol, or included in organelles, such as the endoplasmic reticulum. As in the small intestine, the liver includes CYP enzymes in abundance, as well as phase II enzymes (UGTs, GSTs, sulfotransferases...). The large inter-individual variation observed in human drug clearance for some drugs administered orally, can be partially explained by the substantial inter-individual fluctuation in the expression levels of the different enzymes [17]. CYP3A is the most abundant P450 subfamily expressed in the liver, representing around 40% of total CYP

content, followed by CYP2C (~25%), CYP1A2 (~18%), CYP2E1 (~9%), CYP2A6 (~6%), and CYP2D6 (~2%) [135].

### 1.7.3. Estimation of first-pass metabolism

It is believed that the main reasons for clinical failure of new chemical entities are lack of efficacy, toxicity and unfavourable pharmacokinetic properties [154]. Hence, the development and application of reliable methods to predict human drug disposition may reduce the number of drug candidates that fail due to unacceptable pharmacokinetic characteristics, and decrease the cost and time loss related to selection failure [155]. Clearance is one of the most important pharmacokinetic parameters because it relates directly to drug elimination and bioavailability [156]. Both empirical and physiologically-based approaches have been developed to predict drug clearance in humans that involve the use of preclinical animal data and/or *in vitro* human data [157]. Early determination of pharmacokinetic properties in humans during Phase 0 trials are also useful to guide further drug development.

#### 1.7.3.1. Direct and indirect methods in humans

Direct measurements of the fraction of drug dose that escapes hepatic ( $F_h$ ) and intestinal ( $F_g$ ) elimination, are rarely performed in humans due to ethical reasons [158]. In the case of hepatic elimination, it would require the catheterisation of the brachial artery and hepatic vein after intravenous drug administration [159]. Regarding intestinal elimination, sampling of the portal vein after oral drug intake would be necessary. Nevertheless, an exception to ethical concerns are the studies in anhepatic patients during liver transplant operations, or surgical patients whose portal blood circulation bypasses the liver [139].

Indirect assessment of  $F_g$  and  $F_h$  can be done after preclinical studies, during Phase 0 trials, when sub-therapeutic doses of a new drug are given to a small cohort of patients to determine pharmacodynamic and pharmacokinetic properties. Total clearance (CL) can be derived from the AUC following intravenous dosing. Because CL is an additive property, hepatic clearance ( $CL_h$ ) can then be derived from CL if other contributing factors are known (i.e. renal clearance) or are very limited, and thus negligible. Following the same assumption,  $F_g$  can be estimated

when the absolute oral bioavailability is known, and the orally administered dose is expected to be completely absorbed ( $F_{abs} \sim 1$ ).

Alternatively, for CYP3A substrates only,  $F_g$  can be estimated from interaction studies with grapefruit juice [160]. In this model it is assumed that grapefruit completely inhibits CYP3A-mediated metabolism, and that it shows no effect on the fraction absorbed or on hepatic enzymes.  $F_g$  is estimated by comparing the AUC values after drug oral administration with and without grapefruit juice.

#### 1.7.3.2. *In vivo* methods: Allometric scaling

The best described technique to predict human pharmacokinetics from *in vivo* animal preclinical data is allometric scaling. Pharmacokinetic parameters are a function of anatomical and physiological processes, they can potentially be scaled allometrically across species to extrapolate pharmacokinetic data from animals to humans. Allometric scaling is based on a power function of the form  $y = a \cdot B^x$ , where  $y$  is the parameter of interest (e.g. clearance, volume of distribution...),  $B$  is the body weight, and  $a$  and  $x$  are the allometric coefficient and exponent, respectively [156]. The major drawback in allometric scaling is its empirical nature, although efforts have been made to provide a valid theoretical explanation for commonly accepted scaling exponents [161].

#### 1.7.3.3. *In vitro* methods

Scientific limitations in the *in vivo* methods, the possibility of reducing the use of animals, and the increasing availability of animal and human liver samples, led to the development of *in vitro* to *in vivo* physiologically-based direct scaling approaches [162]. Clearance values can be determined by several approaches, including incubations with recombinant enzymes, subcellular fractions, whole cell systems, and tissue slices [163].

##### 1.7.3.3.1. Recombinant enzymes

One way to understand a complex process like metabolism is to isolate the smallest unit possible, this is, the enzyme responsible for a given metabolic pathway. Recombinantly expressed enzymes provide important information on whether the drug candidate is



metabolized by single or multiple isoforms, and whether highly polymorphic enzymes are the major contributors to its metabolic clearance [164].

#### *1.7.3.3.2. Cell systems*

Freshly isolated hepatocytes and enterocytes present the advantage of being close to the "original" state of the liver and gut [165], but they cannot be pre-characterised, and human cell lines are rarely available. Furthermore, enterocyte harvests are likely to be contaminated with other intestinal cell types, which leads to low activity and difficult interpretation of experimental design. The use of cryopreserved hepatocytes circumvents the problems of availability and are usually well characterised by the manufacturer. Whilst cryopreserved enterocytes, if any, are commercially scarce.

#### *1.7.3.3.3. Tissue slices*

Precision-cut tissue closely resembles the organ from which it is prepared, with all cell types present in their original matrix configuration [166]. Usage of tissue slices allows for maintenance of the functional architecture of the organ and displays metabolism activity from hours to days [167]. However, their use is narrowed to a few laboratories due to limited tissue availability and technical issues, such as difficulties in distributing substrates evenly [168], or the exhibited lag time in Phase II metabolic reactions [169].

#### *1.7.3.3.4. Subcellular fractions*

Subcellular fractions, which include S9, cytosol, and microsomes, continue to be the most widely used *in vitro* system for drug metabolism investigations. During the process of isolation of these fractions (**Figure 1-7**), the co-factors that mediate metabolism are lost. Therefore, the addition of expensive co-factors is necessary for enzyme activation. Nonetheless, it shows the advantage that by excluding or including certain co-factors, it is possible to trigger a specific metabolic pathway for a given compound [164].

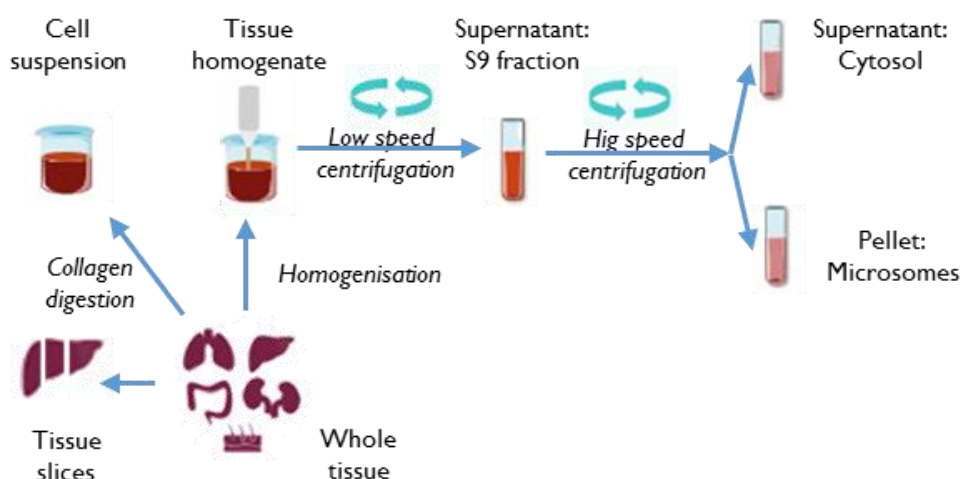


**Figure I-7.** Preparation method of subcellular fractions. S9 is the supernatant fraction obtained from a tissue homogenate by low speed centrifugation ( $\sim 9000$  g). Whilst, the pellet contains unbroken cells, nuclei, and mitochondria. After high speed centrifugation ( $\sim 100,000$  g) of the S9 fraction, pieces of the endoplasmic reticulum sediment out as a pellet (microsomes), and soluble components remain as a supernatant (cytosol).

The S9 fraction contains both cytosolic (transferases) and microsomal components (CYPs), thus it represents almost the complete collection of all Phase I and Phase II metabolic enzymes. However, scale-up factors to predict *in vivo* intrinsic clearance from S9 incubations are rarely covered in the literature [164]. Cytosol is the simplest metabolic system, and only contains soluble drug-metabolising enzymes. Microsomes contain CYPs and UGTs, which are responsible for the bio-transformation of approximately 90% of marketed drugs. However, because they lack cytosolic enzymes, the estimated intrinsic clearance values tend to be underpredicted [168, 170]. Despite limitations, microsomes are the most commonly used *in vitro* approach. This is a reflection of their capacity for long-term storage and high throughput application, commercial availability, ease of use, and thorough characterisation of optimal incubation conditions, enzymology and kinetics [171–175].

#### 1.7.3.3.5. Determination of human clearance

The strategy that allows extrapolation of the *in vitro* clearance to the *in vivo* situation is depicted in **Figure I-8** [176]. The first step consists of determining *in vitro* intrinsic clearance ( $CL_{int}$ ), a pure measurement of enzyme activity that is not influenced by other physiological parameters such as organ blood flow or drug binding to blood matrix. *In vitro*  $CL_{int}$  values should be normalised for cell, microsomal protein or enzyme concentration, and corrected for the

fraction unbound in the incubation ( $CL_{u,int}$ ). The second step involves the determination of *in vivo* hepatic or gut intrinsic clearance ( $CL_{u,h,int}$  or  $CL_{u,g,int}$ ) by extrapolating the activity measured *in vitro* to the whole organ (liver or small intestine) by applying physiologically-based scaling factors. The final stage of the strategy requires the use of a liver/small intestine model that incorporates the effects of blood cell partitioning, organ blood flow, and plasma protein binding to transform  $CL_{u,h,int}$  and  $CL_{u,g,int}$  into hepatic ( $CL_h$ ) and intestinal ( $CL_g$ ) clearances, respectively.

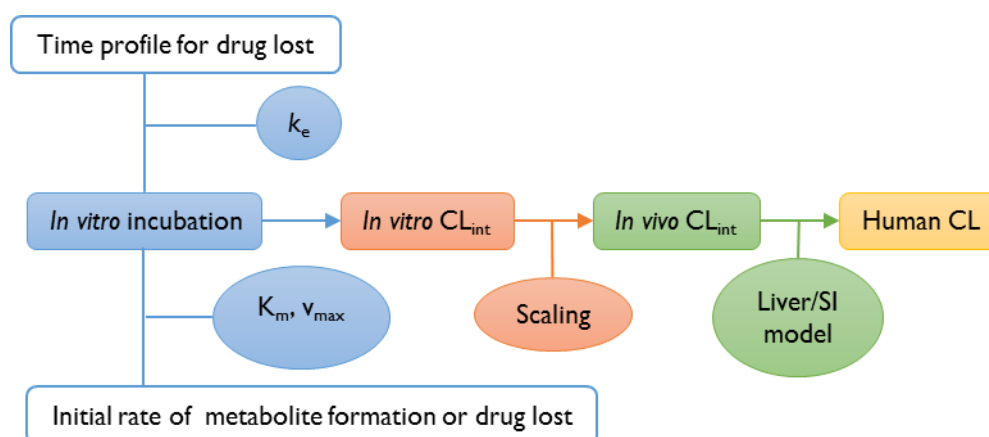


**Figure I-8.** Three-stage strategy for extrapolation of *in vitro* clearance to *in vivo* hepatic metabolic clearance. CL: human clearance (hepatic or intestinal);  $CL_{int}$ : intrinsic clearance;  $k_e$ : drug elimination constant;  $K_m$ : Michaelis–Menten constant; SI: small intestine;  $v_{max}$ : maximum rate of metabolism.

There are several mathematical human hepatic models in the literature, such as the well-stirred and the parallel tube models, which are the simplest and most commonly used. However, the distributed and dispersion models are also well known. In general, differences among the models reside in different assumptions made in terms of anatomical structure and the extent of blood mixing within the liver [151]. In terms of liver anatomy, the well-stirred model views the liver as single compartment, whereas the parallel tube model sees it as a group of identical tubes positioned in parallel. Regarding blood flow, the well-stirred model assumes complete mixing, whereas the parallel tube model considers a bulk flow of blood passing through the tubes. Drug concentration in the well-stirred model is constant and equal to that of emergent venous blood. Whilst, the parallel tube produces a drug concentration gradient from the portal vein to the hepatic vein region. Common assumptions of both models are the following: only unbound drug is subject to elimination, linear kinetics, and no membrane transport barrier [177]. The difference in estimated elimination values of the same drug between the models is

not significant when  $CL_h$  is low ( $F_h > 0.7$ ). However, when  $CL_h$  is high ( $F_h < 0.3$ ), the well-stirred model seems to provide better  $CL_h$  estimates than the parallel tube model, which tends to overestimate them [151, 178].

Scientists first applied the well-stirred liver model to predict intestinal bioavailability ( $F_g$ ). However, this model does not have real physiological meaning since drug molecules are delivered to the metabolic enzymes in the gut lumen, and not by the gut blood flow. Tucker and co-workers [179, 180] developed the “Q-gut” model, which retains the shape of the well-stirred model, but includes a flow term ( $Q_{gut}$ ) which is a hybrid parameter reflecting the volume of the enterocytes, drug absorption rate from the intestinal lumen, and removal of drug from the enterocytes by the enterocytic blood supply.

## **I.8. Research proposal and Objectives**

LFs are mainly used for the delivery of BCS II drugs. The main barriers to the oral bioavailability of these drugs are intestinal micellar solubilisation and first-pass metabolism (rather than membrane permeability). The intraluminal solubility of BCS II drugs in LFs can be estimated using the *in vitro* lipolysis model, and the first-pass extraction ratio can be assessed by performing microsomal stability assays.

The majority of the approaches developed to predict human oral bioavailability typically focus on the behaviour of drugs in the individual processes of absorption, distribution, metabolism, and excretion. However, the body is a complex biological system, and thus the characterisation of a drug's pharmacokinetics would be best described by including these processes in one holistic model [181].

Based on this, the current work proposes, for the first time, the combination of *in vitro* lipolysis and microsomal metabolism studies for the prediction of human oral bioavailability of BCS II drugs administered in LFs.

The overall goal of the present thesis was to further develop and improve the *in vitro* lipolysis model to better characterise lipidic formulations, and thus allow prediction of *in vivo* exposure

in humans. In order to achieve this goal, the objectives of the present PhD thesis were as follows:

- ✓ Simplify and unify the *in vitro* assessment of LFs by proposing a unique and optimised set of working conditions that covers a wide range of LFs (Chapter 2).
- ✓ Gain a better understanding of the lipolysis mechanism by assessing pancreatic lipase activity towards lipidic excipients prone to enzyme digestion (Chapter 3).
- ✓ Select model lipidic formulations and associated clinical data, and perform pharmacokinetic analyses to obtain the oral bioavailability observed in human subjects (Chapter 4).
- ✓ Estimate the fraction of drug dose that is absorbed in those studies by performing *vitro* lipolysis experiments (Chapter 4).
- ✓ Estimate the fraction of drug dose that escapes intestinal and hepatic first-pass metabolism in those studies by performing microsomal metabolism assays (Chapter 5).
- ✓ Propose estimated oral bioavailability values for those studies by combining *in vitro* lipolysis and metabolism data, and check the predictability power of the novel approach by comparing the predicted bioavailability values with the observed ones (Chapter 5).
- ✓ Propose recommendations for future work, including the prediction of oral bioavailability in pre-clinical species and defining a bio-relevant *in vitro* input from the lipolysis model which could be used for *in silico* physiologically-based pharmacokinetic modelling to predict the performance of LFs (Chapter 6).
- ✓ Summarise concluding remarks (Chapter 7).

## **Chapter 2: Optimisation of the *In Vitro* Lipolysis Model Working Conditions**

### **2.1. Introduction**

The *in vitro* lipolysis model has been previously developed and utilised by different research groups [103–106, 122]. The concept and fundamental principles of the model are similar among groups, but different experimental conditions and parameters have been proposed to accommodate the study purposes of each research group. These differences include duration of the test, sampling times, pH, volume and composition of the digestion medium, amounts of formulation added, lipase activity, and source of lipase and bile acids, among others. **Table 2-1** summarises and compares the most important parameters of the experimental media used by established *in vitro* lipolysis research groups, together with Dressman's FaSSIF-V2 (Fasted State Simulated Intestinal Fluids version 2) values, and literature data for average concentrations of major components of human intestinal fluid in the fasted and fed states.

The Lipid Formulation Classification System Consortium has published a number of studies aimed to reduce the variability in the experimental approach between different groups [182–184]. Their focus has been on the characteristics of the experimental medium. However, other important parameters of the *in vitro* lipolysis model, such as time required for digestion, the titrant concentration, or factors associated to the pH-stat titrator working conditions (e.g. rate of titrant addition) have not been assessed.

Based on this, and on the fact that different pH–time profiles were observed during preliminary lipolysis experiments of triglycerides (TGs) with different chain lengths (further described in chapter 3), it was evident that an optimisation of the lipolysis conditions was needed for tighter control over pH levels so as to better mimic *in vivo* conditions. For this reason, the aim of these studies was to find an optimised set of conditions (in terms of titrant concentration and maximum and minimum titrant addition rates) capable of maintaining the pH environment within the physiological range (6.75 – 6.85) during the hydrolysis of TGs with different carbon

chain lengths. The hydrolysis of different volumes of oil was also evaluated to assess a variety of possible scenarios in the intestine, from the ingestion of an oil-containing capsule in fasting conditions to the consumption of a high-fat meal.

**Table 2-1.** Comparison of the composition of digestion media between the human jejunal fluids and several bio-relevant media. Values are expressed as means  $\pm$  SD, or ranges (–).

	pH	Buffer	BS	PL	Ref.
<b><i>In vivo</i> fasted</b>	6.8 $\pm$ 0.4, 7.1 $\pm$ 0.6	8.5 $\pm$ 5 mM, 17, 30 mEq/L HCO <sub>3</sub> <sup>–</sup>	2 $\pm$ 0.2, 0.8–5.5 mM	0.2 $\pm$ 0.07 mM	[114, 185– 188]
<b><i>In vivo</i> fed</b>	6.2 $\pm$ 0.2, 5.2–6.0	2–20, 6–20 mEq/L HCO <sub>3</sub> <sup>–</sup>	8 $\pm$ 0.1, 6.5 $\pm$ 0.9 mM	3 $\pm$ 0.3 mM	[114, 187, 189–192]
<b>FaSSIF-V2</b>	6.5	19 mM Maleic acid	3 mM	0.2 mM	[88]
<b>University of Copenhagen</b>	6.5	2 mM Maleate	5 mM NaTDC	1.25 mM Soy PC	[193]
<b>Monash University</b>	7.5	50 mM Maleate	5 mM NaTDC	1.25 mM Soy PC	[194]
<b>Hebrew University of Jerusalem</b>	6.8	50 mM Maleate	5 mM NaTC	1.25 mM Lecithin	[105, 195]
<b>LFCS Consortium</b>	6.5	2 mM Maleate	3 mM NaTDC	0.75 mM Egg PC	[182]

BS: Bile salt; FaSSIF-V2: Fasted State Simulated Intestinal Fluids version 2; NaTDC: Sodium taurodeoxycholate; NaTC: Sodium Taurocholate; PC: Phosphatidylcholine; PL: Phospholipid; Ref.: exemplary reference.

As mentioned before (see Chapter 1, section 1.4.2), the main enzyme involved in the lipolysis of dietary fat in the intestine is pancreatic lipase [196]. For TG hydrolysis to occur, the participation of another pancreatic protein, co-lipase (~ 10 kDa), is absolutely necessary, as this cofactor prevents the inhibitory effect of bile salts and phospholipids on pancreatic lipase. Lipase and co-lipase are water-soluble pancreatic proteins that in aqueous solution form a 1:1 molar complex [196]. Lipase is glycoprotein with a single chain polypeptide containing 449 amino acids distributed in two domains: a predominant N-terminal domain (amino acids 1–335) and a smaller C-terminal domain (residues 336–449) [197]. On the other hand, co-lipase consists of a single polypeptide chain containing 86 amino acids and is not glycosylated. The interaction between the C-terminal domain of lipase and co-lipase is both electrostatic and hydrophobic and is stabilised by eight hydrogen bonds and around 80 van der Waals contacts.

Pancreatic lipase/co-lipase complex is not significantly active below pH 5.0 and displays its maximum activity at pH 7.0–7.5 (**Figure 2-1**). Hence, lipase is well adapted to the pH conditions measured *in vivo* in the small intestine [198].

In the light of this, for a correct setup of the *in vitro* lipolysis model, the activity of lipase/co-lipase complex was measured prior to optimisation experiments to make sure the enzyme was added in excess, as is the case in *in vivo* conditions [107].

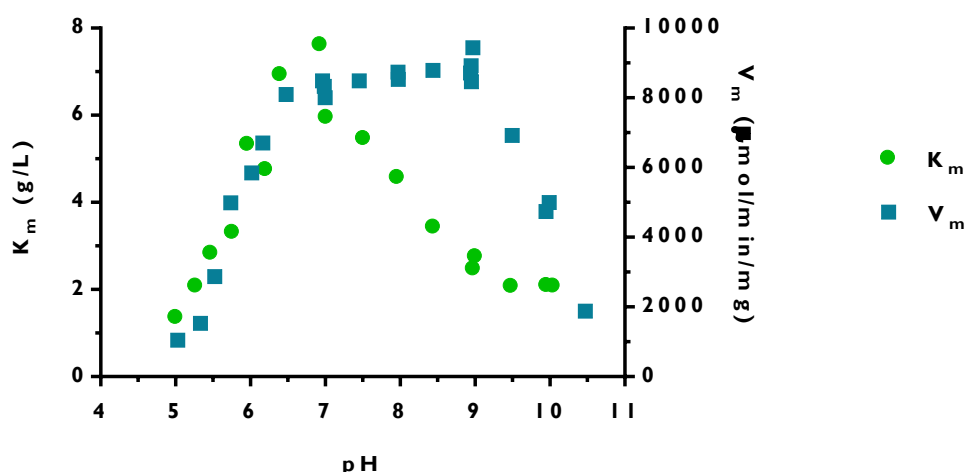


**Figure 2-1.** pH dependence of Michaelis–Menten constant ( $K_m$ , green circles) and maximum reaction rate ( $V_m$ , blue squares). (Adapted with permission from Ref. [199], Copyright© 1971, American Chemical Society)

## 2.2. Materials and Methods

### 2.2.1. Materials

Sodium hydroxide solutions (NaOH, 0.5 M and 1 M), Trizma® maleate, sodium taurocholate hydrate (98% w/w), L- $\alpha$ -lecithin (~60% pure L- $\alpha$ -phosphatidylcholine, from egg yolk), pancreatin powder from porcine pancreas (8 x US Pharmacopeia, USP, specifications activity), glyceryl triacetate ( $\geq 99.9\%$  v/v), glyceryl trioctanoate ( $\geq 99\%$  v/v), and peanut oil were all purchased from Sigma–Aldrich (Dorset, UK). Sodium chloride (99.5% w/w) was a product from Fisher Scientific (Leicester, UK). Calcium chloride anhydrous (93% w/w), and glyceryl tributyrates (98% v/v) were purchased from Alfa Aesar (Heysham, UK). Glyceryl tridecanoate ( $\geq 98\%$  v/v) was obtained from TCI (Tokyo, Japan). The standard buffer solutions (pH 4, 7, 10



and 12), utilised for calibration of the pH-electrode, were purchased from YSI Incorporated (Ohio, USA) and Hanna Instruments (Rhode Island, USA). Water was obtained from a Purelab Ultra Genetic purification system (Elga LabWater, Illinois, USA).

### 2.2.2. Lipidic formulations

Glyceryl triacetate (tri-C2) and glyceryl tributyrates (tri-C4) served as model molecules for short-chain triglycerides (SCTs, < C6). Glyceryl trioctanoate (tri-C8) and glyceryl tridecanoate (tri-C10) represented medium-chain triglycerides (MCTs, C6–C12). In a similar manner to previous publications [105, 200], peanut oil (tri-C18) was chosen as the prototype for long-chain triglycerides (LCTs, > C12). Peanut oil contains mainly LCTs (C16 and C18), the vast majority of which is triolein [201].

### 2.2.3. Preparation of digestion buffers

The preparation of the bio-relevant digestion buffer simulating the contents of the jejunum in the fasted state was based on that developed by the Hebrew University of Jerusalem [105, 195] with a minor modification. This change consisted in decreasing the pH of the buffer from 7.40 to 6.80 to achieve maximum pseudo-physiological conditions [202]. The lipolysis medium contained 50 mM trizma® maleate [123, 203–205], 5 mM calcium chloride, 5 mM sodium taurocholate, and 1.25 mM L- $\alpha$ -lecithin<sup>iii</sup>. The osmolarity of the buffer solution was fixed at around 280 mOsm/kg<sup>iv</sup> with 150 mM NaCl. The pH of the medium was adjusted to  $6.80 \pm 0.05$  at 37 °C using 1 M NaOH solution as titrant, and a pH-stat titrator unit (T50 Graphix, Mettler Toledo Inc., Leicester, UK) coupled to a pH-electrode (DG111-SC, Mettler Toledo Inc., Leicester, UK).

The buffer used for the preparation of the enzyme extract was made in a similar manner, although it did not include bile salts or phospholipids to prevent the deactivation of the lipase prior to the lipolysis experiments.

<sup>iii</sup> L- $\alpha$ -lecithin from egg yolk consist in ~60% pure L- $\alpha$ -phosphatidylcholine, therefore the actual phospholipid levels are 0.75 mM. Lecithin may contain other phospholipids such as phosphatidylethanolamine or phosphatidylinositol.

<sup>iv</sup> Reported osmolarity values of the jejunum in the fasted state are  $271 \pm 15$ ,  $200 \pm 68$ , and  $278 \pm 16$  mOsm/kg [188, 384, 385]. The main electrolytes are Na<sup>+</sup> and Cl<sup>-</sup>, followed by K<sup>+</sup> and Ca<sup>2+</sup>.

#### 2.2.4. Preparation of lipase/co-lipase extract

Porcine pancreatin powder, containing equimolar amounts of lipase and co-lipase [103], was prepared as described by Sek *et al.* [206]. Briefly, one gram of pancreatin powder was added to 5 mL of digestion buffer and vortex-mixed for 15 min at room temperature. After centrifugation at ~1200 g (Harrier 18/80 centrifuge, swing-out rotor, MSE, London, UK) and 4 °C for 15 min, the supernatant was collected and stored on ice to avoid denaturation.

#### 2.2.5. Determination of lipase/co-lipase extract activity

Lipase activity was determined titrimetrically using 20 µL of lipase/co-lipase extract dissolved in 35.5 mL of digestion buffer (pH 6.8, 37 °C). Tri-C4 (6 mL) and NaOH (1 M) were used as enzyme substrate and titration solution, respectively. The lipolysis reaction was left to proceed for 5 minutes. Experiments were performed five times.

The rate of lipolysis ( $k_L$ ) was transformed into enzymatic activity units, as indicated in **Equation 2-1**. The activity of the enzyme was expressed in terms of glyceryl tributyrates units (TBU), where 1 TBU is the amount of enzyme that can release 1 µmol of butyric acid from tri-C4 per minute.

$$\text{Activity (TBU)} = k_L \cdot \left( \frac{\text{mL 1 M NaOH}}{s} \right) \cdot \frac{60 \text{ s}}{\text{min}} \cdot \frac{1000 \text{ µmol NaOH}}{1 \text{ mL 1 M NaOH}} \cdot \frac{1 \text{ µmol butyric acid}}{1 \text{ µmol NaOH}}$$

**Equation 2-1**

According to USP [207], an alternative method for lipase activity determination involves the lipolysis at pH 9 of olive oil emulsified with gum arabic. The triolein method is more robust as it requires the use of a reference standard [107]. However, the tributyrates method is preferred because tri-C4 shows a lower  $pK_a$  than tri-C18 so its lipolysis can be monitored titrimetrically at physiological pH values. Moreover, butyric acid is soluble in water so linear kinetics are obtained for longer times [50].

#### 2.2.6. Optimisation of the *in vitro* lipolysis model working conditions

The set-up of the *in vitro* lipolysis model utilised in the laboratory can be seen in **Figure 2-2**. The procedure of the *in vitro* lipolysis was similar to that described previously [104, 105, 182, 203, 208]. A certain amount of oil was added to 35.5 mL of digestion buffer dispersed in a

reaction vessel with continuous stirring and kept at 37 °C. After 15 min of equilibration, 3.5 mL of lipase/co-lipase extract was added to the mixture to initiate the enzymatic hydrolysis. A pH-stat titrator unit was used to keep experimental pH under control (6.75– 6.85) by titrating the released ionised FAs with NaOH solution. The maximum and minimum rates of titrant addition were set up through the instrument control software (LabX light v3.1). The experiments were considered to be completed when the dosing rate of NaOH was lower than the minimum rate.

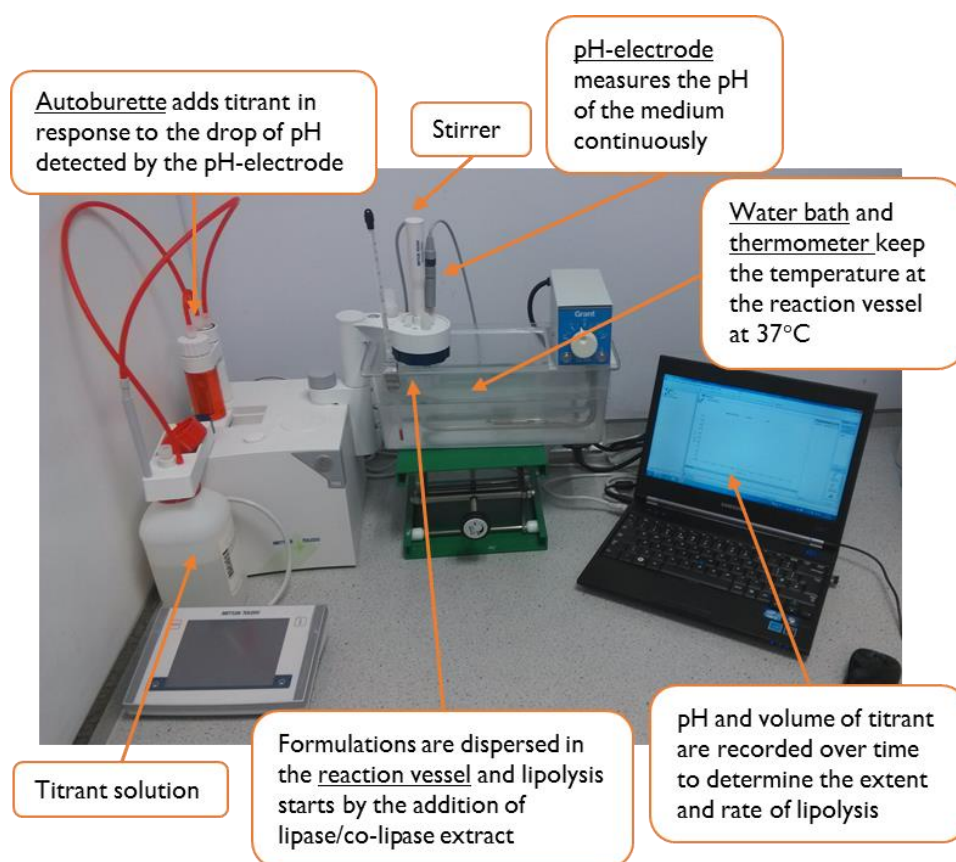


**Figure 2-2.** Set-up of the *in vitro* lipolysis model in the laboratory. The main components and their functions are indicated with arrows.

The lipolysis model was optimised to be able to analyse different volumes of oil and the lipolysis of TGs with different chain lengths with one set of conditions. The titrant concentration and the maximum and minimum rates of addition were varied in order to find a unique set of conditions that maintained the pH between 6.75 and 6.85 during lipolysis. The sets of conditions evaluated during the optimisation of the model are listed in **Table 2-2**. Each set of conditions was assessed for short-, medium-, and long-chain TGs, and with oil volumes of

200, 500 and 1000  $\mu\text{L}$ , five times. The dispersion of 200  $\mu\text{L}$  of TG in the model ( $\sim 40\text{ mL}$ ) would be equivalent to a 1000  $\mu\text{L}$  lipid-containing capsule in the human gastrointestinal tract ( $\sim 250\text{ mL}$  [209]). Similarly, 1000  $\mu\text{L}$  of oil dispersed in the lipolysis medium would be comparable to a high-fat meal in the *in vivo* situation [105]. 500  $\mu\text{L}$  was chosen as a value in between the previous two conditions.

**Table 2-2.** Sets of conditions assessed during the optimisation of the lipolysis model ( $n = 5$ ).

Concentration of titrant (M)	Maximum dosing rate (mL/min)	Minimum dosing rate ( $\mu\text{L}/\text{min}$ ) <sup>a</sup>
0.5	1	10
1	1	10
1	1	3
1	3.5	3

<sup>a</sup> The minimum dosing rate and the termination rate were set to coincide in all experiments. (Reprinted from Ref. [53], under the terms of the Creative Commons Attribution License, CC BY, 2015)

### 2.2.7. Statistical data analysis

All presented data are expressed as mean  $\pm$  standard deviation (SD). A one-way analysis of variance (ANOVA), followed by post hoc Tukey–Kramer multiple comparison test, was used to determine statistically significant differences among the experimental groups. Prior to ANOVA testing, it was confirmed that data followed a normal distribution (Kolmogorov–Smirnov test), and that SDs were not significantly different among groups (Barlett’s test). A  $p$  value (calculated probability) of 0.05 was considered the minimal level of significance to reject the null hypothesis. Statistical analysis was performed using GraphPad Prism version 7.00 for Windows (GraphPad Software, San Diego, California, USA).

## 2.3. Results

### 2.3.1. Lipase extract activity

Lipase activity was determined based on USP recommendations [10]. The amount of NaOH used for titration was represented against time (**Figure 2-3**), and using only the points that fall

on the straight-line segment of the curve, the  $k_L$  (the slope) was calculated and transformed into enzymatic activity units, as indicated in **Equation 2-1**. The activity of the lipase used was 42 TBU/mg of dry pancreatin powder, and 735 TBU/mL of digest.

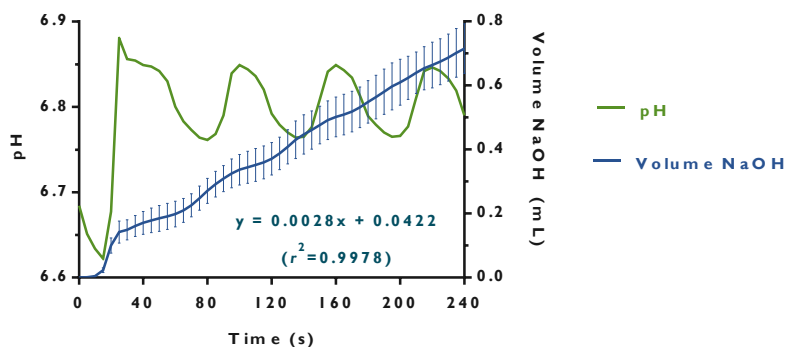


**Figure 2-3.** pH-time (green) and volume of NaOH-time (blue) profiles of the lipolysis of 6 mL of glyceryl tributyrates by 20  $\mu$ L of lipase/co-lipase extract. Conditions: 1 M NaOH, 3.5 mL/min maximum and 3  $\mu$ L/min minimum dosing rate.

### 2.3.2. Optimisation of the *in vitro* lipolysis model working conditions

The effect of the concentration of titrant, and maximum and minimum titrant dosing rates on the control over the lipolysis process was investigated to find an optimised set of conditions capable of keeping the pH environment within the physiological range (6.75–6.85), during the hydrolysis of TGs with different carbon chain lengths. Also the lipolysis of different TG volumes was evaluated in order to assess a variety of possible scenarios in the intestine.

#### 2.3.2.1. 0.5 M NaOH, 1 mL/min maximum rate, 10 $\mu$ L/min minimum rate

The initial set of conditions was characterised by a prolonged time to gain control over pH during the lipolysis of tri-C4, and by a transient drop of pH during the hydrolysis of 500 and 1000  $\mu$ L of tri-C8 (**Figure 2-4**). In addition, high volumes of titrant were required during the lipolysis of 1000  $\mu$ L of tri-C2, tri-C4 and tri-C8 which lead to dilution (approximately 25%) of the experimental medium. Prolonged times to complete the process (e.g. over two hours for 1000  $\mu$ L of tri-C4) were additional issues encountered while assessing the set of conditions.

#### 2.3.2.2. 1 M NaOH, 1 mL/min maximum rate, 10 $\mu$ L/min minimum rate

Titration with 1 M NaOH considerably reduced the time needed to gain initial control over the pH for the lipolysis of tri-C2 and tri-C4, and avoided or decreased the transient loss of control during the lipolysis of tri-C8 (**Figure 2-5**). Despite improvements, these conditions caused a premature cessation of the process for the lipolysis of 200  $\mu$ L of tri-C18. A marked elevation of the pH above the pre-determined threshold at the beginning of the process led to a very slow titrant dosing rate that was recognised by the titrator as lower than the termination rate and the process was terminated after just 90 s.

#### 2.3.2.3. 1 M NaOH, 1 mL/min maximum rate, 3 $\mu$ L/min minimum rate

Reducing the minimum rate of addition from 10 to 3  $\mu$ L/min enabled the continuation of the lipolysis of 200  $\mu$ L of tri-C18 (**Figure 2-6**). Nevertheless, the loss of control over pH (1000  $\mu$ L of tri-C8), the sharp drop of pH and the prolonged time to reach the control band (500 and 1000  $\mu$ L of tri-C4) were still unresolved issues.

#### 2.3.2.4. 1 M NaOH, 3.5 mL/min maximum rate, 3 $\mu$ L/min minimum rate

The increment of the maximum addition rate from 1 to 3.5 mL/min achieved the control over pH throughout the lipolysis of all evaluated TGs and volumes (**Figure 2-7**). In terms of reaction time, lipolysis of short- and medium-chain TGs lasted less than 30 min. Lipolysis of tri-C18 came to an end before reaching 45 min. Statistically significant differences ( $p < 0.05$ ) in NaOH consumption were observed during lipolysis of different volumes of the same TG (except for 500 and 1000  $\mu$ L of tri-C18).

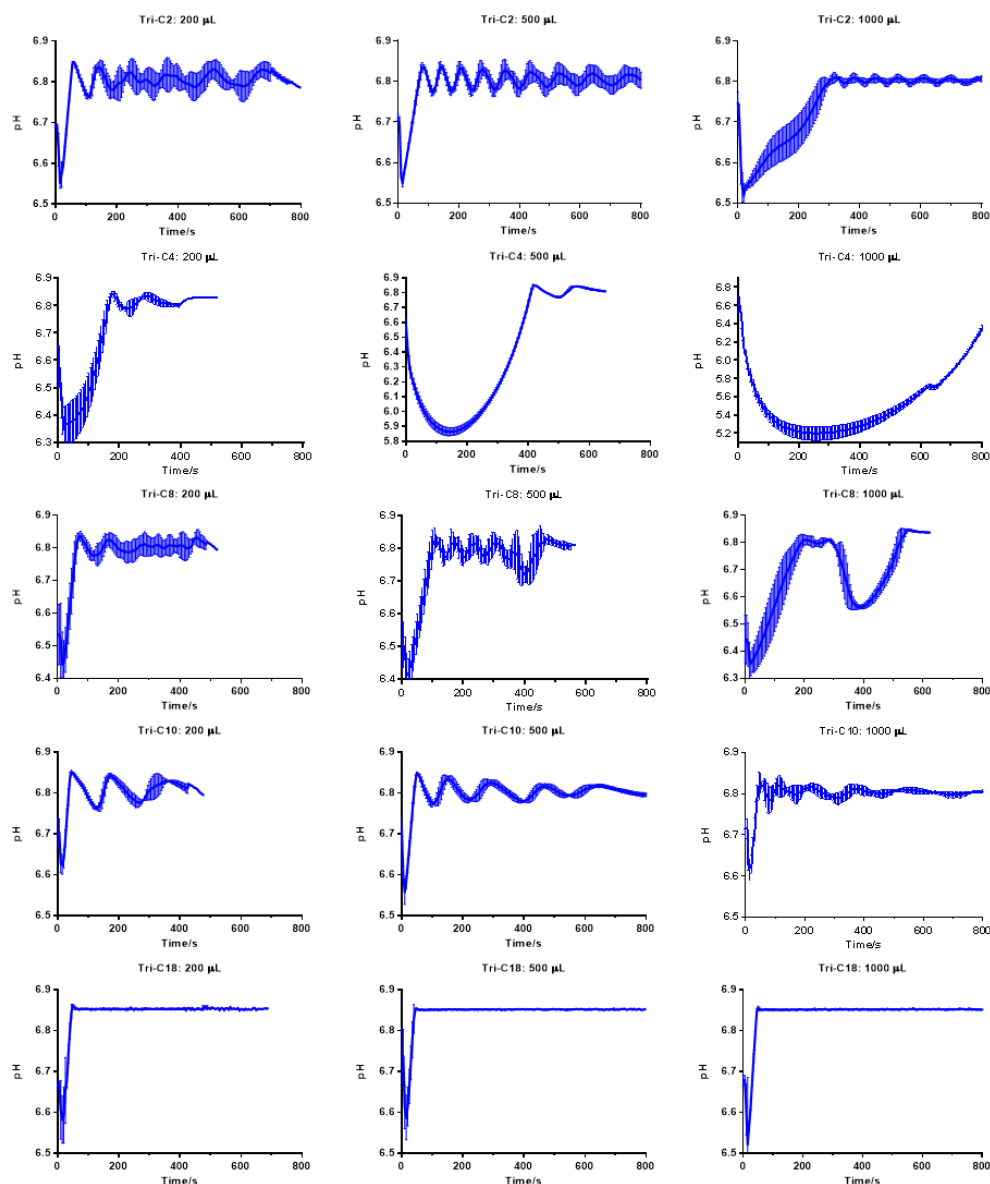


**Figure 2-4.** pH-time lipolysis profiles (mean  $\pm$  SD,  $n = 5$ ) for 200, 500 and 1000  $\mu\text{L}$  of glyceryl triacetate (tri-C2), tributyrates (tri-C4), trioctanoate (tri-C8), tridecanoate (tri-C10), and peanut oil (tri-C18). Conditions: 0.5 M NaOH, 1 mL/min maximum and 10  $\mu\text{L}/\text{min}$  minimum dosing rate. Only the first 800 s of the process are represented for ease of comparison. (Modified from Ref. [53], under the terms of CC BY, 2015)

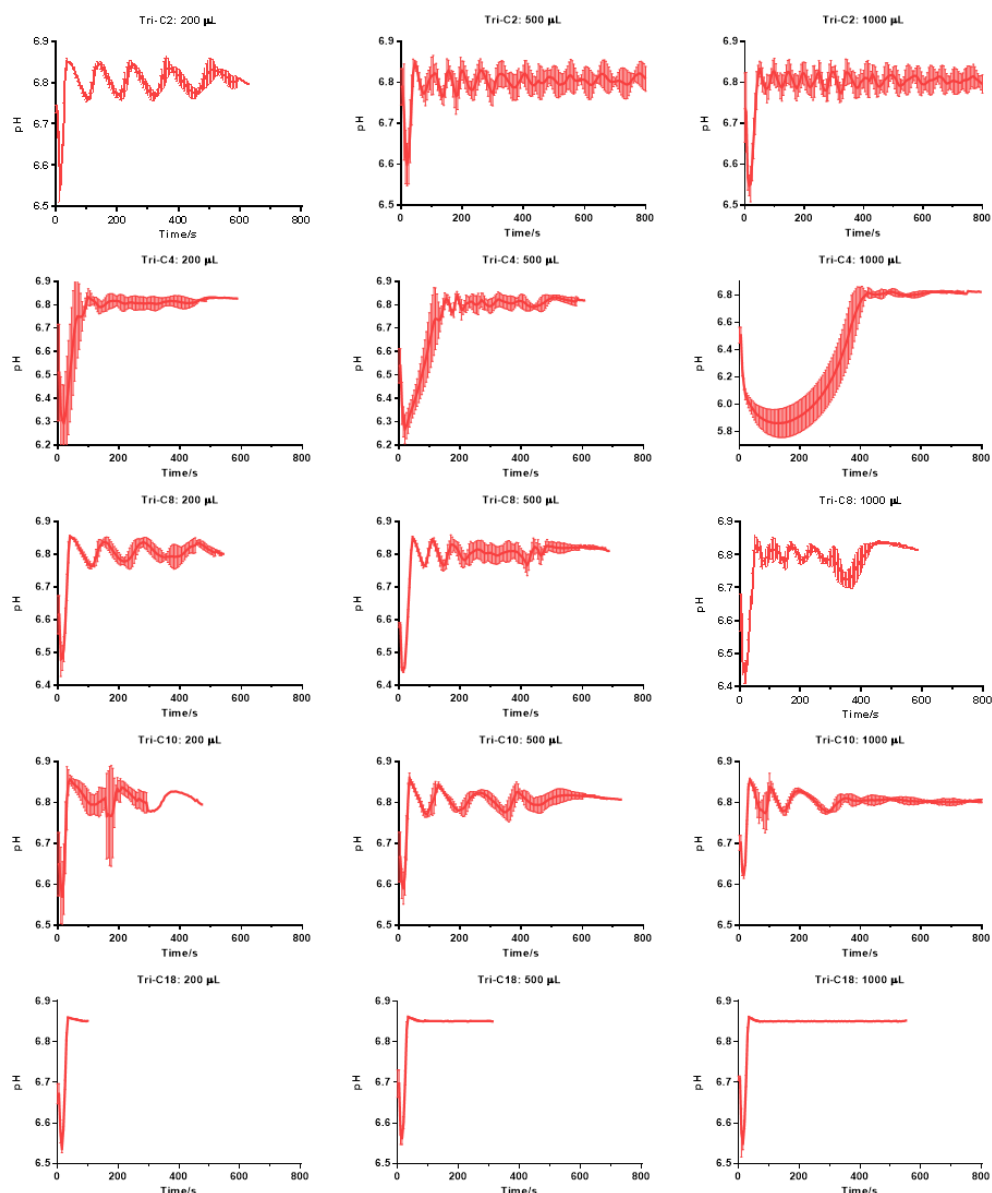


**Figure 2-5.** pH-time lipolysis profiles (mean  $\pm$  SD,  $n = 5$ ) for 200, 500 and 1000  $\mu\text{L}$  of glyceryl triacetate (tri-C2), tributyrates (tri-C4), trioctanoate (tri-C8), tridecanoate (tri-C10), and peanut oil (tri-C18). Conditions: 1 M NaOH, 1 mL/min maximum and 10  $\mu\text{L}/\text{min}$  minimum dosing rate. Only the first 800 s of the process are represented for ease of comparison. (Modified from Ref. [53], under the terms of CC BY, 2015)



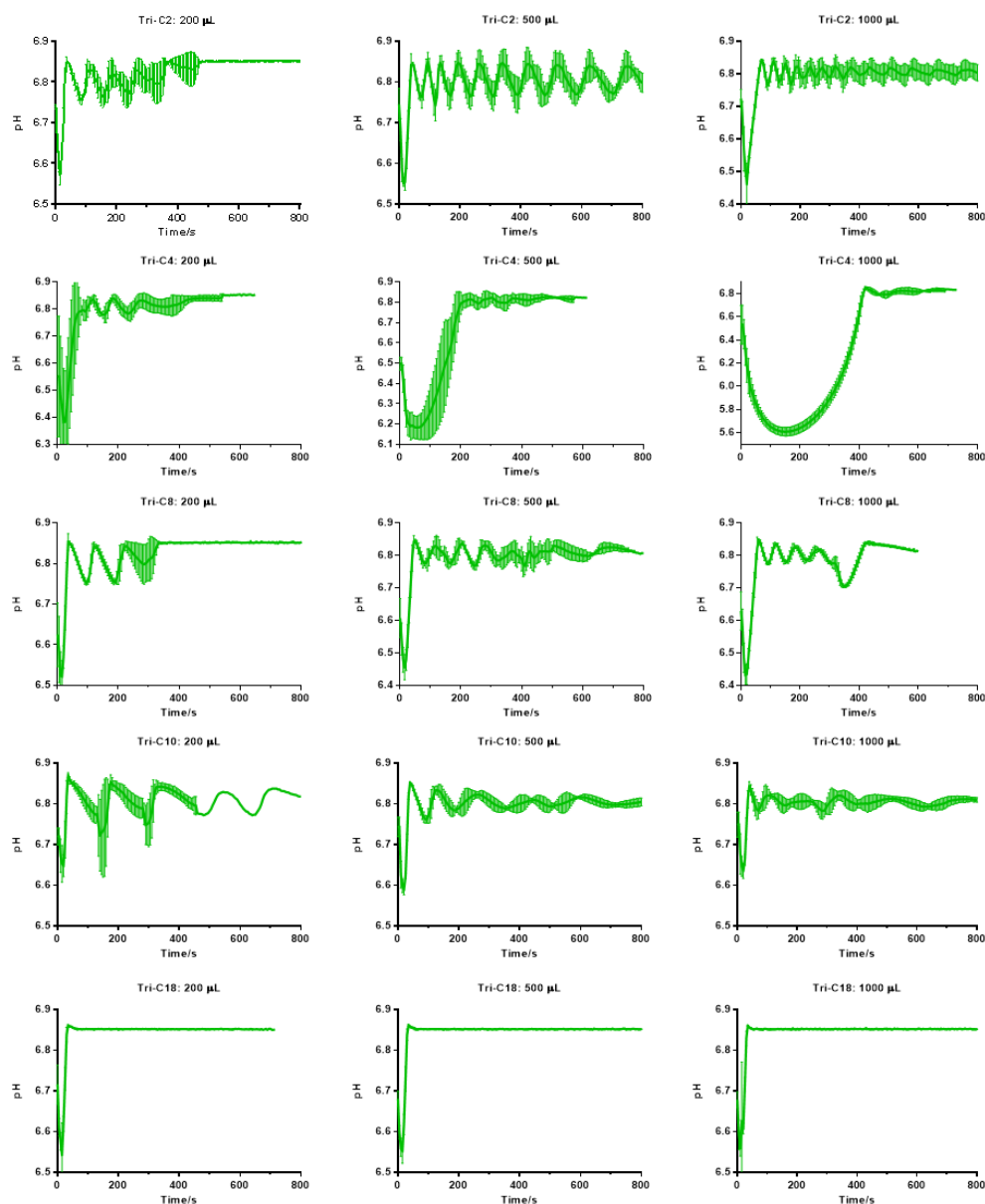


**Figure 2-6.** pH-time lipolysis profiles (mean  $\pm$  SD,  $n = 5$ ) for 200, 500 and 1000  $\mu\text{L}$  of glyceryl triacetate (tri-C2), tributyrat (tri-C4), trioctanoate (tri-C8), tridecanoate (tri-C10) and peanut oil (tri-C18). Conditions: 1 M NaOH, 1 mL/min maximum and 3  $\mu\text{L}/\text{min}$  minimum dosing rate. Only the first 800 s of the process are represented for ease of comparison. (Modified from Ref. [53], under the terms of CC BY, 2015)

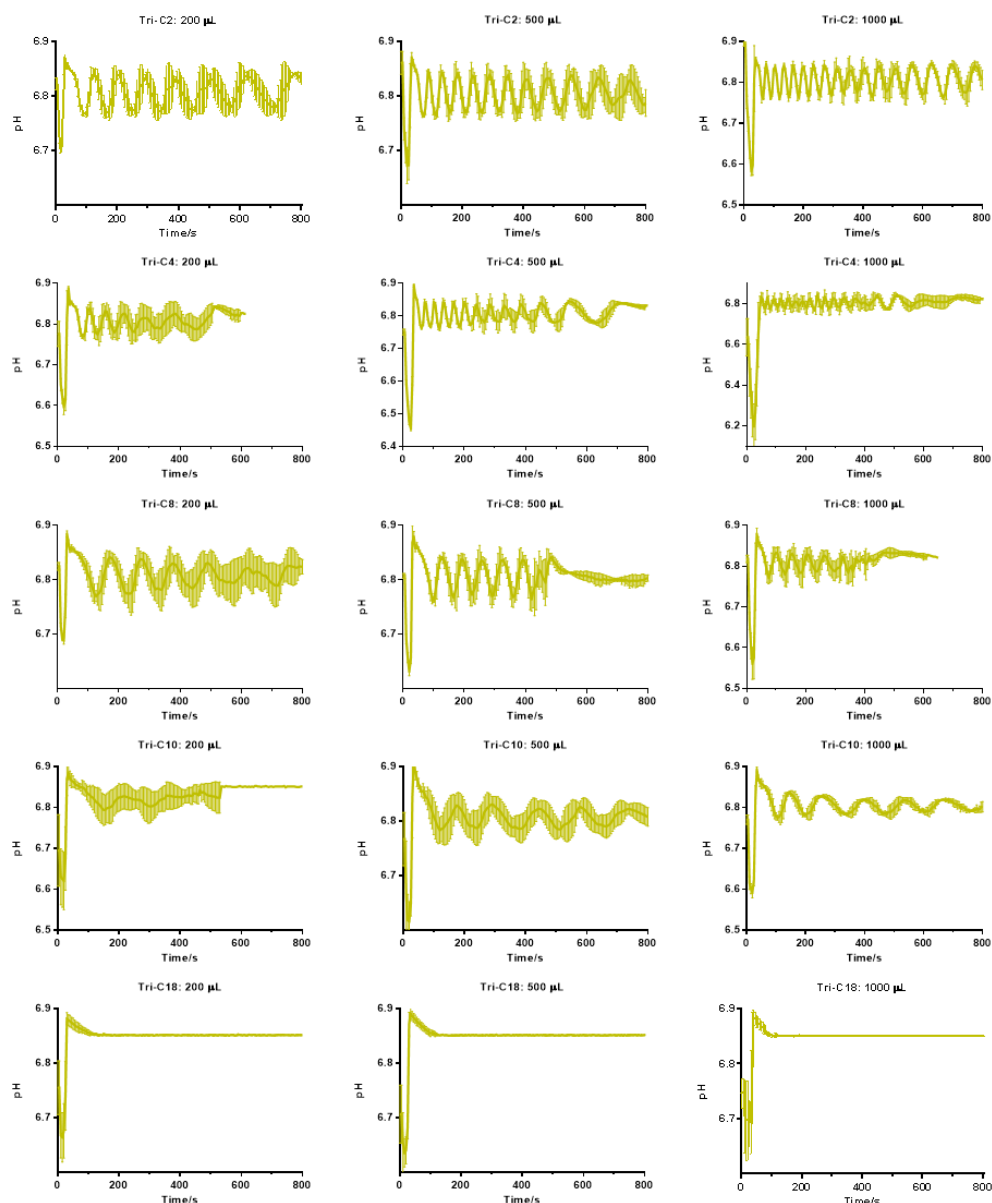


**Figure 2-7.** pH–time lipolysis profiles (mean  $\pm$  SD,  $n = 5$ ) for 200, 500 and 1000  $\mu\text{L}$  of glyceryl triacetate (tri-C2), glyceryl (tri-C4), glyceryl (tri-C8), glyceryl (tri-C10), and peanut oil (tri-C18). Conditions: 1 M NaOH, 3.5 mL/min maximum and 3  $\mu\text{L}/\text{min}$  minimum dosing rate. Only the first 800 s of the process are represented for ease of comparison. (Modified from Ref. [53], under the terms of CC BY, 2015).

## 2.4. Discussion

### 2.4.1. Lipase extract activity

Pancreatic lipase readily adsorbs to TGs droplets. In the small intestine, these droplets are covered with bile salt and phospholipids which prevent the adsorption and lipolytic action of lipase. In this situation the activity of lipase is restored by co-lipase, another pancreatic protein. Lipase and colipase in solution form a 1:1 molar complex. In this investigation, lipase/co-lipase complex activity was determined based on USP recommendations [10], at pH 6.8 (jejunal conditions). The activity of the lipase/co-lipase complex used was 42 TBU/mg of dry pancreatin powder, and 735 TBU/mL of digest. This value was higher than the activity for *in vivo* conditions (500–600 TBU/mL in the fasted state [110]) and confirmed we were working with an excess of enzyme.

### 2.4.2. Optimisation of the *in vitro* lipolysis model working conditions

The role of the concentration of titrant and maximum and minimum titrant addition rates, in the control of the lipolysis process, was investigated to find an optimised set of conditions capable of maintaining the pH environment within physiological range (6.75–6.85) during the hydrolysis of TGs with different carbon chain lengths. The hydrolysis of different volumes of oil (200, 500 and 1000  $\mu$ L) was evaluated to assess a variety of possible scenarios in the intestine, from the ingestion of an oil-containing capsule in fasting conditions to the consumption of a high-fat meal.

The first set of conditions evaluated (0.5 M NaOH with 1 mL/min maximum and 10  $\mu$ L/min minimum dosing rates, **Figure 2-4**) was found to be suitable for tri-C10 and tri-C18, but not for tri-C2, tri-C4 and tri-C8. The high activity that pancreatic lipase showed towards tri-C4 – translated into a large amount of liberated ionised FAs – presented a problem for the titrator when trying to regain control over pH during the initial stages of the process. Most importantly, during the “delayed” periods, pH of the medium dropped to acidic values. If the fate of an ionisable drug across lipolysis phases had been assessed under these conditions, such low pH values could have affected the distribution of the compound, leading to incorrect interpretations of the performance of the lipidic formulation. Regarding the lipolysis of tri-C8,

the drawback was not the initial drop of pH, but the loss of control over pH at a later point in the reaction. Apart from pH control, other reasons to disregard this set of conditions were dilution of the medium due to large volumes of titrant needed during the lipolysis of 1000  $\mu\text{L}$  of tri-C2, tri-C8 and tri-C10 (which could affect the critical micellar concentration of the colloidal species in solution), and prolonged times to complete the process. Based on these results, it was decided to increase the concentration of the titrant up to 1 M but maintain the same maximum and minimum rates of addition of NaOH (**Figure 2-5**). Despite improvements, the new conditions introduced the problem of premature stopping of titration with small volumes of tri-C18. To avoid reaching the termination rate at initial stages of the process, it was decided to reduce the minimum rate to 3  $\mu\text{L}/\text{min}$  (**Figure 2-6**). This new set of conditions enabled the continuation of the lipolysis of 200  $\mu\text{L}$  of tri-C18, but was still suboptimal due to the loss of control over pH during the lipolysis of 1000  $\mu\text{L}$  of tri-C8. There was also a sharp drop of pH and prolonged time to reach the control band at initial stages of the lipolysis for 500 and 1000  $\mu\text{L}$  of tri-C4. Finally, by increasing the maximum addition rate up to 3.5 mL/min, all previous issues (premature stop of titration, loss of control over pH, and prolonged time to reach control band) were avoided and the control over pH throughout the lipolysis of all evaluated TGs and volumes was achieved (**Figure 2-7**). The implementation of this method resulted in shorter reaction times, which allows the assessment of several formulations on the same day. Statistically significant differences ( $p < 0.05$ ) in NaOH consumption were observed during lipolysis of different volumes of the same TG indicating the optimised conditions were capable of distinguishing among the different fat-digesting situations that were mimicked.

## 2.5. Conclusions

1 M NaOH titrant concentration, 3.5 mL/min maximum titrant dosing rate and 3  $\mu\text{L}/\text{min}$  minimum titrant dosing rate, were found to be the conditions that better maintained the pH environment within physiological range (6.75–6.85) during the hydrolysis of TGs with different carbon chain lengths. This optimised set of conditions also allowed the differentiation of the lipolysis of different lipid loads.

This unique set of *in vitro* lipolysis working conditions could facilitate the comparison of data among laboratories, as the impact of method variation on *in vitro* performance would be highly reduced. Besides, these conditions offer better control over pH levels, closely reflecting the buffer capacity *in vivo*, and thus allowing better simulation of physiological digestion of LFs.

## **Chapter 3: Assessment of Pancreatic**

# **Lipase Activity: *In Vitro* Digestion of Equimolar Amounts of Lipids**

### **3.1. Introduction**

Triglycerides (TGs) are the main constituents of dietary lipids [201] and one of the most common excipients used in LFs [210]. Enzymatic hydrolysis of TGs (to yield 2-monoglycerides, 2-MGs, and fatty acids, FAs) occurs at the oil–water interface of the emulsified lipid droplets [40]. The composition and state of this interface affects the characteristics of the lipid droplet, and consequently can modulate the lipase activity [211, 212]. Although 2-MGs and FAs are more water–soluble than the TGs from which they derive, they still show poor solubility in bulk water. As a result, they tend to accumulate on the surface of the lipid droplets forming local liquid crystalline structures. These lipidic structures spontaneously detach from the oil–water interface into the aqueous phase and form large multilamellar vesicles. On further dilution with the intestinal fluids, these multilamellar species transform into smaller unilamellar species, and are eventually incorporated into mixed micelles. Differences in the chain length of 2-MGs and FAs, dictate differences in phase transition behaviour (liquid crystalline to multilamellar and unilamellar vesicles), and in the solubilisation capacity of the colloidal species formed. In long–chain lipid systems vesicular species persist at lower lipid concentrations and are more capable of swelling; hence, they retain drug solubilisation capacity more effectively compared with more polar medium– and short–chain systems. For this reason, chain length largely dictates the absorption fate of poorly water–soluble drug co–administered with lipids [58, 213, 214]. Indeed, the micellar solubilisation capacity of long–chain triglycerides (LCTs) has been reported to be higher than that of short–chain triglycerides (SCTs) [105, 108].

There are other additional mechanisms by which the FA chain length of the TG plays a critical role in the oral bioavailability of the co–administered poorly water–soluble drugs [215]. As an

example, SCTs are known to induce tight junction permeability changes, and thus increase drug intestinal permeation [66]. On the other hand, highly lipophilic drugs ( $\log D_{7.4} > 5$ ) co-administered with LCTs may be incorporated into chylomicrons, and enter the lymphatic system, bypassing the hepatic first-pass metabolism [62] (see section 1.4.3.3 for further details). Although the *in vitro* assessment of the performance of TG-based drug delivery systems with different chain lengths has been carried out before, these studies have only focused on the end result, i.e. drug solubilisation across lipolysis phases [50, 104, 108, 123, 184, 203]. Limited attention has been drawn to assessing the substrate specificity of the pancreatic lipase [216, 217]. A better mechanistic knowledge of the lipolysis process itself, and the factors governing lipase activity, will help to rationalise the performance of LFs and eventually aid in the development of optimised formulations.

Accordingly, the objective of this study was to gain a deeper understanding of the mechanism behind pancreatic lipase activity, by evaluating the *in vitro* lipolysis of equimolar amounts of TGs with different chain lengths. In order to do so, the difference in the lipolysis profiles (extent of digestion, time required to terminate the process, etc.) were investigated. Additionally, the need for a “back-titration” step to overcome underestimation issues addressed in previous literature reports [182, 218] was also assessed.

## 3.2. Materials and Methods

### 3.2.1. Materials

Reagents and solvents used for experimentation were the same as those listed in chapter 2, section 2.2.1. Glycerol triacetate (tri-C2), glycerol tributyrates (tri-C4), glycerol trioctanoate (tri-C8), glycerol tridecanoate (tri-C10) and peanut oil served again as model molecules for short-, medium-, and long-chain triglycerides.

### 3.2.2. Preparation of simulated digestion buffers

The preparation of the bio-relevant digestion buffer simulating the contents of the jejunum in the fasted state was the same as that described in chapter 2, section 2.2.3.

### 3.2.3. Preparation of lipase/co-lipase extract

Lipase/co-lipase extract preparation was identical as that described in chapter 2, section 2.2.4. The activity of the lipase/co-lipase extract used in these studies was 42 tributyrin units (TBU) per mg of dry pancreatic powder (735 TBU/mL of digest).

### 3.2.4. Experimental procedure: Lipolysis of equimolar amounts of different triglycerides

The experimental conditions described in Chapter 2, section 2.2.6 were followed to investigate the lipolysis of a fixed amount (860  $\mu\text{mol}$ ) of triglycerides. This molar amount corresponded to 161, 251, 421, 500, and 829  $\mu\text{L}$  of tri-C2, tri-C4, tri-C8, tri-C10, and tri-C18, respectively<sup>v</sup>. 0.5 M NaOH solution, and 1 mL/min and 10  $\mu\text{L}/\text{min}$  as maximum and minimum rates of titrant addition, were the *in vitro* lipolysis model conditions used for these investigations. The experiments were considered to be completed when the dosing rate of NaOH was lower than 10  $\mu\text{L}/\text{min}$ . Each experiment was repeated five times.

Control experiments ( $n = 5$ ) were performed without any formulation, to correct for the amount of NaOH solution needed to neutralise the acids released as a consequence of the lipolysis of phospholipids, or arising from the lipolysis of impurities in the pancreatin extract.

The extent of digestion was expressed as percentage of the maximum theoretical quantity of lipid susceptible to hydrolysis. Accordingly, it was assumed that one TG releases three FAs and glycerol (**Figure I-3**). The apparent extent of lipolysis at pH 6.80 was calculated from the volume of titrant consumed during the *in vitro* digestion, as expressed in **Equation 3-1**:

$$\text{Extent of lipolysis (\%)} = \frac{V \cdot 0.5 \cdot \text{MW}}{3 \cdot \rho \cdot v} \cdot 100 \quad \text{Equation 3-1}$$

where  $V$  is the volume (L) of titrant consumed during the digestion at pH 6.80, 0.5 (M) is the concentration of the titrant,  $MW$  is the molecular weight (g/mol) of the oil under investigation,

<sup>v</sup> The availability of tri-C10 was very limited, hence the number of experiments with this oil had to be reduced as much as possible. In order to do so, the data collected using the middle volume (500  $\mu\text{L}$ ) of tri-C10 during the optimisation of the model (Chapter 2) was used here. The equivalent molar amount to 500  $\mu\text{L}$  of tri-C10 (860  $\mu\text{L}$ ) was used as a reference to calculate the equivalent volumes of the other triglycerides.



3 is the maximum quantity of FAs than can be released from one TG,  $\rho$  is the density (g/mL) of the oil, and  $v$  is the volume (mL) of oil dispersed in the lipolysis medium.

### 3.2.5. Experimental procedure: Back-titrations

Based on their apparent pKa, FAs released as a consequence of enzymatic hydrolysis at pH 6.80 may be only partially ionised. As a result of this titration by NaOH, lipase activity determination may be underestimated in direct titration experiments. In order to calculate the total extent of lipolysis, back-titrations [182, 218] were performed. In these experiments, the pH of the medium was elevated to pH  $11.50 \pm 0.05$  by quick addition of 0.5 M NaOH. Control experiments without any TG were performed to correct for the amounts of NaOH needed to raise the pH of the medium up to 11.50.

The total extent of lipolysis was calculated using **Equation 3-1**, where  $V$  represented the volume of NaOH added originally at pH 6.80 (titration of ionised FAs) plus the volume of NaOH added during the back-titration experiments (titration of unionised FAs).

### 3.2.6. Solubility effect of glyceryl triacetate on the extent of lipolysis

As opposed to the other model triglycerides, tri-C2 was completely soluble in the bio-relevant media due to its high water solubility (58 g/L at 25 °C, [219]). In order to determine whether this factor would affect pancreatic lipase activity, additional lipolysis experiments ( $n = 3$ ) with higher amounts of tri-C2 were performed. 1500  $\mu$ L and 2100  $\mu$ L of tri-C2, representing values slightly below (49 g/L) and above (68 g/L) the solubility limit, respectively, were lipolysed under the same conditions described in sections 3.2.4 and 3.2.5.

### 3.2.7. Measurement of the droplet size and total surface area of equimolar triglyceride emulsions following dispersion in the lipolysis buffer

Dynamic light scattering (DLS) was used to determine the mean droplet size ( $d_H$ ) of the emulsions in the digestion medium before the addition of pancreatic lipase, just after the equilibration period. DLS measurements were carried out at a scattering angle of  $173^\circ$  and 37 °C, using a Zetasizer Nano ZS ( $\lambda = 633$  nm, Malvern Instruments, Malvern, UK). As the emulsions were too turbid, they were diluted with incomplete lipolysis buffer to  $5 \cdot 10^{-2}\%$  v/v to

avoid multiple scattering effects. Size determinations were performed for all TG emulsions at least 8 times. Diluted digestion buffer was also analysed to account for any contribution of bile salts and phospholipids to DLS measurements. As expected, droplet size of digestion buffer particles was below the detection limit of the instrument [220], and their size could not be determined.

Droplet size measurements were used to calculate the specific surface area ( $S_s$ , surface area per unit volume [221]) of the emulsions formed prior to enzyme addition. Assuming emulsions were formed by spherical droplets, the surface was determined using **Equation 3-2**:

$$S_s = \frac{S_T}{V_T} = \frac{n \cdot S_i}{V_T} = \frac{V_T/V_i \cdot S_i}{V_T} = \frac{S_i}{V_i} = \frac{\pi \cdot d_H^2}{1/6 \cdot \pi \cdot d_H^3} = 6 \cdot \frac{1}{d_H} \quad \text{Equation 3-2}$$

where  $S_T$  is the total surface area of lipid,  $n$  is the number of lipid droplets,  $S_i$  is the surface area of a single lipid droplet,  $V_T$  is the total volume of lipid, and  $V_i$  is the volume of a single lipid droplet.

### 3.2.8. Statistical data analysis

All presented data are expressed as mean  $\pm$  standard deviation (SD). Statistical tests detailed in Chapter 2, section 2.2.7 were used here as well. When only two experimental groups were available, an unpaired Student's *t*-test was used instead of a one-way analysis of variance (ANOVA).

## 3.3. Results

### 3.3.1. *In vitro* lipolysis of equimolar amounts of different triglycerides

The changes in pH over time during the *in vitro* lipolysis of equimolar quantities of selected TGs are depicted in **Figure 3-1**. Regardless of carbon chain length, all pH–time profiles showed an initial drop of pH as a result of the delay between the pH–stat titrator detecting the first ionised FAs and the subsequent addition of NaOH solution for the titration. The initial burst of hydrolysis has already been reported by other authors [103]. Since transit time along the gastrointestinal tract is known to be variable [222], experiments were not performed for a

fixed period of time, but were allowed to proceed until the titrant addition rate was low (10  $\mu\text{L}/\text{min}$ ), indicating the absence of any FAs to titrate, i.e. absence of TG hydrolysis. As a result, the digestion of each lipid took different times, with the hydrolysis of tri-C8 being the longest process ( $\sim 80$  min), followed by tri-C18, tri-C10 and tri-C2 ( $\sim 35$  min). The lipolysis of tri-C4 took the shortest time ( $\sim 20$  min).

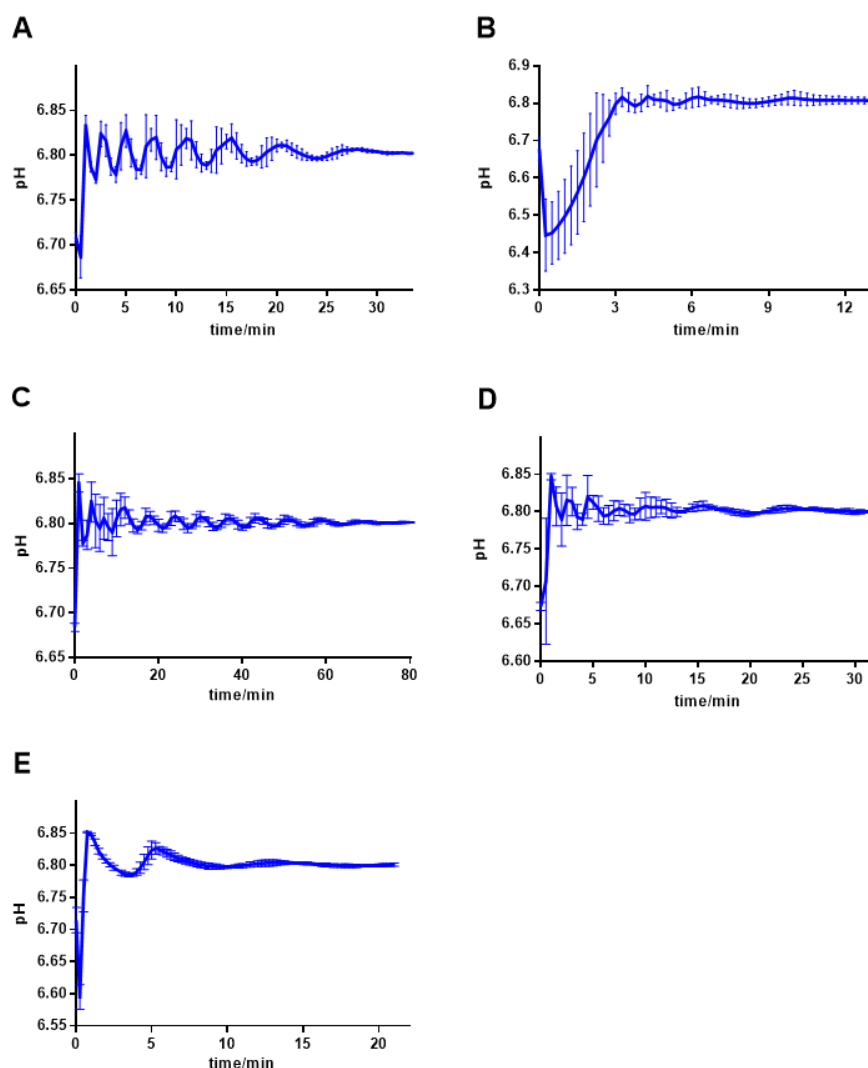


**Figure 3-1.** pH–time profiles obtained during the *in vitro* lipolysis of equimolar amounts of: **(A)** glyceryl triacetate, **(B)** tributyrates, **(C)** trioctanoate **(D)** tridecanoate, and **(E)** peanut oil. Conditions: pH  $6.80 \pm 0.05$ , 0.5 M NaOH titrant concentration, 1 mL/min and 10  $\mu\text{L}/\text{min}$  maximum and minimum titrant dosing rate, respectively. Values are expressed as mean  $\pm$  SD ( $n = 5$ ). (Modified from Ref. [53], under the terms of CC BY, 2015)

The cumulative volumes of 0.5 M NaOH solution required over time during the *in vitro* digestion of equimolar amounts of the selected TGs are represented in **Figure 3-2**. The amount of

titrant consumed was used in **Equation 3-1** to calculate the apparent extent of lipolysis at different time-points, which is also shown in **Figure 3-2**.

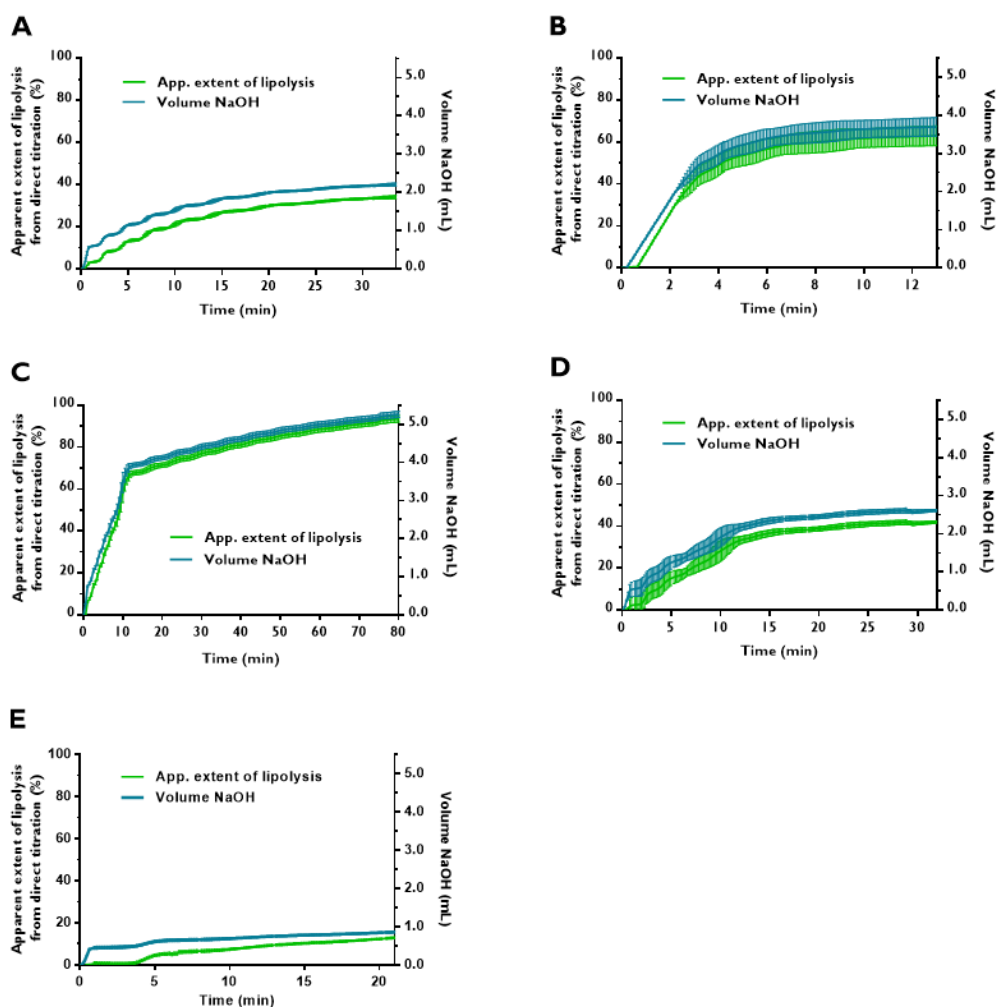


**Figure 3-2.** Apparent extent of lipolysis (green) and volume of titrant (0.5 M NaOH) consumed over time (blue) during the direct *in vitro* lipolysis at pH  $6.80 \pm 0.05$  of equimolar amounts of: (A) glyceryl triacetate, (B) tributyrate, (C) trioctanoate, (D) tridecanoate, and (E) peanut oil. Values are expressed as means ( $n = 5$ )  $\pm$  SD. Note the difference in the time scales (X- axes) among the graphs. (Modified from Ref. [53], under the terms of CC BY, 2015).

All lipids showed a fast initial increase in hydrolysis rate, which subsequently decreased and stayed almost constant for the rest of the process. The lipolysis of tri-C8 resulted in the highest consumption of titrant, and thus in the highest apparent extent of lipolysis by direct titration ( $93 \pm 2\%$ ). Tri-C4 was hydrolysed to a lower extent ( $62 \pm 6\%$ ), but the process was completed one hour earlier. The apparent extents of lipolysis of tri-C10 ( $43 \pm 2\%$ ), tri-C2 ( $33 \pm 0\%$ ) and tri-C18 ( $12 \pm 3\%$ ) were lower than that of tri-C4, despite the longer durations of the reaction.

### 3.3.2. Back-titration studies

The results from the back-titration experiments showed that the extent of lipolysis at pH 6.80 was underestimated by direct titration for all lipids except for tri-C8 (**Figure 3-3**). Based on the cumulative titrant volumes of both direct and back titrations, the lipolysis of tri-C2, tri-C4 and tri-C8 were almost complete ( $98 \pm 2\%$ ,  $91 \pm 9\%$  and  $96 \pm 5\%$ , respectively), and not statistically different from each other ( $p < 0.001$ ). The total extent of hydrolysis of tri-C10 was  $67 \pm 3\%$ , whereas that of tri-C18 was only  $31 \pm 6\%$ .

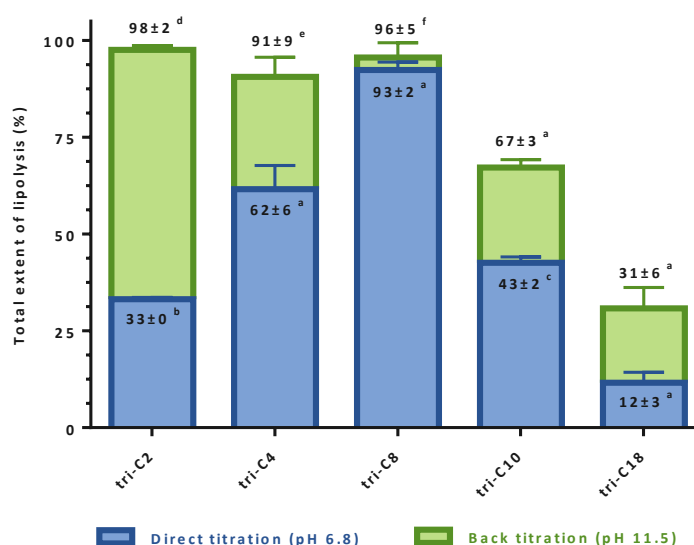


**Figure 3-3.** Comparison of the total extent of lipolysis for the *in vitro* lipolysis of equimolar amounts of different triglycerides: glyceryl triacetate (tri-C2), tributyrates (tri-C4), trioctanoate (tri-C8), tridecanoate (tri-C10) and peanut oil (tri-C18). Blue colours represent the apparent extent of lipolysis calculated during direct titration experiments ( $\text{pH } 6.80 \pm 0.05$ ). Green-shade areas represent the underestimated extent of lipolysis calculated after back-titration experiments ( $\text{pH } 11.50 \pm 0.05$ ). Values are expressed as means ( $n = 5$ )  $\pm$  SD. One-way ANOVA followed by post hoc Tukey-Kramer test was used for statistical analysis.

<sup>a</sup> Statistically significantly different from all other TGs ( $p < 0.001$ ); <sup>b</sup> Statistically significantly different from tri-C4, tri-C8 and tri-C18 ( $p < 0.001$ ), and from tri-C10 ( $p < 0.01$ ); <sup>c</sup> Statistically significantly different from tri-C4, tri-C8 and tri-C18 ( $p < 0.001$ ), and from tri-C2 ( $p < 0.01$ ); <sup>d</sup> Statistically significantly different from all other TGs ( $p < 0.001$ ), except for tri-C4 and tri-C8 ( $p < 0.05$ ); <sup>e</sup> Statistically significantly different from all other TGs ( $p < 0.001$ ), except for tri-C2 and tri-C8 ( $p < 0.05$ ); and <sup>f</sup> Statistically significantly different from all other TGs ( $p < 0.001$ ), except for tri-C2 and tri-C4 ( $p < 0.05$ ).

(Modified from Ref. [53], under the terms of CC BY, 2015)

### 3.3.3. Solubility effect of glyceryl triacetate on the extent of lipolysis

The apparent and total extent of lipolysis of tri-C2 in volumes below and above its solubility limit is shown in **Table 3-1**. No statistically significant differences were found among groups. This result suggests that the lipolysis of 860  $\mu\text{mol}$  of tri-C2 could be compared with that of the other triglycerides even when this oil was completely solubilised in the bio-relevant media and the others were not.

**Table 3-1.** Volumes of titrant used, and calculated apparent and total extent of lipolysis (see **Equation 3-1**), during the hydrolysis of different amounts of glyceryl triacetate representing values below and above its solubility limit. Conditions: 0.5 M NaOH, 1 mL/min maximum and 10  $\mu\text{L}/\text{min}$  minimum dosing rate. Values are expressed as mean  $\pm$  SD.

Volume of oil ( $\mu\text{L}$ )	Direct titration (pH = $6.80 \pm 0.05$ )		Back titration (pH = $11.50 \pm 0.05$ )	
	Volume of NaOH (mL)	Apparent extent of lipolysis (%)	Volume of NaOH (mL)	Total extent of lipolysis (%)
161 (n = 5)	$1.673 \pm 0.021$	$33 \pm 0^*$	$3.299 \pm 0.100$	$98 \pm 2^*$
1500 (n = 3)	$15.333 \pm 0.885$	$32 \pm 2^*$	$40.727 \pm 0.495$	$100 \pm 2^*$
2100 (n = 3)	$21.699 \pm 0.509$	$32 \pm 1^*$	$52.789 \pm 0.527$	$99 \pm 0^*$

\*No statistically significant difference with the other groups (unpaired  $t$ -test).  
(Reprinted from Ref. [53], under the terms of CC BY, 2015)

### 3.3.4. Droplet size and total surface of the equimolar triglyceride emulsions following dispersion in the lipolysis buffer

The particle size and the specific surface area of the equimolar emulsions are shown in **Table 3-2**. All emulsions showed one population and tight peak widths. Tri-C4 had the smallest droplet size ( $124 \pm 6$  nm) and the highest specific surface area ( $436 \cdot 10^{-3} \pm 12 \cdot 10^{-3}$  nm<sup>-1</sup>), followed by tri-C2, tri-C8, tri-C10, and tri-C18. The relatively large droplet sizes are consistent with the poor dispersion properties of Type I lipidic formulations [85].

**Table 3-2.** Hydrodynamic droplet size ( $d_H$ ) and specific surface area ( $S_s$ ) of the diluted ( $5 \cdot 10^{-2}\%$  v/v) triglyceride (TG) emulsions formed upon dispersion of equimolar amounts of oil in the digestion buffer after the equilibration period, prior to enzyme addition (mean  $\pm$  SD,  $n \geq 8$ ). One way ANOVA followed by post hoc Tukey–Kramer test was used for statistical analysis.

Triglyceride	$d_H$ (nm)	$S_s \cdot 10^{-3}$ (nm $^{-1}$ )
Glyceryl triacetate (tri-C2)	$138 \pm 4^a$	$436 \pm 12^a$
Glyceryl tributyrate (tri-C4)	$124 \pm 6^a$	$485 \pm 25^a$
Glyceryl trioctanoate (tri-C8)	$155 \pm 7^b$	$388 \pm 19^b$
Glyceryl tridecanoate (tri-C10)	$162 \pm 7^c$	$371 \pm 17^c$
Peanut oil (tri-C18)	$189 \pm 7^a$	$318 \pm 12^a$

<sup>a</sup> Statistically significantly different from all other TGs ( $p < 0.001$ ); <sup>b</sup> Statistically significantly different from all other TGs ( $p < 0.001$ ), except for tri- C10 ( $p < 0.05$ ); <sup>c</sup> Statistically significantly different from all other TGs ( $p < 0.001$ ), except for tri- C8 ( $p < 0.05$ ). (Reprinted from Ref. [53], under the terms of CC BY, 2015)

### 3.4. Discussion

In this work, the extent of lipolysis of lipidic Type I formulations, based on TGs, has been evaluated by means of an *in vitro* lipolysis model, to better understand the specificity behind pancreatic lipase activity. The assessment of the lipolysis process by direct titration at pH 6.80 showed there are significant differences in the pH–time profiles (**Figure 3-1**) and the amount of titrant consumed (**Figure 3-2**) for each TG. In addition and in agreement with previous studies, there is also more extensive lipolysis (**Figure 3-3**) of medium–chain TGs by pancreatic lipase when compared with long–chain TGs. Most of previous *in vitro* lipolysis reports have compared formulations with the same volume [217] or same mass [49, 123, 182, 203, 218] of lipid. However, to compare pancreatic lipase activity on different TG substrates, the assessment is more informative mechanistically when performed with equimolar amounts as reported here.

Another consideration in the experimental procedure is that the lipolysis of Type I formulations, results in lipolytic products that have a low degree of ionisation at physiologically relevant pH (e.g. pH 6.80). Some authors [121, 182, 217, 218, 223–225] have partially resolved this, by performing back–titrations and defining a correction factor to determine the real extent of lipolysis. In the light of this, back–titration experiments were undertaken at pH 11.50,

immediately after direct titrations had been performed. The pH value of 11.50 was chosen to guarantee both complete FA ionisation and pancreatic lipase inhibition [199].

For tri-C2, the apparent extent of lipolysis was approximately 33%. This value suggests that only triglycerides were hydrolysed. However, back-titration results indicate 66% of the lipolysis extent was underestimated and thus diglycerides and MGs were lipolysed as well. Similarly, the calculated extent of lipolysis at pH 6.80 of tri-C4 was 66%, indicating that all TGs and diglycerides were lipolysed. Subsequent titrations at pH 11.50 revealed that 33% of the extent of the process had been underestimated in direct titrations. Interestingly, pKa values of acetic and butyric acid are 4.74 and 4.82 [226] respectively, and therefore all acid molecules should have been ionised at pH 6.80. However, it has been suggested previously that the apparent pKa of FAs within the aqueous micellar solution is higher than that calculated in standard conditions [182], which could explain the incomplete ionisation. Another possible explanation for this phenomenon is that the lipase was still active, and therefore catalysed the release of one more FA during the time taken (60 s) for the increase of pH levels from 6.80 to 11.50.

For tri-C8 the apparent extent of lipolysis calculated indirectly from the NaOH volume data showed that almost complete hydrolysis was achieved. **Figure 3-2C** shows that for tri-C8 the apparent extent of the lipolysis-time profile is characterised by two distinct slopes, i.e. two different lipolysis rates. The inflection point of this graph falls almost exactly at the 66% value of the lipolysis extent. It could be assumed that the first part of the profile (from 0% to 66%) represents the lipolysis of TGs and diglycerides, and the second part of the profile (the remaining 33%) represents the isomerisation of 2-MG to 1/3-MG and subsequent lipolysis to glycerol and one FA. It is conceivable that the second stage of the process (characterised by the least steep slope) was the slowest, since it involved two steps (isomerisation and hydrolysis), and because the affinity of pancreatic lipase towards monoglycerides is lower than towards TGs and diglycerides [216]. Back-titration data demonstrated that almost all released FAs during the lipolysis of tri-C8 were ionised at  $\text{pH } 6.80 \pm 0.05$ , which is in agreement with the pKa of octanoic acid: 4.89 [226].

Back-titration results for tri-C10 revealed that the total extent of hydrolysis was around 66%; thus, pancreatic lipase catalysed the lipolysis of all TGs and diglycerides, but not monoglycerides.



Although the pKa of decanoic acid (4.90 [217]) is higher than that of octanoic acid, the unionised to ionised FA ratio (~0.5) did not follow theoretically predicted values. However, similar results have been found in other laboratories. Williams *et al.* [182] reported a ratio of 0.43 after the lipolysis of a mixture of tri-C8 and tri-C10 at pH 6.5. Likewise, Fernandez *et al.* [223] determined a ratio of 0.33 while assessing the lipolysis of Gelucire® 44/14 (dodecanoyl polyoxyl-32 glycerides) at different pH values.

Finally, the total extent of lipolysis of LCT tri-C18 indicates that lipase acted on half of the TGs to release two FAs per one molecule of tri-C18. In this case the incomplete ionisation of oleic acid at pH 6.80 was expected since its pKa is 9.85 [117]. Accordingly, around 20% of the extent of the process was undetected by direct titration.

Overall, the trend in extent of lipolysis, and thus lipase activity (tri-C2, tri-C4, tri-C8 > tri-C10 > tri-C18) correlates with results observed by the only two other authors who have undertaken these equimolar lipolysis comparisons. Firstly, Dicklin *et al.* [227] incubated the TGs with pancreatic tissue homogenate for a fixed period of time without titrating the released FAs. In this study, no statistical differences were found among the specific activities that porcine pancreatic tissue homogenates showed towards tri-C4, tri-C6 (glyceryl trihexanoate) and tri-C8, although they were all higher than the lipase activity demonstrated by tri-C10. While, Ciuffreda *et al.* [118] assessed the *in vitro* lipolysis of different TGs by direct titration at pH 8 and reported an ascending order of lipase activity from tri-C18 and tri-C10 to tri-C4, but no lipolytic activity was detected for tri-C2.

A theory as to the increased pancreatic lipase activity for the shorter TG chain lengths could be explained based on a two-step process as described by Lengsfeld *et al.* [198], whereby adsorption at the oil-water interface is followed by a catalysis reaction. Therefore, substrate specificity of lipase could arise from any of these two steps, and could be due to the ability of the lipase to adsorb at the interface, as well as to the chemical affinity the binding site shows towards the TG acyl chain.

Binding site affinity could explain the lower activity observed for tri-C10 and tri-C18 when compared to tri-C2, tri-C4 and tri-C8. X-ray crystallographic studies have shown that the active site of pancreatic lipase is formed by three residues: serine 153 (Ser153), histidine 264 (His264) and aspartate 177 (Asp177) [197].

The catalytic triad is pulled together through hydrogen bonds between the hydroxyl group of Ser153 and one imidazole nitrogen of His264, and between the other imidazole nitrogen and the carboxylic group of Asp177 (**Figure 3-4**). It is under this conformation that the hydrolysis reaction can take place. The hydroxyl group of Ser153 is thought to initiate the reaction through a nucleophilic attack to the first (or third) glyceryl carbon, with the fatty carboxylate being the leaving group [228]. Consequently, the reaction would become faster the more electrophilic the glyceryl carbon is and the better leaving group (more stable) the carboxylate is. In terms of electrophilicity, all TGs are analogous. However, in terms of the leaving group, carboxylates of shorter chain length are better candidates (the stronger the acid, the weaker the conjugate base, the better the leaving group), and accordingly tri-C2, tri-C4 and tri-C8 were lipolysed to the greatest extent.

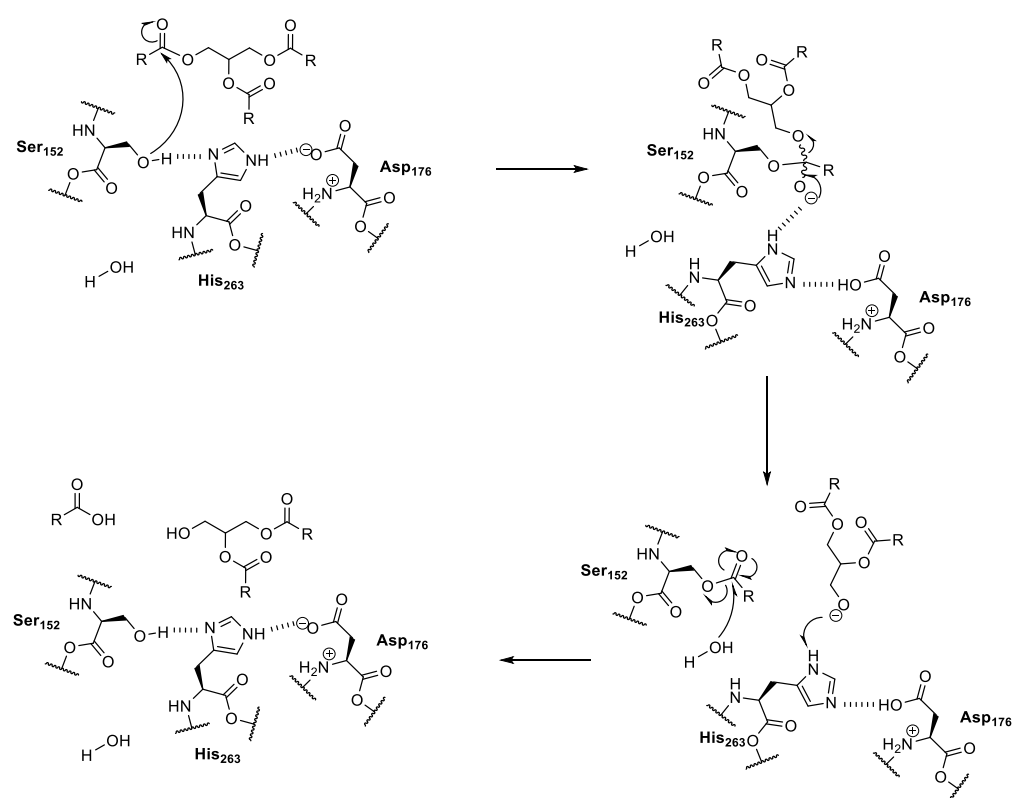


**Figure 3-4.** Proposed molecular mechanism of triglyceride lipolysis by pancreatic lipase focused on the catalytic triad. (Reprinted from Ref. [53], under the terms of the CC BY, 2016)

Regarding the lipase adsorption to the interface, the difference in activity could be attributed to the size of the oil droplets and/or to the inhibitory effects of the lipolysis products. Since pancreatic lipase carries out interfacial catalysis, the higher the substrate surface area, the more

extensive the lipolysis becomes. Therefore, in theory, the TGs with smaller oil droplets, are supposed to be lipolysed to a greater extent. Indeed, results derived from DLS measurements showed that those triglycerides that were lipolysed to a greater extent (tri-C2, tri-C4, and tri-C8) were also characterised by greater specific surface areas (**Table 3-2**).

Alternatively, the lipolysis process could be inhibited by the interfacial activity of amphiphiles such as diglycerides, unionised FAs and, mainly, 2-MGs [229–231]. Unless incorporated within mixed micelles, 2-MGs could form a layer at the droplet surface that efficiently blocks the access of the lipase [231]. Therefore, it could be hypothesised that 2-MGs derived from tri-C10 and tri-C18 are the least solubilised and inhibited the process to a greater extent.

In summary, the results suggest that there is a specific chain length range (C2–C8) for which pancreatic lipase shows higher activity. We hypothesise that this specificity could result from a combination of physicochemical properties of TGs, 2-MGs and FAs, namely the droplet size of the TGs, the solubility of 2-MGs within mixed micelles, and the relative stability of the FAs as leaving groups in the hydrolysis reaction.

### 3.5. Conclusions

In these studies, the *in vitro* lipolysis by pancreatic lipase under bio-relevant conditions at physiological pH of equimolar amounts of TGs with different chain lengths has been evaluated for the first time. The assessment of the process by direct titration at pH 6.80 showed there are significant differences in the pH–time profiles and the amount of titrant consumed for each TG. The combined results of direct and back–titration studies proved there is a specific chain length range (C2–C8) for which pancreatic lipase showed higher activity. Based on the obtained results, it is hypothesised that the specific surface area of the dispersed oil droplets, the solubility of 2-MGs within mixed micelles, and the relative stability of the FAs as leaving groups in the hydrolysis reaction, are the physicochemical properties which could determine the total extent of lipolysis.

Pharmaceutical scientists may consider the extent of digestibility as an additional factor for excipient selection. LCTs may be preferred as their solubilisation capacity is high and have the

potential of increase lymphatic transport. However, since they are slowly and not fully digested, the transfer of drug from the oil droplet to the mixed micelles might be delayed and thus incomplete. SCTs are quickly hydrolysed and therefore the co-administered drug is promptly released. Withal, the solubilisation capacity of their associated micelles is limited, hence the chance for drug precipitation is high. Therefore, the selection of MCTs might be the best option as they are fully digested and their solubilisation capacity is significant.

## **Chapter 4: Estimation of the Fraction**

### **Absorbed of BCS II Drugs in Lipidic**

### **Formulations by *In Vitro* Lipolysis**

#### **4.1. Introduction**

The Biopharmaceutics Classification System (BCS) recognises that drug dissolution and gastrointestinal permeability are the fundamental parameters controlling the rate and the extent of drug absorption. Accordingly, pharmaceutical scientist try to find tools to reliably correlate *in vitro* drug product dissolution and *in vivo* drug performance [9]. Through the successful development and application of *in vitro in vivo* correlations (IVIVC), *in vivo* drug performance can be predicted from its *in vitro* behavior. If successful, IVIVCs can provide a surrogate for bioequivalence studies, improve product quality, and reduce regulatory burdens [232]. Several studies on different levels of IVIVC have been reported in the literature. As an example, Amann *et al.* [233] worked with poly(lactic-co-glycolic) acid implants of risperidone, and obtained a good correlation ( $R^2 = 0.96$ ) between the *in vitro* mean dissolution time (assessed with a USP apparatus) and the *in vivo* mean residence time in rats. As another example, Buch and colleagues [234] combined permeability values (determined with dialysis membranes) and extent of solubilisation data (obtained by using a paddle USP apparatus) of fenofibrate immediate release tablets and related them to the  $C_{\max}$  (maximum plasma concentrations) values gathered from two human studies.

*In vitro* lipolysis digestion methods have been proposed in previous studies as a means to select appropriate lipid vehicles and to rationalise formulation design [63, 103, 235]. Later on, *in vitro* lipolysis studies started focusing on drug solubilisation and distribution across lipolysis phases during lipid digestion. These studies revealed the importance of the lipid component in the formulation to enhance drug absorption, and used the model as a qualitative tool to rank-order the performance of lipidic formulations (LFs) [104, 123, 124, 203, 236]. This was done by correlating the percentage of drug solubilised in the micellar phase with the area under the

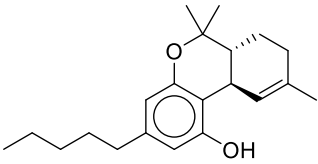
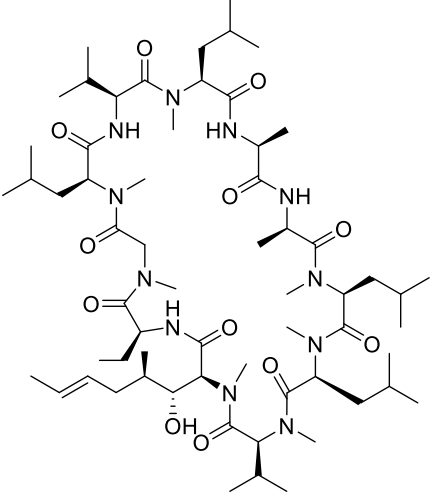
plasma concentration–time curve or the maximum concentration obtained after oral administration of the tested LF to animals. To the best of this author’s knowledge there are no publications describing the correlation between *in vitro* lipolysis data of LFs and drug exposure in humans. The ability of the *in vitro* lipolysis model to predict the actual *in vivo* performance of LFs in humans remains unknown, thus studies that assess IVIVCs are highly needed.

The first aim of the work described in this chapter was to evaluate the solubilisation and distribution across lipolysis phases of two BCS class II drugs, by means of an *in vitro* lipolysis model. The second aim was to propose the fraction of absorbed dose values by using the drug concentration data found in the micellar phase. The last objective consisted in assessing the usefulness of *in vitro* lipolysis for quantitative estimations by comparing the *in vitro* results with *in vivo* bioavailability data, obtained following oral administration of the tested formulations to humans (reported in previously published clinical studies).

Despite entering the market place in 1981, ten years ago oral LFs were still outnumbered 25 to 1 by more “conventional” formulations, and only represented 3% of the total marketed oral formulations (at least in United Kingdom, USA, and Japan) [6, 237]. The small number of commercially available oral LFs considerably reduced the number of model BCS class II drugs suitable for our purposes. Eventually,  $\Delta^9$ -tetrahydrocannabinol (THC) and cyclosporine A (CsA) (**Table 4-1**) were selected for this investigation. THC is an orally active cannabinoid which has complex effects on the central nervous system. THC is a highly lipophilic and poorly water soluble () marketed under the brand name Marinol®. Marinol® is approved for the treatment of anorexia in AIDS patients, as well as for refractory nausea and vomiting in patients undergoing chemotherapy. Marinol® contains dronabinol (synthetic THC) dissolved in sesame oil [238]. CsA acts as an immunosuppressant drug and is broadly used to prevent graft rejection in organ transplantation patients, and for the treatment of severe arthritis and psoriasis, among other indications [239]. CsA is characterised by moderately high lipophilicity, very low solubility in aqueous media, and it is commercialised mainly as Sandimmun Neoral®, a lipid-based self-emulsifying drug delivery system (SEDDS) of CsA. Five published clinical studies were selected as a set of clinical data for the purpose of estimating the human oral bioavailability of THC in Marinol® and CsA in Neoral® [240–244]. The selection process of model LFs and associated

clinical data for the future validation of the *in vitro* lipolysis/metabolism approach will be described. The observed human oral bioavailability of the model LFs was calculated by performing a non-compartmental analysis (NCA) of the pharmacokinetic (PK) data provided in the selected published clinical studies.

**Table 4-1.** Physicochemical properties of  $\Delta^9$ -tetrahydrocannabinol (THC) and cyclosporin A (CsA), and formulation details of Marinol® and Neoral®,

	THC	CsA
<b>Chemical structure</b>		
<b>Molecular formula</b>	C <sub>21</sub> H <sub>30</sub> O <sub>2</sub>	C <sub>62</sub> H <sub>111</sub> N <sub>11</sub> O <sub>12</sub>
<b>Molecular weight</b>	314.47 g/mol	1202.64 g/mol
<b>logP</b>	6.97 [245]	3.35 [245]
<b>Water solubility</b>	0.77-2.8 µg/mL [246]	5 ± 2 µg/mL [247]
<b>pKa</b>	10.17 (acid) [248]	10.3 (acid) [248]
<b>Effective permeability</b>	7.56·10 <sup>-4</sup> cm/s [248]	1.65·10 <sup>-4</sup> cm/s [249]
<b>Lipidic formulation</b>	<b>Marinol®</b>	<b>Neoral®</b>
<b>Dose</b>	2.5, 5 and 10 mg [238]	10, 25, 50, and 100 mg [239]
<b>Composition per capsule</b>	250 µL of sesame oil [238]	1 mL of propylene glycol, Kolliphor® RH40, ethanol, mono-, di-, and triglycerides of corn oil, and α-tocopherol [239]

## 4.2. Materials and Methods

### 4.2.1. Materials

Reagents and solvents used for experimentation were the same as those listed in chapter 2, section 2.2.1. Additional utilised reagents were those listed as follows;  $\alpha$ -tocopherol and Kolliphor® RH40 were purchased from Sigma–Aldrich (Dorset, UK). Vitamin D<sub>3</sub> (VitD<sub>3</sub>, 98% w/w) was obtained from Alfa Aesar (Heysham, UK). Sesame oil and corn oil were purchased from Acros Organics (Geel, Belgium). Dronabinol (synthetic THC), and CsA were products from THC Pharm GmbH (Frankfurt, Germany) and Kemprotec Ltd. (Carnforth, UK), respectively. Cannabidiol (CBD) was kindly donated by GW Pharmaceuticals (Cambridge, UK). Propylene glycol (PG) was purchased from Amresco (Ohio, USA).

### 4.2.2. Lipidic formulations, clinical data, and PK analysis

#### 4.2.2.1. Selection of lipidic formulations and associated clinical data

The selection of model formulations was performed based on availability of published clinical data. An exhaustive search of the literature was performed in order to find publications which would provide the necessary information to accurately reproduce the *in vivo* digestion of the LF using the *in vitro* model. The studies were chosen based on the following criteria:

- a) Volunteers had to be dosed in the fasted state because *in vitro* lipolysis experimental medium consists of simulated intestinal fluids in the fasted state.
- b) Volunteers had to be healthy (no history of renal, hepatic or gastrointestinal diseases) adults (18 to 55 years old), to make sure no additional factors would affect the ADME (absorption, distribution, metabolism, and excretion) properties of the drug. It is known that the age of treated subject represents an additional factor affecting the solubility of drugs. It has been estimated that around 10% of individuals over 65 years of age have a gastric pH greater than pH 6 in the fasted state [250]. Apart from physiological factors, disease states may affect the solubilising capacity in the gastrointestinal tract. As an example, subjects suffering from HIV tend to have a higher gastric pH [251], whereas cystic fibrosis patients have a lower pH [252]. Furthermore, gastric pH can be influenced by concomitant treatment with other drugs [253].



- c) Availability of clear information about the exact amount of lipidic formulation administered since a defined amount of formulation had to be dispersed in the *in vitro* lipolysis medium.
- d) Availability of relevant PK data for a single oral dose, and following intravenous (IV) administration.

The list of selected commercially available oral LFs in the United States, United Kingdom and Japan, collected by Strickley [237], was used as starting point for screening LFs. Some LFs were not considered because sales had been discontinued (Fortovase®, saquinavir [254]), because more than one active pharmaceutical ingredient was included in the medicine (Kaletra®, lopinavir and ritonavir [255]), or because they were extended-release drug products (Ketas®, ibudilast [256]; MXL® capsules, morphine sulphate [257]; and Detrol® LA, tolterodine tartrate [258]). Most of the LFs containing antivirals and antineoplastics were rejected mainly due to available trials referring to non-healthy volunteers, such as HIV patients (Agenerase®, amprenavir [259]; Norvir®, ritonavir [260]; Aptivus®, tipranavir [261]; and Sustiva®, efavirenz [262]) and cancer patients (Targretin®, bexarotene [263]). Other LFs were discarded due to unavailable (Epadel®, ethyl icosapentate; and Fenogal®, fenofibrate), or very limited (Avodart®, dutasteride [264]; and Infree® S capsules, indomethacin farnesyl [265]) oral PK data for single oral doses. Some LFs were rejected because clinical trials included volunteers in the fed state, and/or it was not indicated whether the administered formulation was actually a lipidic one (Juvela N®, tocopherol nicotinate [266]; Selbex®, teprenone [267]; Accutane®, isotretinoin [268]; and Rapamune®, sirolimus [269]). If only one single valid study could be found, the LFs were not taken into account either (Depakene®, valproic acid [270]; Cipro®, ciprofloxacin [271]; Glakay® capsules, menatetrenone [272]; Vesanoïd®, tretinoin [273]; Prometrium®, progesterone [274]; and Hectorol®, doxercalciferol [275]). The LFs of testosterone undecanoate (Andriol® and Restanol®) were discarded as well because the stability of this ester prodrug in the gastrointestinal tract remains unknown.

Eventually, five medicines were short-listed: Marinol® (THC) [240, 241, 276–280], One-Alpha® capsules (alfacalcidol) [281, 282], Rocaltrol® (calcitriol) [282, 283], Heminevrin® (clomethiazole edisilate) [284, 285], and Neoral® (CsA) [138, 242–244, 286–290]. Marinol® (sesame oil), One-Alpha® capsules (sesame oil and  $\alpha$ -tocopherol), Rocaltrol® (fractionated triglycerides of coconut oil or palm oil) and Heminevrin® (fractionated coconut oil) are all Type

I lipidic formulations, whereas Neoral® is a self-emulsifying drug delivery system (SEDDS) consisting of lipids, surfactants and co-solvents (Type IIIA). For the sake of formulation diversity, it was decided to select one Type I formulation (Marinol®, already available in the laboratory), and one Type III (Neoral®).

The clinical studies of the selected LFs were narrowed down further according to the inclusion/exclusion criteria explained above. In the case of Neoral®, numerous studies were rejected because of one of the following reasons: the trials were not performed in healthy volunteers, or were usually conducted in organ transplant patients [287], or the impossibility of confirming whether the administered formulation was actually Neoral® [138, 288, 289], or the impossibility of purchasing the administered dose strength (i.e. 60 mg capsules are not commercially available in UK) [286, 290]. In the case of Marinol®, some studies were not considered because the volunteers were not healthy (cancer patients [276]), because the fed/fasted state of the subjects was not indicated [280], and because of incomplete information about the formulation, such as the volume of co-administered oil [277, 278], or the dose strength of the capsules [279].

Finally, it was possible to select five published clinical studies that described oral administration of THC and CsA and that fulfil the eligibility criteria described above. In the case of Marinol®, the studies described the administration of: (a) 2 × 10 mg capsules (20 mg THC in ~0.5 mL sesame oil) [240], and (b) 1 × 10 mg capsule (10 mg THC in ~0.25 mL sesame oil) [241]. Regarding Neoral®, the studies described the administration of: (a) 2 × 100 mg capsules (200 mg CsA in 2 mL SEDDS) [242, 243], (b) 3 × 100 mg capsules (300 mg CsA in 3 mL SEDDS) [244], and (c) 6 × 100 mg capsules (600 mg CsA in 6 mL SEDDS) [242]. Publications detailing the intravenous administration of THC [280, 291–294] and CsA [138, 295] were collected also to calculate the absolute  $F_{\text{observed}}$ . One of THC studies included frequent Cannabis users [293], which might affect THC PK parameters, such as CL due to induction of metabolism. However, no statistical significant differences were found in the PKs between the users and non-users groups, and thus it was decided to include this data.

#### 4.2.2.2. PK analysis

PK variables for the selected model drugs were collected from the associated published clinical studies. These parameters were as follows: terminal half-life ( $t_{1/2,z}$ ), volume of distribution at the terminal phase ( $V_z$ ) and at the steady-state ( $V_{ss}$ ), maximum plasma (or blood) concentration ( $C_{max}$ ), time at which  $C_{max}$  occurs ( $t_{max}$ ), clearance (CL), and area under the plasma concentration–time curve (AUC) from time zero to the last measurable concentration point ( $AUC_t$ ), and extrapolated to the infinity ( $AUC_{\infty}$ ). When such PK data were not available in the manuscripts, plasma (or blood) concentration–time profiles were extracted using an online tool, WebPlotDigitizer [296], as others researchers have previously done [297–299]. Subsequently, PK parameters were calculated using a NCA in Phoenix WinNonlin® 6.3 (Pharsight, Mountain View, CA, USA). The AUC values were estimated by using the linear and logarithm trapezoidal rules, in the rising and declining phases of drug concentration, respectively. The terminal phase half-life was estimated from at least three of the last measurable concentrations following  $C_{max}$ .  $C_{max}$  and  $t_{max}$  values were derived directly from the profiles. The  $F_{observed}$  values were estimated from the ratio of the  $AUC_{\infty}$  normalised by the dose after IV and oral dosing (**Equation 1-1**). The fraction of drug dose escaping hepatic metabolism ( $F_h$ ) was calculated from the CL values, assuming the compounds are strictly metabolised by the liver when administered intravenously. When plasma CL values were given/calculated, they were transformed into blood CL through the blood to plasma drug concentration ratio (B/P). The combined fractions of the absorbed drug dose and non-metabolised in the gut ( $F_{abs} \cdot F_g$ ) were derived from the estimated  $F_{observed}$  and  $F_h$  values.

#### 4.2.3. Composition and preparation of blank lipidic formulations

Blank formulations mimicking the excipient composition of Marinol® and Neoral®, but lacking the active pharmaceutical ingredients, were prepared and lipolysed in order to generate matrixes from which appropriate calibration curves were constructed. The Marinol® blank formulation consisted of plain sesame oil [238]. The exact composition of Neoral® is not fully disclosed [239], hence some approximations had to be made. Based on available information, and assuming a standard amount of  $\alpha$ -tocopherol of 2.5 mg per unit dose [300], it was calculated that one 100 mg/mL Neoral® capsule contains, in addition to 100 mg CsA, the

following excipients: 100 mg PG, 405 mg Kolliphor® RH40, 0.119 mL ethanol, and 0.35 mL mono-, di-, and triglycerides of corn oil. These specified amounts of excipients were mixed under constant stirring at 37 °C, and stored at room temperature until used.

#### 4.2.4. *In vitro* lipolysis studies

##### 4.2.4.1. Scaling down from *in vivo* to *in vitro* conditions

It has been suggested [301] that for the assessment of the mass of soluble drug in the small intestine an *in vivo* dissolution volume of 80 to 100 mL, rather than the classic 250 mL, would be more accurate. In the current work, it was decided to follow both approaches, and preliminary studies with the Marinol® formulation were done assuming 250 and 100 mL for the *in vivo* dissolution volume. Based on the obtained results, it was decided later on to continue only with the 100 mL approach in the Neoral® studies.

The digestion medium of the *in vitro* lipolysis model consists of approximately 40 mL. Therefore, the amount of formulation corresponding to each clinical study was scaled down accordingly to match the *in vivo* situation, as indicated in **Equation 4-1**:

$$\text{Formulation volume in vitro} = \frac{40 \text{ mL} \cdot \text{Formulation volume in vivo}}{250 \text{ or } 100 \text{ mL}} \quad \text{Equation 4-1}$$

The calculated proportional amounts are summarised in **Table 4-2**.

**Table 4-2.** Scaled amounts of lipidic formulation (Marinol® and Neoral®) dispersed in the *in vitro* lipolysis model (~40 mL) calculated from the quantities administered *in vivo*, according to **Equation 4-1**, assuming different *in vivo* dissolution volumes.

	<i>In vivo</i> dissolution volume (mL)	<i>Formulation in vivo</i>		<i>Formulation in vitro</i>	
		Volume (mL)	Amount of drug (mg)	Volume (mL)	Amount of drug (mg)
Marinol® (THC)	250	0.5	20	0.08	3.2
		0.25	10	0.04	1.6
	100	0.5	20	0.2	8
		0.25	10	0.1	4
Neoral® (CsA)	100	2	200	0.8	80
		3	300	1.2	120
		6	600	2.4	240

THC: Δ<sup>9</sup>-tetrahydrocannabinol; CsA: cyclosporin A

## 4.2.4.2. Simulated intestinal buffers

The effect of the surfactant (bile salts and phospholipids) composition on the *in vitro* digestion of the lipidic formulations was assessed by using two different intestinal fluid compositions simulating the contents of the jejunum in the fasted state (**Table 4-3**). The composition of these digestion media differed in the concentration of sodium taurocholate (bile salt, BS) and phosphatidylcholine (phospholipid, PL). The “classical” buffer, which was used during the experimentation described in Chapters 2 and 3, was analogous to those previously used by other lipolysis research groups [53, 104, 105, 203, 302, 303], and consisted of higher concentrations of surfactants in a proportion 4:1 BS/PL. On the other hand, the “new” buffer, was closer to Fasted-State Simulated Intestinal Fluid-version 2 (FaSSIF-V2) and human physiological conditions, and therefore contained lower surfactant concentrations (3 mM and 0.2 mM BS and PL concentration, respectively) in a ratio 15:1 BS/PL [95].

**Table 4-3.** Comparison of the two different lipolysis media used for the intraluminal processing of Marinol® and Neoral®.

		Classical	New
Concentration (mM)	Trizma® maleate	50	
	Sodium chloride	150	
	Calcium chloride	2	
	Sodium taurocholate	5	3
	Phosphatidylcholine	0.75	0.2
Bile salt to Phospholipid ratio		4:1	15:1

(Adapted from Ref. [304] under the terms of CC BY, 2016)

## 4.2.4.3. Experimental procedure

The experimental conditions described in Chapter 2, section 2.2.6 were followed to investigate the lipolysis of the calculated formulation volumes (**Table 4-2**). The set of conditions (1 M NaOH titrant concentration, and maximum (3.5 mL/min) and minimum (3 µL/min) rates of titrant addition) optimised in Chapter 2 were set up through the instrument control software. The experiments were considered to be completed when the dosing rate of NaOH was lower than 3 µL/min. Each experiment was repeated six times.

Once the lipolysis process was finished, the resulting reaction mixtures were collected in ultra-centrifuge tubes (Beckman Coulter, High Wycombe, UK) for subsequent density gradient separation. The mixtures were ultra-centrifuged (Sorvall Discovery 100SE centrifuge, TH-641 rotor, Thermo Scientific, North Carolina, USA) at  $\sim 197000\text{ g}$  and  $37\text{ }^{\circ}\text{C}$  for 90 minutes. After centrifugation, phases were separated, collected (sediment was re-suspended in water) and stored at  $-80\text{ }^{\circ}\text{C}$  until drug content analysis. The volume recovered for each phase was recorded to determine the drug content.

#### 4.2.5. HPLC–UV analysis

##### 4.2.5.1. Sample preparation

Lipolysis and calibration curve samples were prepared for HPLC–UV (ultraviolet) analysis by liquid–liquid extraction. The procedure for THC samples was similar to that developed by Zgair *et al.* [305], with some modifications. The changes consisted in choosing a different internal standard (VitD<sub>3</sub> instead of probucol) and using 200  $\mu\text{L}$  (or 50  $\mu\text{L}$ ) of sample volume instead of 150  $\mu\text{L}$ . Aliquots of 200  $\mu\text{L}$  of MP and SP (or 50  $\mu\text{L}$  of LP) were mixed with 60  $\mu\text{L}$  of 350  $\mu\text{g/mL}$  VitD<sub>3</sub> in acetonitrile, and vortex-mixed for 2 minutes. Subsequently, 600  $\mu\text{L}$  (or 150  $\mu\text{L}$  for LP) of ice-cold acetonitrile was added, and samples were vortex-mixed for 2 minutes. Six hundred microliters of water was added, and samples were vortex-mixed again for another 2 minutes. Next, 3 mL (or 1.5 mL of LP) of *n*-hexane was added, and samples were vortex-mixed for 5 minutes. After centrifugation at  $\sim 1200\text{ g}$  (Harrier 18/80 centrifuge, swing-out rotor, MSE, London, UK) for 15 min at room temperature, the upper organic layer was transferred to a fresh glass tube and evaporated under a gentle stream of nitrogen gas at  $35\text{ }^{\circ}\text{C}$  (Techne Dri-Block Sample Concentrator, Cambridge, UK). Residues were reconstituted in 200  $\mu\text{L}$  (or 750  $\mu\text{L}$ ) of acetonitrile, and 10  $\mu\text{L}$  was injected into the HPLC system.

The sample treatment of CsA lipolysis samples was similar to that of THC samples. Exceptions were the use of a different initial sample volume (100  $\mu\text{L}$ ), internal standard type, concentration and volume (10  $\mu\text{L}$  of 2  $\text{mg/mL}$  CBD in acetonitrile), extraction solvent type and volume (1.5 mL methyl *tert*-butyl ether), and the volume of solvent added to reconstitute the residue (1000  $\mu\text{L}$ ).

## 4.2.5.2. Chromatographic conditions

The quantitative determination of THC, CsA and corresponding internal standards, was performed using a HPLC system (Waters Alliance 2695, Waters Corporation, Milford, MA, USA) equipped with a photodiode array UV detector (Waters 996, Waters Corp.). Sample temperature was controlled by a fitted chiller at 4 °C. THC and VitD<sub>3</sub> were detected at 220 nm, whereas CsA and CBD were monitored at 211 nm. Separations were achieved using a Sonoma C18(2) 100 x 2.1 mm, 3 µm particle size column (ES Industries, West Berlin, NJ, USA), protected by a Phenomex C18 4 x 2 mm guard cartridge (Phenomenex, Macclesfield, UK). Mobile phases were a mixture of acetonitrile and water in a ratio of 75:25 and 65:35 (v/v), for THC and CsA determination, respectively. The flow rate was set at 0.3 mL/min for 40 minutes at 55 °C, and for 12 minutes at 60 °C, for THC and CsA determination, respectively. Data acquisitions and processing was carried out using Empower™ 2 software (Waters Corp.).

## 4.2.5.3. Method validation

Partial validation of THC and CsA quantitative determinations was performed in accordance with the European Medicines Agency (EMA) and the American FDA Guidelines on bioanalytical method validation [306–308]. Accuracy and precision were expressed as relative error (RE, **Equation 4-2**) and relative standard deviation (RSD, **Equation 4-3**), respectively:

$$RE(\%) = \frac{|\Delta x|}{x} = \frac{|x_{\text{calc}} - x_{\text{nom}}|}{x_{\text{nom}}} \cdot 100 \quad \text{Equation 4-2}$$

$$RSD(\%) = \frac{s_x}{\bar{x}} \cdot 100 \quad \text{Equation 4-3}$$

where  $|\Delta x|$  is the absolute error,  $x_{\text{calc}}$  is the regressed concentration computed from the calibration curve,  $x_{\text{nom}}$  is the nominal standard concentration, and  $s_x$  and  $\bar{x}$  are the standard deviation and average of all  $x_{\text{calc}}$  for a certain concentration, respectively. A method is considered to be accurate and precise if RE and RSD values are  $\leq 15\%$ , except for low limit of quantification (LLOQ), where it should not exceed more than 20%. Intra-day accuracy and precision were determined by analysing six replicates of the same sample batch at concentrations of low, medium and high quality control samples (LQC, MQC and HQC). Inter-day accuracy and precision were calculated by analysing those same concentrations in six different sample batches.

Calibration curves were constructed using a weighting factor of  $1/x^2$ , except for that corresponding to CsA in the SP, for which statistical analysis showed that curve-weighting was not appropriate [309]. Calibration curves consisted of a blank sample (matrix sample processed without internal standard), a zero sample (matrix sample processed with internal standard), and at least six non-zero samples covering the expected concentration range, and meeting the above criteria with regards to RE and RSD values.

#### 4.2.6. Calculation of the predicted fraction absorbed ( $F_{abs}$ )

Following oral administration, drug solubilisation in the intestinal milieu is a prerequisite for the absorption process. Therefore, drug molecules solubilised in the micellar phase of the lipolysis medium are thought to be most readily available for absorption. By contrast, drug molecules in the sediment and lipid phase are not expected to be available for absorption *in vivo* conditions. Since BCS II drugs are highly permeable and lipidic formulations are thought to inhibit drug efflux transporters [310, 311], it was assumed that all the mass of THC and CsA solubilised in the micellar phase would be completely absorbed. To determine the fraction of drug absorbed ( $F_{abs}$ ), the concentration of drug found in the micellar phase ( $C_{MP}$ ) was multiplied by the *in vivo* dissolution volume assumed for scaling down doses (250 or 100 mL), and divided by the administered clinical dose, as indicated in **Equation 4-4**:

$$F_{abs} = C_{MP} \left( \frac{\text{mg}}{\text{mL}} \right) \cdot \frac{250 \text{ or } 100 \text{ mL}}{\text{Clinical dose (mg)}} \quad \text{Equation 4-4}$$

#### 4.2.7. Statistical data analysis

All presented data are expressed as mean (or weighted means, WX)  $\pm$  standard deviation (SD; or overall SD, OSD). Statistical tests detailed in Chapter 3, section 3.2.8 were also used in this chapter. Since PK data from more than one study were available for the same route of administration, weighted mean values were calculated. The overall sum of squared errors (OSSE, **Equation 4-5**) was used to estimate the OSD (**Equation 4-6**), and subsequently the coefficient of variation (CV, **Equation 4-7**).

$$\text{OSSE} = \sum_{i=1}^n [(SD_i^2 + x_i^2) \cdot n_i] - N \cdot WX^2 \quad \text{Equation 4-5}$$



$$\text{OSD} = \sqrt{\text{OSSE}/N} \quad \text{Equation 4-6}$$

$$\text{CV}(\%) = 100 \cdot \sqrt{\text{OSD}/W_X} \quad \text{Equation 4-7}$$

where  $\text{SD}_i$  is the standard deviation from each individual study [312].

A *F*-test was used to analyse the scedasticity of the HPLC–UV method validation data so as to determine whether calibration curve–weighting was needed or not. Homoscedastic data are characterised by SDs that are the same at all sample concentrations; whereas heteroscedastic data present SDs that increase with sample concentration. In the first case, curve weighting is not appropriate; but in the second case, weighting should be used to improve curve performance. Because *F*-test requires variances (SDs squared), i.e. replicates for each concentration on the standard curve, the quality control samples (with  $n = 6$ ) of intra–day analysis were used. The *F*-value ( $F_{\text{exp}}$ ) was calculated as the ratio of the variances ( $s^2$ ) for the HQC and LQC sets of data. If data resulted to be heteroscedastic, the goodness of fit for calibration curves with weighting  $1/x$  or  $1/x^2$  was compared by means of the sum of the RE (%) values, to find the smallest value, i.e., the best fit [309, 313, 314].

### 4.3. Results

#### 4.3.1. PK analysis of selected clinical data

The plasma concentration–time profiles of THC after intravenous and oral administration extracted from the selected clinical publications, are presented in appendix **Figure A-1** and **Figure A-2**, respectively. The blood concentration–time profiles of CsA are shown in appendix **Figure A-3** (intravenous) and **Figure A-4** (oral). The profile corresponding to the oral administration of six Neoral® capsules is missing as it was not provided in the published study. Appendix **Table A-1** and **Table A-2** list the PK parameters for THC and CsA, and **Table 4-4** summarises the derived bioavailability values.

**Table 4-4.** Bioavailability of selected formulations estimated from published clinical data. Absolute oral bioavailability values ( $F_{\text{observed}}$ ) were obtained following the administration of Marinol® [240, 241] and Neoral® [242–244]; hepatic bioavailability values ( $F_h$ ) were calculated from the intravenous administration of  $\Delta^9$ -tetrahydrocannabinol (THC) [280, 291–294] and cyclosporin A (CsA) [138, 295], assuming strictly liver clearance. The fraction absorbed and non-metabolised in the gut ( $F_{\text{abs}} \cdot F_g$ ) were derived from  $F_{\text{observed}}$  and  $F_h$ . Values are expressed as weighted mean  $\pm$  overall SD.

	Dose	$F_{\text{observed}}$ (%)	$F_h$ (%)	$F_{\text{abs}} \cdot F_g$ (%)
<b>Marinol®</b>	2 x 10 mg THC [240]	4.1 $\pm$ 3.6	56.9 $\pm$ 25.5	7.2 $\pm$ 7.7
	1 x 10 mg THC [241]	3.4 $\pm$ 3.8		5.9 $\pm$ 7.5
<b>Neoral®</b>	2 x 100 mg CsA [242, 243]	46.5 $\pm$ 18.1	75.5 $\pm$ 5.5	61.5 $\pm$ 27.7
	3 x 100 mg CsA [244]	41.8 $\pm$ 16.9		55.4 $\pm$ 25.5
	6 x 100 mg CsA [242]	36.6 $\pm$ 12.1		48.4 $\pm$ 19.4

Data showed high variability in PK parameters especially in case of THC. This variability could be partially due to the different analytical methods used, which included radioactivity. Oral and IV AUC values normalised by the dose are markedly different, which indicates that orally administered doses of THC and CsA do not reach the systemic circulation intact. Statistical analysis showed there was no difference ( $p=0.6144$  and  $p=0.0727$ , for THC and CsA, respectively) in the  $F_{\text{observed}}$  values among different strengths of the same formulation. Despite variability in the data, the calculated oral exposure of Neoral® (46.5  $\pm$  18.1%, 41.8  $\pm$  16.9%, and 36.6  $\pm$  12.1%, for two, three and six 100 mg capsules, respectively) was much higher than that of Marinol® (4.1  $\pm$  3.6% and 3.4  $\pm$  3.8%, for two and one 10 mg capsules, respectively).

#### 4.3.2. HPLC–UV method development and validation

Both THC and CsA detection methods showed good selectivity since matrix related peaks from blank lipolysis phases did not interfere with either analyte or corresponding internal standard (VitD<sub>3</sub> and CBD) at the detection wavelengths. Typical chromatograms corresponding to the lipolysis phases obtained following the *in vitro* enzymatic hydrolysis of Marino® and Neoral® are shown in appendix **Figure A-5** and **Figure A-6**, respectively.

For THC, the linearity of the method was confirmed over the concentration ranges of 0.005–0.350 mg/mL, 0.01–6 mg/mL, and 0.25–16 mg/mL for micellar, sediment, and lipid phases, respectively, based on least 9 concentration levels and with correlation coefficient ( $r^2$ ) values  $\geq$  0.99 in all calibration curves (appendix **Figure A-7**). In the case of CsA, the linearity of the

method was confirmed over the concentration ranges of 0.1–8 mg/mL and 0.3–1.5 mg/mL, for micellar and sediment phases, respectively, based on least 8 concentration levels and with correlation coefficient ( $r^2$ ) values  $\geq 0.99$  in all calibration curves, as well (appendix **Figure A-8**). The homoscedasticity of the data was double checked by plotting the absolute errors against the concentration (appendix **Figure A-9** and **Figure A-10**) and by performing *F*-tests (appendix **Table A-3**). In all cases, except for CsA in sediment phase, the calculated *F* value was higher than the tabulated one (5.05) [315], which confirmed the heteroscedasticity of the data and the need for calibration curve-weighting. The weighting scheme  $1/x^2$  was the chosen one as it provided the smallest  $\Sigma$  RE (%) values (appendix **Table A-3**).

The intra-day and inter-day accuracy and precision for THC and CsA in lipolysis phases were within the acceptable limits ( $\leq 15\%$ ) for all quality control samples as indicated by the RE and RSD values shown in appendix **Table A-4**. These results indicate that both THC and CsA detection methods were accurate and precise for the determination of these drugs in lipolysis phases. RE and RSE values for THC and CsA were within the acceptable limits ( $\leq 20\%$ ) at the LLOQ (appendix **Table A-4**), which were found to be 0.002 and 0.05 mg/mL for THC and CsA, respectively.

### 4.3.3. *In vitro* lipolysis

#### 4.3.3.1. Drug distribution across lipolysis phases. The effect of the assumed *in vivo* dissolution volume: 250 versus 100 mL

The intraluminal processing of Marinol® was assessed by *in vitro* lipolysis assuming two different *in vivo* dissolution volumes: 250 and 100 mL. This was done to determine the effect of the scaling factor on the overall digestion process. The total recovery of THC was  $62.0 \pm 5.5\%$ . This value is low but constant, and it is a reflection of the loss of drug during the process of lipolysis, ultracentrifugation and sample preparation, due to non-specific binding to laboratory material. The distribution of THC across micellar, sediment and lipid phases is shown in **Table 4-5**.

**Table 4-5.** Distribution of recovered drug across micellar (MP), sediment (SP) and lipid (LP) phases after the lipolysis (in the “classical” buffer) of diverse doses of Marinol® and Neoral®, assuming two different *in vivo* dissolution volumes. Values are expressed as mean ( $n = 6$ )  $\pm$  SD.

<i>In vivo</i> dissolution volume (mL)	Formulation	% drug MP	% drug SP	% drug LP
250	2 x 10 mg Marinol®	47.3 $\pm$ 3.3	10.9 $\pm$ 1.5	41.6 $\pm$ 4.2
	1 x 10 mg Marinol®	67.1 $\pm$ 3.8	14.8 $\pm$ 1.1	18.1 $\pm$ 3.9
100	2 x 10 mg Marinol®	30.7 $\pm$ 4.3	6.8 $\pm$ 1.4	62.5 $\pm$ 5.4
	1 x 10 mg Marinol®	51.0 $\pm$ 6.6	10.7 $\pm$ 1.1	38.4 $\pm$ 7.2
	2 x 100 mg Neoral®	95.0 $\pm$ 1.0	5.0 $\pm$ 1.0	N/A
	3 x 100 mg Neoral®	96.7 $\pm$ 0.5	3.3 $\pm$ 0.5	
	6 x 100 mg Neoral®	98.4 $\pm$ 0.2	1.6 $\pm$ 0.2	

Statistical analysis showed there were significant differences in the amount of drug recovered in each phase when different *in vivo* dissolution volumes were used ( $p < 0.001$ ). When higher amounts of formulation were dispersed in the model (*in vivo* dissolution volume of 100 mL), the proportion of drug solubilised in the micellar and sediment phases decreased (around 16% and 4%, respectively), whereas the amount of drug solubilised in the lipid phase increased by approximately 20%.

Assuming an *in vivo* dissolution volume of 250 mL, the concentration of THC found in the micellar phase following the lipolysis of the proportional amounts to two and one 10 mg Marinol® capsules were around 19 and 30  $\mu\text{g/mL}$ , respectively. Similarly, assuming a human dissolution volume of 100 mL, the concentrations found for two and one 10 mg Marinol® capsules were around 40 and 47  $\mu\text{g/mL}$ , respectively. These concentration values were used for the estimation of the fraction of absorbed dose values (**Equation 4-4**), which are shown in **Figure 4-1**. Again, statistical analysis showed significant differences between  $F_{\text{abs}}$  values when different *in vivo* dissolution volumes were assumed ( $p < 0.01$ ). When higher amounts of formulation were dispersed in the model (*in vivo* dissolution volume of 100 mL), the estimated  $F_{\text{abs}}$  values decreased for both doses, although this reduction was more pronounced for the digestion of one capsule (76 to 47%), compared to the digestion of two capsules (24 to 20%). The distribution of CsA across the lipolysis phases was only assessed assuming 100 mL as *in vivo* dissolution volume (**Table 4-5**). The recovery of CsA was higher than that of THC (83.8  $\pm$  2.7%), probably due to the fact of CsA being less lipophilic than the cannabinoid, and therefore

showing less tendency towards non-specific binding. After ultracentrifugation, no upper lipid phase was observed, which suggests all tri- and diglycerides in Neoral® were hydrolysed. Almost all recovered drug was present in the micellar phase ( $\geq 95\%$ ) and very little amount of CsA precipitated in the sediment phase. As expected, the CsA concentration in the micellar phase increased with the amount of dispersed lipidic formulation.

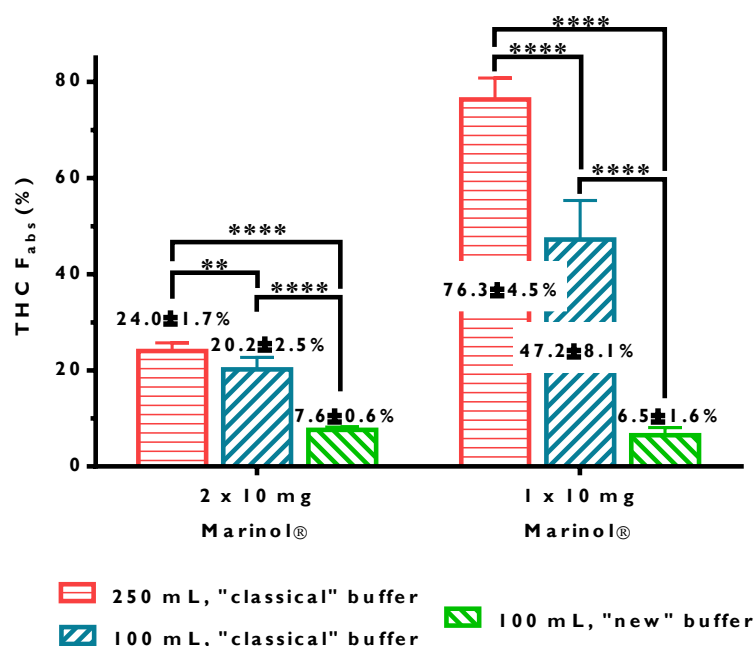


**Figure 4-1.** Fraction of absorbed dose of  $\Delta^9$ -tetrahydrocannabinol (THC) in Marinol® estimated from lipolysis studies. Coral and blue colours correspond to the lipolysis of the formulations using the "classical" buffer, assuming an *in vivo* dissolution volume of 250 mL and 100 mL, respectively. Whilst, green colours represent the lipolysis in the "new" buffer, assuming 100 mL of dissolution volume. Values are expressed as means ( $n = 6$ )  $\pm$  SD. A one-way ANOVA followed by Tukey-Kramer multiple comparison test were used for statistical analysis. Statistically significantly different: \*\*\*\*,  $p < 0.0001$ ; \*\*,  $p < 0.01$

#### 4.3.3.2. Effect of the surfactant concentrations: "classic" versus "new" buffer

The intraluminal processing of Marinol® and Neoral® was assessed by *in vitro* lipolysis using two different digestion buffers (**Table 4-3**). This was done to determine the effect of surfactant (bile salt and phospholipids) concentrations on the overall digestion process. Based on the results obtained in previous experiments, the adequate amount of LF to be dispersed in the 40 mL-volume vessel of the digestion medium was calculated assuming an *in vivo* dissolution volume of 100 mL (**Table 4-2**). According to parsimony concept, only drug concentration in the

micellar phase is considered for  $F_{abs}$  calculation (**Equation 4-4**). Hence, in these experiments only drug content in the micellar phase was determined.

When the classical buffer was used, and 200 and 100  $\mu\text{L}$  of Marinol® were digested, THC concentrations in the micellar phase were  $40 \pm 5 \mu\text{g/mL}$  and  $47 \pm 8 \mu\text{g/mL}$ , respectively. Similarly, when 800, 1200, and 2400  $\mu\text{L}$  of Neoral® were lipolysed, the concentrations of CsA in the micellar phase were  $0.926 \pm 0.012 \text{ mg/mL}$ ,  $1.692 \pm 0.066 \text{ mg/mL}$ , and  $4.709 \pm 0.156 \text{ mg/mL}$ , respectively.

When the new buffer was used instead of the classical one, the concentrations found in the micellar phase decreased for THC and increased for CsA. The concentrations for THC were  $6 \pm 2 \mu\text{g/mL}$ , and  $15 \pm 1 \mu\text{g/mL}$ , respectively for the 200 and 100  $\mu\text{L}$  of Marinol®. For CsA the concentrations were  $1.729 \pm 0.048 \text{ mg/mL}$ ,  $2.637 \pm 0.134 \text{ mg/mL}$ , and  $6.103 \pm 0.703 \text{ mg/mL}$ , following the lipolysis of 800, 1200 and 2400  $\mu\text{L}$  of Neoral®, respectively.

As previously indicated, the working hypothesis of the *in vitro* lipolysis model is that the fraction of drug dose which is solubilised in the micellar phase is most readily available for absorption. In addition, THC and CsA are highly permeable drugs, and LFs are thought to inhibit efflux mechanisms [310, 311]. Therefore, it was assumed that all the amount of THC and CsA solubilised in the micellar phase would completely permeate into the enterocytes. Accordingly, the concentration values found in the micellar phase were next introduced in **Equation 4-4** to calculate the predicted fractions of absorbed dose represented in **Figure 4-1** (THC) and **Figure 4-2** (CsA). The use of lower surfactant concentrations resulted in opposite outcomes: the fraction of THC decreased (from 20.2% and 47.2% to 7.6% and 6.5%), whereas the proportion of absorbed CsA increased (from 46.3%, 56.4% and 78.5% to 87.4%, 87.9%, and 101.7%, respectively).

Statistical analysis showed that there were significant differences ( $p < 0.01$ ) in the estimated  $F_{abs}$ , when the same volume of lipidic formulation was digested using buffers differing in the level of surfactant concentrations. It was also shown that there were significant differences in the estimated  $F_{abs}$  among different doses of the same formulation when using the classical buffer, but no statistically significant differences were detected when the new buffer was used. Exception was the high-dose of six Neoral® capsules study, which turned up to be statistically different from the other two Neoral® studies.

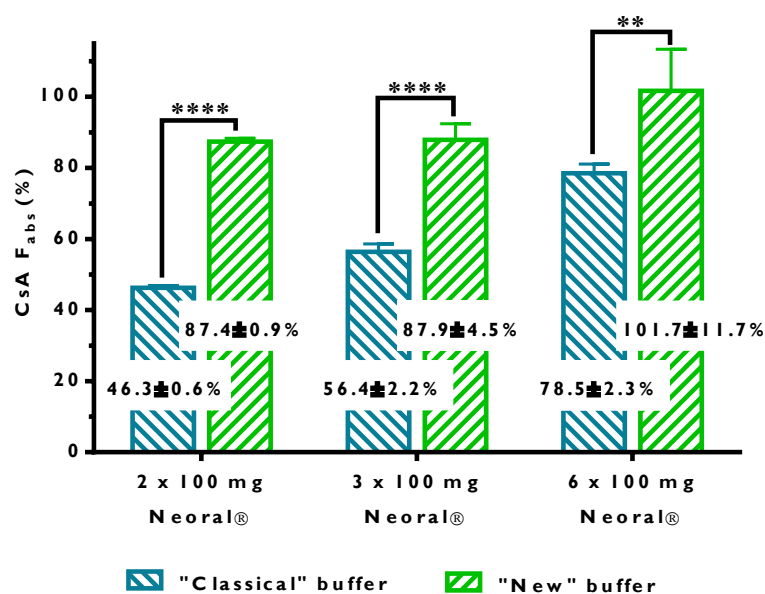


**Figure 4-2.** Fraction of absorbed dose of cyclosporin A (CsA) in Neoral® estimated from lipolysis studies assuming an *in vivo* dissolution volume of 100 mL. Blue colours correspond to the lipolysis of the formulations using the “classical” buffer; whereas green colours represent the “new” buffer. Values are expressed as means ( $n = 6$ )  $\pm$  SD. An unpaired *t*-test followed by Welch’s correction were used for statistical analysis. Statistically significantly different: \*\*\*\*,  $p < 0.0001$ ; \*\*,  $p < 0.01$ .

## 4.4. Discussion

### 4.4.1. PK analysis of selected clinical data

Due to the social stigma associated with smoking cannabis, the harm that smoke may cause, and the marked variable bioavailability when inhaled (it depends on the depth of inhalation, puff duration and breath hold), there is a tendency to administer medicinal cannabinoids orally. As such, Marinol® is approved for use in certain countries including USA or New Zealand [316]. Despite its extremely low oral bioavailability (calculated  $F_{observed}$  values were  $4.1 \pm 3.6\%$  and  $3.4 \pm 3.8$  for two and one capsules, respectively), the systemic exposure with the oral LF formulation is sufficient to produce a therapeutic effect, with only 2 to 44  $\mu\text{g}$  in the brain exerting a pharmacological response [317]). Statistical analysis showed there is no difference between the obtained  $F_{observed}$  values, which suggests Marinol® displays dose proportionality, at least in the range of doses tested. The extremely high, although very variable CL values reported here ( $\sim 9 \pm 5$  mL/min/kg) suggest that THC metabolism is limited by hepatic blood

flow [318]. These values are in accordance with previously reported values (8 and 13.3 mL/min/kg [319]).

In the case of CsA, Mueller *et al.* [242] demonstrated a linear relationship between AUC and Neoral® dose. In the present study, the analysis of the calculated  $F_{\text{observed}}$  values derived from independent clinical studies, suggested there was no statistical differences among doses, and thus confirmed Neoral®'s dose proportionality. The calculated total clearance ( $5.14 \pm 1.15$  mL/min/kg) is in agreement with previous reports [320].

#### 4.4.2. HPLC–UV method development and validation

Two HPLC–UV methods were developed and validated for the determination of THC and CsA concentration in micellar, sediment and lipid phases obtained after the *in vitro* lipolysis of their lipodic formulations (Marinol® and Neoral®, respectively) and subsequent ultra–centrifugation.

##### 4.4.2.1. HPLC–UV method development

First attempts to extract THC from lipolysis matrixes consisted in a liquid–liquid extraction method (tetrahydrofuran and *n*–hexane), based on a previous publication on lipophilic cannabinoids [79]. However, chromatographs resulting from this method showed background lipolysis peaks interfering with the THC signal. As recommended by Zgair *et al.* [305], tetrahydrofuran was substituted for ice–cold acetonitrile, which markedly decreased the size of background noise; and water was introduced in the protocol to yield cleaner spectra.

Initially, compound separation was achieved by using a Phenomenex Luna C18(2) 100 × 2.1 mm, 2 µm particle size column, a simple buffer–free solvent mixture of methanol and water in a ratio of 90:10 (v/v) as mobile phase, a flow rate of 0.2 mL/min and temperature of 35 °C. However, changing to a 3 µm particle size column, using a combination of acetonitrile and water (75:25 (v/v)) as mobile phase, and increasing the flow rate and the temperature up to 0.3 mL/min and 55 °C, respectively, provided better separation efficiency and peak shape, and shorter analysis time.

THC HPLC–UV detection method was used as starting point for the development of a method to quantify CsA in the lipolysis phases. *n*–Hexane did not extract CsA, thus other solvents were tested, such as ethyl acetate or diethyl ether, but it was *tert*–butyl ether that displayed the best



extraction efficiency. CBD was chosen as the most appropriate internal standard, based on its elution being a short time before CsA. Mobile phase solvent ratio and column temperature were optimised also to give the final instrumentation conditions described in section 4.2.5.2.

#### 4.4.2.2. HPLC–UV method validation

Lipolysis data presented acceptable  $r^2$  values ( $\geq 0.99$ ) in all calibration curves, but data were heteroscedastic in all cases, except for CsA in the sediment phase. This was expected since the range of concentration values were of more than one order of magnitude [321], but CsA in the sediment phase only ranged from 350 to 1500  $\mu\text{g/mL}$ . In the light of the evidence of the heteroscedastic situation, the weighted least squared linear regression was used to neutralise the greater influence of the higher concentrations on the fitted regression line. Lipolysis data was tested using the two most common weighting factors,  $1/x$  and  $1/x^2$ , and the latter was chosen as the best fit according to the sum of relative errors (appendix **Table A-3**).

Intra-day and inter-day RE and RSD values derived from  $1/x^2$ -weighted calibration curves (or  $1/x^0$  for CsA in sediment phase) (appendix **Table A-4**) were within the acceptable limits ( $\leq 15\%$ ) for LLOQ and quality control samples of THC and CsA in lipolysis phases. According to EMA and FDA regulations [306–308], these results suggest that the developed HPLC–UV detection methods were accurate and precise for the determination of THC and CsA in lipolysis phases.

#### 4.4.3. *In vitro* lipolysis

*In vitro* digestion experiments were performed to assess the intraluminal processing of the THC and CsA lipidic formulations (Marinol® and Neoral®), to measure and compare the extent of drug solubilisation in the micellar phase, and to estimate the fraction of absorbed drug dose under different experimental conditions.

##### 4.4.3.1. Drug distribution across the lipolysis phases. The effect of the assumed

*in vivo* dissolution volume: 250 versus 100 mL

For the estimation of the amount of drug solubilised in the small intestine, two different *in vivo* dissolution volumes were initially considered: 250 mL and 100 mL. The first value corresponds

to the amount of water given to volunteers in clinical trials, and it has been used by the BCS as the standard volume for assessing the maximum solubility of drugs in the fasted state [322]. However, latest publications [301] suggest that while 250 mL is the reasonable volume for the assessment of solubility of drugs in the stomach, it might be too high for the estimation of drug solubility in the small intestine. Mudie *et al.* suggest using a volume of 80 to 100 mL instead of 250 mL.

Preliminary experiments with Marinol® were performed to determine which volume was more appropriate in the current studies. The digestion medium of *in vitro* lipolysis model has approximately a 40 mL volume, therefore the amounts of two and one 10 mg Marinol® capsules were scaled down accordingly to match the *in vivo* situation (**Table 4-2**). The assumption of a lower *in vivo* dissolution volume (100 vs. 250 mL) led to the dispersion of higher amounts of formulation in the model (200 and 100 µL vs. 80 and 40 µL).

The higher volume of formulation available for digestion was translated into a higher solvent capacity of the micellar phase, as indicated by the observed increment in the drug concentration values. These results were expected since the presence of more oil, if digested, would lead to the production of more triglyceride hydrolysis products. The presence of a higher proportion of 2-monoglycerides and fatty acids in the lipolysis medium generates mixed micelles which are swollen to a greater extent, and thus capable of incorporating higher amounts of the hydrophobic drug.

Nonetheless, the ratio of the volume of sodium hydroxide solution (used to titrate the liberated ionised fatty acids during lipolysis experiments) to the volume of the formulation dispersed in the experimental medium was higher for the lipolysis of 80 and 40 µL of Marinol® (250 mL) than that of 200 and 100 µL of Marinol® (100 mL), which suggests the extent of *in vitro* lipid digestion was lower in the second case. These results are in accordance with the distribution of THC across the lipolysis phases shown in **Table 4-5**. The larger volume of undigested oil remaining after the lipolysis of 200 and 100 µL of the formulation led to a higher sequestration of the lipophilic drug in the lipid phase (62% vs. 42% and 38% vs. 18%) at the expense of the micellar (31% vs. 47% and 51% vs. 64%) and sediment (7% vs. 11% and 11% vs. 15%) phases.

The gastrointestinal volume of liquids in humans (250 and 100 mL) together with the concentrations of drug in the micellar phase and the clinical doses were combined to estimate

the mass of THC soluble in the intestinal milieu (**Equation 4-4**). The  $F_{\text{abs}}$  values (**Figure 4-1**) were higher for the 250 mL approach (24% and 76%), compared to the 100 mL one (20% and 47%). The combination of the fraction absorbed and non-metabolised in the small intestine ( $F_{\text{abs}} \cdot F_g$ ) was estimated based on the oral bioavailability observed in human subjects ( $F_{\text{observed}}$ ) and the fraction of drug non-metabolised in the liver ( $F_h$ ), calculated assuming the drugs were only cleared by the liver when administered intravenously (**Table 4-4**).  $F_{\text{abs}} \cdot F_g$  values were  $7.2 \pm 7.7\%$  and  $5.9 \pm 7.5\%$ , for two and one 10 mg Marinol® capsules respectively. In the best scenario possible, considering the fraction of drug extracted at the intestinal wall to be negligible (i.e.  $F_g \sim 1$ ), the estimated  $F_{\text{abs}}$  would range from 0% to 14.9% and from 0% to 13.4%, for two and one capsules, respectively. Based on this evidence, it seemed that the estimated  $F_{\text{abs}}$  values assuming an *in vivo* dissolution volume of 100 mL (20% and 47%), instead of 250 mL (24% and 76%), were closer to the *in vivo* situation. Therefore, 100 mL was deemed to be more appropriate in the current studies, and doses dispersed in subsequent lipolysis experiments were scaled down according to this volume.

Contrary to Marinol®, the digestion of Neoral® was complete based on the absence of a lipid layer after ultracentrifugation. This discrepancy is interesting from the point of view that both formulations contain long-chain lipids (sesame oil and corn oil), and that higher quantities<sup>vi</sup> of lipid were dispersed in the model when mimicking Neoral® digestion compared to Marinol®. Nonetheless, the lipids in Neoral® are a combination of mono-, di- and triglycerides [239], thus not all the lipid content needs to be digested to be incorporated in the micellar phase. Besides, the self-emulsification properties of Neoral® assists in the formation of smaller oil droplets with increased surface area, thus facilitating the access of pancreatic lipase to the oil-in-water interface and increasing the extent of digestion. The absence of a lipid phase that could lead to the sequestration of CsA molecules, and the enhanced solvent capacity of the micellar phase due to the presence of lipid digestion products and formulation surfactants, accomplished the almost complete solubilisation of CsA in the micellar phase (**Table 4-5**).

<sup>vi</sup> 35% of Neoral® consists of mono-, di- and triglycerides of corn oil. Accordingly 280, 420 and 840  $\mu\text{L}$  of lipid were dispersed when mimicking the digestion of two, three and six 100 mg Neoral® capsules.

## 4.4.3.2. Effect of the surfactant concentrations: “classic” versus “new” buffer

Initially, a lipolysis buffer analogous to those previously used by our and other lipolysis research groups [53, 104, 105, 203, 302, 303], characterised by high concentrations of bile salts and phospholipids (5 mM and 0.75 mM, respectively), was used for digestion of the lipidic formulations. According to literature data [238, 242] and the PK analysis performed herein, both Marinol® and Neoral® showed approximate dose proportionality. However,  $F_{abs}$  results (**Figure 4-1** and **Figure 4-2**) suggested changes in percentage absorbed dependent on dose for both formulations. Hence, it was apparent that a refinement in the lipolysis conditions was needed.

Following the lead of other research groups [323], surfactant levels were reduced down to more bio-relevant concentrations (3 mM bile salt and 0.2 mM phospholipid) [95], and lipolysis experiments were performed again. Interestingly, reduction in surfactant concentrations caused opposite effects for the two tested model drugs.

The solubilised fractions of THC decreased (**Figure 4-1**), whereas the solubilised fractions of CsA increased (**Figure 4-2**). Marinol® is a Type I lipidic formulation [85], therefore it is highly dependent on the presence of bile salts and phospholipids to create mixed micelles within which THC and lipolytic products (fatty acids and 2-monoglycerides) are solubilised. Therefore, the lower the surfactant concentration, the fewer the number of micelles and the lower the solubilised fraction.

On the other hand, Neoral® is a SEDDS (Type IIIA lipidic formulation), for this reason it does not require additional surfactant agents to generate solubilising structures for CsA. The observed variable and reduced solubility of CsA when using the “classical” buffer could be explained by the inhibitory effect on SEDDS formation caused by an excess of bile surfactants in the experimental medium. An excess of bile salt- and phospholipid-derived micellar structures could lead to a higher entrapment of Neoral® components, thus reduce the number of SEDDS particles, and decrease the inherent solubilisation capacity of Neoral®. Results derived from the use of the “new” more bio-relevant buffer, proved to be more consistent within formulations and showed no statistically significant differences between different formulation doses, as seems to occur *in vivo* [242]. The only exception was the study mimicking

the administration of a very high dose of CsA (six Neoral® capsules), which proved to be statistically different from the other two CsA studies.

Interestingly, a higher dose of digested Neoral® *in vitro* led to a higher fraction of solubilised dose, whereas *in vivo* the case seemed to be the opposite. This phenomenon has already been witnessed by Berthelsen *et al.* [323] when working with Kolliphor® RH40 (the main surfactant component in Neoral®), and it was explained by the so-called micellar trapping hypothesis. According to the hypothesis, the reduced bioavailability *in vivo* when using very high levels of Kolliphor® RH40, might be caused by a higher amount of undigested surfactant trapping the drug, thus decreasing the amount of drug available for intestinal permeation.

As previously mentioned, the general assumption made by researchers working with the *in vitro* lipolysis model is that the fraction of drug dose which is solubilised in the micellar phase is most readily available for absorption. This assumption represents an oversimplification of the absorption process, as drug contained in micelles could precipitate in the lower part of the small intestine. Arguably, the estimated fraction of absorbed drug could be slightly overestimated due to gastric degradation, incomplete permeability and the action of efflux transporters (especially P-glycoprotein) expressed on the apical side of enterocytes.

Garret and Hunt [246] proposed in 1974 that THC would be partially degraded in the stomach, after measuring the amount of THC that disappeared in aqueous solution 0.1 M hydrochloric acid over time at 55 °C. However, according to Arrhenius law [324], the rate of THC degradation might have been overestimated, compared to the *in vivo* situation (37 °C). In addition, it is possible that the entrapment of drug molecules within the undigested oil droplets of the formulation could prevent the contact between the drug and the acids of the stomach, and therefore limit gastric degradation. Friis and Bundgaard [325] measured the kinetics of degradation of CsA at pH 1.1 and 3.0 at 37 °C. Based on the calculated half-lives (63 and 79 h, respectively) it was concluded that gastric degradation is of very minor importance for the absorption of CsA upon oral administration.

In terms of permeability, THC and CsA belong to class II of the BCS, thus their membrane permeability is high, mainly passive and a function of lipophilicity ( $P_{\text{eff}} = 7.56 \cdot 10^{-4}$  and  $1.65 \cdot 10^{-4}$  cm/s, for THC [248] and CsA [249], respectively). Therefore, it is expected that most of the fraction of solubilised dose would cross the apical membrane. With regards to efflux proteins,

it has been suggested that high drug permeability would lead to rapid permeation into the enterocytes, making the contribution of intestinal uptake transporters generally insignificant [14]. Furthermore, Ingels *et al.* [310] and Konishi *et al.* [311] have reported the inhibitory effect of monoglycerides on P-glycoprotein activity. Based on this evidence, it can be assumed that efflux transporters do not play a role in the bioavailability of BCS II drugs delivered by means of LFs.

Since the overall aim of this thesis was to quantitatively predict the absolute oral bioavailability, it was evident that lipolysis results alone were not sufficient for this goal. The  $F_{abs}$  values calculated for Marinol® ( $7.6 \pm 0.6\%$  and  $6.5 \pm 1.6\%$ ) were in the very high end of the THC bioavailability range values derived from clinical studies (0.5 to 7.7% and 0 to 7.2%). Whilst, the  $F_{abs}$  values for Neoral® ( $87.4 \pm 0.9\%$ ,  $87.9 \pm 4.5$ , and  $101.7 \pm 11.7\%$ ) markedly overestimated the CsA oral bioavailability range values previously calculated (28.4 to 64.6%, 24.9 to 58.7%, and 24.5 to 48.7%). Because permeability does not represent a barrier to BCS II drugs systemic exposure but first-pass extraction does, the introduction of a metabolism phase in the model deemed to be the most logical future step.

## 4.5. Conclusions

Marinol® (THC) and Neoral® (CsA) were chosen as model LFs for the future validation of the *in vitro* lipolysis/metabolism approach. The selection of these medicines was based on availability of published clinical data. PK analysis of selected clinical studies suggested that both formulations show dose proportionality in the range of the doses tested.

*In vitro* lipolysis has been used to assess the intestinal drug solubilisation of THC in Marinol® and CsA in Neoral®, with the aim to quantitatively predict the fraction absorbed in humans.

An *in vivo* dissolution volume of 100 mL, rather than 250 mL, used for scaling down lipolysis doses, led to better predictions of fraction absorbed in comparison to clinical data.

The use of a digestion buffer with surfactant concentrations closer to bio-relevant conditions, resulted in more accurate prediction of the oral fraction absorbed of THC in Marinol® and

CsA in Neoral® in comparison to data derived from the classical buffer previously used in *in vitro* lipolysis studies.

The digestion of very high dose levels of surfactants might represent a limitation to the estimation of fraction absorbed, since the *in vitro* lipolysis model could not account for the micellar trapping phenomenon that could occur *in vivo*.

The differences observed between predicted fraction absorbed and observed oral bioavailability suggest that *in vitro* lipolysis is not sufficient alone to accurately predict systemic exposure in humans. The combination with a metabolism phase to account for the loss of drug due to first-pass metabolism might increase the accuracy of the predictions.

## **Chapter 5: *In Vitro* Lipolysis/Microsomal Metabolism Model for the Estimation of the Oral Bioavailability of BCS II Drugs in Lipidic Formulations**

### **5.1. Introduction**

There are a few published studies that describe the attempt of linking *in vitro* lipolysis to additional *in vitro* models to improve its predictive value. These studies focused on drug permeability models, such as Caco-2 cells monolayer [236] or Ussing chambers [108]. However, the assessment of intestinal permeability of drugs delivered in lipidic formulations (LFs) is challenging, since lipolysis medium components are toxic for epithelial cells [326, 327]. While the injured mucosa is rapidly repaired *in vivo*, lack of epithelial restitution leads to acute *in vitro* toxicity. Alqahtani *et al.* [236] tried to circumvent this issue by diluting the lipolysis medium exposed to Caco-2 monolayers; but the effect of dilution on the critical micellar concentration of mix-micelles was not assessed, and therefore the obtained results might be of limited relevance. Dahan and Hoffman [108] used perfused rat intestinal tissue instead, and controlled the integrity of the epithelial tissue. However, no correlation was obtained between the *ex vivo* permeation model results and the *in vivo* area under the curve (AUC) values. It was concluded that intestinal permeation studies cannot indicate the actual exposure *in vivo*.

Despite their admirable efforts of trying to add novelty to the *in vitro* lipolysis model, it may be argued that their approach was not adequate for class II drugs of the Biopharmaceutics Classification System (BCS) administered in LFs. These drugs are expected to show high permeability, thus crossing the enterocyte cell membrane does not represent a barrier to oral bioavailability, but pre-systemic metabolism does. It is the opinion of this author that an



improvement in the predictability power of the model could be obtained if linked to a metabolism model that accounts for the percentage of drug lost due to first-pass extraction. Accordingly, the first objective of the experiments described in this chapter was to predict the intestinal and hepatic human clearances, and subsequently quantify the fraction of drug dose that escapes metabolism at the gut wall and in the liver. To this end, human intestinal and hepatic microsomal metabolism data were gathered using the *in vitro* half-life and multiple depletion curves methods [328]. For this investigation, following the work described in Chapter 4,  $\Delta^9$ -tetrahydrocannabinol (THC) and cyclosporine A (CsA) were selected as model drugs, and Marinol® and Neoral® as model LFs. The second objective of the studies presented herein consisted in combining, for the first time, *in vitro* lipolysis and microsomal metabolism data for the prediction of human oral bioavailability of lipophilic drugs administered in LFs. If successful, the novel *in vitro* lipolysis/microsomal metabolism approach (**Figure 5-I**) could possibly transform the lipolysis model from a qualitative tool to a quantitative one. Furthermore, if predictive of the *in vivo* response, this novel approach could drastically reduce the need for animal experiments, improve accuracy and predictability for formulation design, and lead to better designed clinical trials, hence reduce time and cost of pharmaceutical research and development.

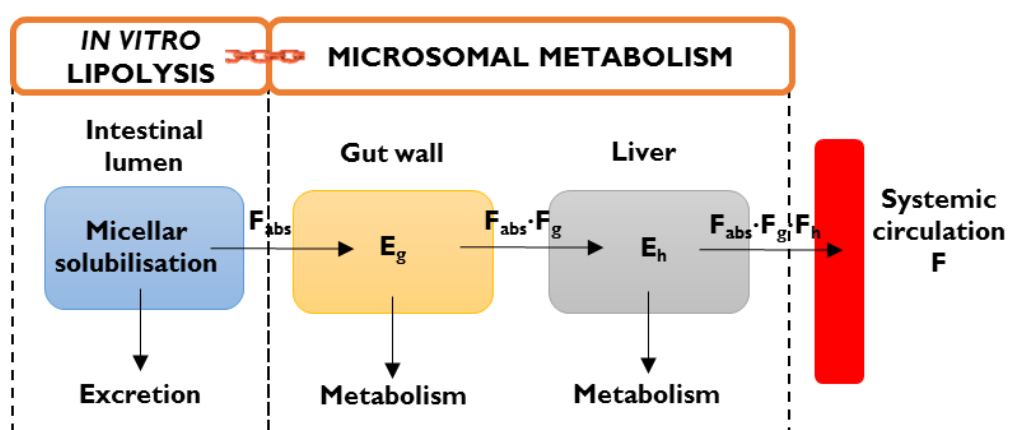


**Figure 5-I.** Proposed *In vitro* lipolysis/microsomal metabolism model for the prediction of the human oral bioavailability of lipophilic drugs administered in lipidic formulations.  $F_{abs}$ : Fraction absorbed;  $F$ : absolute bioavailability;  $F_g$ : intestinal bioavailability;  $F_h$ : hepatic bioavailability;  $E_g$ : intestinal extraction;  $E_h$ : hepatic extraction

## 5.2. Materials and Methods

### 5.2.1. Materials

Verapamil ( $\geq 99\%$  w/w), dexamethasone ( $\geq 98\%$  w/w), chlorpromazine ( $\geq 98\%$  w/w), potassium phosphate dibasic anhydrous ( $\text{K}_2\text{HPO}_4$ ), potassium phosphate monobasic anhydrous ( $\text{KH}_2\text{PO}_4$ ), magnesium chloride ( $\text{MgCl}_2$ ,  $\geq 98\%$  w/w), ammonium acetate ( $\geq 99\%$  w/w), and formic acid ( $\sim 98\%$  v/v) were all purchased from Sigma–Aldrich (Dorset, UK). Nicotinamide adenine dinucleotide phosphate tetrasodium salt hydrate (NADPH, 93% w/w) was a product from Fisher Scientific (Leicester, UK). Dronabinol (synthetic THC), and CsA were products from THC Pharm GmbH (Frankfurt, Germany), and Kemprotec Ltd. (Carnforth, UK), respectively. Vitamin D<sub>3</sub> (VitD<sub>3</sub>, 98% w/w) was obtained from Alfa Aesar (Heysham, UK). Cannabidiol (CBD) was kindly donated by GW Pharmaceuticals (Cambridge, UK). Human liver microsomes pooled from 50 mixed gender donors (20 mg/mL protein content) were obtained from Gibco Invitrogen (Paisley, UK). Intestinal human microsomes pooled from 13 mixed gender donors (10 mg/mL protein content) were a product from Tebu–Bio Ltd. (Peterborough, UK). All solvents were of high-performance liquid chromatography (HPLC) grade or analytical grade and were used without any further purification.

### 5.2.2. *In vitro* microsomal incubations

To determine the fraction of drug dose that escapes metabolism in the gut wall and in the liver, microsomal metabolism stability studies with human intestinal and hepatic microsomes were performed. Clearance values were determined by applying the “*in vitro* half-life approach”, which is based on the measurement of the first-order rate depletion constant of a drug substrate [329]. Microsomal incubations were conducted in a similar manner to that described previously [172]. Reaction mixtures (1200  $\mu\text{L}$  final volume) consisting of 720  $\mu\text{L}$  of 100 mM aqueous potassium phosphate buffer ( $\text{KH}_2\text{PO}_4/\text{K}_2\text{HPO}_4$ , pH 7.4), 240  $\mu\text{L}$  of 2.5 mg/mL human microsomal protein in phosphate buffer, 120  $\mu\text{L}$  of 100 mM aqueous  $\text{MgCl}_2$ , and 24  $\mu\text{L}$  of 0.05–0.5 mM drug substrate (in aqueous acetonitrile, 50% v/v) were placed in a test tube under constant stirring, inside a water bath kept at 37 °C. After 3 minutes of pre-incubation, reactions were initiated by the addition of 96  $\mu\text{L}$  of 125 mM NADPH in phosphate buffer. Final

concentrations of each component of the reaction mixture are listed in **Table 5-1**. Experiments were performed at least five times, and the organic solvent concentration (acetonitrile) in the incubation was less than 1% (v/v). Verapamil and dexamethasone were used as positive and negative controls (extensive and limited hepatic metabolism), respectively. Control experiments without NADPH were carried out as well to monitor the matrix effect on THC and CsA metabolism. At five specified time points (up to 30 and 60 minutes, for hepatic and intestinal assays, respectively), 200  $\mu$ L aliquots were removed and added to glass tubes containing the appropriate internal standard in ice-cold methanol or acetonitrile, (to precipitate the proteins and stop the reaction).

The proportion of drug remaining at each time point was determined immediately after completion of the experiments.

**Table 5-1.** Concentrations of microsomal incubations components at  $t = 0$  minutes.

Compound	Concentration
$\text{KH}_2\text{PO}_4/\text{K}_2\text{HPO}_4$	60 mM
$\text{MgCl}_2$	10 mM
Test compound	1, 2.5, 5, 10 $\mu\text{M}^*$
Human intestinal/hepatic microsomes	0.5 mg/mL
NADPH	1 mM

\* Due to limited availability of intestinal protein, intestinal metabolism studies were performed only at single concentration level (1  $\mu\text{M}$ )

### 5.2.3. Analytical procedures

#### 5.2.3.1. HPLC–UV analysis

##### 5.2.3.1.1. Sample preparation

Verapamil and dexamethasone [330] microsomal incubation samples were prepared for HPLC–UV (ultraviolet) analysis by protein precipitation. Samples were quenched with 1000  $\mu$ L 2  $\mu\text{M}$  chlorpromazine in ice-cold methanol (internal standard for both compounds), vortex-mixed with for 10 seconds, and then centrifuged at  $\sim 1200$  g (Harrier 18/80 centrifuge, swing-out rotor, MSE, London, UK) at room temperature for 10 minutes. The upper organic phase was carefully decanted into fresh glass tubes and the solvent was evaporated under nitrogen gas at 35 °C (Techne Dri-Block Sample Concentrator, Cambridge, UK). The residue was reconstituted in 150  $\mu$ L of aqueous acetonitrile (50%, v/v), vortex-mixed for 5 minutes, and

centrifuged again at ~1200 g for 10 minutes. Finally, 100 µL of the resulting solutions was transferred into HPLC vials and 20 µL was injected into the HPLC instrument.

#### 5.2.3.1.2. Chromatographic conditions

The quantitative determination of verapamil and dexamethasone content in microsomal incubations and internal standard, was performed using a HPLC system (Waters Alliance 2695, Waters Corporation, Milford, MA, USA) equipped with a photodiode array UV detector (Waters 996, Waters Corp.). Samples temperature was controlled by a fitted chiller at 4 °C. Verapamil, dexamethasone and chlorpromazine were detected at 229, 240 and 254 nm, respectively. Separations were achieved using a Phenomenex Gemini-NX 250 x 4 mm, 5 µm particle size column (Phenomenex, Macclesfield, UK), protected by a Phenomenex C18 4 x 2 mm guard cartridge (Phenomenex). Mobile phase was a mixture of acetonitrile and aqueous ammonium acetate (10 mM, pH 4.9) in a ratio of 50:50 (v/v). The flow rate was set at 0.4 mL/min for 17 minutes at 40 °C. Data acquisitions and processing was carried out using Empower™ 2 software (Waters Corp.).

#### 5.2.3.2. HPLC–MS/MS analysis

##### 5.2.3.2.1. Sample preparation

The determination of THC and CsA in microsomal incubation samples was accomplished by means of HPLC–MS/MS (tandem mass spectrometry) analysis since lower limits of quantification had to be achieved compared to lipolysis samples (Chapter 4 section 4.2.5). Microsomal metabolism samples were treated in a similar manner to the lipolysis samples, with the addition of an initial step for protein precipitation. Samples were quenched with 600 µL 1 µM internal standard (VitD<sub>3</sub> for THC, CBD for CsA) in ice–cold acetonitrile, and vortex–mixed for 2 minutes. Subsequently, 600 µL of water was added, and samples were vortex–mixed again for another 2 minutes. Next, 3 mL of *n*–hexane (THC) or methyl *tert*–butyl ether (CsA) was added, and samples were vortex–mixed for 5 minutes. After centrifugation at ~1200 g for 15 min at room temperature, the upper organic layer was transferred to fresh glass tubes and evaporated under a gentle stream of nitrogen gas at 35 °C. Residues were reconstituted in 100 µL of 0.1% (v/v) formic acid in acetonitrile, and 10 µL was injected into the HPLC instrument.

5.2.3.2.2. *Chromatographic conditions*

The chromatographic conditions for the determination THC, VitD<sub>3</sub>, CsA, and CBD in microsomal samples was based on previously validated methods for the quantification of such compounds in biological samples (hair, blood or cod liver oil) [331–334], with small variations around cone and capillary voltages.

The quantitative determination of THC and CsA content in microsomal incubations and corresponding internal standards was performed by using a HPLC system (Agilent 1100 Series, Agilent Technologies, Waldbronn, Germany) equipped with a Quattro Ultima triple–quadrupole mass spectrometer (Waters Corp.), utilising electrospray ionisation for ion production. Sample temperature was controlled by a fitted chiller at 4 °C. Separations were achieved on a Waters XBridge C18 75 x 2.1 mm, 2.5 µm particle size column (Waters Corp.), at a flow rate of 0.3 mL/min and at 60 °C. Elution was conducted with 0.1% (v/v) formic acid in acetonitrile/water 90:10 (v/v) during 7 minutes, and 82.5:17.5 (v/v) during 3.5 minutes, for THC and CsA detection, respectively. Multiple–reaction monitoring in positive ion mode was used to trace ions as follows (*m/z* precursor ion/ product ion): THC (315.2/ 193.0), VitD<sub>3</sub> (385.3/ 259.3), CsA (1219.7/ 1202.7) and CBD (315.2/ 193.0). Nitrogen was used as drying and nebulisation gas at flow rates of 650 L/h and 150 L/h, respectively. The desolvation and source block temperatures were and 350 °C and 125 °C, respectively. The capillary voltages were 3.6 kV and 4.5 kV, for THC and CsA detection, respectively. The cone voltages were 35 V and 45 V for THC and VitD<sub>3</sub> analysis, and CsA and CBD analysis, respectively. Data acquisitions and processing was carried out using MassLynx software (Waters Corp.).

## 5.2.4. Data analysis

5.2.4.1. Determination of *in vitro* intrinsic clearance values

For the determination of the depletion rate constant,  $k_{dep}$ , incubation data were fitted to a mono–exponential model, as shown in **Equation 5-1**:

$$\frac{C_t}{C_0} = e^{-k_{dep} \cdot t} \quad \text{Equation 5-1}$$

where  $C_t$  is the concentration of the compound remaining at each time point, and  $C_0$  is the concentration of the compound at the beginning of the incubation process. However, real concentrations were not determined, since it is not possible to construct calibration curves in

microsomal matrixes. Instead, analyte/internal standard peak area ratios were determined ( $C_t$ ) and normalised to the value obtained at  $t = 0$  ( $C_0$ ). The percentage of drug remaining versus time was then fitted to a first-order decay function to determine  $k_{dep}$ . For hepatic metabolism, the Multiple Depletion Curves Method [328, 335–337] was applied. Depletion rate constants obtained with different initial concentrations (1, 2.5, 5, and 10  $\mu\text{M}$ ) were used to calculate the theoretical depletion constant at infinitesimally low substrate concentration ( $k_{dep,[S] \rightarrow 0}$ ), as indicated in **Equation 5-2**. To facilitate curve fitting, the equation was reorganised to give a linear relationship, as shown in **Equation 5-3**:

$$k_{dep} = k_{dep([S] \rightarrow 0)} \cdot \left(1 - \frac{[S]}{[S] + K_M}\right) \quad \text{Equation 5-2}$$

$$\frac{1}{k_{dep}} = \frac{1}{k_{dep,[S] \rightarrow 0}} + \frac{1}{k_{dep,[S] \rightarrow 0} \cdot K_M} \cdot [S] \quad \text{Equation 5-3}$$

where  $[S]$  is the initial substrate concentration, and  $K_M$  is the Michaelis–Menten constant.

The observed *in vitro* intrinsic clearance ( $CL_{int}$ ) was calculated by multiplying the rate depletion constant ( $k_{dep,[S] \rightarrow 0}$  or  $k_{dep}$ , for hepatic or intestinal metabolism, respectively) by the volume of incubation medium normalised by the amount of microsomal protein. Subsequently,  $CL_{int}$  values were corrected for the fraction of drug unbound in the incubation medium ( $CLu_{int}$ ). For CsA, the extent of non-specific binding ( $fu_{inc}$ ) was predicted using Austin *et al.* equation [338] and a logP value equal to 3.35 [248]. It is known that for highly lipophilic drugs such as THC (logP = 6.97 [248]) either Hallifax and Houston [339] or Austin *et al.* equations lead to poor predictions [340]. On the other hand, experimental measurement of  $fu_{inc}$  of these drugs is also extremely challenging due to non-specific binding to laboratory material [341, 342]. Assuming that THC binds to serum proteins in the same way as to microsomal proteins, it is possible to estimate THC  $fu_{inc}$  using **Equation 5-4**:

$$fu_{100\%} = \frac{fu_{X\%}}{100 - (100 - X) \cdot fu_{X\%}} \quad \text{Equation 5-4}$$

where  $fu_{100\%}$  is the fraction of THC unbound in plasma ( $fu_p = 0.0102$  [248]),  $fu_{X\%}$  is the fraction of THC unbound in the incubation media ( $fu_{inc}$ ), and  $X$  is the ratio between the total concentration of proteins in human serum (approximately 70 mg/mL [343]) and the microsomal concentration in the incubations (0.5 mg/mL).

5.2.4.2. Calculation of the predicted fraction escaping hepatic metabolism ( $F_h$ )

Physiologically-based scaling factors (standard human microsomal recovery of 32 mg microsomes/g liver [173, 175], and average liver weight of 22 g liver/kg body weight [344, 345] were applied to transform  $CL_{u,int}$  (mL/min/mg hepatic protein) into hepatic intrinsic clearances ( $CL_{h,int}$ , mL/min/kg body weight). Hepatic clearances ( $CL_h$ ) were next calculated based on the “well-stirred” model [151], as shown in **Equation 5-5**:

$$CL_h = \frac{Q_h \cdot f_{u_b} \cdot CL_{h,int}}{Q_h + f_{u_b} \cdot CL_{h,int}} \quad \text{Equation 5-5}$$

where  $Q_h$  is the hepatic blood flow (21 mL/min/kg [172, 346]), and  $f_{u_b}$  is the fraction of drug unbound in blood. For CsA, the  $f_{u_b}$  value was found in literature (0.04 [174]), whereas for THC (0.0096), it was calculated based on the fraction of drug unbound in plasma and the blood to plasma concentration ratio (1.063 [248]). The fraction of drug that escapes first-pass metabolism in the liver ( $F_h$ ) was finally derived from the  $CL_h$ , as indicated in **Equation 5-6**:

$$F_h = \left(1 - \frac{CL_h}{Q_h}\right) \quad \text{Equation 5-6}$$

5.2.4.3. Calculation of the predicted fraction escaping gut metabolism ( $F_g$ )

An average of 1410 mg of microsomal content in the human small intestine was used for the transformation of *in vitro* intrinsic clearance ( $CL_{u,int}$ , mL/min/mg intestinal protein) to gut intrinsic clearance ( $CL_{g,int}$ , L/h). The fractions of drug non-metabolised in the gut wall ( $F_g$ ) were estimated using the “Q gut” mathematical model [179, 180], as defined in **Equation 5-9** and **Equation 5-8**:

$$F_g = \frac{Q_{gut}}{Q_{gut} + f_{u_g} \cdot CL_{g,int}} \quad \text{Equation 5-7}$$

$$Q_{gut} = \frac{Q_{villi} \cdot CL_{perm}}{Q_{villi} + CL_{perm}} \quad \text{Equation 5-8}$$

where the gut blood flow ( $Q_{gut}$ ) represents a mixture of villous blood flow ( $Q_{villi} \sim 18$  L/h [347–349]) and permeability across the enterocytes ( $CL_{perm}$ ).  $CL_{perm}$  was calculated through the effective intestinal permeability ( $7.56 \cdot 10^{-4}$  cm/s and  $1.65 \cdot 10^{-4}$  cm/s for THC [248] and CsA [249], respectively) and the small intestine cylindrical surface area ( $0.66$  m<sup>2</sup> [350]). The fraction of drug unbound in the enterocytes ( $f_{u_g}$ ) is commonly assumed to be 1, since this has been shown to provide the greatest accuracy of prediction when using the  $Q_{gut}$  model [8, 132, 312, 351].

Alternatively, gut clearance values were calculated as well from the data obtained with hepatic microsomes. In humans, CYP2C9 [352, 353] and CYP3A4 [354, 355] are the main enzymes involved in THC and CsA metabolism, respectively. The abundance data of these metabolising enzymes per mg of hepatic (73 pmol CYP2C9 and 155 pmol CYP3A4) and intestinal (8.4 pmol CYP2C9 and 43 pmol CYP3A4) microsomes were used to transform  $CL_{u,h,int}$  values into  $CL_{u,g,int}$  [135, 149]. Subsequently  $F_g$  was derived from the resulting  $CL_{u,g,int}$  values as explained above.

#### 5.2.4.4. Calculation of the predicted oral bioavailability ( $F_{predicted}$ )

When several sites of metabolism are in series, bioavailability is defined as the product of the fraction absorbed ( $F_{abs}$ ) times the fractions of drug entering the tissue that escape loss at each site ( $F_g \cdot F_h$ ) [356]. Accordingly, to predict the oral bioavailability of THC in Marinol® and CsA in Neoral®, the  $F_{abs}$  values for the different clinical studies (estimated in Chapter 4) were combined with  $F_g$  and  $F_h$ , as indicated in **Equation 5-9**:

$$F_{predicted}(\%) = F_{abs} \cdot F_g \cdot F_h \cdot 100 \quad \text{Equation 5-9}$$

#### 5.2.5. Statistical data analysis

All presented data are expressed as mean  $\pm$  standard deviation (SD). Statistical tests detailed in Chapter 3, section 3.2.8 were used here as well.

### 5.3. Results

#### 5.3.1. HPLC–MS/MS detection method

Sample preparation using a combination of protein precipitation (with acetonitrile) and liquid–liquid extraction (with *n*–hexane or methyl *tert*–butyl ether) resulted in clean chromatograms with no interfering compounds present, even at concentrations as low as 8 nM (see appendix **Figure A-I I**). THC, CsA and internal standards were clearly separated from the void volume ( $\sim 0.5$  min) and eluted at retention times lower than 5 min, allowing injection–to–injection cycle times much shorter than those required for UV detection (developed for lipolysis samples).



The electrospray ionisation mass spectra of THC and CsA at cone voltages of 35 and 45 V, respectively, are shown in appendix **Figure A-12**.

For THC and CBD, maximum sensitivity was achieved by monitoring the fragmentation of the protonated parent ions  $m/z$  315 ( $[\text{THC}+\text{H}]^+$  and  $[\text{CBD}+\text{H}]^+$ ) to the daughter fragment  $m/z$  193 (see appendix **Figure A-13A** and **D**) [331, 332]. In the case of CsA, the deamination of the ammonium adduct  $m/z$  1220 ( $[\text{CsA}+\text{NH}_4]^+$ ) to form the ion  $m/z$  1203 ( $[\text{CsA}+\text{H}]^+$ ) was monitored (appendix **Figure A-13C**) [333]. The transition of the protonated parent ion  $m/z$  385 ( $[\text{VitD}_3+\text{H}]^+$ ) to the ion  $m/z$  259 (appendix **Figure A-13B**) was used for the quantification of VitD<sub>3</sub> [334].

### 5.3.2. Hepatic microsomal metabolism: Prediction of the fraction non-metabolised in the liver ( $F_h$ )

Apart from intraluminal solubilisation, the other important factor that limits the oral bioavailability of BCS II drugs, is first-pass metabolism. To determine the fraction of drug dose that is not cleared by the liver, microsomal metabolism stability studies with human hepatic microsomes were performed. The metabolism rates ( $k_{\text{dep}}$ ) of THC and CsA at different initial concentrations by human liver microsomes, were obtained by applying the “*in vitro* half-life approach” and fitting the data to mono-exponential decay regressions (see **Equation 5-1**) represented in **Figure 5-2**. These  $k_{\text{dep}}$  values (summarised in appendix **Table A-5**) were next used to determine the theoretical depletion constant at infinitesimally low substrate concentration ( $k_{\text{dep},[S]\rightarrow 0}$ ) and the Michaelis-Menten constant ( $K_M$ ), according to **Equation 5-3**. For THC,  $k_{\text{dep},[S]\rightarrow 0}$  was  $0.6689 \pm 0.2153 \text{ min}^{-1}$ , and  $K_M$  equalled  $2.62 \pm 0.93 \text{ }\mu\text{M}$  ( $r^2 = 0.96$ ). With regards to CsA, the calculated values were  $0.0160 \pm 0.0011 \text{ min}^{-1}$ , and  $5.13 \pm 0.48 \text{ }\mu\text{M}$  ( $r^2 = 0.99$ ), for  $k_{\text{dep},[S]\rightarrow 0}$  and  $K_M$ , respectively.

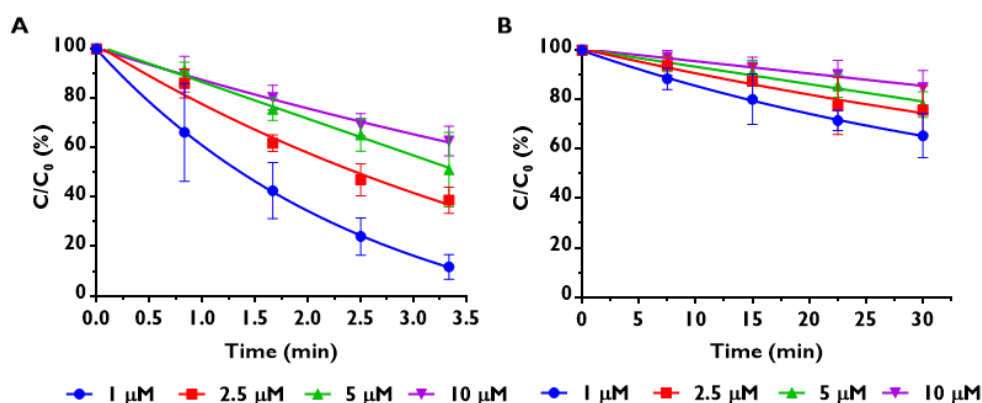


**Figure 5-2.** Depletion curves at different concentration levels derived from hepatic microsomal incubations of  $\Delta^9$ -tetrahydrocannabinol (**A**) and cyclosporin A (**B**). The ratio between the drug concentration remaining at each time point ( $C$ ) and the concentration of drug at the beginning of the incubation process ( $C_0$ ), is represented versus time. Values are expressed as means ( $n = 6$ )  $\pm$  SD. Note the difference in the time scales (X-axes) between the two figures.

Using the microsomal concentration and the fraction unbound in the incubation medium<sup>vii</sup>,  $k_{dep,[S] \rightarrow 0}$  was subsequently transformed into unbound intrinsic clearance:  $CL_{u_{int,THC}} = 2.640 \pm 0.850$  mL/min/mg protein;  $CL_{u_{int,CsA}} = 0.079 \pm 0.006$  mL/min/mg protein). Next, physiologically-based scaling factors (average microsome content in the liver, and average liver weight per kg of body weight), were applied to transform  $CL_{u_{int}}$  into intrinsic hepatic clearance ( $CL_{h_{int}}$ ). Subsequently, the hepatic blood flow and the fraction of drug unbound in blood were introduced in the well-stirred model equation (**Equation 5-5**) to calculate the hepatic clearance ( $CL_{h,THC} = 9.6 \pm 3.1$  mL/min/kg;  $CL_{h,CsA} = 2.0 \pm 0.1$  mL/min/kg). Finally, it was estimated that approximately 54% and 90% of THC and CsA molecules, respectively, would escape first-pass metabolism in the liver (**Equation 5-6**:  $F_{h,THC} = 0.541 \pm 0.174$ ;  $F_{h,CsA} = 0.904 \pm 0.064$ ). For the sake of comparison, clearance and hepatic bioavailability values were estimated as well using the “parallel tube” model<sup>viii</sup> [151, 177]. Nevertheless, these alternative values (see appendix **Table A-6** for THC and **Table A-7** for CsA) were not statistically significantly different ( $p_{THC} = 0.3481$ ,  $p_{CsA} = 0.1119$ ) from those obtained with the well-stirred model.

<sup>vii</sup> To note, when THC metabolism was estimated with  $f_{u_{inc}}$  values derived from either Hallifax and Houston or Austin *et al.* equations, it resulted in a complete loss of prediction, as the  $F_h$  and  $F_g$  values turned up to be  $\sim 0\%$  (see appendix **Table A-6** and **Table A-8**).

<sup>viii</sup>  $CL_h = Q_h \cdot \left(1 - e^{-\frac{f_{ub} \cdot CL_{u_{h,int}}}{Q_h}}\right)$

### 5.3.3. Intestinal microsomal metabolism: Prediction of the fraction non-metabolised in the gut ( $F_g$ )

First-pass metabolism can occur not only in the liver, but also within the enterocytes in the gut wall. Similarly to the hepatic metabolism experimental procedure, the calculation of the fraction of drug dose that escapes metabolism in the gut was performed by means of microsomal metabolism stability studies with human intestinal microsomes. The metabolism rates ( $k_{dep}$ ) of THC and CsA by human intestinal microsomes, were obtained from the fitted mono-exponential decay regressions represented in **Figure 5-3**. The obtained  $k_{dep}$  values were  $0.0462 \pm 0.0009 \text{ min}^{-1}$  ( $r^2 = 0.999$ ) and  $0.0056 \pm 0.0007 \text{ min}^{-1}$  ( $r^2 = 0.95$ ), for THC and CsA, respectively. Again, the microsomal concentration and the fraction unbound in the incubation medium, were used to transform  $k_{dep}$  into unbound intrinsic clearance:  $CL_{u,int,THC} = 0.182 \pm 0.003 \text{ mL/min/mg protein}$ ;  $CL_{u,int,CsA} = 0.028 \pm 0.004 \text{ mL/min/mg protein}$ ). Next, the average microsomal content in the small intestine was used to determine the gut intrinsic clearance values ( $CL_{u,g,int,THC} = 15.4 \pm 0.3 \text{ L/h}$ ;  $CL_{u,g,int,CsA} = 2.3 \pm 0.3 \text{ L/h}$ ). The “Q gut” model, which accounts for mucosal blood flow and permeability across the enterocytes, was applied to finally calculate  $F_g$  (**Equation 5-7** and **Equation 5-8**). It was estimated that around 37% and 58% of THC and CsA molecules, respectively, would escape first-pass metabolism in the small intestine ( $F_{g,THC} = 0.368 \pm 0.070$ ;  $F_{g,CsA} = 0.580 \pm 0.074$ ).

Gut clearance values were calculated as well by extrapolating the data derived from hepatic microsomes, assuming that  $CL_{u,int}$  per pmol of enzyme is the same in both gut and liver. Taking into account the relative abundance data of CYP2C9 and CYP3A4, the extrapolated gut clearances were  $25.7 \pm 8.3 \text{ L/h}$  and  $1.9 \pm 0.1 \text{ L/h}$ , which correspond to  $F_h$  values of  $0.258 \pm 0.083$  and  $0.635 \pm 0.045$ , for THC and CsA, respectively. Statistical analysis showed that there is no significant difference ( $p_{THC} = 0.074$ ,  $p_{CsA} = 0.1876$ ) between the  $F_g$  values calculated either directly from intestinal microsomes or extrapolated from hepatic microsomes.

Additionally, the metabolism of CsA was estimated as well using the  $fu_{inc}$  value calculated with Hallifax and Houston algorithm [339]. Derived values are summarised in appendix **Table A-7** and **Table A-9**. Whereas the estimated  $F_h$  values calculated including either  $fu_{inc, Hallifax}$  or  $fu_{inc, Austin}$  were not statistically significantly different ( $p = 0.3259$ ), the  $F_g$  values statistically differed

( $p = 0.0255$ ). For this reason, it was decided to include both approaches in subsequent calculations of absolute oral exposure.

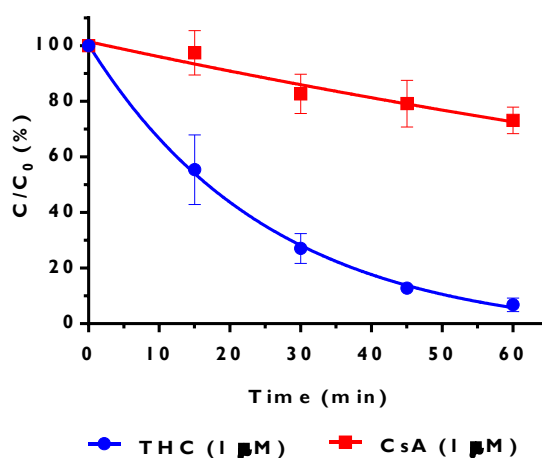


**Figure 5-3.** Depletion curves derived from intestinal microsomal incubations of 1  $\mu$ M  $\Delta^9$ -tetrahydrocannabinol (THC) and 1  $\mu$ M cyclosporin A (CsA). The ratio between the drug concentration remaining at each time point (C) and the concentration of drug at the beginning of the incubation process ( $C_0$ ), is represented versus time. Values are expressed as means ( $n = 6$ )  $\pm$  SD.

#### 5.3.4. Linking *in vitro* lipolysis and metabolism studies: Prediction of the oral bioavailability ( $F_{\text{predicted}}$ )

The estimated absorbed ( $F_{\text{abs}}$ , calculated using two different digestion buffers, see Chapter 4) and non-metabolised ( $F_g \cdot F_h$ ) fractions were combined for the calculation of the predicted oral bioavailability, as indicated in **Equation 5-9**. Bioavailability results are summarised in **Table 5-2**. Pearson's correlation test was used for the measurement of the strength of the association between  $F_{\text{observed}}$  and  $F_{\text{predicted}}$ . Statistical analysis showed there was significant correlation between  $F_{\text{observed}}$  and  $F_{\text{predicted}}$  when the new buffer was used (Pearson's  $r = 0.9638$ ;  $p = 0.0082$ ), but that was not the case for the classical buffer (Pearson's  $r = 0.8291$ ;  $p = 0.0826$ ).

Predicted bioavailability values calculated using  $F_h$  derived from the parallel tube model were not statistically significantly different from those calculated with the well-stirred model (see appendix **Table A-10** for THC, and appendix **Table A-11** for CsA). There were no statistically significant differences either when  $F_{\text{predicted}}$  was calculated with  $F_g$  derived from intestinal data or extrapolated from hepatic data. When CsA oral bioavailability was calculated with data derived from  $f_{u,\text{inc, Halifax}}$  instead of  $f_{u,\text{inc, Austin}}$ , predicted values were statistically

significantly different, but still showed strong correlation ( $p = 0.0083$ ) with the observed ones, according to Pearson's test. Nonetheless, the values derived from  $f_{u_{inc, Austin}}$  were clearly closer to the real ones.

**Table 5-2.** Absolute oral bioavailability values calculated from the data reported in published clinical studies ( $F_{observed}$ ), and calculated with the *in vitro* lipolysis/metabolism approach ( $F_{predicted}$ ), using two different digestion buffers. Values are expressed as weighted means  $\pm$  overall SD ( $F_{observed}$ ) or as means  $\pm$  SD ( $F_{predicted}$ ).

		Marinol®		Neoral®		
		2 x 10 mg THC [240]	1 x 10 mg THC [241]	2 x 200 mg CsA [242, 243]	3 x 200 mg CsA [244]	6 x 200 mg CsA [242]
$F_{observed}$ (%)		4.1 $\pm$ 3.6	3.4 $\pm$ 3.8	46.5 $\pm$ 18.1	41.8 $\pm$ 16.9	36.6 $\pm$ 12.1
$F_{predicted}$ (%)	Classical buffer	4.0 $\pm$ 1.4	7.4 $\pm$ 2.7	24.3 $\pm$ 3.6	29.6 $\pm$ 4.5	41.2 $\pm$ 6.1
	New buffer	1.5 $\pm$ 0.5	1.3 $\pm$ 0.5	45.8 $\pm$ 6.7	46.1 $\pm$ 7.1	53.3 $\pm$ 9.9
$F_{predicted}$ ( $F_g = 1$ ) <sup>a</sup> (%)	Classical buffer	10.9 $\pm$ 3.8	25.5 $\pm$ 9.3	41.0 $\pm$ 9.3	51.0 $\pm$ 4.1	71.0 $\pm$ 5.4
	New buffer	4.1 $\pm$ 1.4	3.5 $\pm$ 1.4	79.0 $\pm$ 5.7	79.5 $\pm$ 6.9	91.9 $\pm$ 12.4
$F_{predicted}$ ( $F_h = 1$ ) <sup>b</sup> (%)	Classical buffer	7.4 $\pm$ 0.9	17.4 $\pm$ 0.3	26.9 $\pm$ 3.4	32.7 $\pm$ 4.4	45.5 $\pm$ 6.0
	New buffer	2.8 $\pm$ 0.2	2.4 $\pm$ 0.6	50.7 $\pm$ 6.5	51.0 $\pm$ 7.0	59.0 $\pm$ 6.8

<sup>a</sup>  $F_{predicted}$  assuming there is not gut metabolism ( $F_g = 1$ ).

<sup>b</sup>  $F_{predicted}$  assuming all the absorbed drug is transported through the lymph, and therefore escapes metabolism in the liver ( $F_h = 1$ ).

THC:  $\Delta^9$ -tetrahydrocannabinol; CsA: cyclosporin A. Classical buffer: 5 mM bile salt, 0.75 mM phospholipid; New buffer: 3 mM bile salt; 0.2 mM phospholipid.

## 5.4. Discussion

LFs are mainly used for the oral delivery of BCS II drugs. Intestinal micellar solubilisation and first-pass metabolism (rather than membrane permeability) are the main barriers to the oral bioavailability of these kind of drugs. *In vitro*, the intraluminal solubility of BCS II drugs administered in LFs can be estimated using the lipolysis model, whereas the first-pass extraction ratio can be assessed by performing microsomal stability assays. The work presented herein

proposes a novel combination of *in vitro* lipolysis and microsomal metabolism studies for the quantitative prediction of human oral bioavailability of BCS II drugs administered in LFs.

Marinol® and Neoral® were selected as model LFs and their observed oral bioavailabilities were calculated from published clinical studies in humans. The predicted fraction absorbed was calculated by measuring the drug concentration in the micellar phase after completion of the lipolysis process (Chapter 4). It was evident that lipolysis results alone were not sufficient for predicting the absolute drug exposure. Thus, hepatic and metabolism phases were introduced to account for the loss of drug due to first-pass metabolism.

In humans, cytochrome 450 (CYP) 2C9 has been identified as the main enzyme involved in THC metabolism. CYP2C9 hydroxylates THC to 11-hydroxy-THC, which may suffer further oxidation to form the carboxylic acid 11-nor-9-carboxy-THC, as depicted in **Figure 5-4**. As for Phase II metabolism of THC, the glucuronidation of 11-nor-9-carboxy-THC by uridinephosphate-glucuronosyltransferases leads to the formation of the O-ester glucuronide, which is the main metabolite found in urine [352, 353, 357]. The other enzyme that catalyses THC metabolism in humans, but to a much lesser extent, is CYP3A4, which is responsible for the 8 $\beta$ -hydroxylation and the 9 $\alpha$ ,10 $\alpha$ -epoxidation of the drug [319, 358].

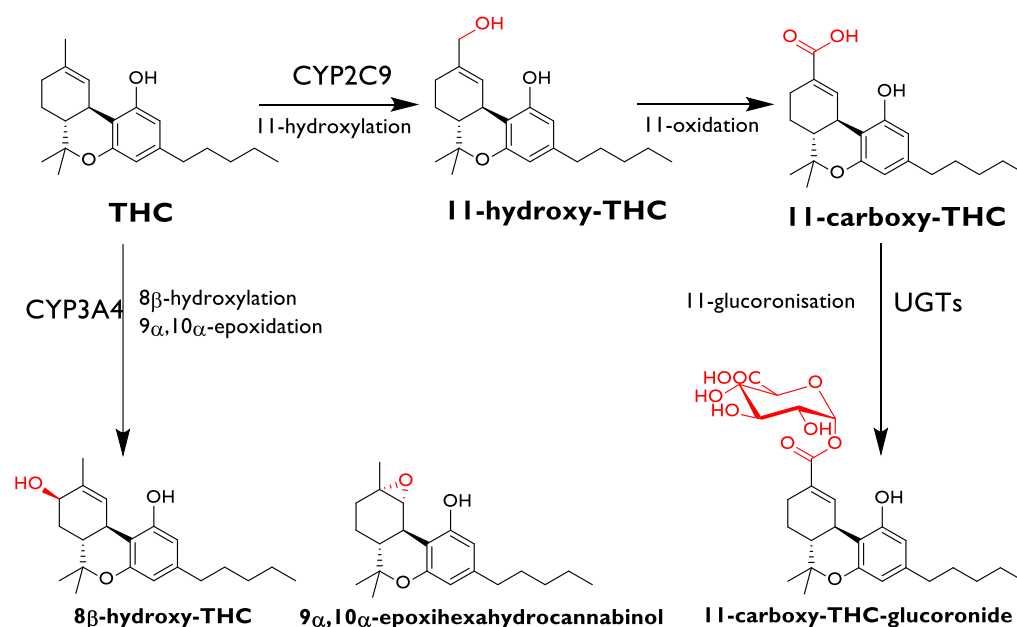


**Figure 5-4.** Most common metabolic pathways and metabolites of  $\Delta^9$ -tetrahydrocannabinol (THC) in humans, catalysed by CYP2C9 and CYP3A4 enzymes. Biotransformations are highlighted in colour red.

CsA is extensively metabolised in the liver and small intestine by CYP3A4 to at least thirty metabolites, all of which are considerably less active than the parent compound [320, 354, 359, 360]. Major metabolic pathways that have been identified include the monohydroxylation of amino acid 1 (4-(2-butenyl)-N-methyl-threonine) and amino acid 9 (N-methyl-leucine), and demethylation of amino acid 4 (N-methyl-leucine). These metabolites represent approximately 70%, 7.5%, and 20% of all CsA degradation products, respectively. Further oxidation of the double bond in amino acid 1 leads to intra-cyclisation and formation of a tetrahydrofuran ring (**Figure 5-5**).

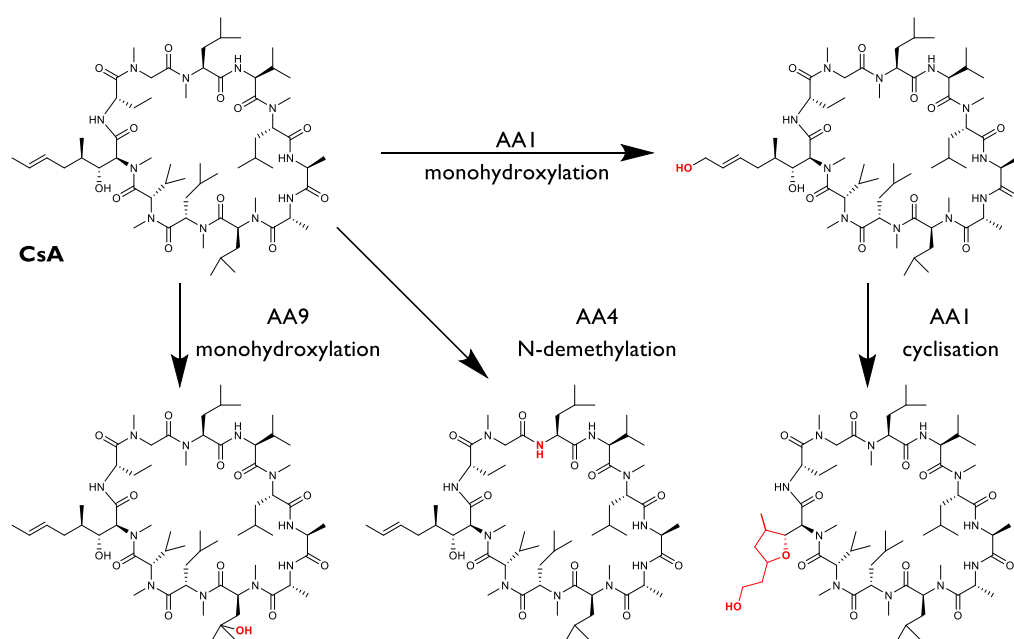


**Figure 5-5.** Most common metabolic pathways and metabolites of cyclosporin A (CsA) in humans, catalysed by CYP3A4 enzyme. Biotransformations are highlighted in colour red. AA stands for amino acid.

In the absence of enzyme saturation,  $CL_{int}$  defined as the ratio between the maximum rate of metabolism ( $v_{max}$ ) and the  $K_M$  (substrate concentration that yields half of  $v_{max}$ ), is used as the link between fundamental enzyme kinetics and *in vivo* pharmacokinetic variables. The “*in vitro* half-life” approach, in which  $CL_{int}$  is derived from the mono-exponential slope of a single depletion curve, is the fastest method but is built on the assumption that the initial substrate concentration is well below  $K_M$ . When this basic condition is experimentally confirmed, the ability to predict clearance *via* an estimate of  $CL_{int}$  is good [361]. However, this method is not suitable when  $K_M$  is unknown and/or  $K_M$  and  $v_{max}$  are required to predict nonlinear kinetics or

to evaluate drug–drug interactions, specific metabolic pathways, and inter–individual variability associated to genetic polymorphism [337]. Obach and Reed–Hagen [328] developed a simple way to assess  $CL_{int}$  and  $K_M$  by carrying out the *in vitro* half–life method at several substrate concentrations (multiple depletion curves method) [328, 336, 337].

#### 5.4.1. Prediction of the fraction non–metabolised in the liver

The fraction of drug that escapes first–pass metabolism in the liver was determined in this work by using human liver microsomes and applying the multiple depletion curves method. To confirm the correct experimental set–up, the metabolism of positive (verapamil) and negative (dexamethasone) control compounds were assessed. The elimination rate constant values calculated for the control compounds ( $k_{verapamil} = 0.0658 \pm 0.0054 \text{ min}^{-1}$ ,  $k_{dexamethasone} = 0.0033 \pm 0.0004 \text{ min}^{-1}$ ) were in accordance to those characteristic of highly (verapamil) and poorly (dexamethasone) metabolised drugs, and were comparable to those values obtained in previous reports with similar experimental conditions [172, 174].  $k_{dep,[S] \rightarrow 0}$  was calculated for THC and CsA by incubating the drugs in hepatic microsomal medium at 4 concentration levels. The obtained  $k_{dep,[S] \rightarrow 0}$  values were then transformed into hepatic clearance data, through corrections for the fraction of drug unbound to microsomes and to blood proteins, physiological scaling factors, and the application of the “well–stirred” model (although the parallel tube model proved to be not statistically significantly different). Traditionally, a value of 45 mg human liver microsomes/g liver has been used [155, 176, 362] to transform  $CL_{u,int}$  into  $CL_{h,int}$ , but this figure was derived from rat rather than human liver [173]. More recent studies performed with human hepatic tissue proposed that a value of 32 or 33 mg human liver microsomes/g liver [173, 175] should be used instead. Reported liver weight values average around 1500 g for a 70 kg man [344, 345], thus a value of 22 g liver/kg body is commonly used for calculations.

In the case of THC, the calculated  $CL_h$  ( $9.6 \pm 3.1 \text{ mL/min/kg}$ ) was slightly higher, but within the same range as the total clearance reported in clinical studies after intravenous administration of THC ( $9.00 \pm 5.3 \text{ mL/min/kg}$ ). For CsA, the estimated  $CL_h$  ( $2.0 \pm 0.1 \text{ mL/min/kg}$ ) was lower than that calculated from literature pharmacokinetic data ( $5.1 \pm 1.1 \text{ mL/min/kg}$ ), and this might be due to CsA being metabolised by other organs in addition to the liver when administered



intravenously. Eventually,  $CL_h$  data were transformed into the fraction non-metabolised in the liver. When  $F_{abs}$  and  $F_h$  values were combined, the *in vitro* lipolysis/hepatic metabolism approach did not sufficiently predict the *in vivo* performance of Marinol® and Neoral® using either of the two buffers (**Table 5-2**). CsA bioavailability was remarkably overestimated, and this fact could be explained by the extensive extraction that the drug suffers at the gut wall [139].

#### 5.4.2. Prediction of the fraction non-metabolised in the gut

Based on the above results, it was evident that the accuracy of the predictions could be improved by the inclusion of an intestinal metabolism phase. Therefore, depletion drug assays in gut microsomal media were next performed. Due to the limited availability of intestinal protein, these studies were done at a single concentration level (1  $\mu$ M). Similar to hepatic metabolism, the intrinsic clearance derived from microsomal incubations was transformed into intestinal clearance and fraction non-metabolised, by applying the “Q gut” model [350]. The transformation of  $CL_{u,int}$  into  $CL_{u,g,int}$  for human intestinal microsomes is not as straight forward as for liver microsomes. To the best of this author’s knowledge, the amount of human intestinal microsomes per g of small intestine has not been reported, presumably because epithelial composition changes from duodenum to ileum. Nonetheless an approximate average value can be calculated from published data. Since the mean intestinal population relative abundance of CYP3A is 50 pmol/mg human intestinal microsomes [132, 135, 147, 363] and the small intestine contains 70.5 nmol CYP3A [147], a value of 1410 mg human intestinal microsomes/small intestine may be used for calculations.

Results derived from CsA experiments ( $CL_{u,int} = 28 \mu\text{L}/\text{min}/\text{mg}$ ;  $F_g = 0.58$ ), were in agreement with those reported by other researchers ( $CL_{u,int} = 27.7 \mu\text{L}/\text{min}/\text{mg}$  [363];  $F_g = 0.53$  [350]). It is important to note that these intestinal clearance values might have been overestimated, as it has been suggested that lipidic excipients may indirectly reduce gut metabolism by inhibition of efflux transporters [70]. The “drug efflux-metabolism alliance” [73, 74] proposes that efflux increases the time available for enterocyte-based metabolism. Accordingly, the impact of lipidic excipients on efflux proteins might reduce the time available for metabolism, and thus decrease pre-systemic extraction (for further details, see Chapter I section I.4.3.3).

### 5.4.3. Prediction of oral bioavailability

Finally, by combining the fractions of drug absorbed and drug non-metabolised, it was possible to propose estimated oral bioavailability values of THC in Marinol® and CsA in Neoral® for different dose levels (**Table 5-2**). Pearson's correlation test showed that there was a strong correlation between  $F_{\text{observed}}$  and  $F_{\text{predicted}}$  values only when  $F_{\text{abs}}$  was calculated with the new buffer.

In the case of Marinol®, the bioavailability was slightly underestimated, but within the range of the clinical values. This underestimation could be attributed to lymphatic transport. As mentioned before (Chapter 1 section 1.4.3.3), when dealing with oral absorption of highly lipophilic drugs co-administered with long-chain triglycerides, such as THC in Marinol®, the lymphatic route should be taken into consideration. Drugs absorbed *via* the intestinal lymphatic system are protected from hepatic first-pass metabolism since the mesenteric lymph enters the systemic circulation by-passing the liver. However, Trevaskis *et al.* [364] suggested that drugs transported via intestinal lymphatics cannot avoid enterocyte-based metabolism, unless extremely large quantities of lipids are administered. Drug association with chylomicrons in the enterocyte is an essential step in the lymphatic absorption pathway [61, 365]. Accordingly, because the vast majority of THC absorbed would associate with chylomicrons [366], and be transported through the lymph, the estimated oral bioavailability of Marinol® could be calculated just taking into account the fractions absorbed and not metabolised in the gut ( $F_h = 1$ ,  $F_{\text{predicted}} = F_{\text{abs}} \cdot F_g$ ). The  $F_{\text{predicted}}$  values obtained ignoring the hepatic phase (**Table 5-2**:  $2.8 \pm 0.2\%$  and  $2.4 \pm 0.6\%$ , for two and one 10 mg Marinol®, respectively), were indeed closer to the average  $F_{\text{observed}}$  ones, which suggests the contribution of lymphatic transport to THC oral bioavailability.

In the case of Neoral®, the bioavailability estimations for Kim *et al.* and Odeberg *et al.* studies (two and three 100 mg capsules) were very accurate. However, when the digestion of exceptionally high doses of formulation was mimicked (Mueller *et al.* study, six 100 mg Neoral®), the *in vitro* lipolysis/metabolism approach did not sufficiently predict the clinical value. As discussed before (Chapter 4, section 4.4.3.2), this is most probably due to CsA micellar trapping occurring when very high amounts of Kolliphor® RH40 are used. This phenomenon

cannot be accurately accounted for with the *in vitro* lipolysis model, and thus it leads to an overestimation of  $F_{abs}$  and subsequent  $F_{predicted}$ .

The general accuracy of the predicted values of bioavailability, and the strong correlation shown with the clinical ones, suggests that the novel *in vitro* lipolysis/microsomal metabolism model could satisfactorily quantitatively estimate the oral bioavailability of BCS II drugs administered in LFs. However, the *in vitro* lipolysis model is not able to predict the micellar trapping of drugs caused by undigested lipidic excipients *in vivo*. Therefore the lipolysis/metabolism approach might have limited applicability when extremely high dose levels of surfactants are ingested.

Some of the parameters used for calculations ( $\log P_{THC}$ ,  $\log P_{CsA}$ ,  $f_{u,p,THC}$ ,  $B/P_{THC}$ ,  $P_{eff,THC}$ ,  $P_{eff,CsA}$ ,  $f_{u,inc,THC}$ , and  $f_{u,inc,CsA}$ ) were *in silico* predictions, due to unavailability of literature data or experimental difficulty in obtaining those parameters in the laboratory. Since each extrapolated parameter is associated with an inherent error, it is highly probable that these uncertainties accumulated and propagated along the final calculation of  $F_{predicted}$ . Accordingly, it is possible that the use of experimental parameters would improve the accuracy of predictions made with the *in vitro* lipolysis/metabolism approach.

## 5.5. Conclusions

*In vitro* lipolysis and microsomal metabolism studies have been combined for the first time with the aim to quantitatively predict the human oral bioavailability of BCS II drugs administered in LFs. This novel approach led to reasonably good predictions of oral bioavailability of THC in Marinol®, and CsA in Neoral® (model formulations) based on the similarity between the predicted bioavailability values and those reported in clinical trials after oral administration of the tested formulations to human subjects.

The use of a digestion buffer with surfactant concentrations closer to bio-relevant conditions, resulted in more accurate predictions of oral bioavailability in comparison to data derived from the classical buffer previously used in *in vitro* lipolysis studies.

The work presented herein suggests that the novel *in vitro* lipolysis/metabolism approach has potential to transform the *in vitro* lipolysis studies from a qualitative tool to a quantitative one.

Further analyses with additional BCS II drugs administered in LFs, might be needed to confirm the predictive power of the model.

## **Chapter 6: Ongoing Experimentation and Recommendations for Future Work**

### **6.1. Introduction**

Further studies should focus on evaluating the predictability power with additional class II drugs of the Biopharmaceutics Classification System (BCS) in lipidic formulations (LFs). However, the main barrier to the validation of the *in vitro* lipolysis/microsomal metabolism approach is the limited availability of appropriate human clinical data. On the contrary, pharmacokinetic data in pre-clinical species is more abundant and/or can be generated more easily at research institutions. For this reasons, ongoing work in the laboratory (see section 6.2) is focused on the validation of the model by using data derived from pharmacokinetic studies performed with rats.

A plausible reason for not obtaining extremely accurate predictions of oral bioavailability with the *in vitro* lipolysis/microsomal metabolism model is that the dynamic and complicated human digesting and metabolic system has been oversimplified for facilitating experimentation (just as any *in vitro* model does). The human body has been represented by 3 theoretical static compartments (small intestine, enterocytes, and liver, see **Figure 5-1**) without specifying anatomy or physiology. However, the relationship among poorly water-soluble compounds, formulation characteristics and systemic exposure after oral administration, is complex and cannot always be captured by solely dissolution and metabolism testing. A more mechanistic link is often required to gain better biopharmaceutical understanding of the *in vivo* absorption, distribution, metabolism and excretion processes. Physiologically-based pharmacokinetic (PBPK) models (e.g. GastroPlus®, PK-Sim®, Chloé®PK, Simcyp®, ADME WorkBench...) are a powerful technology that can help in building this link between experimental data and *in vivo* performance of drug candidates. According to this, it is proposed as future work (although it has already been started in the laboratory, see section 6.3) a further application of the *in vitro*

lipolysis/microsomal metabolism model as an *in vitro* input which could be used for *in silico* modelling in GastroPlus® to predict the plasma concentration–time profiles of BCS II drugs delivered in LFs.

## **6.2. *In vitro* lipolysis/microsomal metabolism model for the prediction in pre-clinical species of oral bioavailability of BCS II drugs in lipidic formulations**

### **6.2.1. Introduction**

Pre-clinical studies of new drug candidates in animals are used to extrapolate pharmacokinetic parameters to man, to select appropriate doses for phase I clinical trials, and to evaluate the safety for humans. Importantly, regulatory guidelines such as the US Food and Drug Administration or the European Medicines Agency require drug testing in at least two mammalian species (murine, canine, primate, porcine, etc.), including one non-rodent species, prior to human trials authorisation [367].

Rats and mice are generally the species of first choice for several reasons, including low cost, small size, simple housing conditions, short reproductive cycle, availability of genetically engineered strains, and short life span. The purpose of utilising additional non-rodent species lies in most cases in the need to obtain confirmatory data that facilitates extrapolation of experimental results to humans (allometric scaling, see Chapter I section 1.7.3.2). On the other hand, sometimes rodents are just not considered the most useful species to obtain scientific answers. In particular, since neither rats nor mice eat on command, and generally consume a low fat diet, they are not thought to be adequate species for pre-clinical food effects, and therefore, for LF testing [368]. For this reason, some researchers have traditionally used dogs for validating *in vitro* lipolysis data [104, 121, 124, 127]. However, some studies suggest that the dog is a poor model of human absorption due to higher luminal bile salt concentrations [142], longer villi length, increased protein binding and higher intestinal pH in the fasted state [369]. Since the dog model has not been proven yet to be more useful than rats in pre-clinical testing of LFs, and due to the (understandable) reluctant use of canines in laboratory

investigations by many researchers, there are many other publications that described the correlation of rat and *in vitro* lipolysis data [105, 203, 204, 236, 323, 370–372].

The ongoing investigation presented herein consisted in applying the *in vitro* lipolysis/microsomal metabolism model to predict oral exposure in pre-clinical species, with the final goal of validating the model not only with human data but also with animal data. In particular, preliminary studies have focused on the prediction of the oral bioavailability of  $\Delta^9$ -tetrahydrocannabinol (THC) in a lipidic and non-lipidic vehicle following oral administration to rats. This *in vivo* study was performed in house by members of Dr. Gerskovich's group, and further details can be found in the publication by Zgair *et al.* [370].

### **6.2.2. Materials and Methods**

#### **6.2.2.1. Materials**

Materials used for *in vitro* lipolysis and microsomal stability assays were the same as those detailed in Chapter 4 section 4.2.1 and Chapter 5 section 5.2.1, with the exception of using rat microsomes instead of human. Pooled rat (male Sprague Dawley) liver (20 mg/mL protein content) and intestinal (10 mg/mL) microsomes were obtained from Gibco Invitrogen (Paisley, UK) and Tebu-Bio Ltd. (Peterborough, UK), respectively. In addition, bovine serum albumin powder ( $\geq 96\%$  w/w) was obtained from Sigma-Aldrich (Dorset, UK).

#### **6.2.2.2. Model formulation and associated pharmacokinetic data**

THC and sesame oil were selected again as the model drug and lipidic vehicle, respectively, for two reasons. Firstly, analytical methods were already developed for the detection of THC in lipolysis phases and microsomal incubations. Secondly, pharmacokinetic experiments in rats had recently been performed in the laboratory, thus reliable data that fulfil the eligibility criteria previously described (see section 4.2.2) was available. In these studies, three groups of male Sprague Dawley rats ( $\sim 365$  g) were used. One group received an intravenous (IV) bolus of THC (4 mg/kg), a second group received an oral dose of 12 mg/kg THC in the LF (12 mg/mL in sesame oil), and the third group received an oral dose of 12 mg/mL THC in a lipid-free formulation (12 mg/mL in propylene glycol/ethanol/water, 80:10:10 v/v). The plasma concentration–time profiles following IV and oral administration of THC are shown in appendix

**Figure A-14A** and **B**, respectively; the pharmacokinetic parameters derived from these graphs are summarised in appendix **Table A-12**. Blood clearance was around 42 mL/min/kg, whereas the absolute oral bioavailability ( $F_{\text{observed}}$ ) values were  $21.5 \pm 8.6\%$  and  $8.5 \pm 5.8\%$  for the lipidic and lipid-free formulations, respectively.

#### 6.2.2.3. *In vitro* lipolysis experiments

Given the volume of the rat gastrointestinal tract in the fasted state being approximately 3.2 mL [373], and taking into consideration that in the *in vivo* study rats were administered with 0.365 mL of formulation and 1 mL of water, the final volume of liquids in the rat gastrointestinal tract was assumed to be approximately 4.565 mL [195]. Because the digestion medium of *in vitro* lipolysis model consists of approximately 40 mL, the amounts of formulation used in the *in vivo* study were scaled-up accordingly. Thus, the 12 mg/kg dose of THC in the *in vivo* study corresponded roughly to 4.38 mg of THC dissolved in 3.2 mL sesame oil or propylene glycol/ethanol/water (80:10:10, v/v) in the lipolysis study.

The impact of digestion on the solubilisation properties of the lipid-based and lipid-free formulations containing THC was examined by means of *in vitro* lipolysis (as described in Chapter 4, section 4.2.4.3) using three different amounts of enzymes, in an attempt to most closely reflect the rat *in vivo* conditions. To facilitate experimentation and data comparison, the experimental medium used for all experiments was the “classic” buffer (see Chapter 4, section 4.2.4.2), which broadly mimics the physiological environment of human and dog small intestine. Initially, lipase activity was kept constant at human levels (500–600 tributyrin units/mL [110]) thus 1 g of pancreatic lipase was utilised ( $n = 6$ ). However, pancreatic activity in the rat has been reported to be at least 5 times lower than that in humans [204]. For this reason, the lipolysis experimentation was carried out as well using enzymatic extracts containing 0.2 g of pancreatic lipase only ( $n = 3$ ). Additionally, a third set of experiments were performed where 0.8 g of bovine serum albumin was added to 0.2 g of pancreatic lipase ( $n = 3$ ), in order to analyse the contribution of enzymes to the reduction in non-specific binding of THC to the lipolysis model material.

A fourth layer was observed in between the lipid and aqueous-micellar phases, following lipolysis and ultra-centrifugation of the lipidic formulation. This gel-like layer is consistent with



previous observations [107, 204, 213, 374], and it has been described as a liquid–crystalline phase (CP) which contains lipids and colloidal structures typical of the micellar but not the lipid phase. For this reason, the amount of drug contained in this layer was considered to be readily available for absorption and was taken into account, together with that found in the micellar phase, for estimation of the fraction absorbed ( $F_{\text{abs}}$ , Chapter 4 section 4.2.6).

High–performance liquid chromatography with ultraviolet detection (HPLC–UV) was used for quantification of THC in lipolysis phases, using the same procedure and chromatographic conditions explained in Chapter 4 sections 4.2.5.1 and 4.2.5.2. Partial method validation of THC quantitative determination in CP was carried out as described in Chapter 4 section 4.2.5.3.

#### 6.2.2.4. *In vitro* microsomal incubations

To determine the fraction of drug dose that escapes metabolism in the gut wall ( $F_g$ ) and in the liver ( $F_h$ ), microsomal metabolism stability studies with rat intestinal ( $n = 3$ ) and hepatic microsomes were performed ( $n = 8$ ). Clearance values were determined by applying the *in vitro* half-life approach at a single substrate concentration level ( $1 \mu\text{M}$ ), as described in Chapter 5 section 5.2.2.

HPLC with tandem mass spectrometry detection (MS/MS) was used for quantification of THC in microsomal media, using the same procedure and chromatographic conditions detailed in Chapter 5 section 5.2.3.2.

Data analysis was performed as indicated in Chapter 5 section 5.2.4. Physiology parameters characteristic of Sprague Dawley rats were used to calculate gut and liver clearances. These factors were as follows: rat microsomal recovery of 61 mg microsomes/g liver [375, 376] and 59.6 mg microsomes/small intestine [8], average liver weight of 40 g liver/kg body weight [376, 377], 55.2 mL/kg/min hepatic blood flow [346, 378], 1.02% fraction unbound to plasma [248], 1.063 blood to plasma ratio [248],  $13.88 \cdot 10^{-4}$  cm/s effective permeability [248], 0.33 L/h villous blood flow, 0.6 m small intestine length, and 0.0022 m small intestine radius [8].

#### 6.2.2.5. Calculation of the predicted oral bioavailability and statistical analysis

The predicted oral bioavailability ( $F_{\text{predicted}}$ ) was calculated by combining  $F_{\text{abs}}$  derived from lipolysis studies and  $F_g \cdot F_h$  derived from microsomal incubations, as indicated in **Equation 5-9**.

The same statistical tests detailed in Chapter 4 section 4.2.7 were used to determine significant differences among the means of the experimental groups and to analyse the scedasticity of the HPLC data.

### 6.2.3. Results and Discussion

#### 6.2.3.1. *In vitro* lipolysis

Typical chromatogram corresponding to the CP phase obtained following *in vitro* enzymatic hydrolysis of 3.2 mL 12 mg/mL THC in sesame oil is shown in appendix **Figure A-15**. The linearity of THC detection method in CP was confirmed over the concentration range of 45–450 µg/mL, based on ten concentration levels and with a correlation coefficient ( $r^2$ ) value  $\geq 0.99$  (appendix **Figure A-16**). Data appeared to be heteroscedastic, based on the residuals graph (appendix **Figure A-17**) and the  $F$ -test value ( $F_{\text{exp}} = 10.82$ ). The weighting scheme  $1/x^2$  was selected, as it provided the best fit. THC detection method in CP was accurate and precise based on the intra-day and inter-day relative errors and relative standard deviations which were  $\leq 15\%$  (see appendix **Table A-13**).

The distribution of THC across lipolysis phases when administered either in a lipid-based or a lipid-free formulation is summarised in **Table 6-1**. The large volume of undigested lipid left and the end of the digestion of the sesame oil solution led to almost complete sequestration of THC in the lipid phase (around 95%), regardless of the amount of pancreatic lipase added (no statistically significantly different). As expected, the extent of digestion was higher when 1 g of lipase was added compared to the 0.2 g scenario, as indicated by the volume of sodium hydroxide needed for titration. However, this was not translated into a higher concentration of drug in the micellar and crystalline phases, as THC molecules were trapped by remaining undigested oil droplets.

Interestingly, the amount of enzyme in the digestion medium markedly affected THC distribution and solubilisation following processing of the lipid-free formulation. When 1 g of protein was present, higher amounts of drug were found in the micellar phase compared to those quantified when only 0.2 g of lipase was utilised, but the amounts in the sediment phase were similar. This phenomenon could originate from the extent of non-specific binding of THC to the lipolysis model instrumentation (stirrer, vessel and pH-electrode). It was hypothesised

that if THC showed stronger affinity to proteins than to laboratory material, higher amounts of proteins in the lipolysis medium would avoid to some extent THC non-specific binding, thus the number of THC molecules in the aqueous phase would increase. To test this hypothesis, lipolysis experiments were performed again using 0.8 g albumin (a protein lacking lipolytic activity) in addition to 0.2 g of lipase. Results confirmed this assumption since THC distribution in micellar and sediment phases did not statistically differ when using either 1 g of lipase or 0.2 g of lipase plus 0.8 g of albumin.

**Table 6-1.** Distribution of recovered drug across micellar (MP), sediment (SP), lipid (LP), and liquid-crystalline (CP) phases after the lipolysis of 3.2 mL of formulations containing  $\Delta^9$ -tetrahydrocannabinol (12 mg/mL) with different amounts of pancreatic lipase and albumin. Data are presented as means  $\pm$  SD.

	$m_{\text{lipase}}$ (g)	% drug MP	% drug SP	% drug LP	% drug CP
<b>Lipidic formulation</b>	1 (n=6)	1.9 $\pm$ 0.2	0.3 $\pm$ 0.0	94.1 $\pm$ 0.7	3.7 $\pm$ 0.7
	0.2 (n=3)	1.9 $\pm$ 0.2	0.2 $\pm$ 0.0	95.9 $\pm$ 1.2	2.1 $\pm$ 1.3
	0.2* (n=3)	2.0 $\pm$ 0.2	0.1 $\pm$ 0.0	94.9 $\pm$ 1.2	3.0 $\pm$ 1.1
<b>Lipid-free formulation</b>	1 (n=6)	38.8 $\pm$ 3.6	61.2 $\pm$ 3.6	N/A	
	0.2 (n=3)	17.9 $\pm$ 5.0	82.1 $\pm$ 5.0		
	0.2* (n=3)	32.8 $\pm$ 6.7	67.2 $\pm$ 8.6		

Lipidic formulation: sesame oil; lipid-free formulation: propylene glycol/ethanol/water (80:10:10, v/v); m: mass.

\* 0.2 of pancreatic lipase and 0.8 g of bovine serum albumin.

Drug concentration determined in micellar and crystalline (if present) phases were used to estimate the fraction of drug dose values shown in **Figure 6-1**. For the LF,  $F_{\text{abs}}$  values did not statistically significantly differ among experimental groups. In the case of the lipid-free formulation, lipolysis experimentation with just 0.2 g of lipase resulted in lower  $F_{\text{abs}}$  values. As explained above this could be attributed to THC non-specific binding to laboratory material. Surprisingly,  $F_{\text{abs}}$  values were not statistically significantly different between lipidic and non lipidic formulations. These results suggest that an excess of long-chain triglycerides in the formulation<sup>ix</sup> (for which pancreatic lipase shows the least affinity as shown in Chapter 3) is counterproductive, as the expected enhancement in the  $F_{\text{abs}}$  attributed to micellar solubilisation

<sup>ix</sup> To put things into perspective, if the same volume of sesame oil formulation were to be administered to humans, a 70 kg person would have to ingest 70 large 1 mL capsules in one go.

does not occur since lipophilic drug molecules are hardly released from the undigested lipid droplets.

Since the addition of 0.2 g of lipase and 0.8 g of albumin was considered to be the experimental set-up that closely reflects the *in vivo* situation, the derived  $F_{abs}$  values from these studies were the ones used for subsequent estimations of oral bioavailability.

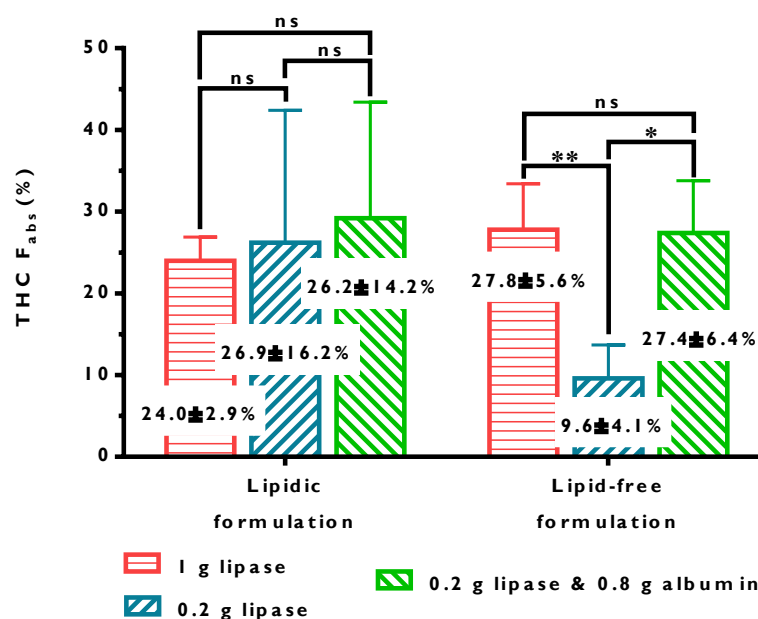


**Figure 6-1.** Fraction of absorbed dose of  $\Delta^9$ -tetrahydrocannabinol (THC) following the lipolysis of 3.2 mL of a lipidic (sesame oil) and lipid-free (propylene glycol/ethanol/water (80:10:10, v/v)) formulations (12 mg/mL) with different amounts of pancreatic lipase and albumin. Coral, blue, and green colours correspond to 1 g of pancreatic lipase ( $n = 6$ ), 0.2 g of pancreatic lipase ( $n = 3$ ), and 0.2 g of pancreatic lipase plus 0.8 g of bovine serum albumin ( $n = 3$ ), respectively. Values are expressed as means  $\pm$  SD. A one-way ANOVA followed by Tukey–Kramer multiple comparison test were used for statistical analysis. Statistically significantly different: \*\*,  $p < 0.01$ ; \*,  $p < 0.05$ ; ns, not significantly different.

#### 6.2.3.2. Microsomal metabolism

Whereas in humans CYP2C9 is the main enzyme involved in THC metabolism, CYP2C11 is responsible for THC enzymatic degradation in rats [379]. The fraction of drug that escapes first-pass metabolism within enterocytes and hepatocytes was determined by using rat intestinal and hepatic microsomes and applying the *in vitro* half-life approach. The metabolism rates ( $k_{dep}$ ) of THC were obtained from the fitted mono-exponential decay regressions represented in **Figure 6-2**. The obtained  $k_{dep}$  values were  $0.2554 \pm 0.0130 \text{ min}^{-1}$  ( $r^2 = 0.98$ ) and  $0.0186 \pm 0.0020 \text{ min}^{-1}$  ( $r^2 = 0.97$ ), for hepatic and intestinal metabolism respectively. The

microsomal concentration and the fraction unbound in the incubation medium, were used to protein;  $CL_{u_{int}} = 0.073 \pm 0.08$  mL/min/mg gut protein). Next, microsomal content in the liver and in the small intestine was used to determine clearance values ( $CL_h = 16.2 \pm 0.2$  mL/min/kg, based on the well-stirred model<sup>x</sup>;  $CL_{u_g} = 0.26 \pm 0.03$  L/h). Clearance values were used to estimate the hepatic and intestinal bioavailabilities:  $F_h = 70.0 \pm 0.6\%$  and  $F_g = 41.2 \pm 4.4\%$  (Q gut model). Reported *in vivo* total blood clearance was 2.5-fold higher than the hepatic clearance derived from these microsomal assays. This could be attributed to THC being metabolised by other organs apart from the liver, when intravenously administered to rats. Direct phase II bio-transformation of THC (i.e. conjugation reactions), which cannot be estimated in microsomal studies since they occur within the cytosolic fraction, could be another plausible reason for the underestimation of THC extraction.

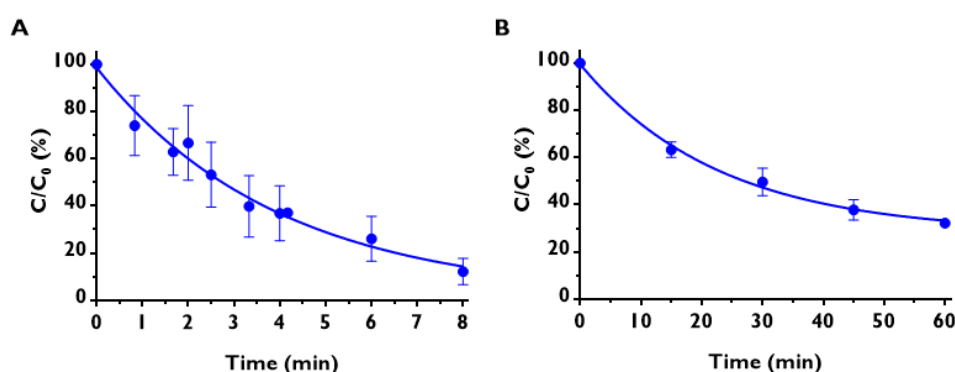


**Figure 6-2.** Depletion curves derived from rat (A) hepatic ( $n = 8$ ) and (B) intestinal ( $n = 3$ ) microsomal incubations of  $1 \mu\text{M}$   $\Delta^9$ -tetrahydrocannabinol (THC). The ratio between the drug concentration remaining at each time point ( $C$ ) and the concentration of drug at the beginning of the incubation process ( $C_0$ ), is represented versus time. Values are expressed as mean  $\pm$  SD. Note the difference in the time scales (X-axes) between the two figures.

#### 6.2.3.3. Prediction of the oral bioavailability in rats

Finally, by combining the predicted fractions of drug absorbed and not metabolised, it was possible to propose estimated oral bioavailability values of THC in a lipid-based and lipid-free formulations when administered to rats in the fasted state (**Table 6-2**). These  $F_{\text{predicted}}$  values were  $8.5 \pm 4.2\%$  and  $7.9 \pm 2.1\%$ , for the lipidic and non lipidic formulations, respectively. Interestingly, the *in vitro* lipolysis/microsomal metabolism model accurately predicted the  $F_{\text{observed}}$

<sup>x</sup>  $CL_h$  calculated with the parallel tube model was not statistically significantly different from the value obtained with the well-stirred model.

for the non lipidic formulation ( $8.5 \pm 5.8\%$ ), but it did not predict the *in vivo* performance of the sesame oil solution ( $21.5 \pm 8.6\%$ ) in rats. In accordance to the assumption proposed in Chapter 5 section 5.4.3, Zgair *et al.* [370] suggested that the primary mechanism of the increased absorption of THC in the presence of lipids is intestinal lymphatic transport, and therefore avoidance of hepatic first-pass extraction. Accordingly, the estimated oral bioavailability of THC corresponding to the lipidic formulation was re-calculated just taking into account the fractions absorbed and not metabolised in the gut ( $F_{abs} \cdot F_g$ , **Table 6-2**). The  $F_{predicted}$  value ignoring the hepatic phase was  $12.2 \pm 6.0\%$ , which is lower than the  $F_{observed}$  value. The reasons for this underestimation could be several. It could be attributed to the differences in composition between the *in vitro* lipolysis digestion medium (which represents human/dog conditions) and rat intestinal fluids. A refinement in the lipolysis buffer concentrations (not only in pancreatic lipase activity) to better mimic rat conditions might lead to enhanced estimation of drug solubilisation and absorption.

The co-administration of extremely large quantities of lipid (such as those given to rats in the *in vivo* study) has been reported to reduce the extent of enterocytic metabolism [364]. Accordingly, it could be reasonable to believe that in this situation the  $F_{abs}$  predicted with the *in vitro* lipolysis model is enough to estimate overall exposure. Indeed, the calculated  $F_{abs}$  ( $\sim 26\%$ ) for the lipidic formulation was closer on average  $F_{observed}$  than  $F_{predicted}$ .

Another explanation for underestimation of  $F_{observed}$  (which can be applied to human predictions too) is that *in vitro* lipolysis, like any other gastrointestinal dissolution model, may have a tendency to underestimate drug absorption *in vivo*, potentially due to non-sink conditions. More detailed investigations of time dependent drug absorption are required in order to improve the *in vitro* model in this aspect.

**Table 6-2.** Absolute oral bioavailability values calculated from the data reported in Ref. [370] ( $F_{\text{observed}}$ ), and calculated with the *in vitro* lipolysis/metabolism approach ( $F_{\text{predicted}}$ ). Values are expressed as means  $\pm$  SD.

	Lipid-based formulation	Lipid free formulation
$F_{\text{observed}}$ (%)	21.5 $\pm$ 8.6	8.5 $\pm$ 5.8
$F_{\text{predicted}}$ (%)	8.5 $\pm$ 4.2	7.9 $\pm$ 2.1
$F_{\text{predicted}} (F_g = 1)^a$ (%)	20.7 $\pm$ 10.0	19.2 $\pm$ 4.6
$F_{\text{predicted}} (F_h = 1)^b$ (%)	12.2 $\pm$ 6.0	11.3 $\pm$ 2.9

<sup>a</sup>  $F_{\text{predicted}}$  assuming there is not gut metabolism ( $F_g = 1$ ).

<sup>b</sup>  $F_{\text{predicted}}$  assuming all the absorbed drug is transported through the lymph, and therefore escapes metabolism in the liver ( $F_h = 1$ ).

#### 6.2.4. Conclusions

These preliminary studies suggest that comparison of *in vivo* drug absorption patterns in the rat with *in vitro* digestion data obtained using bio-relevant intestinal fluids that simulate human/dog conditions may lead to underestimation of solubilisation and absorption of drugs administered in lipidic formulations. Further studies using a digestion buffer that better mimics rat intestinal fluids are needed to check the prediction accuracy of the *in vitro* lipolysis/metabolism model.

### 6.3. *In vitro-in silico/in vivo* Correlation: Prediction of the performance of BCS II drugs in lipidic formulations

#### 6.3.1. Introduction

*In silico* modelling and simulation in drug development is being increasingly applied in the pharmaceutical industry. Indeed, it has been estimated that *in silico* approaches could currently represent up to 15% of research and development expenditure [361]. Simulations are commonly used to support dose selection for first-in-human studies, potential drug–drug interaction effects, and possible exposure differences resulting from a change in formulation. PBPK modelling utilises physiological and anatomical parameters for either *in silico/in vivo* extrapolation, *in vitro/in vivo* extrapolation, or a combination of both, to predict full pharmacokinetics (PKs) in humans and animal species [380]. PBPK modelling implies the use of hundreds of differential equations and biopharmaceutical parameters. Such level of complexity

represented a substantial disadvantage for the application of PBPK modelling in the past. Thankfully, several software products that include whole body PBPK models have been developed and are commercially available nowadays.

At the early stage of a project, it is possible to apply a PBPK model. Absorption and metabolism could be estimated from the *in silico* predictions and *in vitro* measurements of the drug, and taking into account the physiology of the species of interest. Whilst, disposition and elimination could be obtained by fitting a compartmental PK model to *in vivo* intravenous (IV) plasma–concentration profiles (if available). Logically, PBPK modelling of oral exposure does not eliminate the need for *in vivo* experiments, but it can help to reduce the use of laboratory animals by allowing an extrapolation to other dosing regimen within and across animal species, and thus help the design of future studies.

The aim of this preliminary work was to evaluate a further application of the *in vitro* lipolysis model as an *in vitro* solubility input in a PBPK model which could be used, at the early stage of formulation optimisation, to predict the plasma concentration–time profiles of drugs delivered by means of lipidic formulations (LFs). The physicochemical properties and metabolic extraction of  $\Delta^9$ -tetrahydrocannabinol (THC) and cyclosporin A (CsA) were defined by *in silico* predictions and *in vitro* estimations. *In vivo* IV data were included in the model to fit the distribution and elimination phases. Marinol® and Neoral® oral profiles served as observational control.

### 6.3.2. Materials and Methods

#### 6.3.2.1. Software

All simulations were conducted using GastroPlus® version 9.00 (Simulations Plus Inc., Lancaster, CA, US)[248]. For orally administered drugs, GastroPlus® implements an advanced compartmental absorption and transit (ACAT, **Figure 6-3**) model to simulate and predict the fraction of drug absorbed through the gastrointestinal tract. The model offers the possibility of performing non-compartmental and compartmental PK simulations of plasma concentration–time profiles, as long as the minimum PK input values have been provided.



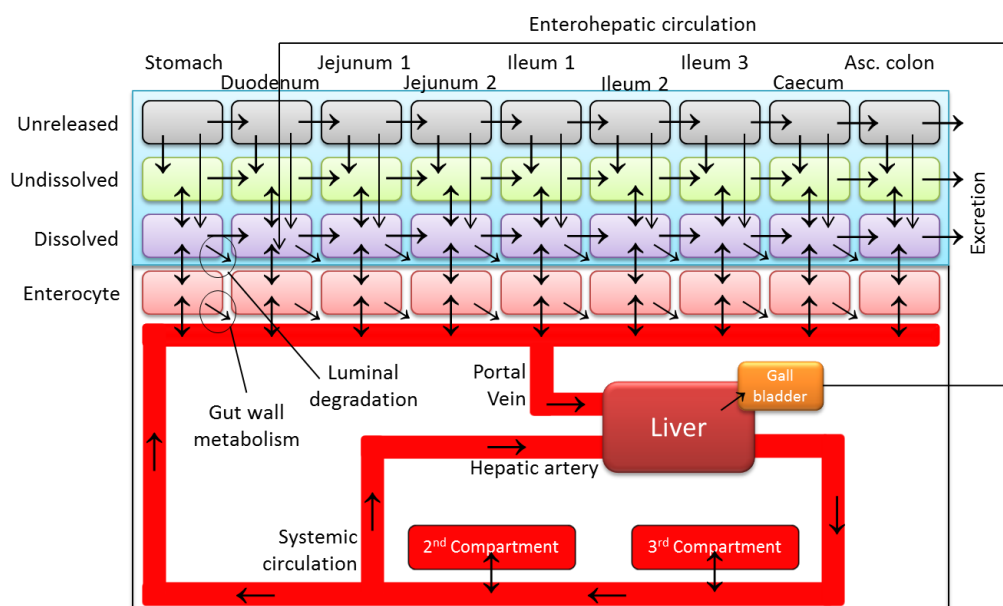


**Figure 6-3.** Advanced compartmental absorption and transit (ACAT) model, by GastroPlus®.

#### 6.3.2.2. *In silico* and *in vitro* input parameters

The input parameters used to perform simulations of bioavailability and plasma concentration–time profiles of THC in Marinol® and CsA in Neoral® are summarised in appendix **Table A-14**. When values were unknown, default GastroPlus® values were used. The ACAT model does not contemplate oil solutions as dosage forms, thus the option “immediate release: solution” was chosen as the most similar input.

The inputs for solubility were the aqueous solubility measured at pH 7.4 and the solubility found in the aqueous–micellar phase following lipolysis and ultra–centrifugation of the LFs in the new buffer (pH 6.8, 3 mM bile salt concentration, and 0.2 mM phospholipid concentration, see Chapter 4 section 4.2.4.2). These values are used by GastroPlus® to calculate the bile salt solubilisation ratio (*SR*), which represents the affinity of a drug to bile salt micelles. Drug solubility in each compartment of the gastrointestinal tract is determined according to **Equation 6-1**:

$$C_{GI,pH} = C_{aq,pH} \cdot \left( 1 + \frac{MW_{H_2O}}{\rho_{H_2O}} \cdot SR \cdot C_{bile} \right) \quad \text{Equation 6-1}$$

where  $C_{aq,pH}$  is the buffer solubility at a given pH calculated from the reference solubility,  $pK_a$  and solubility factor;  $C_{GI,pH}$  is the *in vivo* solubility in a compartment of the gastrointestinal tract with specific pH and bile salt concentration ( $C_{bile}$ ); and  $MW_{H_2O}$  and  $\rho_{H_2O}$  are the molecular weight and density of water, respectively [381].

In order to mimic the delay that LFs provoke in gastric emptying time, this value was fixed at 0.75 h, which broadly represents the semi-fed state. In addition, gastrointestinal volumes corresponding to the different compartments of the ACAT model were reduced to better replicate human physiological conditions<sup>xi</sup>.

The fraction of drug dose escaping metabolism at the gut wall ( $F_g$ ), previously derived from microsomal incubations (see Chapter 5, section 5.3.3) was used to fix the intestinal extraction ratio ( $E_g = 1 - F_g$ ).

#### 6.3.2.3. *In vivo* data

The plasma concentration–time profiles of the IV clinical studies of THC [280, 291–294] and CsA [138, 295] were used as input of the ACAT model to define the PK compartmental model. The plasma–concentration profiles of the oral clinical studies of Marinol® [240, 241] and Neoral® [242–244] were utilised for the validation of the oral predictions.

The distribution and elimination phases were described by a compartmental PK model which was fitted to the *in vivo* IV data. Since more than one PK experiment was available for each compound, the average dose–normalised plasma concentration–time profiles across experiments was calculated and fitted to the PK compartmental model. A three compartment model was chosen for both compounds as it provided the best fit, based on visual inspection and statistical analysis (Akaike and Bayesian information criteria, AIC and BIC).

### 6.3.3. Results and Discussion

In these preliminary studies, a generic ACAT model for predicting oral exposure based on *in silico* predictions (logP, pKa, permeability...), *in vitro* ADME estimations (bio–relevant solubility, and gut microsomal extraction), and the *in vivo* IV plasma concentration–time profiles, was applied to predict the oral *in vivo* performance of THC and CsA when administered to humans as Marinol® and Neoral®, respectively. The ability of the PBPK model to predict oral exposure of these LFs in humans was assessed by comparing the predictions of maximum concentration ( $C_{max}$ ), area under the curve up to the last measurable concentration ( $AUC_t$ ), time at which

---

<sup>xi</sup> Personal communication, Zoe Kane and Alison Wilby, Pharmaceutical Modelling and Simulation Scientists, Quotient Clinical Ltd.

$C_{\max}$  occurs ( $t_{\max}$ ), and profile shape (if available) against observations in the clinical studies. The simulated oral profiles are shown in **Figure 6-4** (THC) and **Figure 6-5** (CsA), whereas the resulting PK parameters are summarised in appendix **Table A-15**.

Interestingly, GastroPlus® predicted that both drugs would be completely absorbed ( $F_{\text{abs}} \sim 100\%$ ). Further investigation (by means of a parameter sensitivity analysis) led to the realisation that the model was not sensitive to any bio-relevant solubility input. The most plausible reason could be an error in the estimation of  $C_{\text{GI,pH}}$  (see **Equation 6-1**). In order to calculate these values, several default values and *in silico* predictions had to be used by the model. Probably, optimum predictability and better quality results could have been obtained if more parameters that influence  $C_{\text{GI,pH}}$  had been measured *in vitro*.

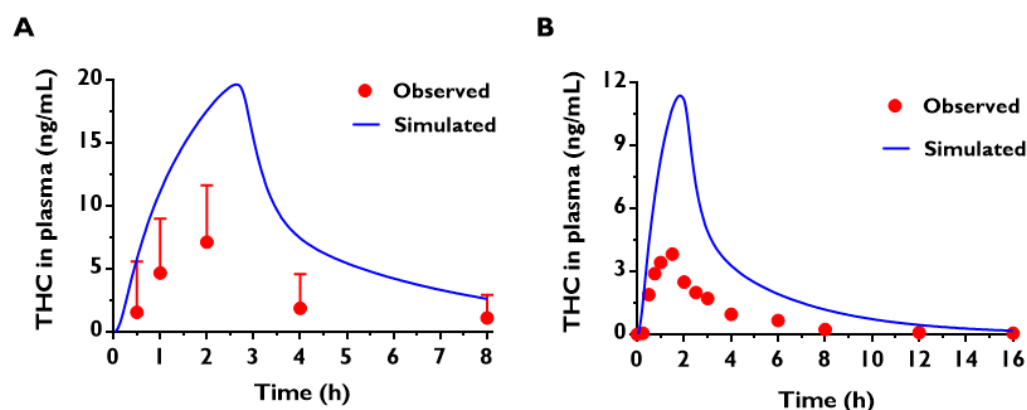


**Figure 6-4.** Simulated (blue line) and observed (red circles) plasma concentration–time profiles following single oral administration of (A) 20 mg and (B) 10 mg Marinol® to humans.

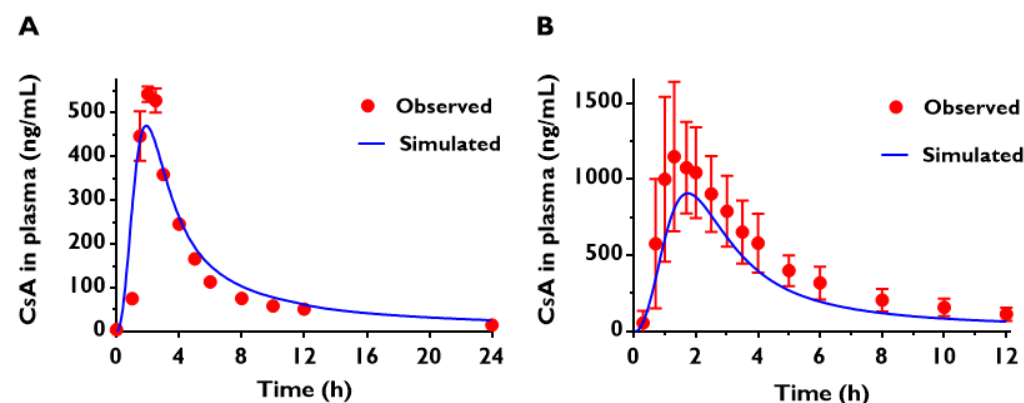


**Figure 6-5.** Simulated (blue line) and observed (red circles) plasma concentration–time profiles following single oral administration of (A) 200 mg and (B) 300 mg Neoral® to humans.

In the case of THC, simulated  $t_{\max}$  values were within the range of the observed ones, and  $C_{\max}$  values were within two-fold (10 mg) and three-fold (20 mg) of the *in vivo* ones. Absolute oral exposure was clearly overestimated, as illustrated by the  $AUC_t$  values, which were around 3 times higher than the reported ones.

In the case of CsA, the simulations were more accurate, as it can be inferred from the similarity between simulated and observed profile shapes.  $T_{\max}$  values were within 25% or less of the observed ones,  $C_{\max}$  values were less than 2-fold of the *in vivo* ones, and absolute bioavailability values were within 5%, 10% and 20% of the clinical values for 200, 300 and 600 mg Neoral® respectively. The higher accuracy in CsA predictions, compared to those of THC, could be due to the fact that more values measured *in vitro* (rather than predicted by *in silico* tools) were included as input parameters.

These results illustrate the value of PBPK simulations for potential use in early discovery and formulation development. Besides, these results demonstrate the importance of quality *in vitro* experimental data when refining the early PBPK results derived from mainly *in silico* predictions.

#### **6.3.4. Conclusions**

In general, the ACAT model provided reasonable predictions despite relying merely on some basic default values, and the use of *in silico* and *in vitro* data combined with average plasma concentration–time profiles from human IV PK studies. Better understanding of the software and underlying equations is needed to correct the lack of sensitivity shown for the *in vitro* lipolysis input.

## **Chapter 7: General Discussion and**

## **Concluding Remarks**

### **7.1. General Discussion: Summary, Future Perspectives, Impact on the Research Field, and Advantages and Limitations of the *In Vitro* Lipolysis/Microsomal Metabolism Model**

In recent years, the discovery of new active lipophilic molecules has increased enormously. The development of effective oral dosage forms for these drug candidates continues to be a pressing problem for the pharmaceutical industry. Many of these compounds are poorly water-soluble but permeate readily across biological membranes (belonging to class II of the Biopharmaceutics Classification System (BCS)). Hence, their dissolution rate and/or maximum solubility in the gastrointestinal tract represents the rate-limiting step to absorption. The co-administration of hydrophobic drugs with food, and in particular fatty food, has been known for some time to enhance absorption. The use of formulations containing lipids to mimic the absorption promotion provided by food has received growing interest in recent years. Lipids are believed to assist absorption by facilitating the formation of colloidal structures within the intestinal milieu that are capable of maintaining hydrophobic drugs in solution, thereby avoiding precipitation. Importantly, the generation of these colloidal species does not often arise directly from the co-administered lipid, but it is more frequently a result from the intraluminal processing (enzymatic digestion and subsequent dispersion) of these lipids prior to absorption.

Unfortunately, a considerable gap exists between the need for lipidic formulations (LFs), as justified by the great number of poorly water-soluble drugs filling the drug discovery pipelines, and its application, as evidenced by the low number of commercially available drug products relying on oral LFs (around 2% to 4% of the market share in US, UK and Japan in 2005 [6, 237]). The reasons for this could be attributed to many different causes, including insufficient drug solubility in the lipidic excipient matrix (which prevents administration of an entire therapeutic

dose in a single oral capsule), or insufficiently assessed physicochemical stability of drugs solubilised in lipidic excipients. Another equally plausible explanation is that the need for a LF cannot be determined with certainty at an early enough point during the drug development process. In order to do so, it would require reliable conviction that a conventional formulation (salt formation, particle size reduction, etc.) of a poorly water-soluble drug will not provide efficient exposure in humans prior to actual clinical testing. Nowadays, this information cannot be reliably estimated from *in vitro* and/or animal studies, and by the time a drug candidate has entered clinical trials, project timelines often simply cannot accommodate the development of an alternative formulation.

However, a growing opinion in the scientific community has suggested that the main contributing factors to the reluctant use LFs are the lack of standardised *in vitro* tests and poor understanding of the biotransformations and behaviour of LFs after oral administration. In this thesis, the causes for substrate specificity of pancreatic lipase have been investigated to provide a better mechanistic knowledge of the lipolysis process itself, and the factors governing lipase activity. The results presented here hopefully help to rationalise the performance of LFs and eventually aid in the development of optimised formulations.

Traditional dissolution testing cannot provide adequate predictions to enable successful rational development of LFs, as they overlook the lipolysis of excipients taking place in the gastrointestinal tract, which greatly influence the solubilisation of a co-administered poorly water-soluble drug. The *in vitro* lipolysis model emerged as a dissolution methodology capable of mimicking the *in vivo* enzymatic lipid digestion process and micellar drug solubilisation. Although this pH-stat method has been increasingly utilised for the assessment of LFs, experimental conditions are still under evaluation. There are several experimental factors that can impact the extent and rate of lipid digestion, and therefore the fate of loaded drugs. Calcium chloride concentration and lipase concentration are some of the factors that have been previously reported in literature. Research data presented in this thesis has contributed to the standardisation and harmonisation of *in vitro* lipolysis by providing a unique set of working conditions (in terms of titrant concentration, and maximum and minimum titrant addition rate) capable of assessing a wide range of LFs. Another important factor known to affect the

performance of LFs is bile concentration. Results presented herein have confirmed the significant impact of the level of bile salts and phospholipids on drug solubilisation; and accordingly it has been proposed the use of concentrations closer to physiological conditions in order to achieve more accurate predictions of *in vivo* performance.

When evaluating LFs by means of *in vitro* lipolysis and subsequent ultra-centrifugation, researchers commonly search for the highest aqueous micellar solubilisation, and the lowest lipid (if present) and sediment recovery among the tested formulations in the hopes of a higher *in vivo* exposure. The reason for this is that drug molecules in the micellar phase are assumed to be absorbed (enter the enterocytes), but the fraction of drug in lipid and sediment phases is expected to have delayed or no absorption. Investigators have usually attempted to achieve rank-order correlations of the performance of LFs by comparing *in vivo* pharmacokinetic parameters obtained in animals with the proportion of drug solubilised in the micellar phase. However, even achievement of rank-order correlation is not always successful. This is not surprising since *in vitro* lipolysis experiments mimic pre-enterocyte processes only. Thus, data gathered from this model might overlook critical processes occurring at earlier and later stages of the absorption process, such as gastric lipid hydrolysis, active drug transport through the gut wall, intra-enterocyte events such as enzymatic degradation, lymphatic transport, and efflux transporters; and post-enterocyte events such as hepatic first-pass metabolism.

To increase the predictivity of *in vivo* performance of LFs, investigations are divided into two “lines of thought”. On one side, some research groups have dedicated efforts to add in a gastric step to the *in vitro* lipolysis model. Gastric lipolysis represents on average 17% of the total extent of lipolysis, thus it is likely to be important for the digestion of some LFs, such as those with great lipidic content (Type I) or those containing long-chain triglycerides (since they are the substrates which are lipolysed to the lowest extent). Arguably, development of predictive gastric lipolysis models in combination with intestinal lipolysis models should be prioritised. However, this is currently hindered by the lack of availability of a suitable gastric lipase. On the other side, to get a more complete picture of the absorption process, researchers have focused on the use of cultured intestinal epithelial cells, Caco2 cell line and Ussing chambers, to investigate drug permeability across the gut wall, following *in vitro* lipolysis. Unfortunately, these

attempts have been relatively unsuccessful, although they are expected to be further researched in the future.

In this thesis it has been hypothesised, for the first time that the coupling of a metabolism phase, instead of a permeability one, to the *in vitro* lipolysis model would enable better predictions of *in vivo* performance of LFs. Since BCS II drugs are highly permeable, and excipients in LFs are expected to reduce or eliminate the effects of influx and efflux transporters, the other remaining factor that is overlooked by the *in vitro* lipolysis model and that affects drug systemic exposure is drug extraction at the gut wall and in the liver. This novel *in vitro* lipolysis/metabolism approach did not aim at qualitative rank-ordering of LFs based on correlation with animal data, but tried to go one step further and quantitatively predict directly the oral bioavailability in humans. The satisfactory predictions obtained in this thesis could be an indication that linking *in vitro* lipolysis and metabolism is the right path to follow for further improvement and development of an *in vitro* model that could accurately predict *in vivo* exposure and therefore facilitate, promote and rationalise the selection of LFs.

## **7.2. Concluding remarks**

The overall goal of this thesis was to further develop and improve the *in vitro* lipolysis model to better characterise lipidic formulations, and thus allow prediction of *in vivo* exposure in humans. In order to do so, different *in vitro* lipolysis model working conditions were evaluated and eventually optimised for tighter control over pH levels so as to better mimic *in vivo* conditions (Chapter 2). Next, the mechanisms behind pancreatic lipase activity was investigated to better understand the lipolysis process (Chapter 3). Once established, the *in vitro* lipolysis model was utilised to assess the fraction of absorbed dose of hydrophobic drugs administered in LFs (Chapter 4) and validate such results by comparing them with the *in vivo* pharmacokinetic data observed in humans, collected from published clinical studies. Because the data derived from *in vitro* lipolysis experimentations did not sufficiently predict the *in vivo* performance of LFs, hepatic and intestinal metabolism phases were introduced to account for the loss of drug due to first-pass metabolism (Chapter 5). Eventually, a novel approach was proposed (named *in*



*vitro* lipolysis/microsomal metabolism model) for the quantitative estimation of human oral bioavailability of BCS II drugs in LFs by combining the predicted fraction absorbed and non-metabolised values (Chapter 5). This novel methodology could drastically reduce the need for animal experiments, improve accuracy and predictability for formulation design, and lead to better designed clinical trials, hence reduce time and cost of industrial research and development.

The key conclusions from these investigations are summarised as follows.

- A) 1 M NaOH titrant concentration, 3.5 mL/min maximum titrant dosing rate and 3  $\mu$ L/min minimum titrant dosing rate, were found to be the conditions that better maintain pH environment within physiological range (6.75–6.85) during the hydrolysis of triglycerides with different carbon chain lengths. This optimised set of conditions also allowed the differentiation of the lipolysis of different lipid loads.
- B) The *in vitro* lipolysis by pancreatic lipase under bio-relevant conditions at physiological pH of equimolar amounts of TGs with different chain lengths was evaluated for the first time. Results proved there is a specific chain length range (C2–C8) for which pancreatic lipase showed higher activity. The specific surface area of the dispersed oil droplets, the solubility of 2-monoglycerides within mixed micelles, and the relative stability of the fatty acids as leaving groups in the hydrolysis reaction, are suggested to be the physicochemical properties which would determine the total extent of lipolysis.
- C) Marinol® (THC in sesame oil) and Neoral® (CsA dissolved in a mixture of lipids, co-solvents and surfactants) were chosen as model LFs for the validation of the *in vitro* lipolysis/metabolism approach. The selection of these medicines was done based on availability of published clinical data.
- D) *In vitro* lipolysis was used to assess the intestinal drug solubilisation of THC in Marinol® and CsA in Neoral®. An *in vivo* dissolution volume of 100 mL, rather than 250 mL, used for scaling down lipolysis doses, led to better predictions of fraction absorbed in comparison to clinical data. The use of a digestion buffer with surfactant concentrations closer to bio-relevant conditions, resulted in more accurate predictions in comparison to data derived from the classical buffer previously used in *in vitro* lipolysis studies. The digestion of very high doses of surfactants might represent a limitation to the model, since

*in vitro* lipolysis, at the moment, can not account for the micellar trapping phenomenon that could occur *in vivo*.

- E) *In vitro* lipolysis and microsomal metabolism studies were combined for the first time with the aim to quantitative predict the human oral bioavailability of BCS II drugs administered in LFs. This novel approach led to reasonably good predictions of oral bioavailability of THC in Marinol®, and CsA in Neoral® based on the similarity between the predicted bioavailability values and those reported in clinical trials after oral administration of the tested formulations to human subjects. The novel *in vitro* lipolysis/metabolism approach has the potential to transform the *in vitro* lipolysis studies from a qualitative tool to a quantitative one.
- F) Further studies are needed to confirm the predictive power of the model. This could be done by predicting the *in vivo* performance of additional BCS II drug in LFs when administered to humans or to pre-clinical species (with prior refinement in the lipolysis buffer concentration to properly mimic animal lipid digestion). A further application of the *in vitro* lipolysis model could be an *in vitro* input for *in silico* modelling to predict the plasma concentration–time profiles of drugs delivered in LFs.

## Appendix

### Appendix A. Pharmacokinetic data following administration of model drugs and lipidic formulations

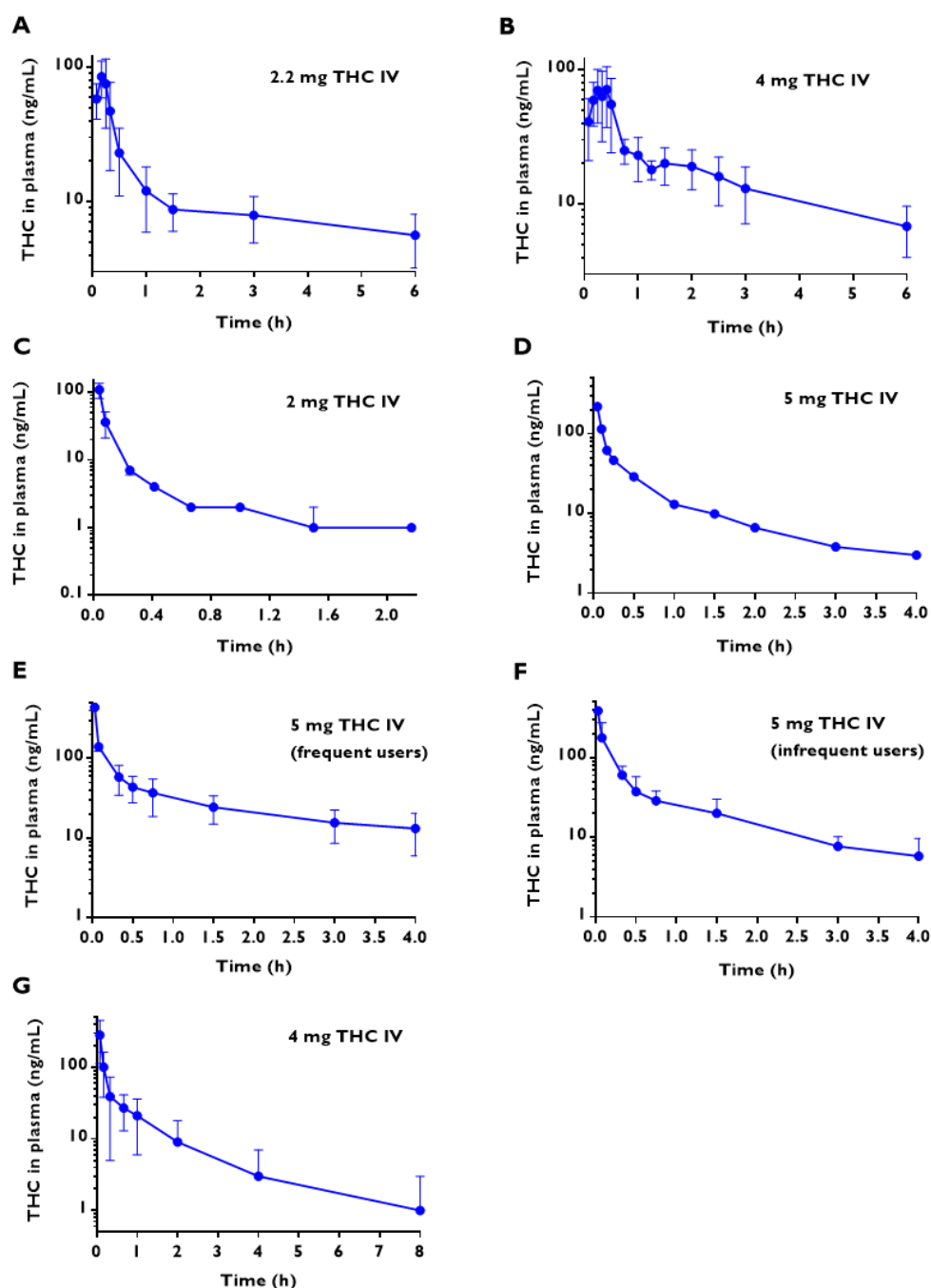


**Figure A-I.** Observed mean  $\pm$  SD plasma concentration–time profiles following intravenous administration of THC, extracted from literature. (Figures **A** and **B**, and **D** adapted with permission from Ref. [280] and [292], Copyright© 1983 and 1980, respectively, American Society for Clinical Pharmacology and Therapeutics; Figure **C** from [291], Copyright© 1981, Plenum Publishing Corporation; Figures **E** and **F** from [293], Copyright© 1992, Oxford University Press; and Figure **G** from [294], Copyright© 2004, Wiley–Liss, Inc.)

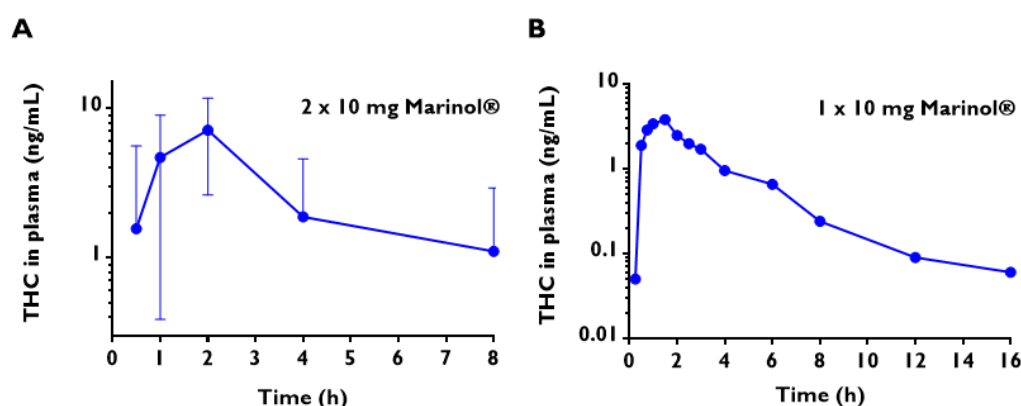


**Figure A-2.** Observed mean  $\pm$  SD plasma concentration–time profiles following oral administration of Marinol®, extracted from literature. (Figure **A** adapted with permission from Ref. [240], Copyright© 2003, Lippincott Williams; and Figure **B** from [241], under the terms of the US Patent and Trademark Office, 2012)

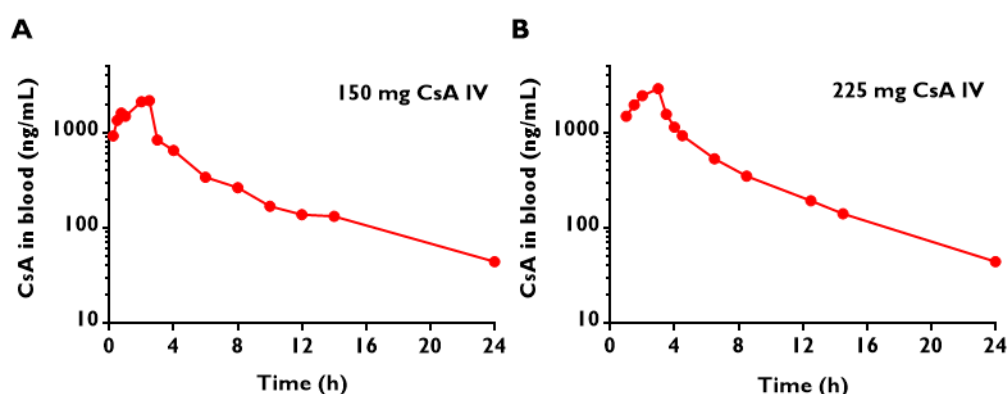


**Figure A-3.** Observed mean  $\pm$  SD blood concentration–time profiles following intravenous administration of CsA, extracted from literature. (Figures **A** and **B** adapted with permission from Ref. [295] and [138], Copyright© 1995 and 1992, respectively, American Society for Clinical Pharmacology and Therapeutics)

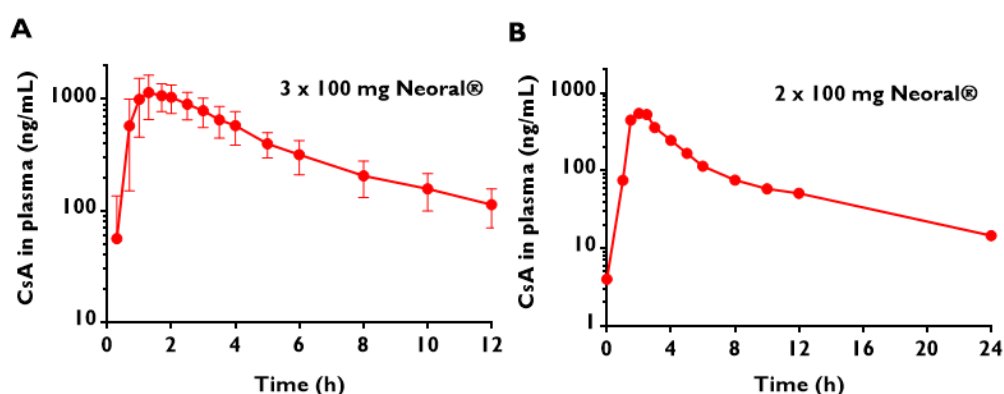


**Figure A-4.** Observed mean  $\pm$  SD plasma concentration–time profiles following oral administration of Neoral®, extracted from literature. (Figure **A** adapted with permissions from Ref. [244], Copyright© 2003, Elsevier B.V.; and Figure **B** from Ref. [243], under the terms of the US Patent and Trademark Office, 1999)

**Table A-I.** Pharmacokinetic parameters reported in literature [240, 241, 280, 292–294] or calculated from the extracted plasma concentration–time profiles (in blue colours), after intravenous and oral (as Marinol®) administration of  $\Delta^9$ -tetrahydrocannabinol. Values are expressed as means  $\pm$  SD, unless otherwise stated.

	Intravenous						Oral		
	Wall et al. [280]		Hunt et al. [291]	Ohlsson et al. [292]	Kelly & Jones [293]		Naef et al. [294]	Naef et al. [240]	Goskonda et al. [241]
n	6 (Women)	6 (Men)	4	11	4 (Users)	4	8	12	18
Dose (mg)	2.2	4	2	5	5	5	4	20	10
t <sub>1/2,z</sub> (min)	1740	2160	1272 ± 90	88	117 ± 17	93 ± 31	98.2	313	392 ± 208
t <sub>max</sub> (min)	–	–	–	–	–	–	–	60 to 120	92 ± 77
C <sub>max</sub> (ng/mL)	–	–	–	–	–	–	–	7.2 ± 2.0	6.12 ± 3.02
AUC <sub>t</sub> (ng·min/mL)	12100 ± 4620	16800 ± 4000	1277	4330 ± 620	9907 ± 3785	7094 ± 2248	7509	1368	734 ± 503
AUC <sub>∞</sub> (ng·min/mL)	15211	22750	1416	4762	9451	8069	7028 ± 5829	1865 ± 1661	762 ± 527
AUC <sub>∞</sub> /dose (ng·min/mL/mg)	5500 ± 2100	4200 ± 1000	636 ± 45	866 ± 124	1981 ± 757	1419 ± 450	1757 ± 1457	93 ± 83	76 ± 53
V <sub>z</sub> (L/kg)	9.9	10.2	0.06 ± 0.03	1.769	1.31 ± 0.57	1.33 ± 0.44	0.982	–	–
V <sub>ss</sub> (L/kg)	4.12	4.63	9.86 ± 2.47	9.44	1.03 ± 0.21	1.00 ± 0.48	0.59 ± 0.29	–	–
CL (mL/min/kg)	3.39 ± 0.85	3.24 ± 0.90	10.22 ± 1.72	13.17	10.01 ± 8.88	9.93 ± 3.69	10.47 ± 5.35	–	–
AUC <sub>∞</sub> /dose (ng·min/mL/mg)	2277 ± 2020 (88.7%)*							93 ± 83 (89.2%)	76 ± 53 (69.7%)
CL (mL/min/kg)	9.05 ± 5.35 (59.1%)*							–	–

t<sub>1/2,z</sub>: terminal phase half-life; C<sub>max</sub>: maximum peak plasma concentration; t<sub>max</sub>: time at which C<sub>max</sub> occurs; AUC: area under the blood concentration–time profile from time zero to the last measurable concentration point (AUC<sub>t</sub>), and extrapolated to the infinity (AUC<sub>∞</sub>); V<sub>z</sub>: terminal phase volume of distribution; V<sub>ss</sub>: volume of distribution in the steady-state; CL: blood clearance (derived from CL<sub>plasma</sub> and blood to plasma ratio = 1.063 [248]); N.P.: not provided either numerically or graphically, (–): not applicable

\* Values are expressed as weighted means  $\pm$  overall standard deviation (coefficient of variation).

**Table A-2.** Pharmacokinetic parameters reported in literature [138, 242–244, 295] or calculated from the extracted blood concentration–time profiles (in blue colours), after intravenous and oral (as Neoral®) administration of cyclosporin A. Values are expressed as means  $\pm$  SD, unless otherwise stated.

	Intravenous		Oral				
	Gomez et al. [295]	Hebert et al. [138]	Odeberg et al. [244]		Kim et al. [243]	Mueller et al. [242]	
<b>n</b>	5	5	3	6	12	24	24
<b>Dose (mg)</b>	150	225	300	300	200	200	600
<b>t<sub>1/2,z</sub> (min)</b>	429	314	232 $\pm$ 15		444	420 $\pm$ 156	558 $\pm$ 150
<b>t<sub>max</sub> (min)</b>	–	–	79.8	109.8	96 $\pm$ 6	90 $\pm$ 24	102 $\pm$ 36
<b>C<sub>max</sub> (ng/mL)</b>	–	–	1307 $\pm$ 127	1256 $\pm$ 438	1243 $\pm$ 35	1026 $\pm$ 218	1813 $\pm$ 400
<b>AUC<sub>t</sub> (ng·min/mL)</b>	541575	741555	302705 $\pm$ 107433		322752 $\pm$ 11646	N.P.	N.P.
<b>AUC<sub>∞</sub> (ng·min/mL)</b>	400968 $\pm$ 112875	608290 $\pm$ 98073	309120 $\pm$ 61680	351480 $\pm$ 127560	333167 $\pm$ 11655	208260 $\pm$ 61740	589860 $\pm$ 142140
<b>AUC<sub>∞</sub>/dose (ng·min/mL/mg)</b>	2673 $\pm$ 753	2704 $\pm$ 436	1030 $\pm$ 206	1172 $\pm$ 425	1666 $\pm$ 58	1041 $\pm$ 309	983 $\pm$ 237
<b>V<sub>z</sub> (L/kg)</b>	2.17	1.79	–	–	–	–	–
<b>V<sub>ss</sub> (L/kg)</b>	1.27 $\pm$ 0.44	1.16 $\pm$ 0.42	–	–	–	–	–
<b>CL (mL/min/kg)</b>	5.30 $\pm$ 1.40	4.97 $\pm$ 0.80	–	–	–	–	–
<b>AUC<sub>∞</sub>/dose (ng·min/mL/mg)</b>	2688 $\pm$ 615 (22.9%)*		1125 $\pm$ 373 (33.1%)*		1250 $\pm$ 389 (31.1%)*		983 $\pm$ 237 (24.1%)
<b>CL (mL/min/kg)</b>	5.14 $\pm$ 1.15 (22.4%)*		–		–		–

t<sub>1/2,z</sub>: terminal phase half-life; C<sub>max</sub>: maximum peak blood concentration; t<sub>max</sub>: time at which C<sub>max</sub> occurs; AUC: area under the blood concentration–time profile from time zero to the last measurable concentration point (AUC<sub>t</sub>), and extrapolated to the infinity (AUC<sub>∞</sub>); V<sub>z</sub>: terminal phase volume of distribution; V<sub>ss</sub>: volume of distribution in the steady-state; CL: clearance; N.P.: not provided either numerically or graphically, (–): not applicable

\* Values are expressed as weighted means  $\pm$  overall standard deviation (coefficient of variation)

**Appendix B. HPLC–UV Method development for the determination of  $\Delta^9$ -tetrahydrocannabinol and cyclosporin A in lipolysis samples**

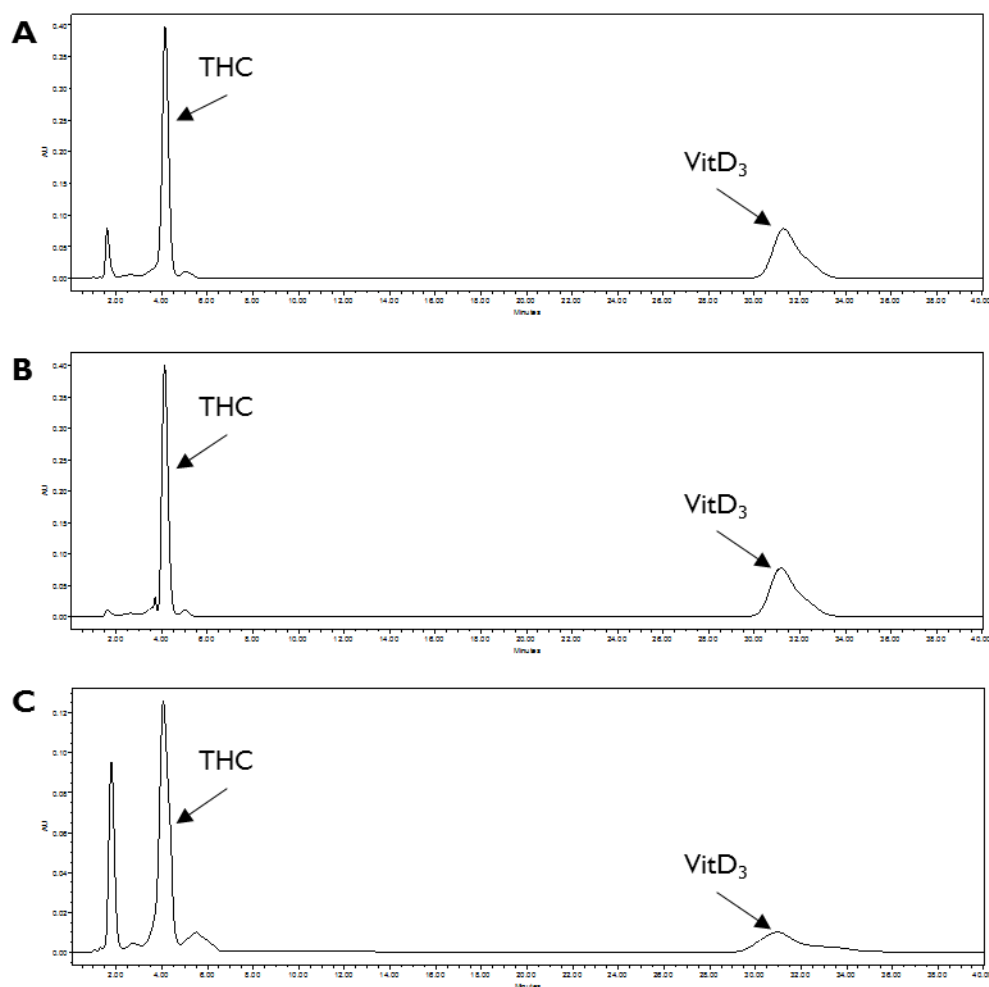


**Figure A-5.** Representative HPLC–UV chromatograms ( $\lambda = 220$  nm), spiked with the internal standard vitamin D<sub>3</sub> (VitD<sub>3</sub>), of micellar (**A**), sediment (**B**) and lipid (**C**) phases obtained after lipolysis and ultra-centrifugation of Marinol® ( $\Delta^9$ -tetrahydrocannabinol, THC, in sesame oil).

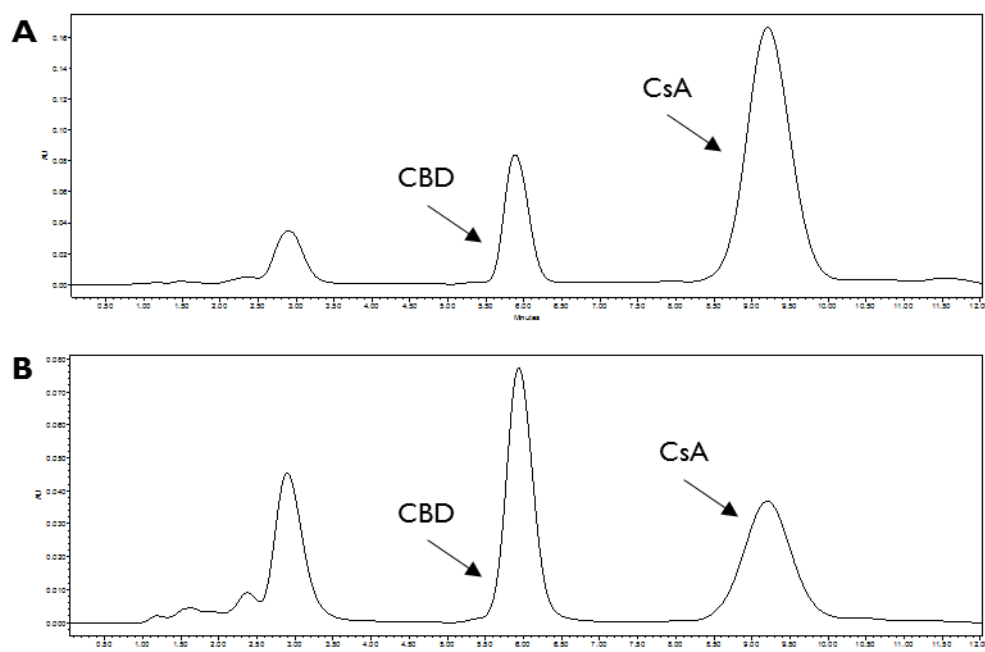


**Figure A-6.** Representative HPLC–UV chromatograms ( $\lambda = 211 \text{ nm}$ ), spiked with the internal standard cannabidiol (CBD), of micellar (**A**) and sediment (**B**) phases obtained after lipolysis and ultra-centrifugation of Neoral® (cyclosporin A, CsA, in a mixture of corn oil, ethanol, propylene glycol, and Kolliphor® RH 40).

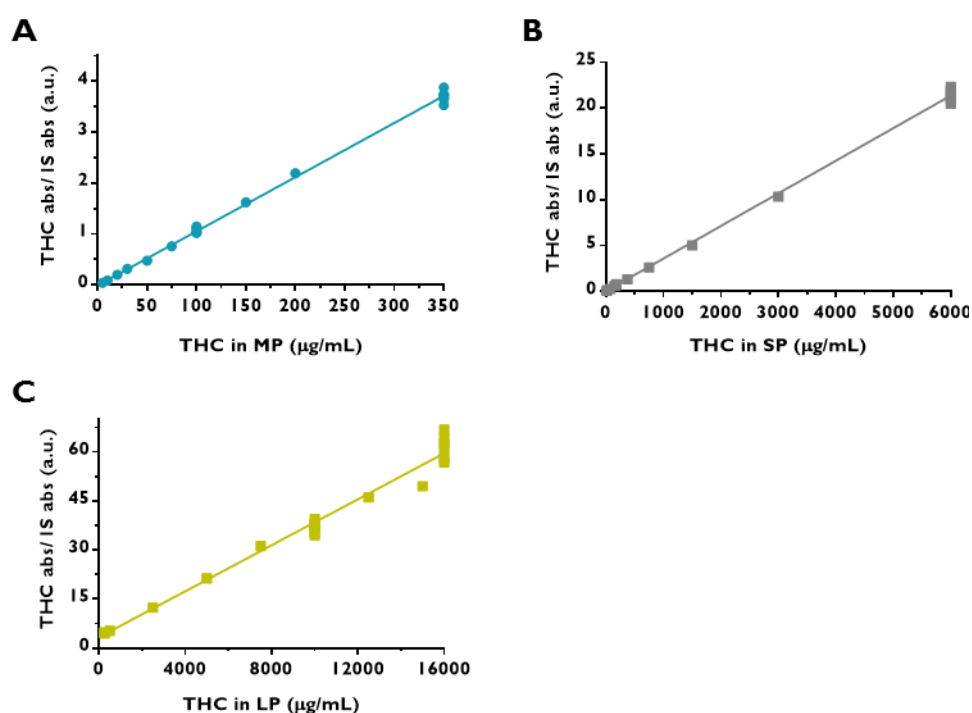


**Figure A-7.** Plot of peak area ratios of  $\Delta^9$ -tetrahydrocannabinol (THC) and internal standard (IS) versus sample concentration in (**A**) micellar (MP), (**B**) sediment (SP), and (**C**) lipid (LP) phases, obtained for the intra-day validation of the HPLC–UV detection method.



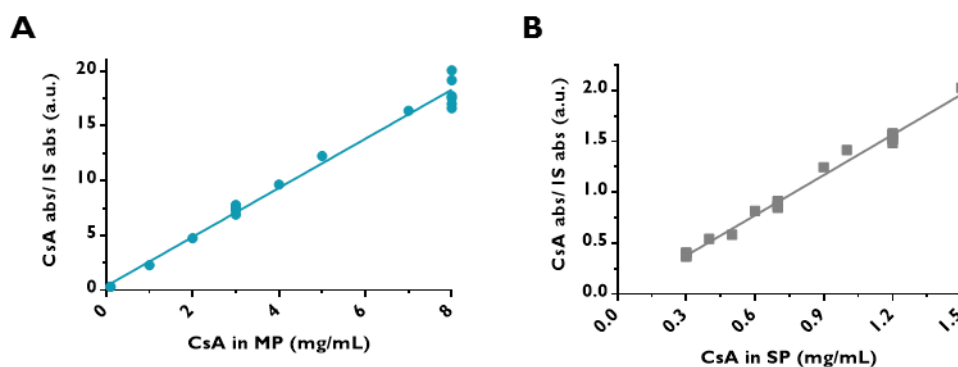


**Figure A-8.** Plot of peak area ratios of cyclosporin A (CsA) and internal standard (IS) versus sample concentration in (A) micellar (MP) and (B) sediment (SP) phases, obtained for the intra-day validation of the HPLC–UV detection method.

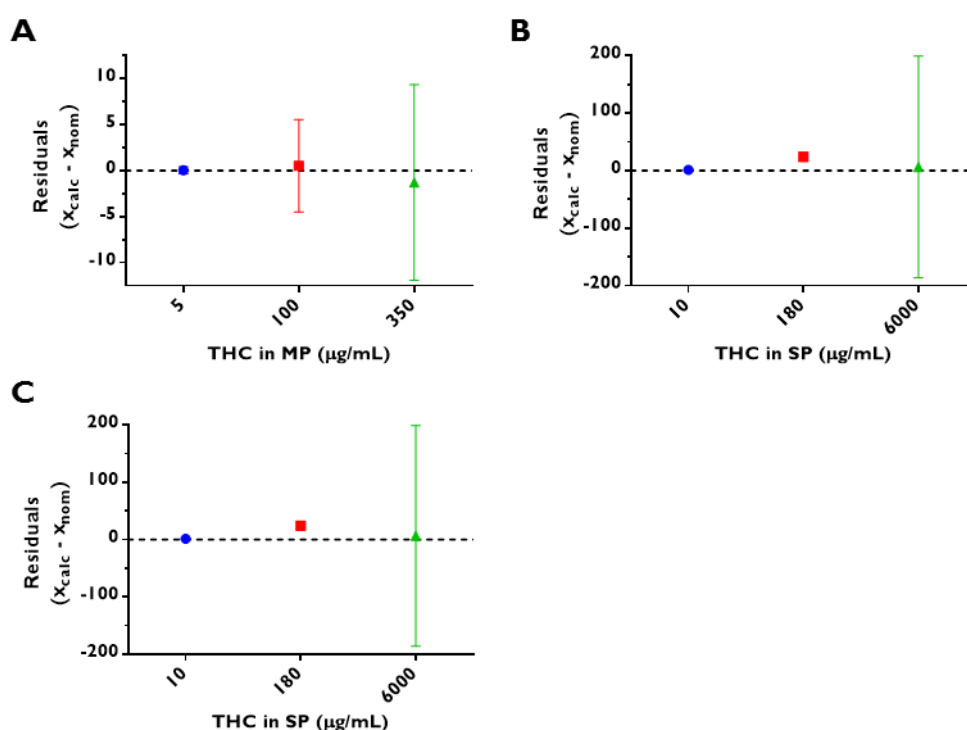


**Figure A-9.** Residuals plotted against low, medium and high quality control concentration samples in (A) micellar (MP), (B) sediment (SP), and (C) lipid (LP) phases, obtained for the intra-day validation of the HPLC–UV detection method of  $\Delta^9$ -tetrahydrocannabinol (THC).  $x_{\text{calc}}$  is the regressed concentration computed from the non-weighted calibration curve, and  $x_{\text{nom}}$  is the nominal standard concentration.

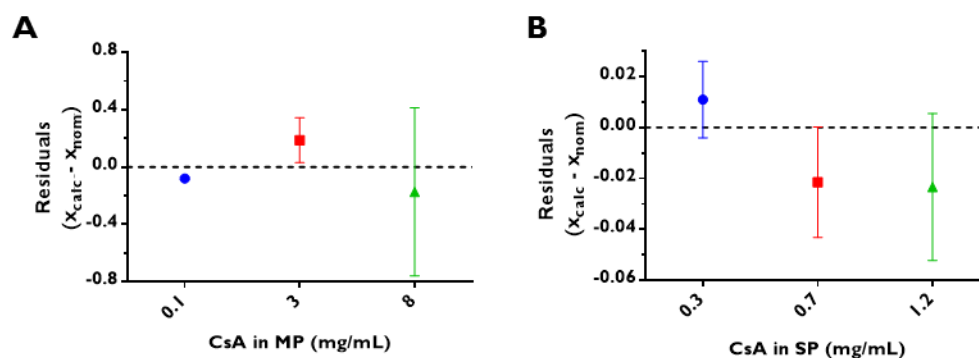


**Figure A-10.** Residuals plotted against low, medium and high quality control concentration samples in **(A)** micellar (MP) and **(B)** sediment (SP) phases, obtained for the intra-day validation of the HPLC–UV detection method of cyclosporin A (CsA).  $x_{\text{calc}}$  is the regressed concentration computed from the non-weighted calibration curve, and  $x_{\text{nom}}$  is the nominal standard concentration.

**Table A-3.** Sum of relative errors (RE) for various curve-weighting values and  $F$  values corresponding to data obtained during intra-day validation of the HPLC–UV detection method of  $\Delta^9$ -tetrahydrocannabinol (THC) and cyclosporin A (CsA) in lipolysis phases.

Drug	Lipolysis phase	$\sum \text{RE} (\%)$		$F_{\text{exp}}$
		$1/x$	$1/x^2$	
THC	MP	100.8266	100.8634	818.3
	SP	254.9426	158.3603	$3.7 \cdot 10^5$
	LP	192.2304	161.7768	988.2
CsA	MP	138.6973	135.5478	3651.6
	SP			3.7

MP: Micellar phase; SP: sediment phase; LP: lipid phase.

**Table A-4.** Intra-day and inter-day accuracy and precision for the detection of  $\Delta^9$ -tetrahydrocannabinol (Marinol®) and cyclosporin A (Neoral®) in lipolysis phases.

	Lipolysis phase	Quality control sample	$x_{nom}$ (mg/mL)	Intra-day (n = 6)			Inter-day (n = 6)		
				$x_{calc}$ (mg/mL)	Accuracy RE (%)	Precision RSD (%)	$x_{calc}$ (mg/mL)	Accuracy RE (%)	Precision RSD (%)
Marinol®	Micellar	LLOQ	0.002	0.002 ± 0.000	9.8	11.9	-	-	-
		Low	0.01	0.01 ± 0.00	3.8	4.8	0.01 ± 0.00	3.6	4.7
		Medium	0.05	0.05 ± 0.001	1.6	1.9	0.051 ± 0.004	6.0	7.9
		High	0.35	349 ± 11	2.2	3.1	0.336 ± 0.020	5.5	5.9
	Sediment	Low	0.01	0.01 ± 0.00	1.9	2.5	0.01 ± 0.00	1.4	1.4
		Medium	0.1	0.11 ± 0.004	9.9	3.2	0.101 ± 0.005	3.6	4.5
		High	6	5.8 ± 1.86	3.6	3.2	5.595 ± 0.296	7.0	5.3
	Lipid	Low	0.25	0.26 ± 0.035	10.3	13.5	0.249 ± 0.019	5.3	7.6
		Medium	5	5.079 ± 0.176	3.0	3.5	5.144 ± 0.120	3.0	2.3
		High	16	16.788 ± 1.099	6.6	6.5	15.040 ± 1.155	7.9	7.7
Neoral®	Micellar	LLOQ	0.05	0.051 ± 0.002	4	4.8	-	-	-
		Low	0.1	0.101 ± 0.009	7.6	9.2	0.102 ± 0.005	3.1	5.1
		Medium	3	3.164 ± 0.151	6.5	4.8	2.895 ± 0.209	6.4	7.2
		High	8	7.651 ± 0.568	7.1	4.8	8.312 ± 0.588	6.4	7.1
	Sediment	Low	0.3	0.304 ± 0.015	4.6	5.0	0.305 ± 0.010	3.0	3.4
		Medium	0.7	0.679 ± 0.022	3.6	3.3	0.694 ± 0.025	3.1	3.6
		High	1.2	1.187 ± 0.029	2.1	2.5	1.193 ± 0.030	2.1	2.5

LLOQ: Lowest validated limit of quantification;  $x_{nom}$ : nominal concentration;  $x_{calc}$ : calculated concentration (means (n=6) ± SD); RE: relative error; RSD: relative standard deviation

**Appendix C. HPLC–MS/MS Method development for the determination of  $\Delta^9$ -tetrahydrocannabinol and cyclosporin A in microsomal incubation samples**

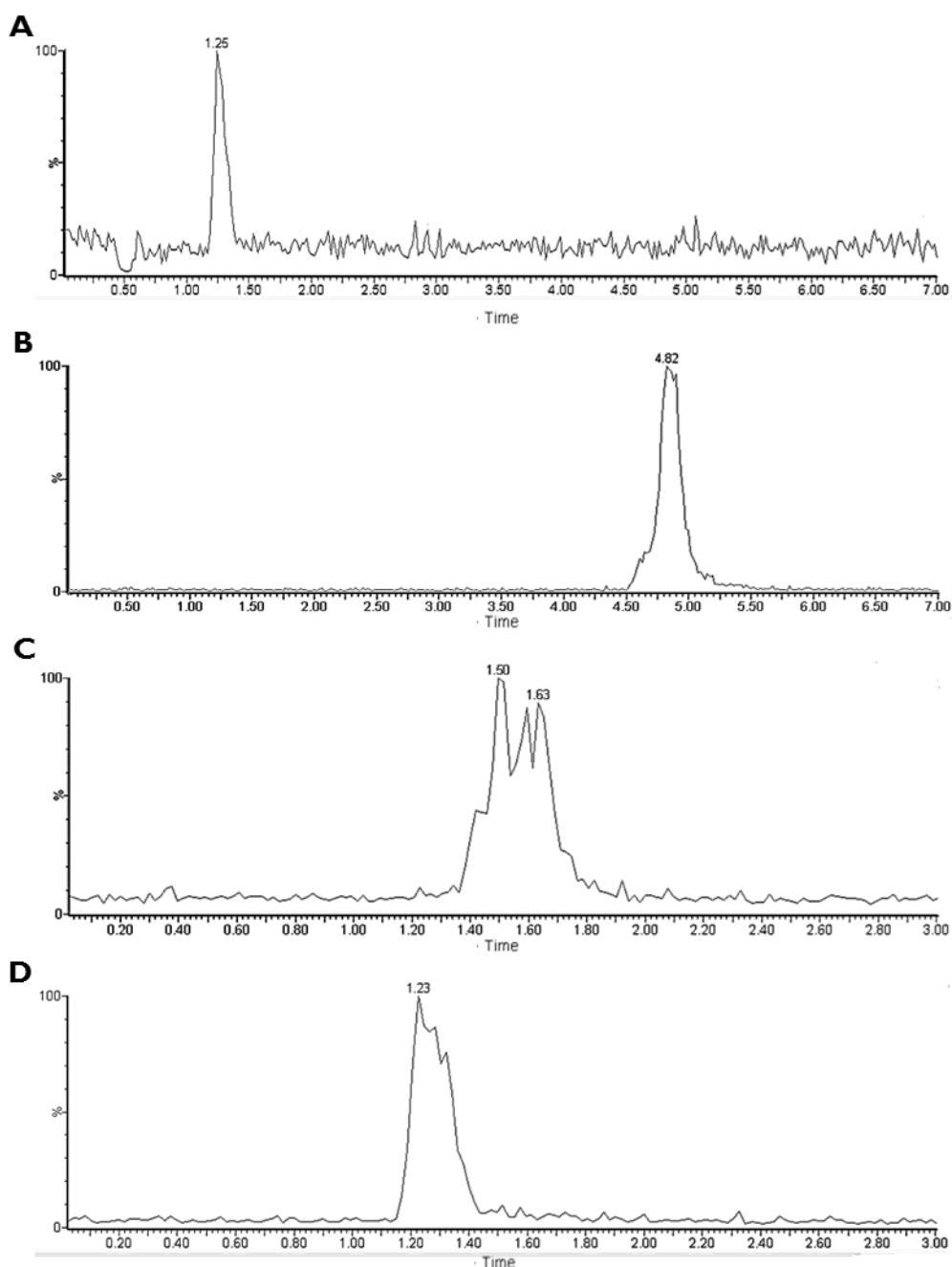


**Figure A-11.** HPLC–MS/MS chromatograms of 2.5 ng/mL of  $\Delta^9$ -tetrahydrocannabinol (**A**) and 9.5 ng/mL cyclosporin A (**C**) in 0.1% (v/v) formic acid in acetonitrile. Representative chromatograms of the internal standards vitamin D<sub>3</sub> (**B**) and cannabidiol (**D**) are also included.

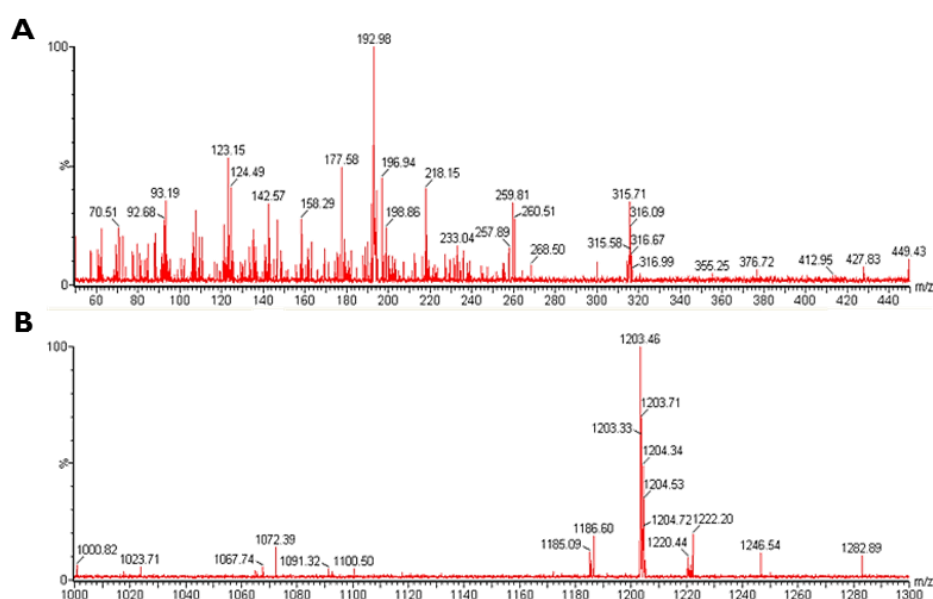


**Figure A-12.** MS/MS spectra of  $\Delta^9$ -tetrahydrocannabinol (**A**) and cyclosporin A (**B**) in 0.1% (v/v) formic acid in acetonitrile.

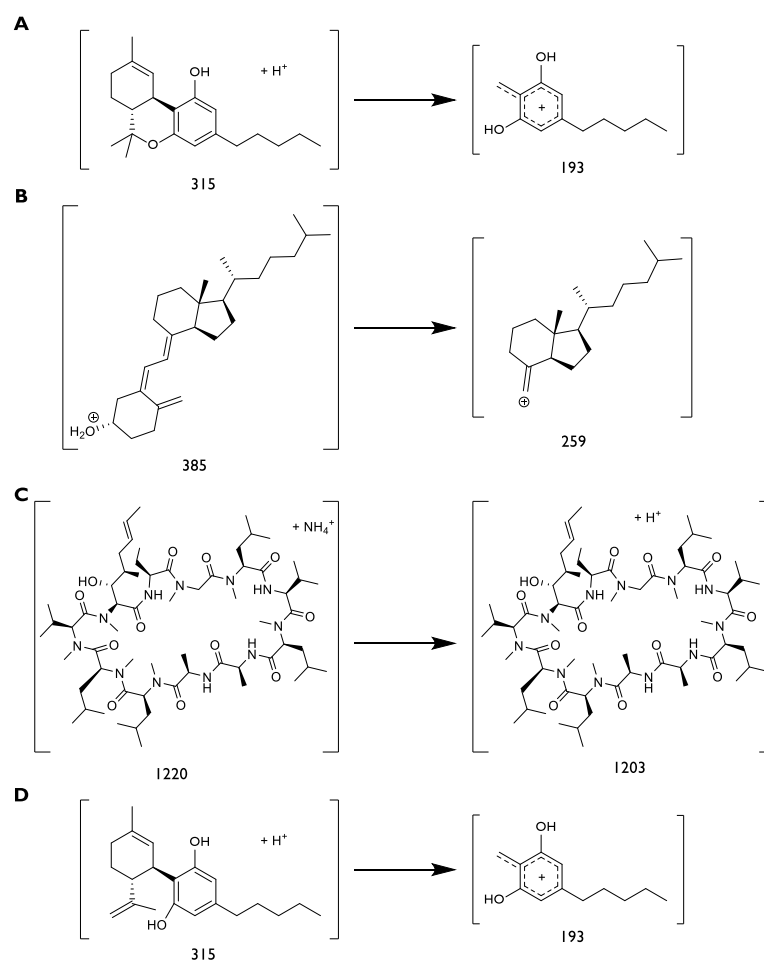


**Figure A-13.** Proposed mechanism for the fragmentation for  $\Delta^9$ -tetrahydrocannabinol (**A**), vitamin D<sub>3</sub> (**B**), cyclosporin A (**C**) and cannabidiol (**D**), in positive ionisation mode. Numbers indicate the *m/z* values for each fragment.

## Appendix D. Additional data derived from the microsomal metabolism of $\Delta^9$ -tetrahydrocannabinol, cyclosporin A, and control compounds

**Table A-5.** Rate depletion constants ( $k_{dep}$ ,  $\text{min}^{-1}$ ) obtained following the incubation of  $\Delta^9$ -tetrahydrocannabinol (THC), cyclosporin A (CsA), and control compounds at different initial substrate concentrations with hepatic microsomes. Values are expressed as means ( $n = 6$ )  $\pm$  SD.

	THC	CsA	Dexamethasone	Verapamil
<b>1 <math>\mu\text{M}</math></b>	$0.6555 \pm 0.0048$	$0.0144 \pm 0.0004$	$0.0033 \pm 0.0004$	$0.0658 \pm 0.0054$
<b>2.5 <math>\mu\text{M}</math></b>	$0.3023 \pm 0.0189$	$0.0102 \pm 0.0011$	N/A	
<b>5 <math>\mu\text{M}</math></b>	$0.2108 \pm 0.0214$	$0.0080 \pm 0.0008$		
<b>10 <math>\mu\text{M}</math></b>	$0.1436 \pm 0.0049$	$0.0055 \pm 0.0005$		

**Table A-6.** Hepatic microsomal data for  $\Delta^9$ -tetrahydrocannabinol, calculated assuming different fractions of drug unbound in the incubations ( $f_{u,inc}$ ). Values are expressed as means ( $n = 6$ )  $\pm$  SD.

$f_{u,inc}$		0.5068 <sup>a</sup>	0.00289 <sup>b</sup>	0.00638 <sup>c</sup>
<b>CL<sub>u,int</sub> (mL/min/mg)</b>		$2.640 \pm 0.850$	$462.904 \pm 148.996$	$209.685 \pm 67.492$
<b>CL<sub>u,h,int</sub> (mL/min/kg)</b>		$1858.3 \pm 598.1$	$32588.4 \pm 10489.3$	$147618.5 \pm 47514.4$
<b>CL<sub>h</sub> (mL/min/kg)</b>	<b>WS</b>	$9.6 \pm 3.1$	$19.7 \pm 6.3$	$20.7 \pm 6.7$
	<b>PT</b>	$12.0 \pm 3.9$	$21.0 \pm 6.8$	$21.0 \pm 6.8$
<b>F<sub>h</sub> (%)</b>	<b>WS</b>	$54.1 \pm 14.4$	$6.3 \pm 2.0$	$1.5 \pm 0.5$
	<b>PT</b>	$42.8 \pm 13.8$	$0.0 \pm 0.0$	$0.0 \pm 0.0$

CL<sub>u,int</sub>: *In vitro* intrinsic clearance; CL<sub>u,h,int</sub>: *in vivo* intrinsic hepatic clearance; CL<sub>h</sub>: hepatic clearance; F<sub>h</sub>: fraction escaping hepatic metabolism; WS: well-stirred model; PT: parallel tube model.

<sup>a</sup> Calculated assuming binding to serum proteins is analogous to binding to microsomal proteins (Equation 5-4); <sup>b</sup> Calculated according to Hallifax and Houston [339]; <sup>c</sup> Calculated according to Austin *et al.* [338].

**Table A-7.** Hepatic microsomal data for cyclosporin A, calculated assuming different fractions of drug unbound in the incubations ( $f_{u_{inc}}$ ). Values are expressed as means ( $n = 6$ )  $\pm$  SD.

$f_{u_{inc}}$		0.7127 <sup>a</sup>	0.4062 <sup>b</sup>
<b>CL<sub>u,int</sub> (mL/min/mg)</b>		0.045 $\pm$ 0.003	0.079 $\pm$ 0.006
<b>CL<sub>u,h,int</sub> (mL/min/kg)</b>		31.6 $\pm$ 2.2	55.5 $\pm$ 3.9
<b>CL<sub>h</sub> (mL/min/kg)</b>	<b>WS</b>	1.2 $\pm$ 0.1	2.0 $\pm$ 0.1
	<b>PT</b>	1.2 $\pm$ 0.1	2.1 $\pm$ 0.1
<b>F<sub>h</sub> (%)</b>	<b>WS</b>	94.3 $\pm$ 6.6	90.4 $\pm$ 6.4
	<b>PT</b>	94.2 $\pm$ 6.6	90.0 $\pm$ 6.3

CL<sub>u,int</sub>: *In vitro* intrinsic clearance; CL<sub>u,h,int</sub>: *in vivo* intrinsic hepatic clearance; CL<sub>h</sub>: hepatic clearance; F<sub>h</sub>: fraction escaping hepatic metabolism; WS: well-stirred model; PT: parallel tube model.

<sup>a</sup> Calculated according to Hallifax and Houston [339]; <sup>b</sup> Calculated according to Austin *et al.* [338].

**Table A-8.** Intestinal microsomal data for  $\Delta^9$ -tetrahydrocannabinol, calculated assuming different fractions of drug unbound in the incubations ( $f_{u_{inc}}$ ). Values are expressed as means ( $n = 6$ )  $\pm$  SD.

$f_{u_{inc}}$	0.5068 <sup>a</sup>	0.00289 <sup>b</sup>	0.00638 <sup>c</sup>
<b>CL<sub>u,int</sub> (mL/min/mg)</b>	0.182 $\pm$ 0.003	45041.938 $\pm$ 848.147	20403.009 $\pm$ 384.192
<b>CL<sub>u,g,int</sub> (L/h)</b>	15.4 $\pm$ 0.3	2702.5 $\pm$ 50.9	1224.2 $\pm$ 23.1
<b>F<sub>g</sub> (%)</b>	36.8 $\pm$ 0.7	0.3 $\pm$ 0.0	0.7 $\pm$ 0.0
<b>CL<sub>u,g,int</sub> (L/h)*</b>	25.7 $\pm$ 8.3	4506.3 $\pm$ 1450.4	2041.2 $\pm$ 657.0
<b>F<sub>g</sub> (%)*</b>	25.8 $\pm$ 8.3	0.2 $\pm$ 0.1	0.4 $\pm$ 0.1

CL<sub>u,int</sub>: *In vitro* intrinsic clearance; CL<sub>u,g,int</sub>: *in vivo* intrinsic gut clearance; F<sub>g</sub>: fraction escaping intestinal metabolism.

<sup>a</sup> Calculated assuming binding to serum proteins is analogous to binding to microsomal proteins (Equation 5-4); <sup>b</sup> Calculated according to Hallifax and Houston [339]; <sup>c</sup> Calculated according to Austin *et al.* [338]; \* Derived from hepatic microsomal data.

**Table A-9.** Intestinal microsomal data for cyclosporin A, calculated assuming different fractions of drug unbound in the incubations ( $f_{u_{inc}}$ ). Values are expressed as means ( $n = 6$ )  $\pm$  SD.

$f_{u_{inc}}$		0.7127 <sup>a</sup>	0.4062 <sup>b</sup>
<b>CL<sub>u,int</sub> (mL/min/mg)</b>		0.016 $\pm$ 0.002	0.028 $\pm$ 0.004
<b>CL<sub>u,g,int</sub> (L/h)</b>		1.3 $\pm$ 0.2	2.3 $\pm$ 0.3
<b>F<sub>g</sub> (%)</b>		70.8 $\pm$ 9.1	58.0 $\pm$ 7.4
<b>CL<sub>u,g,int</sub> (L/h)*</b>		1.1 $\pm$ 0.1	1.9 $\pm$ 0.1
<b>F<sub>g</sub> (%)*</b>		75.3 $\pm$ 5.3	63.5 $\pm$ 4.5

CL<sub>u,int</sub>: *In vitro* intrinsic clearance; CL<sub>u,g,int</sub>: *in vivo* intrinsic gut clearance; F<sub>g</sub>: fraction escaping intestinal metabolism.

<sup>a</sup> Calculated according to Hallifax and Houston [339]; <sup>b</sup> Calculated according to Austin *et al.* [338]; \* Data obtained by extrapolating intestinal metabolism from hepatic microsomal data.



**Table A-10.** Predicted oral bioavailability values of  $\Delta^9$ -tetrahydrocannabinol in Marinol® using the *in vitro* lipolysis/metabolism approach. Values are expressed as means  $\pm$  SD.

		Classical buffer	New buffer	Classical buffer (*)	New buffer (*)
2 x 10 mg Marinol® capsules	WS	4.0 $\pm$ 1.4	1.5 $\pm$ 0.5	2.8 $\pm$ 1.3	1.1 $\pm$ 0.5
	PT	3.2 $\pm$ 1.1	1.2 $\pm$ 0.4	2.2 $\pm$ 1.1	1.2 $\pm$ 0.4
1 x 10 mg Marinol® capsule	WS	9.4 $\pm$ 3.4	1.3 $\pm$ 0.5	6.6 $\pm$ 3.2	0.9 $\pm$ 0.5
	PT	7.4 $\pm$ 2.7	1.0 $\pm$ 0.4	5.2 $\pm$ 1.9	0.7 $\pm$ 0.4

Classical buffer: 5 mM bile salt, 0.75 mM phospholipid; New buffer: 3 mM bile salt; 0.2 mM phospholipid; WS: well-stirred model; PT: parallel tube model.

(\*) Data obtained by extrapolating intestinal metabolism from hepatic microsomal data

**Table A-11.** Predicted oral bioavailability values of cyclosporin A in Neoral® using the *in vitro* lipolysis/metabolism approach. Values are expressed as means  $\pm$  SD

			Classical buffer	New buffer	Classical buffer (*)	New buffer (*)
2 x 100 mg Neoral® capsules	WS	$f_{u_{inc}}$ , Halifax	30.9 $\pm$ 4.5	58.4 $\pm$ 8.6	32.9 $\pm$ 3.3	62.1 $\pm$ 6.2
		$f_{u_{inc}}$ , Austin	24.3 $\pm$ 3.6	45.8 $\pm$ 6.7	26.6 $\pm$ 2.7	50.2 $\pm$ 5.1
	PT	$f_{u_{inc}}$ , Halifax	30.9 $\pm$ 4.5	58.3 $\pm$ 8.6	32.9 $\pm$ 3.6	62.0 $\pm$ 6.2
		$f_{u_{inc}}$ , Austin	24.2 $\pm$ 3.5	45.6 $\pm$ 6.7	26.5 $\pm$ 2.5	49.9 $\pm$ 5.0
3 x 100 mg Neoral® capsules	WS	$f_{u_{inc}}$ , Halifax	37.7 $\pm$ 5.7	58.7 $\pm$ 9.1	40.0 $\pm$ 4.3	62.4 $\pm$ 7.0
		$f_{u_{inc}}$ , Austin	29.6 $\pm$ 4.5	46.1 $\pm$ 7.1	32.4 $\pm$ 3.5	50.5 $\pm$ 5.7
	PT	$f_{u_{inc}}$ , Halifax	37.6 $\pm$ 5.7	58.6 $\pm$ 9.1	37.6 $\pm$ 4.0	62.4 $\pm$ 7.0
		$f_{u_{inc}}$ , Austin	29.4 $\pm$ 4.4	45.9 $\pm$ 7.1	29.4 $\pm$ 3.1	50.2 $\pm$ 5.6
6 x 100 mg Neoral® capsules	WS	$f_{u_{inc}}$ , Halifax	52.4 $\pm$ 7.8	67.9 $\pm$ 12.6	55.7 $\pm$ 5.8	72.2 $\pm$ 11.0
		$f_{u_{inc}}$ , Austin	41.2 $\pm$ 6.1	53.3 $\pm$ 9.9	45.1 $\pm$ 4.7	58.4 $\pm$ 8.9
	PT	$f_{u_{inc}}$ , Halifax	52.4 $\pm$ 7.8	67.9 $\pm$ 11.6	55.7 $\pm$ 5.8	72.2 $\pm$ 11.0
		$f_{u_{inc}}$ , Austin	41.0 $\pm$ 6.1	53.1 $\pm$ 7.1	44.9 $\pm$ 4.7	58.1 $\pm$ 8.8

Classical buffer: 5 mM bile salt, 0.75 mM phospholipid; New buffer: 3 mM bile salt; 0.2 mM phospholipid; WS: well-stirred model; PT: parallel tube model;  $f_{u_{inc}}$ , Halifax and  $f_{u_{inc}}$ , Austin: fraction of drug unbound to microsomes, calculated according to Halifax and Houston [339] and Austin *et al.* [338].

(\*) Data obtained by extrapolating intestinal metabolism from hepatic microsomal data

## Appendix E. Pharmacokinetic data derived from the intravenous and oral administration of $\Delta^9$ -tetrahydrocannabinol to rats

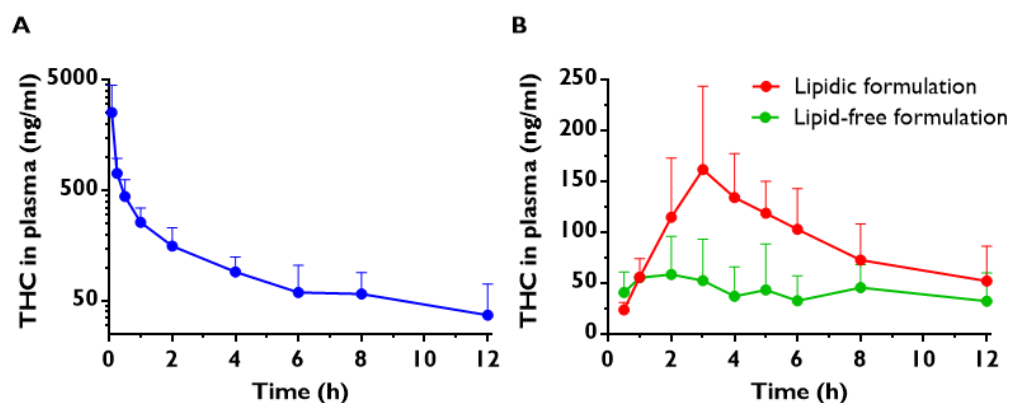


**Figure A-14.** Observed mean + SD plasma concentration–time profiles of  $\Delta^9$ -tetrahydrocannabinol (THC) following (A) intravenous (4 mg/kg, n = 5) and (B) oral (12 mg/kg) administration to rats. Red colours represent the lipidic formulation (sesame oil, n = 6), whereas green colours represent the lipid-free formulation (propylene glycol/ethanol/water (80:10:10, v/v), n = 5). (Adapted with permission from Ref. [370], under the terms of CC BY, 2016)

**Table A-12.** Pharmacokinetic parameters (means  $\pm$  SD) derived from the intravenous and oral administration of  $\Delta^9$ -tetrahydrocannabinol to rats.

	Intravenous	Oral	
		Lipidic formulation	Lipid-free formulation
<b>n</b>	5	6	5
<b>Dose (mg/kg)</b>	4	12	12
<b><math>t_{1/2}</math> (min)</b>	276 $\pm$ 268	444 $\pm$ 382	414 $\pm$ 268
<b><math>t_{max}</math> (min)</b>	–	180	120
<b><math>C_{max}</math> (ng/mL)</b>	–	172 $\pm$ 83	65 $\pm$ 38
<b>AUC<sub>t</sub> (ng·min/mL)</b>	97440 $\pm$ 44811	63000 $\pm$ 24838	24840 $\pm$ 17441
<b>F (%)</b>	–	21.5 $\pm$ 8.6	8.5 $\pm$ 5.8
<b><math>V_d</math> (L/kg)</b>	7.9 $\pm$ 4.6	–	
<b>CL (mL/min/kg)</b>	41.9 $\pm$ 23.8	–	

Lipidic formulation: sesame oil; lipid-free formulation: propylene glycol/ethanol/water (80:10:10, v/v);  $t_{1/2}$ : half-life;  $C_{max}$ : maximum peak plasma concentration;  $t_{max}$ : time at which  $C_{max}$  occurs; AUC<sub>t</sub>: area under the plasma concentration–time profile from time zero to the last measurable concentration point; F: observed oral bioavailability;  $V_d$ : volume of distribution; CL: blood clearance (derived from CL<sub>plasma</sub> and blood to plasma ratio = 1.063 [248]). (Adapted with permission from Ref. [370], under the terms of CC BY, 2016)

## Appendix F. Additional data resulting from the *in vitro* lipolysis of the lipidic and lipid-free formulations of $\Delta^9$ -tetrahydrocannabinol

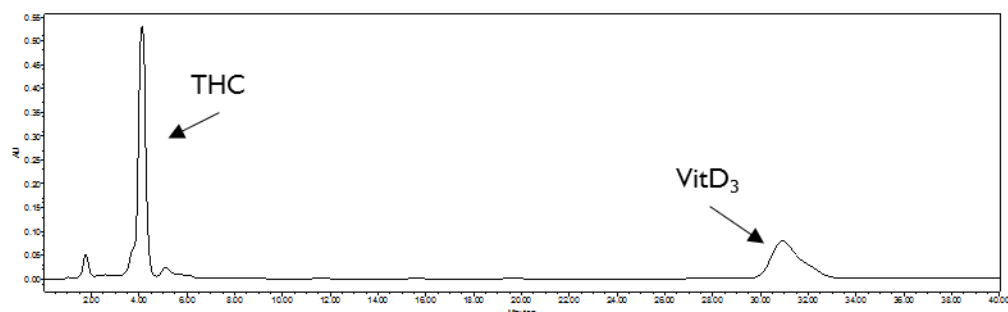


**Figure A-15.** Representative HPLC–UV chromatograms ( $\lambda = 220$  nm) of the liquid–crystalline phase obtained after lipolysis and ultra–centrifugation of 3.2 mL 12 mg/mL  $\Delta^9$ -tetrahydrocannabinol (THC) in sesame oil, spiked with the internal standard vitamin D<sub>3</sub> (VitD<sub>3</sub>).

**Table A-13.** Intra–day and inter–day accuracy and precision for the detection of  $\Delta^9$ -tetrahydrocannabinol in the liquid–crystalline phase obtained after lipolysis and ultra–centrifugation of 3.2 mL of 12 mg/mL sesame oil.

Quality control sample		Low	Medium	High
$x_{\text{nom}}$ (mg/mL)		45	200	450
Intra–day (n = 6)	$x_{\text{calc}}$ (mg/mL)	44 ± 5	195 ± 21	437 ± 15
	Accuracy RE (%)	9.8	7.1	2.9
	Precision RSD (%)	11.9	10.7	3.3
Inter–day (n = 6)	$x_{\text{calc}}$ (mg/mL)	49 ± 5	205 ± 11	450 ± 5
	Accuracy RE (%)	12.3	4.5	5.0
	Precision RSD (%)	10.8	5.0	2.5

$x_{\text{nom}}$ : nominal concentration;  $x_{\text{calc}}$ : calculated concentration (means (n=6) ± SD); RE: relative error; RSD: relative standard deviation.

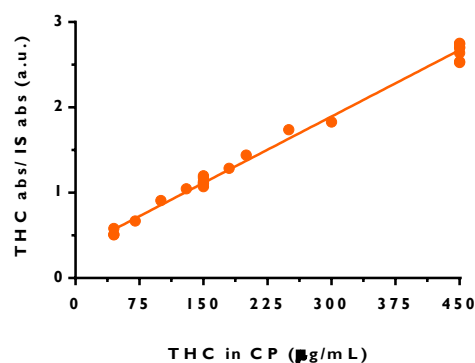


**Figure A-16.** Plot of peak area ratios of  $\Delta^9$ -tetrahydrocannabinol (THC) and internal standard (IS) versus sample concentration in the liquid-crystalline phase (CP), obtained for the intra-day validation of the HPLC-UV detection method.

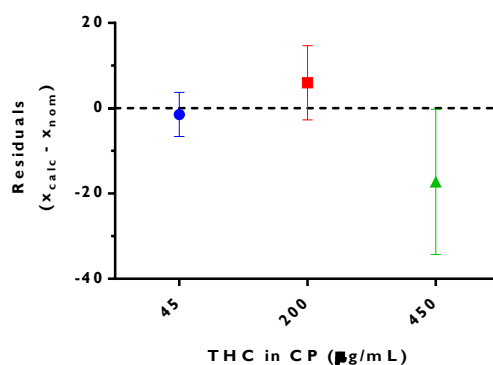


**Figure A-17.** Residuals plotted against low, medium and high quality control concentration samples in the liquid-crystalline (CP) phase, obtained for the intra-day validation of the HPLC-UV detection method of  $\Delta^9$ -tetrahydrocannabinol (THC).  $x_{\text{calc}}$  is the regressed concentration computed from the non-weighted calibration curve, and  $x_{\text{nom}}$  is the nominal standard concentration.

## Appendix G. Additional data derived from the *in silico* simulations of the oral profiles of Marinol® and Neoral®

**Table A-14.** *In silico* estimates and *in vitro* experimental values for  $\Delta^9$ -tetrahydrocannabinol and cyclosporin A physicochemical and biopharmaceutical properties.

	$\Delta^9$ -Tetrahydrocannabinol		Cyclosporin A	
	Estimate ( <i>in silico</i> )*	Observed ( <i>in vitro</i> )	Estimate ( <i>in silico</i> )*	Observed ( <i>in vitro</i> )
<b>Molecular formula</b>	$C_{21}H_{30}O_2$		$C_{62}H_{111}N_{11}O_{12}$	
<b>Molecular weight</b>	314.47 g/mol		1202.64 g/mol	
<b>logP/logD</b>	6.97	–	3.35	–
<b>Acid pK<sub>a</sub></b>	10.17	–	10.3	–
<b>Solubility factor</b>	7143 <sup>a</sup>		4000 <sup>a</sup>	–
<b>Solubility at pH 7.4</b>		2.8 µg/mL [246]		5 µg/mL [247]
<b>Effective permeability</b>	7.56 µm/s			1.65 µm/s [249]
<b>Dosage form</b>	Immediate release: solution			
<b>Gastric emptying time</b>	0.75 h			
<b>Initial dose</b>		10, 20 mg [240, 241]		200, 300, 600 [242–244]
<b>Dosage volume</b>	240 mL			
<b>Mean precipitation time</b>	900 s			
<b>Diffusion coefficient</b>	$3 \cdot 10^{-6}$ cm <sup>2</sup> /s			
<b>Drug particle density</b>	1.2 g/mL			
<b>SGF solubility</b>	0 mg/mL (pH 1.2, bile salt concentration: 0 mM) <sup>b</sup>			
<b>FaSSIF solubility (pH 6.8, bile salt concentration: 3 mM)</b>		15, 6 µg/mL <sup>c</sup>		1.729, 2.637, 6.103 g/mL <sup>c</sup>
<b>FeSSIF solubility</b>	0 mg/mL (pH 5, bile salt concentration: 15 mM) <sup>b</sup>			
<b>Body weight</b>	70 kg			
<b>Blood/plasma ratio</b>	1.063			2 [382]
<b>f<sub>u</sub> (%)</b>	1.02			8 [174, 382]
<b>E<sub>g</sub> (%)</b>		74.2 <sup>d</sup>		42.0 <sup>d</sup>

SGF: Simulated gastric fluids; FaSSIF: fasted state simulated intestinal fluids; FeSSIF: fed state simulated intestinal fluids; f<sub>u</sub>: fraction of drug unbound to plasma; E<sub>g</sub>: gut extraction.

\* Obtained using ADMET Predictor® (Simulations Plus, Inc.) [248] or ACD/I-Lab [245].

<sup>a</sup> Value estimated by dividing the number 20 by the intrinsic aqueous solubility in mg/mL, as indicated in the manual (based on the publication by Bergstrom et al. [383]). <sup>b</sup> According to the manual, if the experimental value is unknown, the input should be zero. <sup>c</sup> Solubility found in the micellar phase following *in vitro* lipolysis of the formulation. <sup>d</sup> Estimated from intestinal microsomal incubations.

**Table A-15.** Pharmacokinetic output parameters obtained following the simulations of the oral profiles of Marinol® and Neoral® at different dose levels with GastroPlus®.

	Marinol®				Neoral®					
	10 mg		20 mg		200 mg		300 mg		600 mg	
	Observed	Simulated	Observed	Simulated	Observed	Simulated	Observed	Simulated	Observed	Simulated
<b>F<sub>abs</sub> (%)</b>	–	100	–	100	–	99.8	–	97.6	–	97.6
<b>F<sub>abs</sub>•F<sub>g</sub> (%)</b>	–	26	–	26	–	57.8	–	56.6	–	56.6
<b>F (%)</b>	3.4 ± 3.8	15.4	4.1 ± 3.6	15.4	46.5 ± 18.1	48.1	41.8 ± 16.9	47.0	37 ± 12	47
<b>C<sub>max</sub> (ng/mL)</b>	6.12 ± 3.02	11.3	7.2 ± 2.0	19.6	549 ± 103	471	572.5	906.45	906 ± 200	1806
<b>t<sub>max</sub> (h)</b>	1.53 ± 1.28	2.64	1 to 2	1.81	1.5 ± 0.33	1.92	1.33	1.72	1.7 ± 0.6	1.68
<b>AUC<sub>t</sub> (ng•h/mL)</b>	12.23 ± 8.38	38.32	22.8	66.8	2691 ± 97	2677	2522	3519	4915 ± 1184	7894

F<sub>abs</sub>: Fraction absorbed; F<sub>g</sub>: intestinal bioavailability; F: absolute bioavailability; C<sub>max</sub>: maximum plasma concentration; t<sub>max</sub>: time at which C<sub>max</sub> occurs; AUC<sub>t</sub>: area under the plasma concentration–time profile.

Observed values were collected from references [240–244]

## References

1. Lipinski, C. A., Lombardo, F., Dominy, B. W., & Feeney, P. J. (2001). Experimental and computational approaches to estimate solubility and permeability in drug discovery and development settings. *Advanced Drug Delivery Reviews*, 46(1–3), 3–26.
2. Lipinski, C. A. (2000). Drug-like properties and the causes of poor solubility and poor permeability. *Journal of Pharmacological and Toxicological Methods*, 44(1), 235–249.
3. Fahr, A., & Liu, X. (2007). Drug delivery strategies for poorly water-soluble drugs. *Opinion on Drug Delivery*, 4(4), 403–416.
4. Williams, H. D., Trevaskis, N. L., Charman, S. A., Shanker, R. M., Charman, W. N., Pouton, C. W., & Porter, C. J. H. (2013). Strategies to Address Low Drug Solubility in Discovery and Development. *Pharmacological Reviews*, 65(1), 315–499.
5. Takagi, T., Ramachandran, C., Bermejo, M., Yamashita, S., Yu, L. X., & Amidon, G. L. (2006). A Provisional Biopharmaceutical Classification of the Top 200 Oral Drug Products in the United States, Great Britain, Spain, and Japan. *Molecular Pharmaceutics*, 3(6), 631–643.
6. Hauss, D. J. (2007). Preface. In D. J. Hauss (Ed.), *Oral Lipid-Based Formulations: Enhancing the Bioavailability of Poorly Water-Soluble Drugs*. Princeton, New Jersey, USA: Bristol-Myers Squibb Company.
7. Fasano, A. (1998). Innovative strategies for the oral delivery of drugs and peptides. *Trends in biotechnology*, 16(4), 152–157.
8. Hatley, O. (2013). *Mechanistic prediction of intestinal first-pass metabolism using in vitro data and preclinical species and in man*. Pharmacy School. The University of Manchester, Manchester.
9. Amidon, G., Lennernäs, H., Shah, V., & Crison, J. (1995). A Theoretical Basis for a Biopharmaceutic Drug Classification: The Correlation of in Vitro Drug Product Dissolution and in Vivo Bioavailability. *Pharmaceutical Research*, 12(3), 413–420.
10. US Food and Drug Administration. (2016). USP Monographs: Pancrelipase, available at: [http://www.pharmacopeia.cn/v29240/usp29nf24s0\\_m60320.html](http://www.pharmacopeia.cn/v29240/usp29nf24s0_m60320.html) (Accessed: May 2016).
11. Rautio, J., Kumpulainen, H., Heimbach, T., Oliyai, R., Oh, D., Jarvinen, T., & Savolainen, J. (2008). Prodrugs: design and clinical applications. *Nat Rev Drug Discov*, 7(3), 255–270.
12. Pouton, C. W. (2006). Formulation of poorly water-soluble drugs for oral administration: Physicochemical and physiological issues and the lipid formulation classification system. *European Journal of Pharmaceutical Sciences*, 29(3–4), 278–287.
13. Müllertz, A., Ogbonna, A., Ren, S., & Rades, T. (2010). New perspectives on lipid and surfactant based drug delivery systems for oral delivery of poorly soluble drugs. *Journal of Pharmacy and Pharmacology*, 62(11), 1622–1636.
14. Custodio, J. M., Wu, C.-Y., & Benet, L. Z. (2008). Predicting Drug Disposition, Absorption / Elimination / Transporter Interplay And The Role Of Food On Drug Absorption. *Advance Drug Delivery Reviews*, 60(6), 717–733.
15. Benet, L. Z. (2009). The Role of Transporters in the Pharmacokinetics of Orally Administered Drugs. *Pharmaceutical Research*, 26(9), 2039–2054.

16. Dahan, A., Miller, J., & Amidon, G. (2009). Prediction of Solubility and Permeability Class Membership: Provisional BCS Classification of the World's Top Oral Drugs. *The AAPS Journal*, 11(4), 740–746.
17. Wilkinson, G. R. (2005). Drug Metabolism and Variability among Patients in Drug Response. *New England Journal of Medicine*, 352(21), 2211–2221.
18. van de Waterbeemd, H., & Gifford, E. (2003). ADMET in silico modelling: towards prediction paradise? *Nature Review Drug Discovery*, 2(3), 192–204.
19. Serajuddin, A. T. M. (2007). Salt formation to improve drug solubility. *Advanced Drug Delivery Reviews*, 59(7), 603–616.
20. Bowker, M. J. (2002). Procedure for Salt Selection and Optimisation. In P. H. Stahl & C. G. Wermuth (Eds.), *Handbook of Pharmaceutical Salts: Properties, Selection, and Use* (pp. 161–89). Weinheim: Wiley-VCH.
21. Singhal, D., & Curatolo, W. (2004). Drug polymorphism and dosage form design: a practical perspective. *Advanced Drug Delivery Reviews*, 56(3), 335–347.
22. Pudipeddi, M., & Serajuddin, A. T. M. (2005). Trends in solubility of polymorphs. *J Pharm Pharm Sci*, 94, 929–39.
23. Yu, L. (2001). Amorphous pharmaceutical solids: preparation, characterization and stabilization. *Advance Drug Delivery Reviews*, 48, 27–42.
24. Serajuddin, A. T. M. (1999). Solid dispersion of poorly water-soluble drugs: Early promises, subsequent problems, and recent breakthroughs. *J Pharm Pharm Sci*, 88(10), 1058–66.
25. Giri, T. K., Alexander, A., & Tripathi, D. K. (2010). Physicochemical Classification and Formulation Development Of Solid Dispersion Of Poorly Water Soluble Drugs: An Updated Review. *International Journal of Pharmaceutical & Biological Archives*, 1(4), 309–24.
26. Challa, R., Ahuja, A., Ali, J., & Khar, R. K. (2005). Cyclodextrins in drug delivery: An updated review. *AAPS PharmSciTech*, 6(2), E329–E357.
27. Loftsson, T., & Duchêne, D. (2007). Cyclodextrins and their pharmaceutical applications. *International Journal of Pharmaceutics*, 329(1–2), 1–11.
28. Stella, V. J., & Rajewski, R. A. (1997). Cyclodextrins: their future in drug formulation and delivery. *Pharmaceutical Research*, 14, 556–567.
29. Khadka, P., Ro, J., Kim, H., Kim, I., Kim, J. T., Kim, H., ... Lee, J. (2014). Pharmaceutical particle technologies: An approach to improve drug solubility, dissolution and bioavailability. *Asian Journal of Pharmaceutical Sciences*, 9(6), 304–316.
30. Liversidge, G. G., & Cundy, K. C. (1995). Particle size reduction for improvement of oral bioavailability of hydrophobic drugs: I. Absolute oral bioavailability of nanocrystalline danazol in beagle dogs. *International Journal of Pharmaceutics*, 125(1), 91–97.
31. Nykamp, G., Carstensen, U., & Müller, B. W. (2002). Jet milling—a new technique for microparticle preparation. *International Journal of Pharmaceutics*, 242(1–2), 79–86.
32. Van Eerdenbrugh, B., Van den Mooter, G., & Augustijns, P. (2008). Top-down production of drug nanocrystals: Nanosuspension stabilization, miniaturization and transformation into solid products. *International Journal of Pharmaceutics*, 364(1), 64–75.



33. Müller, R. H., Jacobs, C., & Kayser, O. (2001). Nanosuspensions as particulate drug formulations in therapy: Rationale for development and what we can expect for the future. *Advanced Drug Delivery Reviews*, 47(1), 3–19.
34. Chakraborty, S., Shukla, D., Mishra, B., & Singh, S. (2009). Lipid – An emerging platform for oral delivery of drugs with poor bioavailability. *European Journal of Pharmaceutics and Biopharmaceutics*, 73(1), 1–15.
35. Benito-Gallo, P., Gershkovich, P., Marlow, M., Zann, V., & Wasan, K. M. (2016). Smart Lipid-Based Drug Delivery Systems. In V. P. Torchilin (Ed.), *Smart Pharmaceutical Nanocarriers* (pp. 309–371). Imperial College Press.
36. McClements, D. J., Decker, E. A., & Park, Y. (2008). Controlling Lipid Bioavailability through Physicochemical and Structural Approaches. *Critical Reviews in Food Science and Nutrition*, 49(1), 48–67.
37. Mu, H., & Høy, C.-E. (2004). The digestion of dietary triacylglycerols. *Progress in Lipid Research*, 43(2), 105–133.
38. Carey, M. C., Small, D. M., & Bliss, C. M. (1983). Lipid digestion and absorption. *Annu Rev Physiol.*, 45(1), 651–677.
39. Nordskog, B. K., Phan, C. T., Nutting, D. F., & Tso, P. (2001). An examination of the factors affecting intestinal lymphatic transport of dietary lipids. *Advanced Drug Delivery Reviews*, 50(1–2), 21–44.
40. Charman, W. N., Porter, C. J. H., Mithani, S., & Dressman, J. B. (1997). Physicochemical and physiological mechanisms for the effects of food on drug absorption: The role of lipids and pH. *Journal of Pharmaceutical Sciences*, 86(3), 269–282.
41. DeNigris, S. J., Hamosh, M., Kasbekar, D. K., Lee, T. C., & Hamosh, P. (1988). Lingual and gastric lipases: species differences in the origin of prepancreatic digestive lipases and in the localization of gastric lipase. *Biochimica et Biophysica Acta (BBA) - Lipids and Lipid Metabolism*, 959(1), 38–45.
42. Hamosh, M., & Scow, R. O. (1973). Lingual Lipase and Its Role in the Digestion of Dietary Lipid. *The Journal of Clinical Investigation*, 52(1), 88–95.
43. Dahan, A., & Hoffman, A. (2008). Rationalizing the selection of oral lipid based drug delivery systems by an in vitro dynamic lipolysis model for improved oral bioavailability of poorly water soluble drugs. *Journal of Controlled Release*, 129(1), 1–10.
44. Maljaars, P. W. J., Peters, H. P. F., Mela, D. J., & Masclee, A. A. M. (2008). Ileal brake: A sensible food target for appetite control. A review. *Physiology & Behavior*, 95(3), 271–281.
45. Tso, P. (2008). Gastrointestinal Secretion, Digestion, and Absorption. In R. A. Rhoades & D. Bell (Eds.), *Medical Physiology: Principles for Clinical Medicine* (3rd ed., Vol. 497–539). Baltimore - Philadelphia: Lippincott Williams & Wilkins.
46. Wickham, M., Garrood, M., Leney, J., Wilson, P. D. G., & Fillery-Travis, A. (1998). Modification of a phospholipid stabilized emulsion interface by bile salt: effect on pancreatic lipase activity. *Journal of Lipid Research*, 39(3), 623–632.
47. Lowe, M. E. (1997). Colipase Stabilizes the Lid Domain of Pancreatic Triglyceride Lipase. *Journal of Biological Chemistry*, 272(1), 9–12.
48. Bezzine, S., Ferrato, F., Ivanova, M. G., Lopez, V., Verger, R., & Carrière, F. (1999). Human Pancreatic Lipase: Colipase Dependence and Interfacial Binding of Lid Domain

- Mutants. *Biochemistry*, 38(17), 5499–5510.
49. Christensen, J. Ø., Schultz, K., Mollgaard, B., Kristensen, H. G., & Mullertz, A. (2004). Solubilisation of poorly water-soluble drugs during in vitro lipolysis of medium- and long-chain triacylglycerols. *European Journal of Pharmaceutical Sciences*, 23(3), 287–296.
  50. Desnuelle, P., & Savary, P. (1963). Specificities of lipases. *Journal of Lipid Research*, 4(4), 369–384.
  51. Entressangles, B., Savary, P., Constantin, M. J., & Desnuelle, P. (1964). Comportement In vitro et In vivo des chaînes courtes situées en position interne dans les triglycérides. *Biochim Biophys Acta*, 84, 140–148.
  52. Greenberger, N. J., & Skillman, T. G. (1969). Medium-chain triglycerides. Physiologic Considerations and Clinical Implications. *The New England Journal of Medicine*, 280(19), 1045–1058.
  53. Benito-Gallo, P., Franceschetto, A., Wong, J. C. M., Marlow, M., Zann, V., Scholes, P., & Gershkovich, P. (2015). Chain length affects pancreatic lipase activity and the extent and pH–time profile of triglyceride lipolysis. *European Journal of Pharmaceutics and Biopharmaceutics*, 93(0), 353–362.
  54. Wilson, F. A., Sallee, V. L., & Dietschy, J. M. (1971). Unstirred Water Layers in Intestine: Rate Determinant of Fatty Acid Absorption from Micellar Solutions. *Science*, 174(4013), 1031–1033.
  55. Shiau, Y. F., Kelemen, R. J., & Reed, M. A. (1990). Acidic mucin layer facilitates micelle dissociation and fatty acid diffusion. *American Journal of Physiology - Gastrointestinal and Liver Physiology*, 259(4), G671–G675.
  56. Strauss, E. W. (1966). Electron microscopy study of intestinal fat absorption in vitro from mixed micelles containing linolenic acid, monoolein, and bile salt. *Journal of Lipid Research*, 7, 307–723.
  57. Stremmel, W. (1988). Uptake of fatty acids by jejunal mucosal cells is mediated by fatty acid binding membrane protein. *Journal of Clinical Investigation*, 82, 2001–2010.
  58. Porter, C. J. H., Trevaskis, N. L., & Charman, W. N. (2007). Lipids and lipid-based formulations: optimizing the oral delivery of lipophilic drugs. *Nature Reviews Drug Discovery*, 6, 231–248.
  59. Charman, W. N. A., & Stella, V. J. (1986). Estimating the maximal potential for intestinal lymphatic transport of lipophilic drug molecules. *International Journal of Pharmaceutics*, 34(1–2), 175–178.
  60. Wasan, K. M., & Cassidy, S. M. (1998). Role of plasma lipoproteins in modifying the biological activity of hydrophobic drugs. *Journal of Pharmaceutical Sciences*, 87(4), 411–424.
  61. Gershkovich, P., & Hoffman, A. (2005). Uptake of lipophilic drugs by plasma derived isolated chylomicrons: Linear correlation with intestinal lymphatic bioavailability. *European Journal of Pharmaceutical Sciences*, 26(5), 394–404.
  62. Mansbach, C. M., & Siddiqi, S. A. (2010). The Biogenesis of Chylomicrons. *Annual Review of Physiology*, 72(1), 315–333.
  63. Porter, C. J. H., & Charman, W. N. (2001). In vitro assessment of oral lipid based formulations. *Advanced Drug Delivery Reviews*, 50, Supple(0), S127–S147.

64. Day, J. P. R., Rago, G., Domke, K. F., Velikov, K. P., & Bonn, M. (2010). Label-Free Imaging of Lipophilic Bioactive Molecules during Lipid Digestion by Multiplex Coherent Anti-Stokes Raman Scattering Microspectroscopy. *Journal of the American Chemical Society*, 132(24), 8433–8439.
65. Sek, L., Porter, C. J. H., Kaukonen, A. M., & Charman, W. N. (2002). Evaluation of the in-vitro digestion profiles of long and medium chain glycerides and the phase behaviour of their lipolytic products. *Journal of Pharmacy and Pharmacology*, 54(1), 29–41.
66. Ohata, A., Usami, M., & Miyoshi, M. (2005). Short-chain fatty acids alter tight junction permeability in intestinal monolayer cells via lipoxxygenase activation. *Nutrition*, 21(7–8), 838–847.
67. Yeh, P. Y., Smith, P. L., & Ellens, H. (1994). Effect of medium-chain glycerides on physiological properties of rabbit intestinal epithelium in vitro. *Pharmaceutical Research*, 11(8), 1148–1154.
68. Prasad, Y. V. R., Puthli, S. P., Eaimtrakarn, S., Ishida, M., Yoshikawa, Y., Shibata, N., & Takada, K. (2003). Enhanced intestinal absorption of vancomycin with Labrasol and d- $\alpha$ -tocopheryl PEG 1000 succinate in rats. *International Journal of Pharmaceutics*, 250(1), 181–190.
69. Rama Prasad, Y. V., Minamimoto, T., Yoshikawa, Y., Shibata, N., Mori, S., Matsuura, A., & Takada, K. (2004). In situ intestinal absorption studies on low molecular weight heparin in rats using Labrasol as absorption enhancer. *International Journal of Pharmaceutics*, 271(1–2), 225–232.
70. Orlowski, S., Selosse, M. A., Boudon, C., Micoud, C., Mir, L. M., Belehradek, J. J., & Garrigos, M. (1998). Effects of detergents on P-glycoprotein atpase activity: differences in perturbations of basal and verapamil-dependent activities. *Cancer biochemistry biophysics*, 16(1–2), 85–110.
71. Barta, C. A., Sachs-Barrable, K., Feng, F., & Wasan, K. M. (2008). Effects of Monoglycerides on P-Glycoprotein: Modulation of the Activity and Expression in Caco-2 Cell Monolayers. *Molecular Pharmaceutics*, 5(5), 863–875.
72. Regev, R., Assaraf, Y. G., & Eytan, G. D. (1999). Membrane fluidization by ether, other anesthetics, and certain agents abolishes P-glycoprotein ATPase activity and modulates efflux from multidrug-resistant cells. *European Journal of Biochemistry*, 259(1–2), 18–24.
73. Benet, L. Z., & Cummins, C. L. (2001). The drug efflux–metabolism alliance: biochemical aspects. *Advanced Drug Delivery Reviews*, 50, Supple, S3–S11.
74. Benet, L. Z., Cummins, C. L., & Wu, C. Y. (2004). Unmasking the dynamic interplay between efflux transporters and metabolic enzymes. *International Journal of Pharmaceutics*, 277(1–2), 3–9.
75. Gershkovich, P., Fanous, J., Qadri, B., Yacovan, A., Amselem, S., & Hoffman, A. F. (2009). The role of molecular physicochemical properties and apolipoproteins in association of drugs with triglyceride-rich lipoproteins: in-silico prediction of uptake by chylomicrons. *Journal of Pharmacy and Pharmacology*, 61(1), 31–39.
76. Charman, W. N., & Porter, C. J. H. (1996). Lipophilic prodrugs designed for intestinal lymphatic transport. *Advanced Drug Delivery Reviews*, 19(2), 149–169.
77. Ipp, H., & Zemlin, A. (2013). The paradox of the immune response in HIV infection: When inflammation becomes harmful. *Clinica Chimica Acta*, 416(0), 96–99.
78. Glechner, A., Wöckel, A., Gartlehner, G., Thaler, K., Strobelberger, M., Griebler, U., &

- Kreienberg, R. (2013). Sentinel lymph node dissection only versus complete axillary lymph node dissection in early invasive breast cancer: A systematic review and meta-analysis. *European Journal of Cancer*, 49(4), 812–825.
79. Gershkovich, P., Qadri, B., Yacovan, A., Amselem, S., & Hoffman, A. (2007). Different impacts of intestinal lymphatic transport on the oral bioavailability of structurally similar synthetic lipophilic cannabinoids: Dexanabinol and PRS-211,220. *European Journal of Pharmaceutical Sciences*, 31(5), 298–305.
  80. Khoo, S.-M., Shackleford, D., Porter, C. H., Edwards, G., & Charman, W. (2003). Intestinal Lymphatic Transport of Halofantrine Occurs After Oral Administration of a Unit-Dose Lipid-Based Formulation to Fasted Dogs. *Pharmaceutical Research*, 20(9), 1460–1465.
  81. Noguchi, T., Charman, W. N. A., & Stella, V. J. (1985). Lymphatic appearance of DDT in thoracic or mesenteric lymph duct cannulated rats. *International Journal of Pharmaceutics*, 24(2–3), 185–192.
  82. Trevaskis, N. L., Kaminskas, L. M., & Porter, C. J. H. (2015). From sewer to saviour: targeting the lymphatic system to promote drug exposure and activity. *Nat Rev Drug Discov*, 14(11), 781–803.
  83. Shah, A. K., & Agnihotri, S. A. (2011). Recent advances and novel strategies in pre-clinical formulation development: An overview. *Journal of Controlled Release*, 156(3), 281–296.
  84. Cole, E. T., Cadé, D., & Benameur, H. (2008). Challenges and opportunities in the encapsulation of liquid and semi-solid formulations into capsules for oral administration. *Advanced Drug Delivery Reviews*, 60(6), 747–756.
  85. Pouton, C. W. (2000). Lipid formulations for oral administration of drugs: non-emulsifying, self-emulsifying and “self-microemulsifying” drug delivery systems. *European Journal of Pharmaceutical Sciences*, 11, Supple(0), S93–S98.
  86. Schott, H. (1985). Surfactant systems: Their chemistry, pharmacy and biology. By D. Attwood and A. T. Florence. Chapman & Hall, London EC4P 4EE, United Kingdom. 1983. 794 pp. *Journal of Pharmaceutical Sciences*, 74(10), 1140–1141.
  87. Sjögren, E., Abrahamsson, B., Augustijns, P., Becker, D., Bolger, M. B., Brewster, M., ... Langguth, P. (2014). In vivo methods for drug absorption – Comparative physiologies, model selection, correlations with in vitro methods (IVIVC), and applications for formulation/API/excipient characterization including food effects. *European Journal of Pharmaceutical Sciences*, 57, 99–151.
  88. Jantratid, E., Janssen, N., Reppas, C., & Dressman, J. (2008). Dissolution Media Simulating Conditions in the Proximal Human Gastrointestinal Tract: An Update. *Pharmaceutical Research*, 25(7), 1663–1676.
  89. United States Pharmacopeia and National Formulary. (2006). USP 29. Rockville, MD: United States Pharmacopeial Convention Inc.
  90. Gray, V. A., & Dressman, J. B. (1996). Change of pH requirements for simulated intestinal fluid TS. *Pharmacopeial Forum*, 22, 1943–1945.
  91. Dressman, J., Amidon, G., Reppas, C., & Shah, V. (1998). Dissolution Testing as a Prognostic Tool for Oral Drug Absorption: Immediate Release Dosage Forms. *Pharmaceutical Research*, 15(1), 11–22.
  92. Galia, E., Nicolaidis, E., Hörter, D., Löbenberg, R., Reppas, C., & Dressman, J. B. (1998).

- Evaluation of Various Dissolution Media for Predicting In Vivo Performance of Class I and II Drugs. *Pharmaceutical Research*, 15(5), 698–705.
93. Fadda, H. M., & Basit, A. W. (2005). Dissolution of pH responsive formulations in media resembling intestinal fluids: bicarbonate versus phosphate buffers. *Journal of Drug Delivery Science and Technology*, 15(4), 273–279.
  94. Merchant, H. A., Frost, J. A., & Basit, A. W. (2012). Apparatus and method for testing medicaments. PCT/GB2013/051145.
  95. Bergström, C. A. S., Holm, R., Jørgensen, S. A., Andersson, S. B. E., Artursson, P., Beato, S., ... Mullertz, A. (2014). Early pharmaceutical profiling to predict oral drug absorption: Current status and unmet needs. *European Journal of Pharmaceutical Sciences*, 57, 173–199.
  96. Kleberg, K., Jacobsen, F., Fatouros, D. G., & Müllertz, A. (2010). Biorelevant Media Simulating Fed State Intestinal Fluids: Colloid Phase Characterization and Impact on Solubilization Capacity. *Journal of Pharmaceutical Sciences*, 99(8), 3522–3532.
  97. United States Pharmacopeia and National Formulary. (2012). USP 35 - NF 30. United States Pharmacopeial Convention.
  98. Washington, N., Washington, C., & Wilson, C. G. (2001). The Stomach. In *Physiological Pharmaceutics. Barriers to drug absorption* (2nd ed., pp. 75–103). London: Talyor and Francis.
  99. Kostewicz, E. S., Abrahamsson, B., Brewster, M., Brouwers, J., Butler, J., Carlert, S., ... Augustijns, P. (2014). In vitro models for the prediction of in vivo performance of oral dosage forms. *European Journal of Pharmaceutical Sciences*, 57, 342–366.
  100. Kostewicz, E. S., Wunderlich, M., Brauns, U., Becker, R., Bock, T., & Dressman, J. B. (2004). Predicting the precipitation of poorly soluble weak bases upon entry in the small intestine. *Journal of Pharmacy and Pharmacology*, 56(1), 43–51.
  101. Gu, C., Rao, D., Gandhi, R. B., Hilden, J. o n, & Raghavan, K. (2005). Using a Novel Multicompartment Dissolution System to Predict the Effect of Gastric pH on the Oral Absorption of Weak Bases with Poor Intrinsic Solubility. *Journal of Pharmaceutical Sciences*, 94(1), 199–208.
  102. Reymond, J.-P., Sucker, H., & Vonderscher, J. (1988). In Vivo Model for Ciclosporin Intestinal Absorption in Lipid Vehicles. *Pharmaceutical Research*, 5(10), 677–679.
  103. Zangenberg, N. H., Müllertz, A., Kristensen, H. G., & Hovgaard, L. (2001). A dynamic in vitro lipolysis model: I. Controlling the rate of lipolysis by continuous addition of calcium. *European Journal of Pharmaceutical Sciences*, 14(2), 115–122.
  104. Porter, C. J. H., Kaukonen, A. M., Taillardat-Bertschinger, A., Boyd, B. J., O'Connor, J. M., Edwards, G. A., & Charman, W. N. (2004). Use of in vitro lipid digestion data to explain the in vivo performance of triglyceride-based oral lipid formulations of poorly water-soluble drugs: Studies with halofantrine. *Journal of Pharmaceutical Sciences*, 93(5), 1110–1121.
  105. Dahan, A., & Hoffman, A. (2006). Use of a Dynamic in Vitro Lipolysis Model to Rationalize Oral Formulation Development for Poor Water Soluble Drugs: Correlation with in Vivo Data and the Relationship to Intra-Enterocyte Processes in Rats. *Pharmaceutical Research*, 23(9), 2165–2174.
  106. Zangenberg, N. H., Müllertz, A., Gjelstrup Kristensen, H., & Hovgaard, L. (2001). A dynamic in vitro lipolysis model: II: Evaluation of the model. *European Journal of*

- Pharmaceutical Sciences*, 14(3), 237–244.
107. Larsen, A. T., Sassene, P., & Müllertz, A. (2011). In vitro lipolysis models as a tool for the characterization of oral lipid and surfactant based drug delivery systems. *International Journal of Pharmaceutics*, 417(1–2), 245–255.
  108. Dahan, A., & Hoffman, A. (2007). The effect of different lipid based formulations on the oral absorption of lipophilic drugs: The ability of in vitro lipolysis and consecutive ex vivo intestinal permeability data to predict in vivo bioavailability in rats. *European Journal of Pharmaceutics and Biopharmaceutics*, 67(1), 96–105.
  109. Ibrahim, F., Gershkovich, P., Sivak, O., Wasan, E. K., & Wasan, K. M. (2012). Assessment of novel oral lipid-based formulations of amphotericin B using an in vitro lipolysis model. *European Journal of Pharmaceutical Sciences*, 46(5), 323–328.
  110. Di Maio, S., & Carrier, R. L. (2011). Gastrointestinal contents in fasted state and post-lipid ingestion: In vivo measurements and in vitro models for studying oral drug delivery. *Journal of Controlled Release*, 151(2), 110–122.
  111. Dressman, J. B., Vertzoni, M., Goumas, K., & Reppas, C. (2007). Estimating drug solubility in the gastrointestinal tract. *Advanced Drug Delivery Reviews*, 59(7), 591–602.
  112. Fadda, H. M., Sousa, T., Carlsson, A. S., Abrahamsson, B., Williams, J. G., Kumar, D., & Basit, A. W. (2010). Drug Solubility in Luminal Fluids from Different Regions of the Small and Large Intestine of Humans. *Molecular Pharmaceutics*, 7(5), 1527–1532.
  113. Kalantzi, L., Goumas, K., Kalioras, V., Abrahamsson, B., Dressman, J., & Reppas, C. (2006). Characterization of the Human Upper Gastrointestinal Contents Under Conditions Simulating Bioavailability/Bioequivalence Studies. *Pharmaceutical Research*, 23(1), 165–176.
  114. Persson, E., Gustafsson, A.-S., Carlsson, A., Nilsson, R., Knutson, L., Forsell, P., ... Abrahamsson, B. (2005). The Effects of Food on the Dissolution of Poorly Soluble Drugs in Human and in Model Small Intestinal Fluids. *Pharmaceutical Research*, 22(12), 2141–2151.
  115. Moreno, M. P. de la C., Oth, M., Deferme, S., Lammert, F., Tack, J., Dressman, J., & Augustijns, P. (2006). Characterization of fasted-state human intestinal fluids collected from duodenum and jejunum. *Journal of Pharmacy and Pharmacology*, 58(8), 1079–1089.
  116. Carrière, F., Renou, C., Lopez, V., de Caro, J., Ferrato, F., Lengsfeld, H., ... Verger, R. (n.d.). The specific activities of human digestive lipases measured from the in vivo and in vitro lipolysis of test meals. *Gastroenterology*, 119(4), 949–960.
  117. Kanicky, J. R., & Shah, D. O. (2002). Effect of Degree, Type, and Position of Unsaturation on the pKa of Long-Chain Fatty Acids. *Journal of Colloid and Interface Science*, 256, 201–207.
  118. Ciuffreda, P., Manzocchi, A., Loseto, A., & Santaniello, E. (2001). Lipolytic activity of porcine pancreas lipase on fatty acidesters of dialkylglycerols: a structural basis for the design of new substrates for the assay of pancreatic lipases activity. *Chemistry and Physics of Lipids*, 111, 105–110.
  119. Carriere, F., Barrowman, J. A., Verger, R., & Laugier, R. (1993). Secretion and contribution to lipolysis of gastric and pancreatic lipases during a test meal in humans. *Gastroenterology*, 105, 876–888.
  120. Bakala-N'Goma, J.-C., Williams, H., Sassene, P., Kleberg, K., Calderone, M., Jannin, V., ... Carrière, F. (2015). Toward the Establishment of Standardized In Vitro Tests for

- Lipid-Based Formulations. 5. Lipolysis of Representative Formulations by Gastric Lipase. *Pharmaceutical Research*, 32(4), 1279–1287.
121. Christophersen, P. C., Christiansen, M. L., Holm, R., Kristensen, J., Jacobsen, J., Abrahamsson, B., & Müllertz, A. (2014). Fed and fasted state gastro-intestinal in vitro lipolysis: In vitro in vivo relations of a conventional tablet, a SNEDDS and a solidified SNEDDS. *European Journal of Pharmaceutical Sciences*, 57, 232–239.
  122. Fernandez, S., Chevrier, S., Ritter, N., Mahler, B., Demarne, F., Carrière, F., & Jannin, V. (2009). In Vitro Gastrointestinal Lipolysis of Four Formulations of Piroxicam and Cinnarizine with the Self Emulsifying Excipients Labrasol® and Gelucire® 44/14. *Pharmaceutical Research*, 26(8), 1901–1910.
  123. Griffin, B. T., Kuentz, M., Vertzoni, M., Kostewicz, E. S., Fei, Y., Faisal, W., ... Dressman, J. B. (2013). Comparison of in vitro tests at various levels of complexity for the prediction of in vivo performance of lipid-based formulations: Case studies with fenofibrate. *European Journal of Pharmaceutics and Biopharmaceutics*, 86(3), 427–437.
  124. Larsen, A. T., Ohlsson, A. G., Polentarutti, B., Barker, R. A., Phillips, A. R., Abu-Rmaileh, R., ... Müllertz, A. (2013). Oral bioavailability of cinnarizine in dogs: Relation to SNEDDS droplet size, drug solubility and in vitro precipitation. *European Journal of Pharmaceutical Sciences*, 48(1–2), 339–350.
  125. Khoo, S.-M., Humberstone, A. J., Porter, C. J. H., Edwards, G. A., & Charman, W. N. (1998). Formulation design and bioavailability assessment of lipidic self-emulsifying formulations of halofantrine. *International Journal of Pharmaceutics*, 167(1–2), 155–164.
  126. Thomas, N., Holm, R., Garmer, M., Karlsson, J. J., Müllertz, A., & Rades, T. (2013). Supersaturated Self-Nanoemulsifying Drug Delivery Systems (Super-SNEDDS) Enhance the Bioavailability of the Poorly Water-Soluble Drug Simvastatin in Dogs. *The AAPS Journal*, 15(1), 219–227.
  127. McEvoy, C. L., Trevaskis, N. L., Edwards, G. A., Perlman, M. E., Ambler, C. M., Mack, M. C., ... Porter, C. J. H. (2014). In vitro–in vivo evaluation of lipid based formulations of the CETP inhibitors CP-529,414 (torcetrapib) and CP-532,623. *European Journal of Pharmaceutics and Biopharmaceutics*, 88(3), 973–985.
  128. de Graaf, I. A. M., de Kanter, R., de Jager, M. H., Camacho, R., Langenkamp, E., van de Kerkhof, E. G., & Groothuis, G. M. M. (2006). Empirical validation of a rat in vitro organ slice model as a tool for in vivo clearance prediction. *Drug Metabolism and Disposition*, 34(4), 591–599.
  129. De Kanter, R., Monshouwer, M., Draaisma, A. L., De Jager, M. H., De Graaf, I. A. M., Proost, J. H., ... Groothuis, G. M. M. (2004). Prediction of whole-body metabolic clearance of drugs through the combined use of slices from rat liver, lung, kidney, small intestine and colon. *Xenobiotica*, 34(3), 229–241.
  130. Gill, K. L., Houston, J. B., & Galetin, A. (2012). Characterization of In Vitro Glucuronidation Clearance of a Range of Drugs in Human Kidney Microsomes: Comparison with Liver and Intestinal Glucuronidation and Impact of Albumin. *Drug Metabolism and Disposition*, 40(4), 825–835.
  131. Cubitt, H. E., Houston, J. B., & Galetin, A. (2011). Prediction of Human Drug Clearance by Multiple Metabolic Pathways: Integration of Hepatic and Intestinal Microsomal and Cytosolic Data. *Drug Metabolism and Disposition*, 39(5), 864–873.
  132. Gertz, M., Harrison, A., Houston, J. B., & Galetin, A. (2010). Prediction of Human Intestinal First-Pass Metabolism of 25 CYP3A Substrates from In Vitro Clearance and Permeability Data. *Drug Metabolism and Disposition*, 38(7), 1147–1158.

133. Jakoby, W. B., & Ziegler M., D. (1990). The Enzymes of Detoxication. *The Journal of Biological Chemistry*, 265(34), 20715–20718.
134. Lin, J. H., Chiba, M., & Baillie, T. A. (1999). Is the Role of the Small Intestine in First-Pass Metabolism Overemphasized? *Pharmacological Reviews*, 51(2), 135–158.
135. Paine, M. F., Hart, H. L., Ludington, S. S., Haining, R. L., Rettie, A. E., & Zeldin, D. C. (2006). The Human Intestinal Cytochrome P450 “Pie.” *Drug Metabolism and Disposition*, 34(5), 880–886.
136. Fromm, M. F., Busse, D., Kroemer, H. K., & Eichelbaum, M. (1996). Differential induction of prehepatic and hepatic metabolism of verapamil by rifampin. *Hepatology*, 24(4), 796–801.
137. Paine, M. F., Shen, D. D., Kunze, K. L., Perkins, J. D., Marsh, C. L., McVicar, J. P., ... Thummel, K. E. (1996). First-pass metabolism of midazolam by the human intestine. *Clinical Pharmacology & Therapeutics*, 60(1), 14–24.
138. Hebert, M. F., Roberts, J. P., Prueksaritanont, T., & Benet, L. Z. (1992). Bioavailability of cyclosporine with concomitant rifampin administration markedly less than predicted by hepatic enzyme induction. *Clin Pharmacol Ther*, 52, 453–457.
139. Kolars, J. C., Watkins, P. B., Merion, R. M., & Awni, W. M. (1991). First-pass metabolism of cyclosporin by the gut. *The Lancet*, 338(8781), 1488–1490.
140. Holtbecker, N., Fromm, M. F., Kroemer, H. K., Ohnhaus, E. E., & Heidemann, H. (1996). The nifedipine-rifampin interaction. Evidence for induction of gut wall metabolism. *Drug Metabolism and Disposition*, 24(10), 1121–1123.
141. Wu, C.-Y., Benet, L. Z., Hebert, M. F., Gupta, S. K., Rowland, M., Gomez, D. Y., & Wachter, V. J. (1995). Differentiation of absorption and first-pass gut and hepatic metabolism in humans: Studies with cyclosporine. *Clinical Pharmacology & Therapeutics*, 58(5), 492–497.
142. Kararli, T. T. (1995). Comparison of the gastrointestinal anatomy, physiology, and biochemistry of humans and commonly used laboratory animals. *Biopharmaceutics & Drug Disposition*, 16(5), 351–380.
143. Lennernäs, H. (1995). Does fluid flow across the intestinal mucosa affect quantitative drug absorption? Is it time for a reevaluation? *Pharmaceutical Research*, 12(11), 1573–1582.
144. Sugano, K., Kansy, M., Artursson, P., Avdeef, A., Bendels, S., Di, L., ... Senner, F. (2010). Coexistence of passive and carrier-mediated processes in drug transport. *Nature Reviews Drug Discovery*, 9(8), 597–614.
145. Lennernäs, H. (2007). Animal data: The contributions of the Ussing Chamber and perfusion systems to predicting human oral drug delivery in vivo. *Advanced Drug Delivery Reviews*, 59(11), 1103–1120.
146. Lennernäs, H. (2007). Modeling Gastrointestinal Drug Absorption Requires More In Vivo Biopharmaceutical Data: Experience from In Vivo Dissolution and Permeability Studies in Humans. *Curr Drug Metab.*, 8(7), 645–657.
147. Paine, M. F., Khalighi, M., Fisher, J. M., Shen, D. D., Kunze, K. L., Marsh, C. L., ... Thummel, K. E. (1997). Characterization of Interintestinal and Intraintestinal Variations in Human CYP3A-Dependent Metabolism. *Journal of Pharmacology and Experimental Therapeutics*, 283(3), 1552–1562.



148. Yang, J., Tucker, G. T., & Rostami-Hodjegan, A. (2004). Cytochrome P450 3A expression and activity in the human small intestine. *Clinical Pharmacology & Therapeutics*, 76(4), 391.
149. Galetin, A., & Houston, J. B. (2006). Intestinal and Hepatic Metabolic Activity of Five Cytochrome P450 Enzymes: Impact on Prediction of First-Pass Metabolism. *Journal of Pharmacology and Experimental Therapeutics*, 318(3), 1220–1229.
150. Evans, W. H. (1980). A Biochemical Dissection of the Functional Polarity of the Plasma Membrane of the Hepatocyte. *Biochimica et Biophysica Acta*, 604(1), 27–64.
151. Kwon, Y. (2001). Clearance. In Y. Kwon (Ed.), *Handbook of Essential Pharmacokinetics, Pharmacodynamics and Drug Metabolism for Industrial Scientists* (pp. 83–103). Hingham, MA, USA: Kluwer Academic Publishers Publishers.
152. Zamek-Gliszczyński, M. J., Hoffmaster, K. A., Nezasa, K., Tallman, M. N., & Brouwer, K. L. R. (2006). Integration of hepatic drug transporters and phase II metabolizing enzymes: Mechanisms of hepatic excretion of sulfate, glucuronide, and glutathione metabolites. *European Journal of Pharmaceutical Sciences*, 27(5), 447–486.
153. Roberts, M. S., Magnusson, B. M., Burczynski, F. J., & Weiss, M. (2002). Enterohepatic Circulation. *Clinical Pharmacokinetics*, 41(10), 751–790.
154. Chaturvedi, P. R., Decker, C. J., & Odinecs, A. (2001). Prediction of pharmacokinetic properties using experimental approaches during early drug discovery. *Current Opinion in Chemical Biology*, 5(1), 452–463.
155. Obach, R. S., Baxter, J. G., Liston, T. E., Silber, B. M., Jones, B. C., Macintyre, F., ... Wastall, P. (1997). The Prediction of Human Pharmacokinetic Parameters from Preclinical and In Vitro Metabolism Data. *Journal of Pharmacology and Experimental Therapeutics*, 283(1), 46–58.
156. Lavé, T., Coassolo, P., & Reigner, B. (1999). Prediction of Hepatic Metabolic Clearance Based on Interspecies Allometric Scaling Techniques and In Vitro-In Vivo Correlations. *Clinical Pharmacokinetics*, 36(3), 211–231.
157. Ito, K., & Houston, B. J. (2005). Prediction of Human Drug Clearance from in Vitro and Preclinical Data Using Physiologically Based and Empirical Approaches. *Pharmaceutical Research*, 22(1), 103–112.
158. Galetin, A., Gertz, M., & Houston, J. B. (2008). Potential role of intestinal first-pass metabolism in the prediction of drug–drug interactions. *Expert Opinion on Drug Metabolism & Toxicology*, 4(7), 909–922.
159. DOWLING, J. T., APPLETON, W. G., & MUSA, B. U. (1968). Direct Measurement of Hepatic Thyroxine Flux in Normal Man. *The Journal of Clinical Endocrinology & Metabolism*, 28(10), 1503–1507.
160. Hollander, A. A. M. J., van Rooij, J., Lentjes, E. G. W. M., Arbouw, F., van Bree, J. B., Schoemaker, R. C., ... Cohen, A. F. (1995). The effect of grapefruit juice on cyclosporine and prednisone metabolism in transplant patients. *Clinical Pharmacology & Therapeutics*, 57(3), 318–324.
161. Martin, R. D., Genoud, M., & Hemelrijk, C. K. (2005). Problems of allometric scaling analysis: examples from mammalian reproductive biology. *Journal of Experimental Biology*, 208(9), 1731–1747.
162. Lavé, T., Chapman, K., Goldsmith, P., & Rowland, M. (2009). Human clearance prediction: shifting the paradigm. *Expert Opinion on Drug Metabolism & Toxicology*, 5(9),

1039–1048.

163. Jolivet, L. J., & Ekins, S. (2007). Methods for predicting human drug metabolism. *Advances in Clinical Chemistry*, 43(1), 131–176.
164. Zhang, D., Luo, G., Ding, X., & ChuangLud. (2012). Preclinical experimental models of drug metabolism and disposition in drug discovery and development. *Acta Pharmaceutica Sinica B*, 2(6), 549–561.
165. Gómez-Lechón, M. J., Donato, M. T., Castell, J. V., & Jover, R. (2003). Human hepatocytes as a tool for studying toxicity and drug metabolism. *Current Drug Metabolism*, 4(4), 292–312.
166. Graaf, I. A. M. de, Groothuis, G. M. M., & Olinga, P. (2007). Precision-cut tissue slices as a tool to predict metabolism of novel drugs. *Expert Opinion on Drug Metabolism & Toxicology*, 3(6), 879–898.
167. Thohan, S., Zurich, M. C., Chung, H., Weiner, M., Kane, A. S., & Rosen, G. M. (2001). Tissue Slices Revisited: Evaluation and Development of a Short-Term Incubation for Integrated Drug Metabolism. *Drug Metabolism and Disposition*, 29(10), 1337–1342.
168. Brian Houston, J., & Carlile, D. J. (1997). Prediction of Hepatic Clearance from Microsomes, Hepatocytes, and Liver Slices. *Drug Metabolism Reviews*, 29(4), 891–922.
169. van de Kerkhof, E. G., Ungell, A.-L. B., Sjöberg, Å. K., de Jager, M. H., Hilgendorf, C., de Graaf, I. A. M., & Groothuis, G. M. M. (2006). Innovative Methods to Study Human Intestinal Drug Metabolism in Vitro: Precision-Cut Slices Compared with Ussing Chamber Preparations. *Drug Metabolism and Disposition*, 34(11), 1893–1902.
170. Obach, R. S., Zhang, Q.-Y., Dunbar, D., & Kaminsky, L. S. (2001). Metabolic Characterization of the Major Human Small Intestinal Cytochrome P450s. *Drug Metabolism and Disposition*, 29(3), 347–352.
171. Ekins, S., Ring, B. J., Grace, J., McRobie-Belle, D. J., & Wrighton, S. A. (2000). Present and future in vitro approaches for drug metabolism. *Journal of Pharmacological and Toxicological Methods*, 44(1), 313–324.
172. Obach, R. S. (1999). Prediction of Human Clearance of Twenty-Nine Drugs from Hepatic Microsomal Intrinsic Clearance Data: An Examination of In Vitro Half-Life Approach and Nonspecific Binding to Microsomes. *Drug Metabolism and Disposition*, 27(11), 1350–1359.
173. Wilson, Z. E., Rostami-Hodjegan, A., Burn, J. L., Tooley, A., Boyle, J., Ellis, S. W., & Tucker, G. T. (2003). Inter-individual variability in levels of human microsomal protein and hepatocellularity per gram of liver. *British Journal of Clinical Pharmacology*, 56(4), 433–440.
174. Riley, R. J., McGinnity, D. F., & Austin, R. P. (2005). A Unified Model For Predicting Human Hepatic, Metabolic Clearance From In Vitro Intrinsic Clearance Data In Hepatocytes And Microsomes. *Drug Metabolism and Disposition*, 33(9), 1304–1311.
175. Barter, Z. E., Bayliss, M. K., Beaune, P. H., Boobis, A. R., Carlile, D. J., Edwards, R. J., ... Rostami-Hodjegan, A. (2007). Scaling factors for the extrapolation of in vivo metabolic drug clearance from in vitro data: reaching a consensus on values of human microsomal protein and hepatocellularity per gram of liver. *Curr Drug Metab.*, 8(1), 33–45.
176. Brian Houston, J. (1994). Utility of in vitro drug metabolism data in predicting in vivo metabolic clearance. *Biochemical Pharmacology*, 47(9), 1469–1479.

177. Pang, K. S., & Rowland, M. (1977). Hepatic clearance of drugs. I. Theoretical considerations of a “well-stirred” model and a “parallel tube” model. Influence of hepatic blood flow, plasma and blood cell binding, and the hepatocellular enzymatic activity on hepatic drug clearance. *Journal of Pharmacokinetics and Biopharmaceutics*, 5(6), 625–653.
178. Ahmad, A. B., Bennett, P. N., & Rowland, M. (1983). Models of hepatic drug clearance: discrimination between the “well stirred” and “parallel-tube” models. *Journal of Pharmacy and Pharmacology*, 35(4), 219–224.
179. Rostami-Hodjegan, A., & Tucker, G. T. (2002). The effects of portal shunts on intestinal cytochrome P450 3A activity. *Hepatology (Baltimore, Md.)*, 35(6), 1549–50–1.
180. Yang, J. S., Rostami-Hodjegan, A., & Tucker, G. T. (2001). Prediction of ketoconazole interaction with midazolam, alprazolam and triazolam: Incorporating population variability. *British Journal of Clinical Pharmacology*, 52, 472–473.
181. De Buck, S. S., Sinha, V. K., Fenu, L. A., Nijssen, M. J., Mackie, C. E., & Gilissen, R. A. H. J. (2007). Prediction of Human Pharmacokinetics Using Physiologically Based Modeling: A Retrospective Analysis of 26 Clinically Tested Drugs. *Drug Metabolism and Disposition*, 35(10), 1766–1780.
182. Williams, H., Sassene, P., Kleberg, K., Bakala-N’Goma, J.-C., Calderone, M., Jannin, V., ... Pouton, C. W. (2012). Toward the Establishment of Standardized In Vitro Tests for Lipid-Based Formulations, Part I: Method Parameterization and Comparison of In Vitro Digestion Profiles Across a Range of Representative formulations. *J. Pharm. Sci.*, 101(9), 3360–3380.
183. Williams, H. D., Anby, M. U., Sassene, P., Kleberg, K., Bakala-N’Goma, J.-C., Calderone, M., ... Porter, C. J. H. (2012). Toward the Establishment of Standardized in Vitro Tests for Lipid-Based Formulations. 2. The Effect of Bile Salt Concentration and Drug Loading on the Performance of Type I, II, IIIA, IIIB, and IV Formulations during in Vitro Digestion. *Molecular Pharmaceutics*, 9(11), 3286–3300.
184. Williams, H., Sassene, P., Kleberg, K., Calderone, M., Igonin, A., Jule, E., ... Porter, C. H. (2013). Toward the Establishment of Standardized In Vitro Tests for Lipid-Based Formulations, Part 3: Understanding Supersaturation Versus Precipitation Potential During the In Vitro Digestion of Type I, II, IIIA, IIIB and IV Lipid-Based Formulations. *Pharmaceutical Research*, 1–18.
185. Banwell, J. G., Gorbach, S. L., Pierce, N. F., Miltra, R., & Mondal, A. (1971). Accute Undifferentiated Human Diarrhea in Tropics 2. Alterations in Intestinal Fluid and Electrolyte Movement. *J. Clin. Invest.*, 50, 890–900.
186. Bucher, G. R., Flynn, J. C., & Robinson, C. S. (1944). The Action of the Human Small Intestine in Altering the Composition of Physiological Saline. *J. Biol. Chem.*, 155, 305–13.
187. Mudie, D. M., Amidon, G. L., & Amidon, G. E. (2010). Physiological Parameters for Oral Delivery and in Vitro Testing. *Molecular Pharmaceutics*, 7(5), 1388–1405.
188. Perez de la Cruz Moreno, M., Deferme, S., Lammert, F., Tack, J., Dressman, J., & Augustijns, P. (2006). Characterization of Fasted-Stated Human Intestinal Fluids Collected from Duodenum and Jejunum. *J. Pharm. Pharmacol.*, 58, 1079–89.
189. McGee, L. C., & Hastings, A. B. (1942). The Carbon Dioxide Tension and Acid-Base Balance of Jejunal Secretions in Man. *J. Biol. Chem.*, 142, 893–904.
190. Bown, R. L., Sladen, G. E., Clark, M. L., & Dawson, A. M. (1971). The Production and Transport of Ammonia in the Human Colon. *Gut*, 12, 863.

191. Ovesen, L., Bendtsen, F., Tage-Jensen, U., Pedersen, N. T., Gram, B. R., & Rune, S. J. (1986). Intraluminal pH in the Stomach, Duodenum, and Proximal Jejunum in Normal Subjects and Patients with Exocrine Pancreatic Insufficiency. *Gastroenterology*, 90, 958–62.
192. Rautureau, M., Bisalli, A., & Rambaud, J. C. (1981). Bile Salts and Lipids in Aqueous Intraluminal Phase During the Digestion of a Standard Meal in Normal Man. *Gastroenterol. Clin. Biol.*, 5, 417–25.
193. Parmentier, J., Thomas, N., Müllertz, A., Fricker, G., & Rades, T. (2012). Exploring the fate of liposomes in the intestine by dynamic in vitro lipolysis. *International Journal of Pharmaceutics*, 437(1–2), 253–263.
194. Han, S., Quach, T., Hu, L., Wahab, A., Charman, W. N., Stella, V. J., ... Porter, C. J. H. (2014). Targeted delivery of a model immunomodulator to the lymphatic system: Comparison of alkyl ester versus triglyceride mimetic lipid prodrug strategies. *Journal of Controlled Release*, 177(0), 1–10.
195. Gershkovich, P., Sivak, O., Contreras-Whitney, S., Darlington, J. W., & Wasan, K. M. (2012). Assessment of cholesterol absorption inhibitors nanostructured aluminosilicate and cholestyramine using in vitro lipolysis model. *Journal of Pharmaceutical Sciences*, 101(1), 291–300.
196. Erlanson-Albertsson, C. (1983). The interaction between pancreatic lipase and colipase: a protein-protein interaction regulated by a lipid. *FEBS Letters*, 162(2), 225–229.
197. Embleton, J. K., & Pouton, C. W. (1997). Structure and function of gastro-intestinal lipases. *Advanced Drug Delivery Reviews*, 25(1), 15–32.
198. Lengsfeld, H., Beaumier-Gallon, G., Chahinian, H., De Caro, A., Verger, R., Laugier, R., & Carrière, F. (2004). Physiology of Gastrointestinal Lipolysis and Therapeutical Use of Lipases and Digestive Lipase Inhibitors. In G. Müller & S. Petry (Eds.), *Lipases and Phospholipases in Drug Development: From Biochemistry to Molecular Pharmacology*. Weinheim: WILEY-VCH Verlag GmbH & Co. KGaA.
199. Desnuelle, P., Semeriva, M., & Dufour, C. (1971). Probable involvement of a histidine residue in the active site of pancreatic lipase. *Biochemistry*, 10(11), 2143–2149.
200. Gershkovich, P., & Hoffman, A. (2007). Effect of a high-fat meal on absorption and disposition of lipophilic compounds: The importance of degree of association with triglyceride-rich lipoproteins. *European Journal of Pharmaceutical Sciences*, 32(1), 24–32.
201. Gibson, L. (2007). Lipid-based excipients for oral drug delivery. In D. J. Hauss (Ed.), *Oral Lipid-Based Formulations*. New York, USA: Informa Healthcare.
202. Lalanne, M., Khoury, H., Deroussent, A., Bosquet, N., Benech, H., Clayette, P., ... Andrieux, K. (2009). Metabolism evaluation of biomimetic prodrugs by in vitro models and mass spectrometry. *International Journal of Pharmaceutics*, 379(2), 235–243.
203. Han, S., Yao, T., Zhang, X., Gan, L., Zhu, C., Yu, H., & Gan, Y. (2009). Lipid-based formulations to enhance oral bioavailability of the poorly water-soluble drug anethol trithione: Effects of lipid composition and formulation. *International Journal of Pharmaceutics*, 379(1), 18–24.
204. Anby, M. U., Nguyen, T.-H., Yeap, Y. Y., Feeney, O. M., Williams, H. D., Benameur, H., ... Porter, C. J. H. (2014). An in Vitro Digestion Test That Reflects Rat Intestinal Conditions To Probe the Importance of Formulation Digestion vs First Pass Metabolism in Danazol Bioavailability from Lipid Based Formulations. *Molecular Pharmaceutics*.

205. Elgart, A., Cherniakov, I., Aldouby, Y., Domb, A., & Hoffman, A. (2013). Improved Oral Bioavailability of BCS Class 2 Compounds by Self Nano-Emulsifying Drug Delivery Systems (SNEDDS): The Underlying Mechanisms for Amiodarone and Talinolol. *Pharmaceutical Research*, 30(12), 1–16.
206. Sek, L., Porter, C. J. H., & Charman, W. N. (2001). Characterisation and quantification of medium chain and long chain triglycerides and their in vitro digestion products, by HPTLC coupled with in situ densitometric analysis. *Journal of Pharmaceutical and Biomedical Analysis*, 25(3–4), 651–661.
207. US Pharmacopeia. (2016). USP Monographs: Pancrelipase, available at: [http://www.pharmacopeia.cn/v29240/usp29nf24s0\\_m60320.html](http://www.pharmacopeia.cn/v29240/usp29nf24s0_m60320.html) (Accessed: May 2016).
208. Kaukonen, A., Boyd, B., Charman, W., & Porter, C. H. (2004). Drug Solubilization Behavior During in Vitro Digestion of Suspension Formulations of Poorly Water-Soluble Drugs in Triglyceride Lipids. *Pharmaceutical Research*, 21(2), 254–260.
209. Dubois, A. (1998). What is the correlation between gastric secretory volume and reflux frequency? In R. Giuli, J.-P. Galmiche, G. G. Jamieson, & C. Scarpignato (Eds.), *The Esophagogastric Junction*. OESO.
210. Hauss, D. J. (2007). Oral lipid-based formulations. *Advanced Drug Delivery Reviews*, 59(7), 667–676.
211. Larsson, A., & Erlanson-Albertsson, C. (1986). Effect of phosphatidylcholine and free fatty acids on the activity of pancreatic lipase-colipase. *Biochim Biophys Acta.*, 876(3), 543–550.
212. Peters, G., & Toxvaerd, S. (1995). Structure and dynamics of lipid monolayers: implications for enzyme catalised lipolysis. *Nature Structural Biology*, 2, 395–401.
213. Patton, J. S., & Carey, M. C. (n.d.). Watching fat digestion. *Science*, 13(204(4389)), 145–148.
214. Westergaard, H., & Dietschy, J. M. (1976). The mechanism whereby bile acid micelles increase the rate of fatty acid and cholesterol uptake into the intestinal mucosal cell. *The Journal of Clinical Investigation*, 58(1), 97–108.
215. Porter, C. J. H., Pouton, C. W., Cuine, J. F., & Charman, W. N. (2008). Enhancing intestinal drug solubilisation using lipid-based delivery systems. *Advanced Drug Delivery Reviews*, 60(6), 673–691.
216. Brockerhoff, H. (1968). Substrate specificity of pancreatic lipase. *Biochimica et Biophysica Acta (BBA) - Enzymology*, 159(2), 296–303.
217. Armand, M., Borel, P., Ythier, P., Dutot, G., Melin, C., Senft, M., ... Lairon, D. (1992). Effects of droplet size, triacylglycerol composition, and calcium on the hydrolysis of complex emulsions by pancreatic lipase: an in vitro study. *The Journal of Nutritional Biochemistry*, 3(7), 333–341.
218. Fernandez, S., Jannin, V., Rodier, J.-D., Ritter, N., Mahler, B., & Carrière, F. (2007). Comparative study on digestive lipase activities on the self emulsifying excipient Labrasol®, medium chain glycerides and PEG esters. *Biochimica et Biophysica Acta (BBA) - Molecular and Cell Biology of Lipids*, 1771(5), 633–640.
219. Riddick, J. A., Bunger, W. B., & Sakano, T. K. (1985). *Techniques of Chemistry. Volume II. Organic Solvents* (p. 402). New York, NY: John Wiley and Sons.

220. Malvern Instruments Ltd. (2014). (n.d.). Zetasizer Nano ZS, available at: <http://www.malvern.com/en/products/product-range/zetasizer-range/zetasizer-nano-range/zetasizer-nano-zs/default.aspx> (Accessed: October 2014) .
221. Li, Y., & McClements, D. J. (2010). New Mathematical Model for Interpreting pH-Stat Digestion Profiles: Impact of Lipid Droplet Characteristics on in Vitro Digestibility. *Journal of Agricultural and Food Chemistry*, 58(13), 8085–8092.
222. Yu, L. X., Crison, J. R., & Amidon, G. L. (1996). Compartmental transit and dispersion model analysis of small intestinal transit flow in humans. *International Journal of Pharmaceutics*, 140(1), 111–118.
223. Fernandez, S., Rodier, J.-D., Ritter, N., Mahler, B., Demarne, F., Carrière, F., & Jannin, V. (2008). Lipolysis of the semi-solid self-emulsifying excipient Gelucire® 44/14 by digestive lipases. *Biochimica et Biophysica Acta (BBA) - Molecular and Cell Biology of Lipids*, 1781(8), 367–375.
224. Eydoux, C., Caro, J. De, Ferrato, F., Boullanger, P., Lafont, D., Laugier, R., ... De Caro, A. (2007). Further biochemical characterization of human pancreatic lipase-related protein 2 expressed in yeast cells. *Journal of Lipid Research*, 48, 1539–1549.
225. Pedersen, P. B., Vilmann, P., Bar-Shalom, D., Müllertz, A., & Baldursdottir, S. (2013). Characterization of fasted human gastric fluid for relevant rheological parameters and gastric lipase activities. *European Journal of Pharmaceutics and Biopharmaceutics*, 85(3, Part B), 958–965.
226. National Center for Biotechnology Information. (n.d.). PubChem Compound Database, CID=176, 264, 379, 2969, <https://pubchem.ncbi.nlm.nih.gov> (Accessed: September 2014).
227. Dicklin, M. E., Robinson, J. L., Lin, X., & Odle, J. (2006). Ontogeny and chain-length specificity of gastrointestinal lipases affect medium-chain triacylglycerol utilization by newborn pigs. *J Anim Sci*, 84, 818–825.
228. Lüthi-Peng, Q., Märki, H. P., & Hadvary, P. (1992). Identification of the active-site serine in human pancreatic lipase by chemical modification with tetrahydrolipstatin. *FEBS Letters*, 299(1), 111–115.
229. Reis, P., Miller, R., Leser, M., Watzke, H., Fainerman, V. B., & Holmberg, K. (2008). Adsorption of Polar Lipids at the Water– Oil Interface. *Langmuir*, 24(11), 5781–5786.
230. Salentinig, S., Sagalowicz, L., Leser, M. E., Tedeschi, C., & Glatzer, O. (2011). Transitions in the internal structure of lipid droplets during fat digestion. *Soft Matter*, 7(2), 650–661.
231. Paris, G. Y., Garmaise, D. L., Cimon, D. G., Swett, L., Carter, G. W., & Young, P. (1980). Glycerides as prodrugs. 3. Synthesis and antiinflammatory activity of [1-(p-chlorobenzoyl)-5-methoxy-2-methylindole-3-acetyl]glycerides (indomethacin glycerides). *Journal of Medicinal Chemistry*, 23(1), 9–13.
232. Emami, J. (2006). In vitro - in vivo correlation: from theory to applications. *J Pharm Pharm Sci.*, 9(2), 169–89.
233. Amann, L. C., Gandal, M. J., Lin, R., Liang, Y., & Siegel, S. J. (2010). In Vitro--In Vivo Correlations of Scalable PLGA-Risperidone Implants for the Treatment of Schizophrenia. *Pharmaceutical Research*, 27(8), 1730–1737.
234. Buch, P., Holm, P., Thomassen, J. Q., Scherer, D., Branscheid, R., Kolb, U., & Langguth, P. (2010). IVIVC for Fenofibrate Immediate Release Tablets Using Solubility and Permeability as In Vitro Predictors for Pharmacokinetics. *Journal of Pharmaceutical*

- Sciences*, 99(10), 4427–4436.
235. Kossena, G. A., Boyd, B. J., Porter, C. J. H., & Charman, W. N. (2003). Separation and characterization of the colloidal phases produced on digestion of common formulation lipids and assessment of their impact on the apparent solubility of selected poorly water-soluble drugs. *Journal of Pharmaceutical Sciences*, 92(3), 634–648.
  236. Alqahtani, S., Alayoubi, A., Nazzal, S., Sylvester, P., & Kaddoumi, A. (2014). Enhanced Solubility and Oral Bioavailability of  $\gamma$ -Tocotrienol Using a Self-Emulsifying Drug Delivery System (SEDDS). *Lipids*, 49(8), 819–829.
  237. Strickley, R. G. (2007). Currently Marketed Oral Lipid-Based Dosage Forms: Drug Products and Excipients. In D. J. Hauss (Ed.), *Oral Lipid-Based Formulations: Enhancing the Bioavailability of Poorly Water-Soluble Drugs*. Princeton, New Jersey, USA: Bristol-Myers Squibb Company.
  238. U.S. Food and Drug Administration. (2015). Marinol® (Dronabinol Capsules), available at: <http://www.fda.gov/ohrms/dockets/dockets/05n0479/05N-0479-emc0004-04.pdf> (Accessed: March 2016).
  239. European Medicines Agency. (2015). Sandimmun Neoral® (Annex III), available at: [http://www.ema.europa.eu/docs/en\\_GB/document\\_library/Referrals\\_document/Sandimmun\\_Neoral\\_30/WC500144886.pdf](http://www.ema.europa.eu/docs/en_GB/document_library/Referrals_document/Sandimmun_Neoral_30/WC500144886.pdf) (Accessed: March 2016).
  240. Naef, M., Curatolo, M., Petersen-Felix, S., Arendt-Nielsen, L., Zbinden, A., & Brenneisen, R. (2003). The analgesic effect of oral delta-9-tetrahydrocannabinol (THC), morphine, and a THC-morphine combination in healthy subjects under experimental pain conditions. *Pain*, 105(1–2), 79–88.
  241. Goskonda, V. R., Chavan, A., Kokate, A., & Gill, H. (2012). Liquid cannabinoid formulations (Patent No.: US 8222292 B2). (U.S. Patent and Trademark Office, Ed.). Phoenix, AZ (US): Insys Therapeutics, Inc.
  242. Mueller, E., Kovarik, J., van Bree, J., Tetzloff, W., Grevel, J., & Kutz, K. (1994). Improved Dose Linearity of Cyclosporine Pharmacokinetics from a Microemulsion Formulation. *Pharmaceutical Research*, 11(2), 301–304.
  243. Kim, J. W., Shin, H. J., & Yang, S. G. (1999). Cyclosporin-containing pharmaceutical composition (Patent No.: 5980939). (U.S. Patent and Trademark Office, Ed.). Seoul, Rep. of Korea: Chong Kun Dang, Corp.
  244. Odeberg, J. M., Kaufmann, P., Kroon, K.-G., & Höglund, P. (2003). Lipid drug delivery and rational formulation design for lipophilic drugs with low oral bioavailability, applied to cyclosporine. *European Journal of Pharmaceutical Sciences*, 20(4–5), 375–382.
  245. Advanced Chemistry Developmen Inc. (2014). ACD/I-Lab version 12.1.0.50375 . [www.acdlabs.com](http://www.acdlabs.com). Toronto, ON, Canada.
  246. Garrett, E. R., & Hunt, C. A. (1974). Physicochemical properties, solubility, and protein binding of  $\Delta^9$ -tetrahydrocannabinol. *Journal of Pharmaceutical Sciences*, 63(7), 1056–1064.
  247. Varma, M. V. S., & Panchagnula, R. (2005). Prediction of in vivo intestinal absorption enhancement on P-glycoprotein inhibition, from rat in situ permeability. *Journal of Pharmaceutical Sciences*, 94(8), 1694–1704.
  248. Simulations Plus Inc. (Ed.). (2016). GastroPlus software. Lancaster, CA.
  249. Chiu, Y.-Y., Higaki, K., Neudeck, B. L., Barnett, J. L., Welage, L. S., & Amidon, G. L.

- (2003). Human Jejunal Permeability of Cyclosporin A: Influence of Surfactants on P-Glycoprotein Efflux in Caco-2 Cells. *Pharmaceutical Research*, 20(5), 749–756.
250. Russell, T. L., Berardi, R. R., Barnett, J. L., O'Sullivan, T. L., Wagner, J. G., & Dressman, J. B. (1994). pH-Related Changes in the Absorption of Dipyridamole in the Elderly. *Pharmaceutical Research*, 11(1), 136–143.
  251. Herzlich, B. C., Schiano, T. D., Moussa, Z., Zimbalist, E., Panagopoulos, G., Ast, A., & Nawabi, I. (1992). Decreased intrinsic factor secretion in AIDS: relation to parietal cell acid secretory capacity and vitamin B12 malabsorption. *American Journal of Gastroenterology*, 87(12), 1781–1788.
  252. Youngberg, C. A., Berardi, R. R., Howatt, W. F., Hyneck, M. L., Amidon, G. L., Meyer, J. H., & Dressman, J. B. (1987). Comparison of gastrointestinal pH in cystic fibrosis and healthy subjects. *Digestive Diseases and Sciences*, 32(5), 472–480.
  253. Blum, R. A., D'Andrea, D. T., Florentino, B. M., Wilton, J. H., Hilligoss, D. M., Gardner, M. J., ... Schentag, J. J. (1991). Increased Gastric pH and the Bioavailability of Fluconazole and Ketoconazole. *Annals of Internal Medicine*, 114(9), 755–757.
  254. News Medical. (2005). Roche to discontinue the sale and distribution of Fortovase (saquinavir). Retrieved from <http://www.news-medical.net/news/2005/05/18/10187.aspx>
  255. AbbVie Inc. (2015). Kaletra® (lopinavir/ritonavir), available at: <https://www.kaletra.com/> (Accessed: June 2016).
  256. Kyorin Pharmaceutical Co. (2013). Ketas® (ibudilast), available at: [http://www.kyorin-pharm.co.jp/prodinfo/medicine/pdf/KETAS\\_Capsules.pdf](http://www.kyorin-pharm.co.jp/prodinfo/medicine/pdf/KETAS_Capsules.pdf), (Accessed: May 2016).
  257. Napp Pharmaceuticals. (n.d.). MXL® capsules (morphine sulphate), available at: <http://www.chardeh.com.tw/file/Product/201302191405252687.pdf>, (Accessed: May 2016).
  258. Pfizer - Pharmacia and Upjohn Company. (2013). Detrol® LA (tolterodine tartrate), available at: <http://labeling.pfizer.com/showlabeling.aspx?id=719> (Accessed: May 2016).
  259. RxList Inc. (2014). AGENERASE® (amprenavir) Capsules, available at: <http://www.rxlist.com/agenerase-drug.htm> (Accessed on June 2016).
  260. U.S. Food and Drug Administration. (2016). Norvir® (Ritonavir), available at: [http://www.accessdata.fda.gov/drugsatfda\\_docs/label/2011/020945s032lbl.pdf](http://www.accessdata.fda.gov/drugsatfda_docs/label/2011/020945s032lbl.pdf) (Accessed: May 2016).
  261. U.S. Food and Drug Administration. (2011). APTIVUS® (tipranavir), available at: [http://www.accessdata.fda.gov/drugsatfda\\_docs/label/2011/021814s011lbl.pdf](http://www.accessdata.fda.gov/drugsatfda_docs/label/2011/021814s011lbl.pdf) (Accessed: June 2016).
  262. Csajka, C., Marzolini, C., Fattinger, K., Decosterd, L. A., Fellay, J., Telenti, A., ... Buclin, T. (2003). Population pharmacokinetics and effects of efavirenz in patients with human immunodeficiency virus infection. *Clinical Pharmacology & Therapeutics*, 73(1), 20–30.
  263. Duvic, M., Hymes, K., Heald, P., Breneman, D., Martin, A. G., Myskowski, P., ... Group, for M. of the B. W. S. (2001). Bexarotene Is Effective and Safe for Treatment of Refractory Advanced-Stage Cutaneous T-Cell Lymphoma: Multinational Phase II-III Trial Results. *Journal of Clinical Oncology*, 19(9), 2456–2471.
  264. U.S. Food and Drug Administration. (2006). Avodart® (dutasteride), available at [http://www.accessdata.fda.gov/drugsatfda\\_docs/label/2008/021319s015lbl.pdf](http://www.accessdata.fda.gov/drugsatfda_docs/label/2008/021319s015lbl.pdf),



(Accessed: March 2016).

265. Eisai Co. (2009). Infree® S Capsules (indometacin farnesil), available at: [http://www.eisai.jp/medical/products/di/EPI/INF\\_C-SC-EPI.pdf](http://www.eisai.jp/medical/products/di/EPI/INF_C-SC-EPI.pdf), (Accessed: May 2016).
266. Eisai Co. (2009). Juvela N® (tocopherol nicotinate), available at: [http://www.eisai.jp/medical/products/di/EPI/EN\\_C-SC-FG-EPI.pdf](http://www.eisai.jp/medical/products/di/EPI/EN_C-SC-FG-EPI.pdf) (Accessed: May 2016).
267. Eisai Co. (2014). Selbex® (teprenone), available at: <http://www.shijiebiaopin.com/upload/product/201431323032020.pdf>, (Accessed: May 2016).
268. Colburn, W. A., Vane, F. M., & Shorter, H. J. (1983). Pharmacokinetics of isotretinoin and its major blood metabolite following a single oral dose to man. *European Journal of Clinical Pharmacology*, 24(5), 689–694.
269. Brattström, C., Säwe, J., Jansson, B., Lönnebo, A., Nordin, J., Zimmerman, J. J., ... Groth, C. G. (2000). Pharmacokinetics and Safety of Single Oral Doses of Sirolimus (Rapamycin) in Healthy Male Volunteers. *Therapeutic Drug Monitoring*, 22(5), 537–544.
270. Albright, P. S., Bruni, J., & Suria, D. (1984). Pharmacokinetics of Enteric-Coated Valproic Acid. *Therapeutic Drug Monitoring*, 6(1), 21–23.
271. Shah, A., Liu, M.-C., Vaughan, D., & Heller, A. H. (1999). Oral bioequivalence of three ciprofloxacin formulations following single-dose administration: 500 mg tablet compared with 500 mg/10 mL or 500 mg/5 mL suspension and the effect of food on the absorption of ciprofloxacin oral suspension. *Journal of Antimicrobial Chemotherapy*, 43(suppl 1), 49–54.
272. Eisai Co. (2009). Glakay® capsules (vitamin K2), available at: [http://www.eisai.jp/medical/products/di/EPI/GLA\\_SC-EPI.pdf](http://www.eisai.jp/medical/products/di/EPI/GLA_SC-EPI.pdf) (Accessed: May 2016).
273. Thudi, N. R., Shrivastav, V. K., Monif, T., Khuroo, A., Gurule, S., Partani, P. O., ... Mathur, R. (2011). Pharmacokinetic and bioequivalence study of endogenous compound tretinoin 10 mg capsules in healthy volunteers by base line correction approach. *Clinical Research and Regulatory Affairs*, 28(3), 68–73.
274. Levine, H., & Watson, N. (2000). Comparison of the pharmacokinetics of Crinone 8% administered vaginally versus Prometrium administered orally in postmenopausal women. *Fertility and Sterility*, 73(3), 516–521.
275. Upton, R. A., Knutson, J. C., Bishop, C. W., & LeVan, L. W. (2003). Pharmacokinetics of doxercalciferol, a new vitamin D analogue that lowers parathyroid hormone. *Nephrology Dialysis Transplantation*, 18(4), 750–758.
276. Frytak, S., Moertel, C. G., & Rubin, J. (1984). Metabolic studies of Delta-9-Tetrahydrocannabinol in Cancer Patients. *Cancer Treatment Reports*, 68(12), 1427–1431.
277. Joerger, M., Wilkins, J., Fagagnini, S., Baldinger, R., Brenneisen, R., Schneider, U., ... Weber, M. (2012). Single-dose pharmacokinetics and tolerability of oral delta-9-tetrahydrocannabinol in patients with amyotrophic lateral sclerosis. *Drug Metab Lett.*, 6(2), 102–108.
278. Karschner, E. L., Darwin, W. D., Goodwin, R. S., Wright, S., & Huestis, M. A. (2011). Plasma Cannabinoid Pharmacokinetics following Controlled Oral  $\Delta$  9-Tetrahydrocannabinol and Oromucosal Cannabis Extract Administration. *Clinical Chemistry*, 57(1), 66–75.

279. Schwilke, E. W., Schwoppe, D. M., Karschner, E. L., Lowe, R. H., Darwin, W. D., Kelly, D. L., ... Huestis, M. A. (2009).  $\Delta$  9-Tetrahydrocannabinol (THC), 11-Hydroxy-THC, and 11-Nor-9-carboxy-THC Plasma Pharmacokinetics during and after Continuous High-Dose Oral THC. *Clinical Chemistry*, 55(12), 2180–2189.
280. Wall, M. E., Sadler, B. M., Brine, D., & Taylor, H. (1983). Metabolism, disposition, and kinetics of delta-9-tetrahydrocannabinol in men and women. *Clin. Pharmacol. Ther.*, 34(3), 352–363.
281. Medicines and Healthcare products Regulatory Agency. (2009). Alfacalcidol capsules, available at: <http://www.mhra.gov.uk/home/groups/par/documents/websiteresources/con065723.pdf> (Accessed: May 2016).
282. Brandi, L., Egfjord, M., & Olgaard, K. (2002). Pharmacokinetics of 1,25(OH)<sub>2</sub>D<sub>3</sub> and 1 $\alpha$  (OH)D<sub>3</sub> in normal and uraemic men. *Nephrology Dialysis Transplantation*, 17(5), 829–842.
283. Jin, S.-E., Park, J.-S., & Kim, C.-K. (2009). Pharmacokinetics of oral calcitriol in healthy human based on the analysis with an enzyme immunoassay. *Pharmacological Research*, 60(1), 57–60.
284. Jostell, K. G., Agurell, S., Allgén, L. G., Kuylensstierna, B., Lindgren, J. E., Åberg, G., & G. Österlöf. (1978). Pharmacokinetics of Clomethiazole in Healthy Adults. *Acta Pharmacologica et Toxicologica*, 43, 180–89.
285. Ratz, A. E., Schlienger, R. G., Linder, L., Langewitz, W., & Haefeli, W. E. (1999). Pharmacokinetics and pharmacodynamics of clomethiazole after oral and rectal administration in healthy subjects. *Clinical Therapeutics*, 21, 829–40.
286. Kovarik, J. M., Mueller, E. A., Van Bree, J. B., Tetzloff, W., & Kutz, K. (1994). Reduced inter- and intraindividual variability in cyclosporine pharmacokinetics from a microemulsion formulation. *Journal of Pharmaceutical Sciences*, 83(3), 444–446.
287. Ptachcinski, R., Venkataramanan, R., & Burckart, G. (1986). Clinical Pharmacokinetics of Cyclosporin. *Clinical Pharmacokinetics*, 11(2), 107–132.
288. Postolache, P., Petrescu, O., Dorneanu, V., & Zanini, A. C. (2002). Cyclosporine bioavailability of two physically different oral formulations. *Eur Rev Med Pharmacol Sci.*, 6(6), 127–131.
289. Drewe, J., Meier, R., Vonderscher, J., Kiss, D., Posanski, U., Kissel, T., & Gyr, K. (1992). Enhancement of the oral absorption of cyclosporin in man. *British Journal of Clinical Pharmacology*, 34(1), 60–64.
290. Mueller, E., Kovarik, J., van Bree, J., Grevel, J., Lückner, P., & Kutz, K. (1994). Influence of a Fat-Rich Meal on the Pharmacokinetics of a New Oral Formulation of Cyclosporine in a Crossover Comparison with the Market Formulation. *Pharmaceutical Research*, 11(1), 151–155.
291. Hunt, C. A., & Jones, R. T. (1980). Tolerance and disposition of tetrahydrocannabinol in man. *Journal of Pharmacology and Experimental Therapeutics*, 215(1), 35–44.
292. Ohlsson, A., Lindgren, J.-E., Wahlen, A., Agurell, S., Hollister, L. E., & Gillespie, H. K. (1980). Plasma delta-9-tetrahydrocannabinol concentrations and clinical effects after oral and intravenous administration and smoking. *Clin Pharmacol Ther*, 28(3), 409–16.
293. Kelly, P., & Jones, R. T. (1992). Metabolism of tetrahydrocannabinol in frequent and infrequent marijuana users. *Journal of analytical toxicology*, 16(4), 228–235.

294. Naef, M., Russmann, S., Petersen-Felix, S., & Brenneisen, R. (2004). Development and pharmacokinetic characterization of pulmonal and intravenous delta-9-tetrahydrocannabinol (THC) in humans. *Journal of Pharmaceutical Sciences*, 93(5), 1176–1184.
295. Gomez, D. Y., Wacher, V. J., Tomlanovich, S. J., Hebert, M. F., & Benet, L. Z. (1995). The effects of ketoconazole on the intestinal metabolism and bioavailability of cyclosporine. *Clin Pharmacol Ther*, 58, 15–19.
296. Rohatgi, A. (2015). WebPlotDigitizer v3.8, <http://arohatgi.info/WebPlotDigitizer>.
297. Lin, Z., Monteiro-Riviere, N. A., & Riviere, J. E. (2016). A physiologically based pharmacokinetic model for polyethylene glycol-coated gold nanoparticles of different sizes in adult mice. *Nanotoxicology*, 10(2), 162–172.
298. Kuo, I., & Akpa, B. S. (2013). Validity of the Lipid Sink as a Mechanism for the Reversal of Local Anesthetic Systemic Toxicity: A Physiologically Based Pharmacokinetic Model Study. *Anesthesiology*, 118(6), 1350–1361.
299. Lin, Z., Li, M., Gehring, R., & Riviere, J. E. (2015). Development and Application of a Multiroute Physiologically Based Pharmacokinetic Model for Oxytetracycline in Dogs and Humans. *Journal of Pharmaceutical Sciences*, 104(1), 233–243.
300. Joint FAO/WHO Expert Committee on Food Additives. (1987). Evaluation of certain food additives and contaminants, available at: [http://apps.who.int/iris/bitstream/10665/44515/1/WHO\\_TRS\\_960\\_eng.pdf](http://apps.who.int/iris/bitstream/10665/44515/1/WHO_TRS_960_eng.pdf) (Accessed: May 2016).
301. Mudie, D. M., Murray, K., Hoad, C. L., Pritchard, S. E., Garnett, M. C., Amidon, G. L., ... Marciani, L. (2014). Quantification of Gastrointestinal Liquid Volumes and Distribution Following a 240 mL Dose of Water in the Fasted State. *Molecular Pharmaceutics*, 11(9), 3039–3047.
302. Kaukonen, A., Boyd, B., Porter, C. H., & Charman, W. (2004). Drug Solubilization Behavior During in Vitro Digestion of Simple Triglyceride Lipid Solution Formulations. *Pharmaceutical Research*, 21(2), 245–253.
303. Williams, H. D., Sassene, P., Kleberg, K., Calderone, M., Igonin, A., Jule, E., ... Communicated on Behalf of the, L. C. (2014). Toward the Establishment of Standardized In Vitro Tests for Lipid-Based Formulations, Part 4: Proposing a New Lipid Formulation Performance Classification System. *Journal of Pharmaceutical Sciences*, 103(3), 2441–55.
304. Benito-Gallo, P., Marlow, M., Zann, V., Scholes, P., & Gershkovich, P. (2016). Linking in Vitro Lipolysis and Microsomal Metabolism for the Quantitative Prediction of Oral Bioavailability of BCS II Drugs Administered in Lipidic Formulations. *Molecular Pharmaceutics*, 13(10), 3526–3540.
305. Zgair, A., Wong, J. C. M., Sabri, A., Fischer, P. M., Barrett, D. A., Constantinescu, C. S., & Gershkovich, P. (2015). Development of a simple and sensitive HPLC-UV method for the simultaneous determination of cannabidiol and  $\Delta^9$ -tetrahydrocannabinol in rat plasma. *Journal of Pharmaceutical and Biomedical Analysis*, 114(0), 145–51.
306. U.S. Food and Drug Administration. (2006). Guidance for Industry. Bioanalytical Method Validation, available at: <http://www.fda.gov/downloads/Drugs/Guidance/ucm070107.pdf> (Accessed: June 2016).
307. European Medicines Agency. (2015). Guideline on bioanalytical method validation, available at:

- [http://www.ema.europa.eu/docs/en\\_GB/document\\_library/Scientific\\_guideline/2011/08/WC500109686.pdf](http://www.ema.europa.eu/docs/en_GB/document_library/Scientific_guideline/2011/08/WC500109686.pdf) (Accessed: June 2016).
308. Briggs, R. J., Nicholson, R., Vazvaei, F., Busch, J., Mabuchi, M., Mahesh, K. S., ... Abbott, R. W. (2014). Method Transfer, Partial Validation, and Cross Validation: Recommendations for Best Practices and Harmonization from the Global Bioanalysis Consortium Harmonization Team. *The AAPS Journal*, 16(6), 1143–1148.
  309. Almeida, A. M., Castel-Branco, M. M., & Falcao, A. C. (2002). Linear regression for calibration lines revisited: weighting schemes for bioanalytical methods. *Journal of Chromatography B*, 774(1), 215–222.
  310. Ingels, F., Deferme, S., Destexhe, E., Oth, M., Van den Mooter, G., & Augustijns, P. (2002). Simulated intestinal fluid as transport medium in the Caco-2 cell culture model. *International Journal of Pharmaceutics*, 232(1–2), 183–192.
  311. Konishi, T., Satsu, H., Hatsugai, Y., Aizawa, K., Inakuma, T., Nagata, S., ... Shimizu, M. (2004). A bitter melon extract inhibits the P-glycoprotein activity in intestinal Caco-2 cells: monoglyceride as an active compound. *Biofactors*, 22(1–4), 71–74.
  312. Howgate, E. M., Rowland Yeo, K., Proctor, N. J., Tucker, G. T., & Rostami-Hodjegan, A. (2006). Prediction of in vivo drug clearance from in vitro data. I: Impact of inter-individual variability. *Xenobiotica*, 36(6), 473–497.
  313. Edgerley, D. A. (1998). Techniques for improving the accuracy of calibration in the environmental laboratory. In *14th Annual Waste Testing & Quality Assurance Symposium* (pp. 181–87).
  314. Kiser, M. M., & Dolan, J. W. (2004). Selecting the Best Curve Fit. *LC-GC Europe*, 17(3), 138–43.
  315. Miller, J. N., & Miller, J. C. (2010). Appendix 2: Statistical tables. In J. N. Miller & J. C. Miller (Eds.), *Statistics and Chemometrics for Analytical Chemistry* (6th ed., p. 267). Harlow, UK: Pearson Education Limited.
  316. Grow Shop Blog Alchimia. (2015). Marijuana and Medicine: Cesamet®, Marinol®, Sativex®. Retrieved from <https://www.alchimiaweb.com/blogen/marijuana-and-medicine-cesamet-marinol-sativex/>
  317. Adams, I. B., & Martin, B. R. (1996). Cannabis: pharmacology and toxicology in animals and humans. *Addiction*, 91(11), 1585–1614.
  318. Hunt, C. A., Jones, R. T., Herning, R. I., & Bachman, J. (1981). Evidence that Cannabidiol Does Not Significantly Alter the Pharmacokinetics of Tetrahydrocannabinol in Man. *Journal of Pharmacokinetics and Biopharmaceutics*, 9(3), 245–260.
  319. Grotenhermen, F. (2003). Pharmacokinetics and Pharmacodynamics of Cannabinoids. *Clinical Pharmacokinetics*, 42(4), 327–360.
  320. Dunn, C., Wagstaff, A., Perry, C., Plosker, G., & Goa, K. (2001). Cyclosporin. *Drugs*, 61(13), 1957–2016.
  321. Johnson, E. L., Reynolds, D. L., Scott Wright, D., & Pachla, L. A. (1988). Biological Sample Preparation and Data Reduction Concepts in Pharmaceutical Analysis. *Journal of Chromatographic Science*, 26(8), 372–379.
  322. U.S. Food and Drug Administration. (2000). Guidance for Industry: Waiver of In Vivo Bioavailability and Bioequivalence Studies for Immediate-Release Solid Oral Dosage Forms Based on a Biopharmaceutics Classification System. (U.S. Department of Health

- and Human Services, Food and Drug Administration, & Center for Drug Evaluation and Research (CDER), Eds.).
323. Berthelsen, R., Holm, R., Jacobsen, J., Kristensen, J., Abrahamsson, B., & Müllertz, A. (2015). Kolliphor Surfactants Affect Solubilization and Bioavailability of Fenofibrate. Studies of in Vitro Digestion and Absorption in Rats. *Molecular Pharmaceutics*, 12(4), 1062–1071.
  324. Pauling, L. (1947). *General Chemistry*. New York: Dover Publications, Inc.
  325. Friis, G. J., & Bundgaard, H. (1992). Kinetics of degradation of cyclosporin A in acidic aqueous solution and its implication in its oral absorption. *International Journal of Pharmaceutics*, 82(1), 79–83.
  326. Kleberg, K., Jacobsen, J., & Müllertz, A. (2010). Characterising the behaviour of poorly water soluble drugs in the intestine: application of biorelevant media for solubility, dissolution and transport studies. *Journal of Pharmacy and Pharmacology*, 62(11), 1656–1668.
  327. Vertzoni, M., Markopoulos, C., Symillides, M., Goumas, C., Imanidis, G., & Reppas, C. (2012). Luminal Lipid Phases after Administration of a Triglyceride Solution of Danazol in the Fed State and Their Contribution to the Flux of Danazol Across Caco-2 Cell Monolayers. *Molecular Pharmaceutics*, 9(5), 1189–1198.
  328. Obach, R. S., & Reed-Hagen, A. E. (2002). Measurement of Michaelis Constants for Cytochrome P450-Mediated Biotransformation Reactions Using a Substrate Depletion Approach. *Drug Metabolism and Disposition*, 30(7), 831–837.
  329. Nath, A., & Atkins, W. M. (2006). A Theoretical Validation of the Substrate Depletion Approach to Determining Kinetic Parameters. *Drug Metabolism and Disposition*, 34(9), 1433–1435.
  330. Lee, J. B. (2015). *HPLC-UV assays for Verapamil and Dexamethasone (Unpublished work)*.
  331. Mercolini, L., Mandrioli, R., Protti, M., Conti, M., Serpelloni, G., & Raggi, M. A. (2013). Monitoring of chronic Cannabis abuse: An LC–MS/MS method for hair analysis. *Journal of Pharmaceutical and Biomedical Analysis*, 76, 119–125.
  332. Roth, N., Moosmann, B., & Auwärter, V. (2013). Development and validation of an LC–MS/MS method for quantification of  $\Delta^9$ -tetrahydrocannabinolic acid A (THCA-A), THC, CBN and CBD in hair. *Journal of Mass Spectrometry*, 48(2), 227–233.
  333. Keevil, B. G., Tierney, D. P., Cooper, D. P., & Morris, M. R. (2002). Rapid Liquid Chromatography-Tandem Mass Spectrometry Method for Routine Analysis of Cyclosporin A Over an Extended Concentration Range. *Clinical Chemistry*, 48(1), 69–76.
  334. Bartolucci, G., Giocaliere, E., Boscaro, F., Vannacci, A., Gallo, E., Pieraccini, G., & Moneti, G. (2011). Vitamin D3 quantification in a cod liver oil-based supplement. *Journal of Pharmaceutical and Biomedical Analysis*, 55(1), 64–70.
  335. Thörn, H. A., Lundahl, A., Schrickx, J. A., Dickinson, P. A., & Lennernäs, H. (2011). Drug metabolism of CYP3A4, CYP2C9 and CYP2D6 substrates in pigs and humans. *European Journal of Pharmaceutical Sciences*, 43(3), 89–98.
  336. Jigorel, E., & Houston, J. B. (2012). Utility of Drug Depletion-Time Profiles in Isolated Hepatocytes for Accessing Hepatic Uptake Clearance: Identifying Rate-Limiting Steps and Role of Passive Processes. *Drug Metabolism and Disposition*, 40(8), 1596–1602.

337. Sjögren, E., Lennernäs, H., Andersson, T. B., Gråsjö, J., & Bredberg, U. (2009). The Multiple Depletion Curves Method Provides Accurate Estimates of Intrinsic Clearance (CL<sub>int</sub>), Maximum Velocity of the Metabolic Reaction (V<sub>max</sub>), and Michaelis Constant (K<sub>m</sub>): Accuracy and Robustness Evaluated through Experimental Data and Monte Carlo Si. *Drug Metabolism and Disposition*, 37(1), 47–58.
338. Austin, R. P., Barton, P., Cockcroft, S. L., Wenlock, M. C., & Riley, R. J. (2002). The Influence of Nonspecific Microsomal Binding on Apparent Intrinsic Clearance, and Its Prediction from Physicochemical Properties. *Drug Metabolism and Disposition*, 30(12), 1497–1503.
339. Hallifax, D., & Houston, J. B. (2006). Binding of Drugs to Hepatic Microsomes: Comment and Assessment of Current Prediction Methodology With Recommendation for Improvement. *Drug Metabolism and Disposition*, 34(4), 1078.
340. Gertz, M., Kilford, P. J., Houston, J. B., & Galetin, A. (2008). Drug Lipophilicity and Microsomal Protein Concentration as Determinants in the Prediction of the Fraction Unbound in Microsomal Incubations. *Drug Metabolism and Disposition*, 36(3), 535–542.
341. Minder, R., Weder, H. J., & Bickel, M. H. (1970). Experimental errors resulting from uptake of lipophilic drugs by soft plastic materials. *Biochemical Pharmacology*, 19, 2179–80.
342. Hammarlund-Udenaes, M. (2013). Microdialysis in CNS PKPD Research: Unraveling Unbound Concentrations. In M. Muller (Ed.), *Microdialysis in Drug Development* (p. 83). New York - Hiedelberg - Dordrecht - London: Springer.
343. Yang, C. X., Li, Y. F., & Huang, C. Z. (2002). Determination of Total Protein Content in Human Serum Samples with Fast Red Vr by Resonance Light Scattering Technique. *Analytical Letters*, 35(12), 1945–1957.
344. McGinnity, D. F., Soars, M. G., Urbanowicz, R. A., & Riley, R. J. (2004). Evaluation Of Fresh And Cryopreserved Hepatocytes As In Vitro Drug Metabolism Tools For The Prediction Of Metabolic Clearance. *Drug Metabolism and Disposition*, 32(11), 1247–1253.
345. Molina, D. K., & DiMaio, V. J. (2012). Normal organ weights in men: part II-the brain, lungs, liver, spleen, and kidneys. *Am J Forensic Med Pathol.*, 33(4), 368–72.
346. Davies, B., & Morris, T. (1993). Physiological Parameters in Laboratory Animals and Humans. *Pharmaceutical Research*, 10(7), 1093–1095.
347. Matheson, P. J., Wilson, M. A., & Garrison, R. N. (2016). Regulation of Intestinal Blood Flow. *Journal of Surgical Research*, 93(1), 182–196.
348. Valentin, J. (2002). Basic anatomical and physiological data for use in radiological protection: reference values: ICRP Publication 89. *Annals of the ICRP*, 32(3–4), 1–277.
349. Granger, D. N., Richardson, P. D., Kvietys, P. R., & Mortillaro, N. A. (1980). Intestinal blood flow. *Gastroenterology*, 78, 837–863.
350. Yang, J., Jamei, M., Yeo, K. R., Tucker, G. T., & Rostami-Hodjegan, A. (2007). Prediction of Intestinal First-Pass Drug Metabolism. *Current Drug Metabolism*, 8(7), 676–684.
351. Karlsson, F. H., Bouchene, S., Hilgendorf, C., Dolgos, H., & Peters, S. A. (2013). Utility of In Vitro Systems and Preclinical Data for the Prediction of Human Intestinal First-Pass Metabolism during Drug Discovery and Preclinical Development. *Drug Metabolism and Disposition*, 41(12), 2033–2046.
352. Mazur, A., Lichti, C. F., Prather, P. L., Zielinska, A. K., Bratton, S. M., Gallus-Zawada, A.,

- ... Moran, J. H. (2009). Characterization of Human Hepatic and Extrahepatic UDP-Glucuronosyltransferase Enzymes Involved in the Metabolism of Classic Cannabinoids. *Drug Metabolism and Disposition*, 37(7), 1496–1504.
353. Bland, T. M., Haining, R. L., Tracy, T. S., & Callery, P. S. (2005). CYP2C-catalyzed delta(9)-tetrahydrocannabinol metabolism: Kinetics, pharmacogenetics and interaction with phenytoin. *Biochemical Pharmacology*, 70(7), 1096–1103.
  354. Kolars, J. C., Schmiedlin-Ren, P., Schuetz, J. D., Fang, C., & Watkins, P. B. (1992). Identification of rifampin-inducible P450III A4 (CYP3A4) in human small bowel enterocytes. *J Clin Invest*, 90(5), 1871–1878.
  355. Kronbach, T., Fischer, V., & Meyer, U. A. (1988). Cyclosporine metabolism in human liver: Identification of a cytochrome P-450III gene family as the major cyclosporine-metabolizing enzyme explains interactions of cyclosporine with other drugs. *Clin. Pharm. Ther.*, 43(6), 630–635.
  356. Pond, S. M., & Tozer, T. N. (1984). First-Pass Elimination Basic Concepts and Clinical Consequences. *Clinical Pharmacokinetics*, 9(1), 1–25.
  357. Watanabe, K., Matsunaga, T., Yamamoto, I., Funae, Y., & Yoshimura, H. (1995). Involvement of CYP2C in the Metabolism of Cannabinoids by Human Hepatic Microsomes from an Old Woman. *Biological & pharmaceutical bulletin*, 18(8), 1138–1141.
  358. Bornheim, L. M., Lasker, J. M., & Raucy, J. L. (1992). Human hepatic microsomal metabolism of delta 1-tetrahydrocannabinol. *Drug Metabolism and Disposition*, 20(2), 241–246.
  359. Yatscoff, R. W., Malcolm, A. J., & Naicker, S. S. (2004). Immunoassay method for measuring a cyclosporine and its metabolites. *Google Patents*.
  360. Yatscoff, R. W., Rosano, T. G., & Bowers, L. D. (1991). The clinical significance of cyclosporine metabolites. *Clinical Biochemistry*, 24(1), 23–25.
  361. Rostami-Hodjegan, A., & Tucker, G. T. (2007). Simulation and prediction of in vivo drug metabolism in human populations from in vitro data. *Nat Rev Drug Discov*, 6(2), 140–148.
  362. Andersson, T. B., Sjöberg, H., Hoffmann, K.-J., Boobis, A. R., Watts, P., Edwards, R. J., ... Pelkonen, O. (2001). An Assessment of Human Liver-Derived in Vitro Systems to Predict the in Vivo Metabolism and Clearance of Almqalant. *Drug Metabolism and Disposition*, 29(5), 712–720.
  363. Gertz, M., Houston, J. B., & Galetin, A. (2011). Physiologically Based Pharmacokinetic Modeling of Intestinal First-Pass Metabolism of CYP3A Substrates with High Intestinal Extraction. *Drug Metabolism and Disposition*, 39(9), 1633–1642.
  364. Trevaskis, N. L., Porter, C. J. H., & Charman, W. N. (2006). An Examination Of The Interplay Between Enterocyte-Based Metabolism And Lymphatic Drug Transport In The Rat. *Drug Metabolism and Disposition*, 34(5), 729–733.
  365. Dahan, A., & Hoffman, A. (2005). Evaluation of a chylomicron flow blocking approach to investigate the intestinal lymphatic transport of lipophilic drugs. *European Journal of Pharmaceutical Sciences*, 24(4), 381–388.
  366. Wong, J., Sivak, O., Wasan, K. M., Fischer, P. M., & Gershkovich, P. (2013). The Role of Lymphatic Transport in the Intestinal Absorption of Lipophilic Cannabinoids. *AAPS . San Antonio (TX, USA)*.

367. van der Laan, J. W., Brightwell, J., McAnulty, P., Ratky, J., & Stark, C. (2010). Regulatory acceptability of the minipig in the development of pharmaceuticals, chemicals and other products. *Journal of Pharmacological and Toxicological Methods*, 62(3), 184–195.
368. Porter, C. J. H., & Charman, W. N. (2007). Oral Lipid-based Formulations: Using Preclinical Data to Dictate Formulation Strategies for Poorly Water-Soluble Drugs. In D. J. Hauss (Ed.), *Oral Lipid-Based Formulations: Enhancing the Bioavailability of Poorly Water-Soluble Drugs* (pp. 185–207). Princeton, New Jersey, USA: Bristol-Myers Squibb Company.
369. Chiou, W., Jeong, H., Chung, S., & Wu, T. (2000). Evaluation of using dog as an animal model to study the fraction of oral dose absorbed of 43 drugs in humans. *Pharm Res.*, 17, 135–40.
370. Zgair, A., Wong, J. C., Lee, J. B., Mistry, J., Sivak, O., Wasan, K. M., ... Gershkovich, P. (2016). Dietary fats and pharmaceutical lipid excipients increase systemic exposure to orally administered cannabis and cannabis-based medicines. *Am J Transl Res*, 8(7), In Press.
371. Avramoff, A., Khan, W., Ezra, A., Elgart, A., Hoffman, A., & Domb, A. J. (2012). Cyclosporin pro-dispersion liposphere formulation. *Journal of Controlled Release*, 160(2), 401–406.
372. Dahan, A., Mendelman, A., Amsili, S., Ezov, N., & Hoffman, A. (2007). The effect of general anesthesia on the intestinal lymphatic transport of lipophilic drugs: Comparison between anesthetized and freely moving conscious rat models. *European Journal of Pharmaceutical Sciences*, 32(4–5), 367–374.
373. McConnell, E. L., Basit, A. W., & Murdan, S. (2008). Measurements of rat and mouse gastrointestinal pH, fluid and lymphoid tissue, and implications for in-vivo experiments. *Journal of Pharmacy and Pharmacology*, 60(1), 63–70.
374. Holt, P. R., Fairchild, B. M., & Weiss, J. (1986). A liquid crystalline phase in human intestinal contents during fat digestion. *Lipids*, 21(7), 444–446.
375. Smith, R., Jones, R. D. O., Ballard, P. G., & Griffiths, H. H. (2008). Determination of microsome and hepatocyte scaling factors for in vitro/in vivo extrapolation in the rat and dog. *Xenobiotica*, 38(11), 1386–1398.
376. Carlile, D. J., Zomorodi, K., & Houston, J. B. (1997). Scaling Factors to Relate Drug Metabolic Clearance in Hepatic Microsomes, Isolated Hepatocytes, and the Intact Liver: Studies with Induced Livers Involving Diazepam. *Drug Metabolism and Disposition*, 25(8), 903–911.
377. Lu, C., Li, P., Gallegos, R., Uttamsingh, V., Xia, C. Q., Miwa, G. T., ... Gan, L.-S. (2006). Comparison of Intrinsic Clearance in Liver Microsomes and Hepatocytes from Rats and Humans: Evaluation of Free Fraction and Uptake in Hepatocytes. *Drug Metabolism and Disposition*, 34(9), 1600–1605.
378. Plowchalk, D. R., & Teeguarden, J. (2002). Development of a Physiologically Based Pharmacokinetic Model for Estradiol in Rats and Humans: A Biologically Motivated Quantitative Framework for Evaluating Responses to Estradiol and Other Endocrine-Active Compounds. *Toxicological Sciences*, 69(1), 60–78.
379. Watanabe, K., Yamaori, S., Funahashi, T., Kimura, T., & Yamamoto, I. (2007). Cytochrome P450 enzymes involved in the metabolism of tetrahydrocannabinols and cannabinol by human hepatic microsomes. *Life Sciences*, 80(15), 1415–1419.
380. Chaudhuri, S. R., Bolger, M. B., Lawless, M., Balakrishnan, A., & Morrison, J. (2016).



- Physiologically based pharmacokinetic modeling and simulation for drug candidate optimization and selection. *AAPS magazine*, June, 14–18.
381. Honório, T. da S., Pinto, E. C., Rocha, H. V. A., Esteves, V. S. D., dos Santos, T. C., Castro, H. C. R., ... Cabral, L. M. (2013). In Vitro–In Vivo Correlation of Efavirenz Tablets Using GastroPlus®. *AAPS PharmSciTech*, 14(3), 1244–1254.
382. Akhlaghi, F., Ashley, J., Keogh, A., & Brown, K. (1999). Cyclosporine Plasma Unbound Fraction in Heart and Lung Transplantation Recipients. *Therapeutic Drug Monitoring*, 21(1), 8–16.
383. Bergström, C. A. S., Luthman, K., & Artursson, P. (2004). Accuracy of calculated pH-dependent aqueous drug solubility. *European Journal of Pharmaceutical Sciences*, 22(5), 387–398.
384. Lindahl, A., Ungell, A.-L., Knutson, L., & Lennernäs, H. (1997). Characterization of Fluids from the Stomach and Proximal Jejunum in Men and Women. *Pharmaceutical Research*, 14(4), 497–502.
385. Pedersen, B. L., Mullertz, A., Bronsted, H., & Kristensen, H. G. (2000). A comparison of the solubility of danazol in human and simulated gastrointestinal fluid. *Pharm Res.*, 17, 891–894.